Dynamics of spontaneous activity in the cerebral cortex across brain states

Daniel Alejandro Jercog

Universitat de Barcelona

Programa de Doctorado en Biomedicina

Dynamics of spontaneous activity in the cerebral cortex across brain states

Memoria de Tesis Doctoral

Daniel Alejandro Jercog

Trabajo dirigido y supervisado por
Albert Compte Braquets [(1)]
Jaime De la Rocha Vázquez [(2)]
Maria Victoria Sánchez Vives [(3,4)]

Barcelona, 2013

[(1)] Theoretical Neurobiology of Cortical Networks, [(2)] Cortical Circuit Dynamics Group, [(3)] Cortical Networks and EVENT Lab, Systems Neuroscience Group, Institut d'investigacions Biomèdiques August Pi i Sunyer (IDIBAPS). [(4)] Tutor designado.

Área: Neurociencia. **Línea**: Neurofisiología y computación en sistemas corticales.

A mi familia,

A Emily.

Agradecimientos

Agradezco a mis directores, por creer en mis capacidades y darme la oportunidad de realizar mi tesis doctoral y crecer en múltiples aspectos con ellos. A Mavi por haberme dado la oportunidad de venir a Barcelona para poder dar mis primeros pasos en neurociencia y permitirme meter mis manos en los experimentos. A Albert por su eterna paciencia para sentarse conmigo a enseñarme a encarar problemas con una nueva perspectiva, desde cuentas en papel y lápiz hasta cuestiones de la vida. A Jaime por enseñarme a pensar de manera aguda, crítica y precisa, y sobre todo por su predisposición y energía positiva que transmite (incluso en los momentos más difíciles).

A mis compañeros de laboratorio durante estos años: Diego, Thomas, Ramón, Marcel, Lucila, Enrique, Marie, Maira, Juan Pablo, Klaus, Rita, Alex, David, Carola, Pavel, Ainhoa, Gabriela, Jaime, Albert, João... Agradecerles no solo por todo lo aprendido gracias a ellos, sino también porque hicieron que el laboratorio (subterráneo) sea un lugar más agradable para pasar infinidad de horas. Y a mis amigos por llevarme a la vida más allá de la ciencia (que existe) Especialmente a Miguel, Vere, Ingo, Javirlo, Negro, Lucila, Kike... Lo mismo que mis compañeros de la gloriosa Violeta FC. A los Terrazas Pepo, Zisko y Marco. Gracias totales por la música, "misteriosa forma del tiempo".

Gracias a mis padres Sonio y Chiche, y mis hermanos Sonia y Pablo por su amor incondicional y apoyo en todo momento. A Pablo por nuestras charlas desde la "pizzería de Kandel", que siempre me hicieron reir y sentirme más acompañado de la gente que quiero tanto y está tan lejos. Lo mismo que mi otro hermano, Santi. A pesar de los miles de kilómetros de distancia y tanto tiempo, siempre estuvieron cerca de mi. Y a Emily por su paciencia infinita, por cuidar y hacer de mí cada día una mejor persona. Voy a parar aquí antes de que explote el *cursi*-metro...

Este ha sido un viaje inolvidable. Esta tesis va dedicada a todos ellos.

Resumen

La corteza cerebral conforma la mayor parte del volumen total del cerebro humano y es a su vez el área mayormente responsable de funciones cognitivas y de procesamiento de orden superior. Desde los primeros estudios a principios del siglo XX tras el desarrollo de la electroencefalografía, se entendió que el cerebro exhibe abundante actividad electroquímica espontánea. Dicha actividad eléctrica, registrada mediante el electroencefalograma, proviene de neuronas que se activan durante la ausencia de estímulos sensoriales o de la ejecución de un comportamiento motor.

La actividad espontánea de la corteza cerebral se manifiesta de manera permanente durante los distintos "estados cerebrales" (*brain states*) presentes entre el sueño y la vigilia, donde la dinámica interna del cerebro interacciona con la actividad desencadenada por estímulos sensoriales. A pesar que inicialmente se pensó que dicha actividad espontánea era meramente "ruido neuronal", i.e. actividad que no representaba información relevante alguna, durante las últimas décadas se ha enfatizado su participación en posibles funciones computacionales que van desde la exploración de experiencias sensoriales previas a la formación de nuevas memorias. De hecho, estudios recientes durante los últimos años refuerzan las teorías de que la actividad espontánea cortical producida durante el sueño - más precisamente durante el sueño de onda lenta - tiene un rol esencial en la consolidación de la memoria.

El estado cerebral de un sujeto está definido en base a la estructura de su actividad espontánea. El cerebro opera en un aparente continuo de regímenes en cuyos extremos se encuentran, respectivamente, los estados desincronizados (tales como con vigilia activo, atención o sueño MOR) y sincronizados (tales como sueño de onda lenta, anestesia, vigilia reposo). Durante los estados desíncronizados, poblaciones de neuronas de la corteza cerebral disparan potenciales de acción de manera tónica, aparentemente estocástica y no correlacionada entre ellas. Por otra parte, durante los estados sincronizados, las neuronas de la corteza cerebral muestran de manera coherente la alternancia entre intervalos de ausencia de actividad (*DOWN*) e intervalos donde eventualmente descargan potenciales de acción (*UP*). Más aún, la actividad generada por las redes corticales durante los intervalos UP muestra aparente similitud con aquella observable en el animal

despierto, y por lo tanto sugiere que durante estos intervalos se llevan a cabo procesamientos de información o computaciones similares a aquellos que tienen lugar durante la vigilia. En estos últimos años se ha entendido también que los estados cerebrales no definen categorías discretas, sino más bien un continuo de posibles estados. De hecho, se ha visto recientemente que los intervalos DOWN pueden aparecer incluso en el animal despierto. A pesar de décadas de investigación acerca de la actividad espontánea cortical, su importancia y significado para el correcto funcionamiento del cerebro permanecen mayormente inciertos, así como también los mecanismos que la generan.

La presente Tesis Doctoral se dedica al estudio y caracterización de la actividad espontánea de la corteza cerebral en distintos estados cerebrales, y de los posibles mecanismos que la generan. Concretamente en esta Tesis Doctoral se abordan los siguientes objetivos:

1. Determinar el perfil laminar de la sincronización[1] de la actividad intracortical de frecuencias rápidas en la columna cortical durante los intervalos UP de estados cerebrales sincronizados *in vivo* y en el circuito cortical aislado *in vitro*.
2. Mediante el estudio detallado de la estadística de la actividad de poblaciones de neuronas durante los estados sincronizados *in vivo*, construir un modelo computacional para explorar los mecanismos de red que causan las transiciones entre intervalos UP y DOWN durante los estados cerebrales sincronizados.
3. Mediante el análisis de la actividad de poblaciones de neuronas en distintos estados cerebrales, determinar cómo los estados cerebrales modulan la dinámica y la estadística de la actividad espontánea en los circuitos corticales.

A continuación se detallan los resultados obtenidos en relación a cada uno de estos puntos.

1 El termino sincronización se refiere a la actividad colectiva de neuronas en una escala de tiempo del orden de milisegundos, y no debe ser confundido con los estados cerebrales sincronizados o desincronizados, que se refieren a escalas de tiempo del orden de minutos.

1. La actividad de la corteza cerebral del animal despierto se caracteriza por la presencia de oscilaciones rápidas (10-100Hz) en las señales de potencial de campo local. Dichas oscilaciones se encuentran circunscritas en dos dominios conformados por capas supra e infra granulares (capas superficiales y profundas de la corteza, respectivamente). No está claro, si esta es una característica general de la activación cortical, si depende de neuromoduladores o de *inputs* característicos del estado de vigilia. Por otra parte, las redes corticales producen oscilaciones rápidas, no sólo durante el estado de vigilia y tareas cognitivas, sino también durante el sueño de onda lenta o anestesia profunda. También se han observado oscilaciones rápidas durante los intervalos UP generados espontáneamente en rodajas de neo-corteza mantenidas *in vitro*. El estudio presentado en el Capítulo 4.1 de esta Tesis tiene como fin determinar si dicha segregación laminar de las oscilaciones rápidas observada durante la vigilia también se produce durante la actividad espontánea observada durante los intervalos UP. Con este objetivo, se registraron señales extracelulares de múltiples capas en rodajas de corteza visual de hurones *in vitro* y también registros laminares *in vivo* en la corteza visual de hurones anestesiados.

Registros laminares de dieciséis canales *in vivo* revelaron la existencia de compartimentos laminares de oscilaciones rápidas a través de la columna cortical durante los intervalos UP. Observamos altos niveles de coherencia para los electrodos del mismo dominio laminar (supra/infra granulares), mientras que se encontraron niveles más bajos de coherencia entre electrodos de dominios laminares distintos. Por una parte, las capas infragranulares mostraron oscilaciones rápidas de mayor frecuencia que las capas supragranulares durante los intervalos UP, un hallazgo que resultó coherente tanto *in vivo* como *in vitro*. Específicamente, la potencia de las fluctuaciones en la banda de frecuencias beta (10-30Hz) fue mayor en capas supragranulares mientras que los picos de potencia sobre la banda de frecuencias gamma (30-100Hz) fueron la característica espectral más prominente de las capas infragranulares. Las oscilaciones gamma en capas infragranulares *in vivo* resultaron más fuertes y más robustas que aquellas observadas *in vitro*. Con el fin de probar si la diferencia observada en la potencias de las oscilaciones *in vivo* e *in vitro* podría ser explicada por una excitabilidad más alta del circuito cortical *in situ*, se incrementó la excitabilidad en rodajas mediante la aplicación de ácido kaínico, un agonista de los receptores de kainato a menudo utilizado con este fin. El ácido kaínico indujo un aumento significativo en la potencia de las oscilaciones gamma en capas infragranulares, pero también generó un desacoplamiento entre capas supra y capas infragranulares durante la alternancia entre intervalos UP y DOWN, un efecto

que no se observa en circunstancias fisiológicas *in vivo*.

Estos resultados demuestran que la segregación en diferentes dominios laminares es también una característica de actividad de la red cortical espontánea durante los intervalos UP, a pesar de la fuerte conectividad vertical intracolumnar y los patrones de activación cortical altamente síncronos durante la alternancia entre intervalos UP y DOWN. Por otra parte, nuestro estudio *in vitro* demuestra que la modulación de la excitabilidad local puede controlar acoplamientos entre laminas y la dinámica oscilatoria en circuitos corticales.

Este trabajo ha sido[2] presentado en:

Annual Meeting of the Society for Neuroscience 2013, San Diego (Estados Unidos)
Laminar profile of fast oscillations during cortical Up states in vivo and in vitro
D Jercog, M Ruiz-Mejias, R Reig, A Compte and MV Sanchez-Vives

FENS 2010, Amsterdam, (Holanda)
Oscillations in the beta/gamma range during spontaneous up states in supra versus infragranular layers of the cerebral cortex in vitro and in vivo
DA Jercog, S De La Torre, A Compte & MV Sanchez-Vives

2. Como fue descrito anteriormente, durante el sueño de onda lenta y bajo los efectos de anestesia, los circuitos corticales muestran fluctuaciones globales lentas en su actividad, consistentes en la alternancia de intervalos UP y DOWN. Aunque este patrón de actividad es ubicuo durante el sueño de onda lenta y bajo el efecto de muchos anestésicos, todavía carecemos de una descripción clara de los mecanismos que lo generan. La hipótesis estándar de generación de dicho patrón en redes corticales con conexiones recurrentes supone la existencia de un mecanismo celular o sináptico de fatiga (e.g., *corrientes transmembrana de adaptación*) que se acumula durante los intervalos UP en los que las neuronas disparan de modo tónico. Progresivamente la fatiga neuronal disminuye la excitabilidad de las neuronas hasta que la actividad recurrente ya no puede ser sostenida y el circuito pasa a un intervalo DOWN. Durante los períodos de "descanso" en los que las neuronas permanecen en silencio, las redes corticales se recuperan de dicha fatiga hasta que el circuito se auto-excita y transiciona a un nuevo intervalo UP. Este mecanismo produce una alternancia oscilatoria entre intervalos UP y DOWN. Alternativamente,

2 Neuroscience 2013 tendrá lugar en Noviembre de 2013.

se ha propuesto que estructuras subcorticales tales como el tálamo, ganglios basales o el propio hipocampo, generan *inputs* sobre los circuitos corticales que pueden causar transiciones entre UP/DOWN y en consecuencia, asumiendo la independencia en el tiempo de dichos *inputs*, generar transiciones UP/DOWN estocásticas.

Para comprender la contribución de los diferentes mecanismos, se analizaron registros extracelulares de la actividad de poblaciones de neuronas de la corteza cerebral de ratas anestesiadas con uretano. Basado en la actividad de potenciales de acción de la población de neuronas, se determinaron las duraciones de los intervalos UP (U) y DOWN (D). Se encontró que las distribuciones de U y D se asemejan a distribuciones gamma sesgadas - con alto coeficiente de variación (CV promedio = 0.7). Además dichas duraciones exhibieron correlaciones significativamente positivas entre las duraciones de intervalos consecutivos (corr(DU)=0,15 y corr(UD) = 0.1). Adicionalmente, la tasa de descarga de potenciales de acción durante los intervalos UP reveló rastros débiles de la presencia de adaptación (decaimiento de la tasa de descarga). Esta evidencia, puede sugerir que los mecanismos de fatiga tienen un papel débil pero significativo en la determinación de la duración de los intervalos U y D, mientras que los *inputs* externos o las fluctuaciones de la actividad durante los U, podrían tener un gran impacto generando las transiciones entre UP/DOWN. Por otra parte, basada en la forma de la espiga promedio de cada una de las neuronas registradas extracelularmente, clasificamos las neuronas en putativa inhibitoria (I) y putativa excitatoria (E). La segregación de neuronas en I y E reveló que las neuronas I durante períodos U mostraron más adaptación en la tasa de descarga que las neuronas E, contrario a las respuestas típicas de estos dos tipos de células frente a la inyección de impulsos de corriente despolarizantes.

Mediante el uso de un modelo de red de baja dimensión representando poblaciones de neuronas umbral-lineal (*linear-threshold*) E e I, se encontró que por medio de la combinación de adaptación celular en las neuronas E y la presencia de fluctuaciones externas se podría producir la alternancia entre períodos UP y DOWN describiendo una dinámica que coincide con las estadísticas obtenidas en los experimentos. Además, el modelo propuesto se basa en un nuevo tipo de biestabilidad entre un intervalo de ausencia de actividad (DOWN) y un intervalo de descarga de potenciales de acción (UP), cuya tasa de descarga puede ser arbitrariamente baja. La biestabilidad surge de la asimetría entre las poblaciones I y E, donde la ganancia y el umbral de disparo de las neuronas I deben ser más grandes

que las de las neuronas E, ambas características observadas experimentalmente. En estas condiciones, a pesar de que la adaptación celular sólo afecta a la subpoblación E, la adaptación de la tasa la descarga durante los intervalos UP es más pronunciada para la subpoblación I, tal como se observa en los experimentos.

En resumen, nuestros análisis sobre los datos experimentales revelaron que la estadística de duraciones de los intervalos UP y DOWN durante estados cerebrales sincronizados observados bajo el efecto de uretano son más irregulares que lo descrito previamente bajo otros anestésicos. Además observamos trazas débiles de decaimiento en la tasa de descarga promedio de la población durante intervalos UP. Estas dos características enfatizan el rol de las fluctuaciones causando transiciones UP/DOWN. Por otra parte, la presencia de correlaciones positivas entre intervalos UP/DOWN indirectamente revela la existencia de un proceso de fatiga lento que contribuye a la generación de dichas transiciones. Asimismo, el modelo propuesto proporciona una explicación mecanística a la estadística de los intervalos UP y DOWN de la corteza *in vivo*, basada en un nuevo régimen de biestabilidad que se basa en intervalos UP estabilizados por inhibición y a una tasa de descarga baja.

Este trabajo ha sido presentado en:

Barcelona Computational & Systems Neuroscience 2013, Barcelona, (España)
Mechanisms underlying UP and DOWN states in the neocortex
D Jercog, A Roxin, P Barthó, A Luczak, A Compte & J de la Rocha

Annual Meeting of the Society for Neuroscience 2011, Washington, (Estados Unidos)
Slow global fluctuations in cortical circuits under urethane anesthesia
DA Jercog, A Roxin, A Renart, P Bartho, L Hollender, KD Harris, A Compte, J de la Rocha

3. Los estados desincronizados se caracterizan por pequeñas fluctuaciones rápidas de baja amplitud en el potencial de campo local, que corresponden con la descarga tónica de neuronas individuales. Por otro lado, los estados síncronos se caracterizan por fluctuaciones lentas de gran amplitud en la LFP que corresponde con la alternancia entre intervalos UP y DOWN, que se expresan coherentemente en las neuronas individuales del circuito cortical local. Como ha sido mencionado anteriormente, los estados sincronizado y desincronizado no son estados cerebrales discretos sino, más bien , los extremos en un continuo de estados posibles .

El objetivo de este estudio fue entender cómo los diferentes estados cerebrales en dicho espacio continuo afectan la dinámica de la alternancia entre intervalos UP-DOWN y, por otra parte, estudiar si un modelo simple que muestra adaptación y fluctuaciones puede explicar dichos cambios en la dinámica de los circuitos corticales .

El análisis de los datos experimentales reveló que las variaciones espontáneas en el estado del cerebro durante los experimentos impacta la dinámica UP-DOWN en una forma sistemática en casi todos los experimentos analizados. A pesar de que los estados desincronizados extremos no muestran la presencia de intervalos DOWN, en principio, para una amplia gama de niveles de estados sincronizados pudimos detectar transiciones UP-DOWN. Hemos cuantificado las estadísticas de U y D y de la actividad durante diferentes niveles de sincronización del estado cerebral. Este análisis revela que hacia los estados más desincronizados : *i.* los intervalos UP aumentan su duración y variabilidad, mientras que los intervalos DOWN las disminuyen, *ii.* la correlación entre intervalos consecutivos disminuye. Un modelo de red sencillo que incluye tanto adaptación y fluctuaciones puede producir la alternancia entre intervalos UP y DOWN y, más aún, mediante cambios en la adaptación y las fluctuaciones puede reproducir cualitativamente los cambios observados entre los extremos de estados cerebrales desincronizados y sincronizados.

Este trabajo ha sido presentado en:

FENS 2012, Barcelona, (España)

Dynamics Of Up And Down States In Cortical Circuits Under Urethane Anesthesia

DA Jercog, A Roxin, P Barthó, A Luczak, A Renart, KD Harris, A Compte & J de la Rocha

Table of Contents

1. Introduction

1.1. Cortical Spontaneous activity

Even during the absence of sensory input or behavioral output, the brain exhibits abundant ongoing activity in many structures. As a matter of fact, from resting state imaging studies in humans we know that the ongoing brain activity consumes 20% of the body energy and moreover, task-related increases in neuronal metabolism only represents a remarkably small increase of <5% compared with baseline levels (Raichle and Mintun, 2006). Despite the prominence and several decades of research about ongoing spontaneous activity, its importance and significance during normal brain functioning is still poorly understood. The following sections will discuss some basic aspects of what we know regarding this still mysterious phenomenon.

Not just noise

When an identical stimulus is presented repeatedly, cortical neurons exhibit variability in their responses, approximately following Poisson statistics (Dean, 1981; Tolhurst et al., 1981). A common procedure to extract the signal from the variable responses obtained during electrophysiological recordings is to average over repeated presentations of the stimulus. This procedure assumes that the variability of neural responses is an annoyance for cortical processing that the brain somehow must overcome. If this variability is uncorrelated across a population of neurons, averaging the single-trial responses over the many cells in the population would average out the noise and result in a reliable estimate of the stimulus input (van Kan et al., 1985; Shadlen and Newsome, 1998a; Softky and Koch, 1993; Tolhurst et al., 1983). This commonly assumed "signal-plus-noise" model of cortical responses downgrades the meaning of the spontaneous activity, which might provide a source of this variability as it has a strong impact on sensory evoked responses. Moreover, it has been proposed that the variability of the neuronal response might be important for coding purposes (reviewed in (Stein et al., 2005), (Ma et al., 2006)).

The spontaneous activity is not an independent random process of individual neurons, but it is generated by the synaptic inputs from other coherently activated neurons. This effect is observed when without any sensory input, spontaneous activity can be as large as the evoked activity (Arieli et al., 1995; Petersen et al., 2003a). Moreover, activity can be correlated across millimeters of the cortex as reported by Amos Arieli and colleagues (1995), but also over different time scales ranging from milliseconds to seconds (Kohn and Smith, 2005). The magnitude and spatio-temporal correlations of the spontaneous activity demonstrate that this is not just random independent noise coming from individual neurons.

Additionally, it has been proposed that responses in single trials can be predicted by linear summation of a deterministic component (the average response over trials) and the preceding ongoing activity in paralyzed cats (Arieli et al., 1996). However, average responses and trial-to-trial responses variability strongly depend

on the level of anesthesia which might lead to failure of the simple linear model interactions (Kisley and Gerstein, 1999; Petersen et al., 2003b). It is however an appealing idea that sensory input processing might be a combination of a deterministic response and ongoing cortical dynamics (Curto et al., 2009).

Anyhow, spontaneous activity is one of the factors that account for the inter-trial variability in cortical responses. In this case, evoked sensory responses are a result of the interaction between spontaneous activity and external stimulation rather than an overtake of the cortical circuit by the external input, reflecting the structure of the input signal itself, and this interaction might depend on the stimulus strength (Fiser et al., 2004; Nauhaus et al., 2009).

As mentioned before, the interaction with the external world can lead to response patterns across cortical populations that are similar to those observed during the spontaneous activity, as if thalamic input would be a triggering signal to produce stereotypical responses, resembling the idea of attractor networks or ingrained trajectories in the state space (Cossart et al., 2003; MacLean et al., 2005). The spontaneous activity may replay previous experienced sensory responses, since the spatio-temporal structure of activity on engaged networks are likely to be similar to those observed during evoked-responses (Tsodyks et al., 1999; Kenet et al., 2003; Fiser et al., 2004; Han et al., 2008; Luczak et al., 2009). Consequently, it has been suggested that the patterns of spontaneous activity reveal the realm of possible cortical network responses (Luczak et al., 2009).

In this way, spontaneous activity is more than noise and possibly an instrumental part of cortical processing by modulation cortical responses in a context dependent manner.

Reveals the underlying connectivity

During development, spontaneous activity is crucial in defining cell properties (i.e. receptive field, tuning) and early patterns of connections that are built even without any sensory perception experience (Ruthazer and Stryker, 1996; Weliky and Katz, 1997) (reviewed in (Feller, 1999)). The inherent mechanisms generating such structured patterns of ongoing spontaneous activity are unknown. However, it is reasonable to rely on the hypothesis that spontaneous activity reflects the underlying connectivity of cortex. A clear example is provided by primary visual cortex orientation maps found in cats, monkeys and tree-shews (but not in mice and rats). Whether is evoked or spontaneous activity from a cell tuned for a particular orientation are used to trigger averaging of optical imaging signal from a piece of cortical surface, a pattern emerges highlighting those cortical columns matching the orientation preference of the cell (Bonhoeffer and Grinvald, 1991; Tsodyks et al., 1999). The connectivity map unveiled in this way confirms results from anatomical studies and cross-correlation analysis of pairs of single-unit recordings (Ts'o et al., 1986). These same orientation maps can interestingly emerge during spntaneous activity (Kenet et al., 2003; Murphy and Miller, 2009). However, this result occur mostly under anesthesia, as the spatio-temporal structure of spontaneous activity changes during waking. Thus, even though spontaneous activity is clearly affected by the circuit connectivity, this is not the only factor that determines its structure as

the same networks can display very different patterns of spontaneous activity.

At a larger spatial scale, a similar approach is commonly used in imaging studies to find anatomically separate cortical networks observed as covariation of measured activity, a procedure called functional connectivity analysis (Friston et al., 1997; Biswal et al., 2010). The spontaneous activity can reveal those global networks as measured by functional-Magnetic-Resonance-Imaging (fMRI) during resting-state conditions (Vincent et al., 2007; van den Heuvel et al., 2009). Additionally, this spontaneous activity that covariates is relatively stable across a wide range of cognitive states, ranging from fully awake to light sleep and anesthesia (Fox and Raichle, 2007). Therefore, spontaneous activity reveals to the same extent, both the underlying functional and structural connectivity of cortical networks.

During sleep: a window for perception & the link with learning

During sleep, the brain is not "turned-off" or disconnected from the external world. Indeed, initially shown by a number of behavioral experiments in humans during the 1970s, during sleep we are capable of fairly complex processing, such as auditory (Perrin et al., 1999; Portas et al., 2000) or somatosensory (Nishihara and Horiuchi, 1998). In such way, the spontaneous activity observed during sleep has been proposed as a way of providing a gate of information processing in the cortex (Massimini et al., 2003; Schabus et al., 2012; Luczak et al., 2013).

Moreover, during the last decade there has been an explosion in the number of studies concerning the spontaneous activity produced during sleep, which replay sequential firing patterns observed during prior behaviour in the hippocampus (Skaggs and McNaughton, 1996; Wilson, 1996; Diba and Buzsáki, 2007; Ji and Wilson, 2007) and neocortex (Qin et al., 1997; Hoffman and McNaughton, 2002; Ribeiro et al., 2004; Euston et al., 2007; Ji and Wilson, 2007; Peyrache et al., 2009). This replay of activity may be involved in the process of memory consolidation by producing a structural re-organization of the wiring of brain circuitry (Walker and Stickgold, 2006; Marshall et al., 2006; Ngo et al., 2013) inducing synaptic potentiation (Chauvette et al., 2012). It seems unlikely that sequential firing patterns would be purely related with learning, instead they might reflect a constraint of the cortical circuitry on the possible response patterns - "the vocabulary"- that local cortical circuits are able to generate, since sequences are observable even before a stimulus is ever presented (Luczak et al., 2009). However, it seems clear that after repetitive presentation of a given stimulus, the evoked activity patterns strongly reverberates modifying the patterns of ongoing cortical activity during several minutes in this way mimicking the evoked activity patterns (Han et al., 2008), and learning processes alters the patterns of subsequent ongoing spontaneous activity (Maquet et al., 2000; Ohl et al., 2001). This learning-dependent plasticity process may alter the underlying circuitry, reflected as changes produced in the strength of networks correlation structures (Lewis et al., 2009). According to the Hebbian theory of learning, persistence or repetition of interaction between cells tends to induce long lasting cellular changes such as an increase in their associative strength (Hebb, 1949). In this sense, reverberation of the activity in cell assemblies carried out by the spontaneous activity could serve as a mechanism of short-term memory

formation or as facilitation of long-term perceptual learning (Han et al., 2008). Overall, spontaneous activity during sleep may sculpt traces within the cortical circuit for memory formation.

1.2. Laminar architecture and physiology of neocortex

Perhaps one of the most striking features of the anatomical structure of the mammalian cortex is the laminar organization, defined primarily by the density and size of cell bodies. Given the amount of layers, cortex can be broadly categorized into neocortex (with 6 layers) and allocortex (with less than 6 layers). The allocortex is composed by the hippocampus and olfactory cortex. On the other hand, the neocortex is an area of the brain responsible for "higher functions" such as sensory perception, motor commands, spatial reasoning, abstract planning, working memory or language, and different functional areas are topographically organized (Brodmann, 1909; von Economo and Koskinas, 1925).

The use and improvements of the Golgi staining technique during early XX century, lead to the suggestion from anatomists like Campbell and Bolton that superficial layers of cortex might be involved in “receptive and associative” functions whereas deep layers had “corticofugal and commissural” functions. The fine degree of laminar functional organization, however, was first assessed with the combination of tracers and intracellular recordings performed in the visual cortex of cats during the 1970s (reviewed by (Douglas and Martin, 2004))

Cortical cells can be classified into excitatory or inhibitory, according to the effect of their action potentials in the postsynaptic neuron. Excitatory cells use the excitatory neurotransmitter glutamate, whereas inhibitory cells use the inhibitory neurotransmitter g-amino-butyric acid (GABA). Cortical cells can also be classified into projection neurons and interneurons, according to their spatial connectivity in the local circuit. Excitatory cells are composed of the projection neuron class, namely the pyramidal cells (located in layers III, V and VI), and the interneuron type spiny stellate cells (located in layer IV). On the other hand, several types of inhibitory GABA-ergic interneurons have been distinguished based on their connection-pattern and the co-transmitters they contain (Ascoli et al., 2008; Markram et al., 2004). Pyramidal cells constitute 70-80% of the cortical cells, while the remaining percentage are mostly inhibitory neurons which exhibit several sub-families of diverse morphology (reviewed in (Markram et al., 2004)). The similarity of certain response properties (e.g. orientation tunning of V1 neurons) of nearby cells across all layers suggested that the cortex is organized into elementary processing units, arranged in columns (Mountcastle, 1957; Jones, 2000).

Analysis of *in vivo* intracellular recordings across different neuronal types and layers combined with micro-anatomical data suggests the existence of a canonical microcircuit within the neocortex (Douglas et al., 1989; Binzegger et al., 2004). Many details regarding the connectivity structure at laminar level are preserved across different areas to the most extent for excitatory (Barbour and Callaway, 2008; Shepherd and Svoboda, 2005; Weiler et al., 2008; Xu et al., 2010)

and inhibitory (Kätzel et al., 2011) connections. Even if stereotypy is an appealing concept for understanding how the brain works, the diversity of neuronal types and the complex connectivity observed suggest that a unique stereotypical neocortical microcircuit seems unlikely (Silberberg et al., 2002).

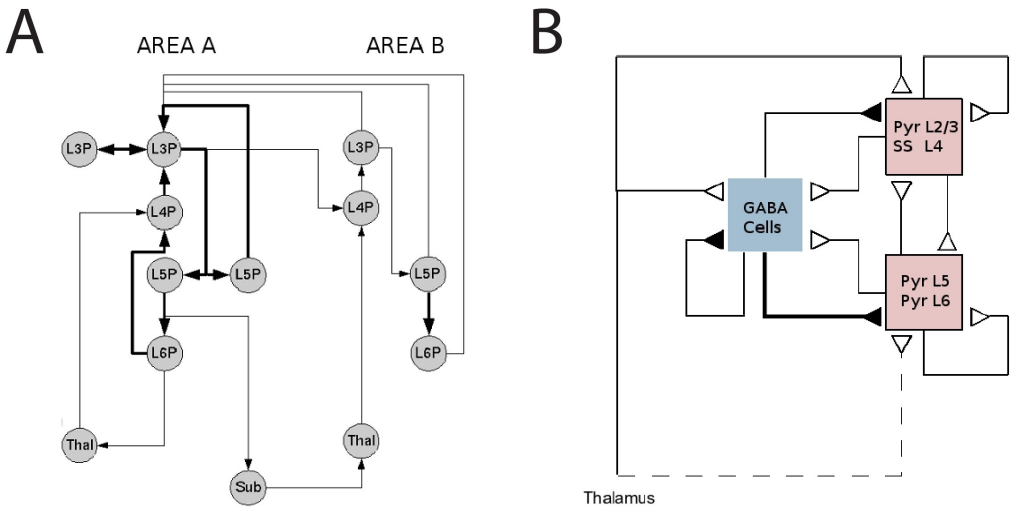

Figure 1. *Cortical laminar connectivity organization.* **A.** Connectivity structure of excitatory neurons within and across different cortical areas (A and B) and their sub-cortical relations. Thick lines represent the connectivity within the cortical column whereas thin lines represent subcortical and inter-areal connections (LX: layer, Thal: thalamus, Sub: sub-cortical structure such as basal ganglia). Modified from (Douglas and Martin, 2004). **B,** Minimal cortical "canonical microcircuit" that explains intracellular responses of visual cortical neurons to stimulation of thalamic afferents, composed by inhibitory (GABA) and excitatory (Pyr: pyramidal, SS: spiny stellate) cortical neurons within a column. Modified from (Douglas et al., 1989).

The layer IV is the major thalamo-recipient layer, which provides incoming sensory information to neocortex, and the prominence or lack of prominence of layer IV is associated with the amount of thalamic input received. Moreover, layer VI provides feedback to thalamic relay nuclei and projects towards superficial and deeper cortical layers, whereas layer V/VI projects to pulvinar and motor structures like superior culliculus other cortical areas and the spinal cord (Binzegger et al., 2004) (extensively reviewed in (Thomson and Bannister, 2003)). Although this model has been the dogma of the cortical microcircuit for decades, recent multiple patch clamp recordings challenge this flow of information across the cortical column (Constantinople and Bruno, 2013). Furthermore, the laminar structure of cortical activity can vary under different behavioural conditions (Sakata and Harris, 2009; Buffalo et al., 2011). Despite the increasing amount of studies concerning cortical layer specific properties, the precise function of neocortical layers remains unclear. In Chapter 4.1 of this thesis we will study the laminar profile of neocortical fast oscillations occurring during periods of spontaneous activity.

The input-output function of cortical neurons

The relationship between output firing as a function of the amplitude of the

injected input current, often called *f-I* curve or input-output transfer function, is one of the basic electrophysiological properties of neurons. Input-output relationships are typically described as sigmoidal-shaped functions: enhancing the output of weak inputs leads to a gradual increase in the firing response, where intermediate inputs elicit steep increase in firing response, while larger inputs exhibit response saturation (Haider and McCormick, 2009). However, in the absence of background activity in some *in vitro* preparations the Input/output relationship cam be modeled as pice-wise linear function (Schiff and Reyes, 2012; Stafstrom et al., 1984), usually called threshold-linear relationship. The linear relationship between input-output holds for a range of firing rates (<30Hz) for some *in vitro* preparations (Mason and Larkman, 1990) because the response saturation is generally achieved at higher firing rates (La Camera et al., 2006; McCormick et al., 1985), while in other *in vitro* preparations response saturation can sometimes be observed at lower firing rates (Amatrudo et al., 2012). Saturation *in vivo* tends to occur at high firing rates (Anderson et al., 2000b; Nowak et al., 2003; Priebe and Ferster, 2008). On the other

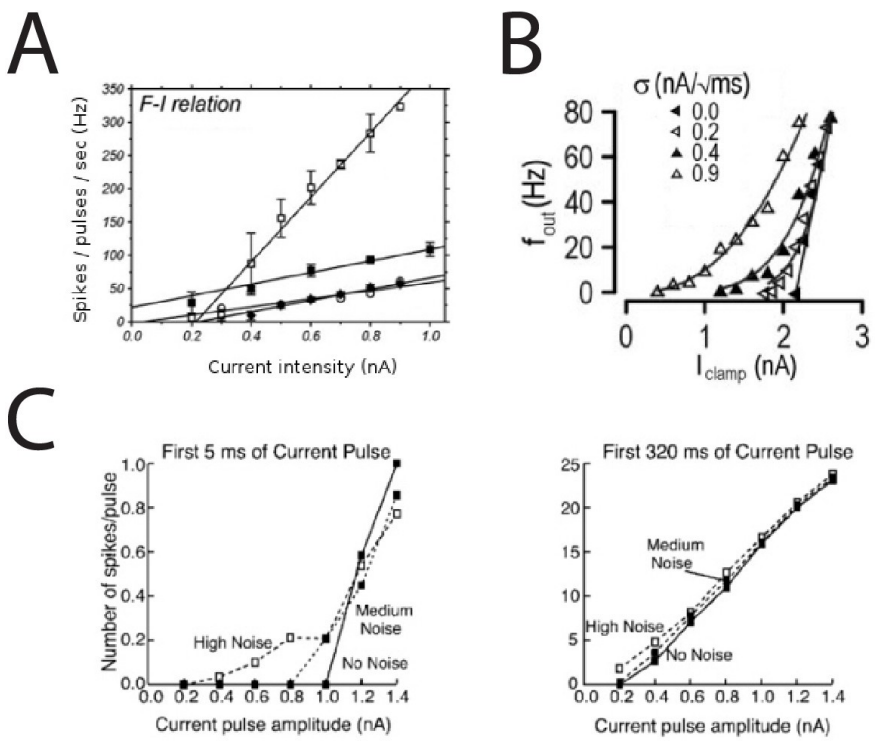

Figure 2. *Cortical f-I curves*. **A.** Some examples of *f-I* curves *in vivo* showing little saturation effects in their *f-I* curves for different neuronal types in the anesthetized cat (Modified from (Nowak et al., 2003)). **B and C,** *In vitro*, injecting noisy current inputs to model synaptic background smooths the "hard" threshold nonlinearity (B modified from (Prescott and De Koninck, 2003) C modified from (Shu et al., 2003a)).

hand, the hard threshold defined by the union of the pice-wise linear functions (i.e., the “sharp knee”) observed in the Input-output relationship *in vitro* when generated using DC current with no fluctuations is smoothed in the *in vivo* condition, where background synaptic input shape the Input-output relationship in an exponential manner by causing firing when the mean input current is subthreshold (Anderson et

al., 2000b; Priebe and Ferster, 2008). Moreover, this smooth effect of the hard threshold can be reproduced by the injection of input noisy current into cells (Prescott and De Koninck, 2003; Shu et al., 2003a). In Chapter 4.3 from Results, we will show that the choice of the transfer function has consequences as the on the dynamics exhibited by recurrently connected networks.

Classification of cortical neurons

Apart from the excitatory and inhibitory classification, cortical neurons can be classified with regard to their intrinsic electrophysiological properties. Under controlled conditions *in vitro*, differences in biophysical membrane properties of individual neurons are manifested in distinct patterns of responses. Therefore, an electrophysiological classification is possible taking into account both the onset and the steady-state response to a current step injection into the soma of neurons (McCormick et al., 1985; Connors and Gutnick, 1990). In this way, cortical neurons can be divided into the following, more standard, cell classes: regular spiking (RS), fast spiking (FS), intrinsically bursting (IB), fast repetitive bursting or chattering or stuttering (FRB) and low-threshold spiking (LTS) (Nowak et al., 2003) (reviewed in (Contreras, 2004)). Nevertheless, recently the Petilla Interneuron Nomenclature Group (PING) — composed by several laboratories specialized in interneuron related studies during many years — established a detailed landmark of possible firing patterns of interneurons given the diversity of their electrical properties previously reported (Ascoli et al., 2008; Druckmann et al., 2012).

Anatomically, RS, IB and FRB cells are almost always pyramidal neurons and, therefore, excitatory. The electrophysiological phenotype of the spiny stellate cells is also RS, leaving them as the only class of excitatory non-pyramidal cell (McCormick et al., 1985). On the other hand, FS and LTS cells are almost exclusively GABA-ergic interneurons, although RS GABA-ergic interneurons also have been observed (Contreras, 2004). In layer V, parvalbumin-expressing GABAergic neurons account for approximatley 60% of the total inhibitory neurons, and all of them exhibit FS properties (Ascoli et al., 2008; Gonchar et al., 2007; Kawaguchi and Kubota, 1997; Markram et al., 2004).

The intrinsic properties of some electrophysiological classes of neurons have different signatures in the input-output relationships. It has been shown *in vitro* that FS cells have higher gain and steeper input-output curves than RS cells, which exhibit spike frequency adaptation or accommodation to steady-state current responses (Connors and Gutnick, 1990; McCormick et al., 1985; Nowak et al., 2003). Moreover, FS cells require several times higher input current than RS cells to reach spike threshold when studied in thalamocortical slices *in vitro* under the absence of background synaptic activity (Cruikshank et al., 2007; Schiff and Reyes, 2012). On the contrary, the FS inhibitory partners LTS, need a lower amount of current to evoke an action potential and also show steeper input-output relationship when compared to RS (Fanselow et al., 2008).

Subsets of excitatory and inhibitory – but not LTS (Cruikshank et al., 2010; Gibson et al., 1999) - cells are innervated by the excitatory thalamic relay neurons, which are the main source of extrinsic input to the neocortex. FS show less input resistance and higher thresholds than RS, however, they respond stronger than RS

cells to thalamic input (Cruikshank et al., 2007, 2010; Gibson et al., 1999) even if cortico-thalamic synapses are depressed after repetitive firing of thalamic cells as observed both *in vitro* and *in vivo* (Castro-Alamancos, 2004; Gabernet et al., 2005). Perhaps due to these differences in synaptic transmission and in the impact of background synaptic activity across cell types there are only few reports regarding the input-output relationship of cortical neurons *in vivo* (Nowak et al., 2003). In Chapter 4.3 from Results, we will implement these differences in gain and thresholds between inhibitory and excitatory neurons in a computational model of a cortical network.

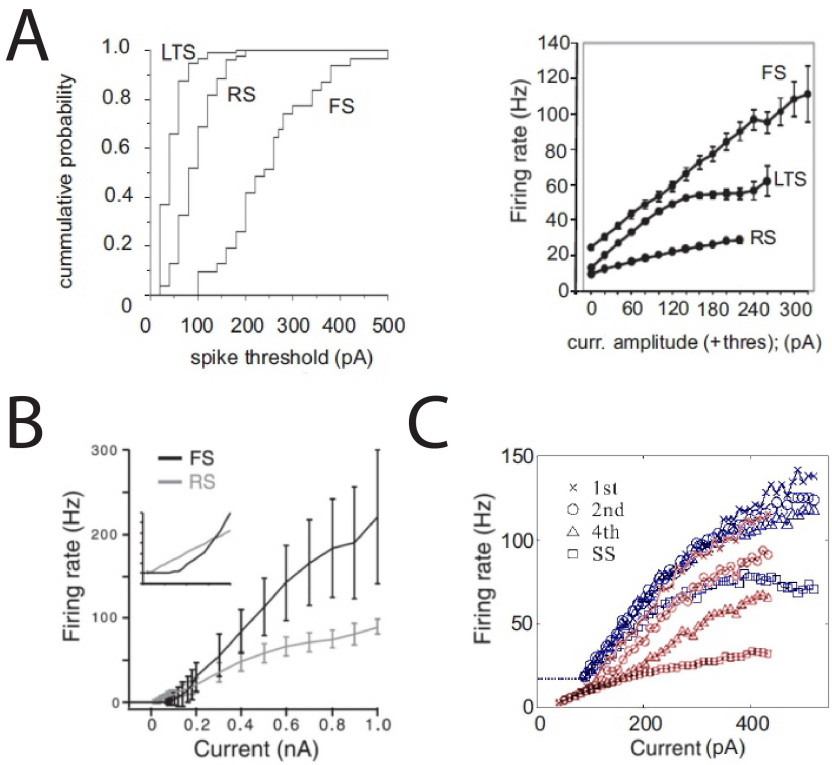

Figure 3. *Cortical f-I curves on steady state responses to constant current injection for excitatory and inhibitory neurons in vitro*. **A.** *f-I* curves for different neuronal types LTS, RS and FS in the somatosensory cortex. **B.** *f-I* curves of RS and FS neuronal types from auditory cortex. **C.** *f-I* curves of RS (red) and FS (blue) neuronal types from somatosensory cortex where firing rate is also shown for 1st, 2nd and 4th interspike interval along with the steady state responses (SS). (A, Modified from (Fanselow et al., 2008). B, Modified from (Schiff and Reyes, 2012). C, Modified from (Tateno et al., 2004).)

Although the characterization of electrophysiological neuronal types from an intracellular perspective is relatively well established, to date there is no agreed criteria available for a reliably classification of extracellular recorded neurons *in vivo* (Ascoli et al., 2008). However, FS neurons are characterized by "narrow" spikes (Mountcastle et al., 1969) compared to spikes from other cells due to the

existence of Kv3 potassium channels in the first case (Rudy and McBain, 2001). Therefore, classification methods into either putative inhibitory FS or excitatory cells for cortical neurons have been proposed based on the spike-waveform dynamics and properties of the spiking statistics (Barthó et al., 2004) and it is used both in rodent (Fujisawa et al., 2008; Sirota et al., 2008) and monkey (Mitchell et al., 2007) electrophysiological studies. In Chapter 4.2 we will use this categorization to study the dynamics of putative excitatory and inhibitory neurons during spontaneous activity.

Spike Frequency adaptation

The ability of neurons to fire action potentials is dependent on their previous electrical activity. One clear example is the absolute refractory period produced by Na+ channel inactivation. However, the history on the electrical activity can also affect the neuronal firing abilities on much longer timescales. Spike-frequency adaptation (SFA) for instance refers to a decrease in instantaneous discharge rate during a sustained current injection and is a common feature of many types of neurons in mammal and non-mammal species.

In neocortex, SFA has been observed in most pyramidal neurons, in particular those classified as RS, whereas their counterpart cells, FS cells, shows little or no adaptation effects (Connors and Gutnick, 1990; McCormick et al., 1985), although they show slow adaptation in the timescales of tens of seconds *in vitro* (Descalzo et al., 2005). The underlying mechanism is usually attributed to the accumulation of an afterhyperpolarization current (AHP), which is an outward current triggered in the wake of action potentials (Baldissera and Gustafsson, 1971; Partridge and Stevens, 1976). Some possible roles have been proposed for SFA including the stabilization of oscillations (Crook et al., 1998), the "forward masking" effect (Wang, 1998), perceptual bistability (Moreno-Bote et al., 2007).
SFA also has been shown as a possible mechanism to reduce output variability (Farkhooi et al., 2011) improving coding accuracy (Cortes et al., 2012). Moreover, adaptation has been proposed as a crucial factor of constraining the preferred frequency of synchronization over neuronal assemblies, setting the frequency of population rhythms in neocortex (Fuhrmann et al., 2002; Sanchez-Vives and McCormick, 2000). It has also been shown that, the presence of neuromodulators like acetylcholine blocks or reduces the magnitude of K+ conductances that are responsible for spike frequency adaptation in cortical neurons (McCormick, 1992). In Chapter 4.3 and 4.4 we will implement SFA in a computational network model of spontaneous activity.

1.3. Neocortical oscillations

Ever since the studies done by Luigi Galvani during the end of XVIII century, the electrical nature of nerve impulses started to dismiss previous theories by which the nervous system was essentially hydraulic (originally proposed by the Greek physician Galen during II century). Modern electrophysiology was developed during the XIX century even if it was not until 1929 that Hans Berger for the first

time reported that the electrical activity of the brain could be recorded through the scalp, leading to the origin of the electroencephalogram (EEG). One striking finding by Berger was that the EEG signal could display an oscillatory pattern at particular frequencies (~10 Hz) when subjects closed their eyes. Since then, the characterization of oscillatory brain activity and the theoretical investigation of their role in brain normal function has grown enormously.

Oscillations can arise from intrinsic neuronal mechanisms, from the interaction among neurons in a network, or from the dynamic interplay between both intrinsic and network properties (for a review see (Buzsáki and Draguhn, 2004)). On a single cell level, oscillations can be observed in the subthreshold membrane potential or in the temporal pattern of spike trains. On the other hand, oscillations on the macroscopic level as shown by EEG, or by the mesoscopic local field potential (LFP) that presumably reflect the pooled synaptic activity from of a population of neurons in a certain volume of tissue (Buzsáki et al., 2012), although the contribution of intrinsic properties may be larger than commonly considered (Reimann et al., 2013).

The term “oscillator” in neuroscience was not used until recent times — popularized by Steriade and Deschênes in 1984 — perhaps because “brain rhythms are not usually oscillators as described by physics textbooks” (Buzsáki, 2006). The tendency of cortical circuits to exhibit oscillations suggests that they could be considered analogous to central pattern generators commonly observed in vertebrates, which are self-contained functional circuits in which sensory input provides primarily a modulation of the function like respiration, walking or swallowing (reviewed in (Yuste et al., 2005)). The principle governing central pattern generators can be studied in the framework of systems composed by coupled oscillators, whereas for cortical circuits the applicability of this framework is more questionable since cortical oscillations are usually reflected by weak and broad-band power spectral signatures which can occur intermingled in short periods of time and are typically confined to small neuronal populations (Wang, 2010). Another feature of cortical activity which seems at odds with the idea of central pattern generators, is the stochasticity exhibited by spike trains. In particular, cortical cells tend to emit Poisson-like spike trains which differ qualitatively from those displayed by oscillators.

In the cerebral cortex, neural activity exhibits a continuous presence and modulation of oscillations, which is suggestive of a role as one of the fundamental mechanisms for information processing. Cortical oscillations not only occur during sleep or anesthesia (Steriade et al., 1993a, 1996), but also during the awake state and cognitive performance. The frequencies of oscillations observed in the cortex spans from infra-slow 0.5 Hz to ultra fast 500 Hz (Buzsáki and Draguhn, 2004), and electrophysiological studies have shed some light on the different underlying mechanism. Next, I will focus on discussing aspects of slow-wave activity, comprising the slow-oscillation (0.1-1 Hz), delta waves (1-4 Hz) and spindles (7-15 Hz). Then I will continue with fast-oscillations (20-80 Hz), which includes the oscillations in the beta (15-30 Hz) and gamma (30-80 Hz) range of frequencies.

The slow-wave activity

During slow-wave sleep and under the effect of several anesthetics (Steriade et al., 1993a; Achermann and Borbély, 1997) or during drowsy or quite-wakefulness periods (Buzsaki et al., 1988; Petersen et al., 2003b; Crochet and Petersen, 2006; Luczak et al., 2009), EEG/LFP signal are dominated by high amplitude slow fluctuations in the slow/delta range (0.1 to 4 Hz). Intracellularly, this pattern of activity is characterized by alternations between an hyperpolarizing phase where neurons mostly show no firing – so-called DOWN state-, and a depolarizing phase were neurons fire tonically at low rates – so-called UP state – (Buzsaki et al., 1988; Steriade et al., 1993a; Crochet and Petersen, 2006) (see below).

Although delta waves and slow-oscillation are considered to represent different phenomena (Achermann and Borbély, 1997), the definition for both follows the same criteria and from this perspective some authors suggested that they are not separate patterns but delta waves represent DOWN intervals from the slow oscillation (Sirota and Buzsáki, 2005). Moreover, delta waves have also been proposed to have both thalamic and cortical origin, for example, thalamectomy in cats does not prevent delta waves (reviewed in (Villablanca, 2004)) and thalamic slice preparations show delta waves (see review by (Sirota and Buzsáki, 2005)). In anesthetized animals, both types of delta waves are nested on top of the slow-oscillation (Steriade et al., 1993b; Steriade, 2006).

Another rhythm grouped as slow oscillation are the spindles (7-15 Hz), displaying waxing-and-waning oscillation at 7-14Hz appearing irregularly in-between 5-15 sec. The thalamic origin of this rhythm is well established since spindles are absent in thalamectomized animals (Steriade and Contreras, 1998) while they appear in isolated thalamic slices (von Krosigk et al., 1993). Nevertheless, in the same way as delta waves, spindles also appear over imposed on slow-oscillations which suggest at least a cortical coordination (Steriade et al., 1993b).

Slow waves during sleep propagate in a fast way across the cortex, covering the whole human cortex in 115 ms in average, as revealed by high-density EEG recordings (Massimini et al., 2004). The propagation of the slow waves are also observed in anesthetized rodents by means of voltage sensitive dyes (Petersen et al., 2003b; Mohajerani et al., 2010) or indirectly using electrode arrays (Nauhaus et al., 2009; Ruiz-Mejias et al., 2011) yielding similar values of about 20-30 mm/s. Simultaneous intracellular recordings reveal that neighboring cortical neurons undergo synchronous transitions on spontaneous slow fluctuations (Lampl et al., 1999), something that was originally observed in striatal neurons (Stern et al., 1998). This synchronization in the transitions can span several millimeters (Amzica and Steriade, 1995a; Volgushev et al., 2006), and horizontal cortico-cortical connections seems to play a fundamental role in the wave propagation since pharmacological disruption of these connections between pairs of neurons largely reduce the synchronization of these slow-waves (Amzica and Steriade, 1995b). Although slow waves are considered a global cortical phenomenon, some evidence from the last years suggest that slow waves can take place locally as well (Volgushev et al., 2006; Nir et al., 2008), even within few hundreds of microns (Sirota and Buzsáki, 2005). In humans, the propagation generation of slow-waves in

the cortex tends to originate at prefrontal areas (Massimini et al., 2004). However, a more recent study shows that this locus of generation could be age dependent and move from occipital areas in the child towards prefrontal areas in adults (Kurth et al., 2010). In anesthetized mice (age>2 months), the predominant propagation is in the anteroposterior direction (Ruiz-Mejias et al., 2011) and the locus of generation tends to be at motor/sensory areas (Mohajerani et al., 2010), whereas simultaneous intracellular recordings in adult cats suggest that take place at parietal cortex (Volgushev et al., 2006).

Steriade and colleagues have suggested that the origin of slow-waves is cortical since extensive thalamic lesions, even several days after producing the intervention, does not prevent their appearance (Steriade et al., 1993c). The same group has also shown that the thalamus (the main input to neocortex) of one-hemisphere-decorticated cats does not display slow-waves (Timofeev and Steriade, 1996a) and that slow waves are present in cortical slabs (Timofeev et al., 2000). Furthermore, slow-waves can appear in a robust manner *in vitro,* resembling those slow-waves observed under anesthesia *in vivo* (Sanchez-Vives and McCormick, 2000).

Nevertheless, the cortical origin of slow waves, and in particular the slow oscillation, is still an ongoing debate and an active role of the thalamus in the generation and shaping of the rhythm has also been proposed (Crunelli and Hughes, 2010). Supporting this idea it has been shown that a thalamic *in vitro* preparation can generate a similar a slow rhythm if metabotropic gluatamate receptors are activated (Hughes et al., 2002, 2004). Moreover, certain type of thalamic neurons seem to exhibit oscillatory behaviour in the delta band, observed in the deafferented thalamus of cats (Steriade et al., 1991). *In vivo*, thalamic low-threshold Ca2+ potential neurons that bursts at the onset of the UP state present them as good candidates of UP state triggers (Contreras and Steriade, 1995; Crunelli and Hughes, 2010). More recent *in vivo* evidence in anesthetitzed rats support this idea showing that some thalamo cortical neurons fire prior to the onset of active phases of cortical slow waves (Slézia et al., 2011; Ushimaru et al., 2012). Crunelli and Hughes in their review from 2010 suggest "... the illustrated examples of cortical UP and DOWN states from the cat *in vivo* [referring to the studies carried by Steriade and colleagues] appear less regular and rhythmic in the absence of thalamic input" (Crunelli and Hughes, 2010). This idea suggests that even though the cortex in isolation might be able to generate slow-waves, thalamic input can entrain those waves which inherit to some extent the rhythmic behaviour generated in the thalamus. Nevertheless, a recent study combining calcium-imaging and optogenetics tools has shown that : (i) the stimulation of a small subset of layer V pyramidal cells from visual cortex of mice is sufficient to initiate UP global cortical states similar that are to those observed spontaneously, (ii) activity is first propagated in cortex and secondly in thalamus (Stroh et al., 2013).

Fast oscillations

Fast oscillations refer to oscillations occurring in the range of tens of Hz. At these frequencies, spikes locked to a certain phase tend to occur in synchrony. Neuronal synchrony, on the other hand, is a potential mechanism for information

encoding and transfer simply because neurons are very sensitive to the coincident arrival of input spikes versus asynchronous inputs (Nowak et al., 1997; Salinas and Sejnowski, 2000). Neuronal synchrony may play a role in well timed coordination and communication between neural populations simultaneously engaged in a certain cognitive process. Originally proposed as a way to solve the "binding problem" (Singer, 1993), synchrony and the role of fast oscillations in a neural code is still a matter of intense research.

During awake and REM sleep, the EEG of spontaneous activity exhibits fluctuations at high frequencies (14-80Hz) with low amplitude and apparently asynchronous across distant areas. Fast oscillations in the beta and gamma range of frequencies, have been associated with cognitive processing such as attention (Fries et al., 2001), working memory (Lisman and Idiart, 1995; Palva et al., 2005), decision making (Haegens et al., 2011), but also with motor functions (MacKay and Mendonça, 1995; Baker et al., 1997), and sensory processing in primates and rodents (extensively reviewed in (Wang, 2010)).

However, fast oscillations are not only present during the wakefulness domain since they are also present in the depolarizing phase of slow-waves in the EEG (Steriade et al., 1996; Le Van Quyen et al., 2010), better observed in human intracraneal EEG (Valderrama et al., 2012). Moreover, ultra-fast short oscillatory episodes (80-400Hz), also called "ripples" are observed superimposed over the depolarizing phase of the slow oscillation in neocortex (Grenier et al., 2001), which might also be fundamental for memory consolidation (Eschenko et al., 2008; Girardeau et al., 2009). The similarity of these fast oscillations with those observed during wakefulness, suggested that they might reflect previous acquired experiences which are subsequently stored by highly synchronized events such as the slow-waves in the EEG (Sejnowski and Destexhe, 2000).

Oscillations across the cortical layers

The slow oscillation is a nearly synchronous event across the cortical layers (Steriade et al., 1996), although detailed analysis in multi-site laminar LFP recordings suggest that deep layers of cortex tend to precede the depolarizing phase (Chauvette et al., 2010). Moreover, the leading firing of layers V cortical neurons in the depolarizing phase suggest a role of deep layers in the initiation of this pattern of activity *in vitro* (Sanchez-Vives and McCormick, 2000) and *in vivo* (Sakata and Harris, 2009; Chauvette et al., 2010; Stroh et al., 2013; Beltramo et al., 2013). However, slow waves with leading firing at superficial layers are observed in the human cortex surrounding epileptic foci (Csercsa et al., 2010). Another remarkable feature of the slow-waves is the laminar profile, exhibiting a phase reversal occurring between the border of layer IV and layer V (Buzsaki et al., 1988), which is suggested to occur due to differential location of recording electrodes relative to the dipoles of large pyramidal cells (Chauvette et al., 2010).

Recent studies have reported the existence of laminar differences regarding the presence of fast oscillations during cognitive tasks in monkeys, where gamma-band synchrony (40-80 Hz) predominates in superficial layers and slower rhythms (10-30Hz) rules the synchronization in deep layers of visual areas (Buffalo et al., 2011; Spaak et al., 2012). The synchrony of the fast oscillations across the layers in

the cortical circuit is not restricted to specific layers but both group of supragranular (SG) and infragranular (IG) layers act like independent compartments, in which coherence values within layers from the same compartment are high and coherence values between layers from different compartments are low and, furthermore, this occurs during visual processing and rest in awake monkeys (Maier et al., 2010).

Laminar differences in oscillations can also be observed in a number of different *in vitro* preparations by activating slices in various different ways: kainate receptor activation (Cunningham et al., 2003; Roopun et al., 2006, 2008; Ainsworth et al., 2011), the cholinergic agonist carbachol (van Aerde et al., 2009), a combination of the aforementioned agonists (Oke et al., 2010; Roopun et al., 2010), or electrically (Metherate and Cruikshank, 1999). Some of these pharmacological models suggest that local cortical circuits from SG and IG can generate fast oscillations independently (Roopun et al., 2006). Moreover, the different profiles observed in the laminar oscillatory content depend on the pharmacological manipulation: for example, faster frequency oscillations in SG than in IG in auditory area A1 under carbachol perfusion (Roopun et al., 2010) or the opposite profile under kainate perfusion (Ainsworth et al., 2011).

As mentioned above, fast oscillations are also present during the depolarizing phase of *in vivo* slow-waves in the EEG, and simultaneous LFP laminar recordings suggest that these oscillations are synchronized across all layers within a column (Steriade and Amzica, 1996; Steriade et al., 1996). Moreover, during the depolarizing phase of the slow-oscillation in cortical slices (Sanchez-Vives and McCormick, 2000), beta/gamma (10-100Hz) oscillations are observed as an emergent property of the cortical circuit (Compte et al., 2008), although the compartmentalization and the detailed laminar specificity of these fast oscillations remains to be elucidated. In Chapter 4.1 of this Thesis we will address this specific question.

1.4. UP-DOWN states

The definition of UP and DOWN states refers to the condition by which the membrane potential of neurons exhibits two different preferred sub threshold values. This effect can be observed as a bimodality in the histogram of the voltage membrane values of individual neurons. This property was observed *in vivo* for the first time in spiny neurons from neostriatum of anesthetized rats (Wilson and Groves, 1981).

Since the discovery made by Wilson and colleagues, much of the work about UP and DOWN states has been performed in anesthetized animals. However, UP and DOWN states has been described to appear naturally in the cortex during the slow-wave-sleep (SWS) phase in cats (Steriade et al., 1993a). In the seminal work of Steriade and colleagues, mentioned in previous sections, it has been shown that UP and DOWN states are observed in intracellular recordings in the presence of slow waves (<1Hz) under deep ketamine or urethane anesthesia. Although the terms UP and DOWN states and slow oscillations are commonly intermixed, we interpret the term UP and DOWN states as a pattern contingent to the occurrence of slow

waves complexes observed during sleep or anesthesia: DOWN states might occasionally appear e.g. when rats perform a behavioral task under sleep pressure (Vyazovskiy et al., 2011), during periods of drowsiness or quite-wakefulness (Crochet and Petersen, 2006; Poulet and Petersen, 2008; Poulet et al., 2012), under different anesthetics (Steriade et al., 1993a), in cortical slabs (Timofeev et al., 2000) and also in different *in vitro* slices preparations exhibiting diverse UP and DOWN states dynamics (Sanchez-Vives and McCormick, 2000; Cossart et al., 2003; Rigas and Castro-Alamancos, 2007; Sanchez-Vives et al., 2008; Mann et al., 2009; Fanselow and Connors, 2010).

The UP and DOWN states *in vivo* have been observed across many different species including mice (Petersen et al., 2003b), rats (Cowan and Wilson, 1994), ferrets (Hasenstaub et al., 2005), cats (Steriade et al., 1993a) and there are also indirect evidence of their presence in humans analyzing EEG (Achermann and Borbély, 1997) and multiple LFP and single unit recordings (Cash et al., 2009; Le Van Quyen et al., 2010; Csercsa et al., 2010). Moreover, they are also observed in numerous different cortical areas such as frontal (Lewis and O'Donnell, 2000; Léger et al., 2005; Isomura et al., 2006), somatosensory (Petersen et al., 2003b; Sachdev et al., 2004; Steriade et al., 2001), visual (Lampl et al., 1999; Steriade et al., 2001), olfactory (Murakami et al., 2005), auditory (Metherate and Ashe, 1993; Saleem et al., 2010), enthorinal (Isomura et al., 2006; Hahn et al., 2012), to name some studies. Although they recur to spread across the entire cortex, there are differences in their profile and statistics across areas (Ruiz-Mejias et al., 2011).

Despite the intracellular definition, UP and DOWN states are commonly inferred indirectly from LFP signals (Mukovski et al., 2007; Steriade et al., 1993a; Compte et al., 2008; McFarland et al., 2011), given that synaptic barrages of activity occur during UP states and are absent during DOWN states (Haider and McCormick, 2009) and that neighboring neurons undergo UP-DOWN transitions in a synchronous way (Amzica and Steriade, 1995a; Volgushev et al., 2006). Another procedure to infer UP and DOWN states is from multi-unit activity (MUA) (Hasenstaub et al., 2007; Luczak et al., 2007; Sanchez-Vives et al., 2010), given that action potentials in MUA are observed almost exclusively during UP states (Luczak et al., 2007). However, the detection of these periods is not a straight forward process and comparison across studies is problematic since there is no universal definition concerning what constitutes an UP or DOWN state, and it is not clear how the detection using different signals (i.e., intracellular membrane potentials, MUA spikes, LFPs) are comparable (but see (Hasenstaub et al., 2007; Saleem et al., 2010)). Anyhow, this dynamical pattern seems to be a ubiquitous feature of cortex but the underlying mechanism and functional role and the are still under debate. In the following sections I will briefly go over on what is known regarding the nature and possible mechanisms.

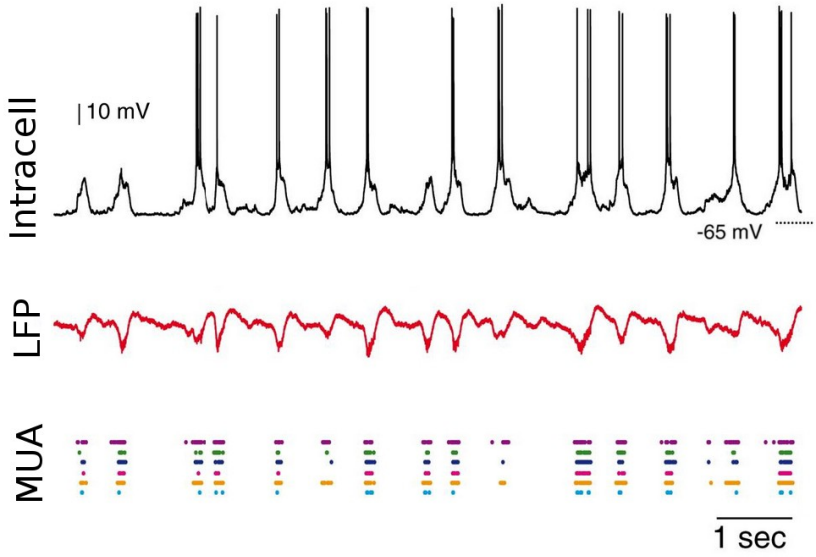

Figure 4. Simultaneous intracellular (top), LFP (middle) and Multi single-unit activity (bottom) recordings in the auditory cortex of urethane anesthetized rats (modified from (Saleem et al., 2010)).

Intra-cortical mechanisms underlying cortical UP and DOWN states

Some neurons in the brain are intrinsically bistable, like motoneurons (Hounsgaard and Kiehn, 1985) or purkinje cells from cerebellum (Loewenstein et al., 2005). In those cases, the hyperpolarization of the membrane potential eliminates the bimodality of the membrane potential histogram whereas the brief depolarization/hyperpolarization of a neuron can induce different plateau potentials, which is a sufficient proof in order to asses bistability of the cells.

Persistent activity in the absence of synaptic input is reported to be observed *in vitro* in a minority of cortical cells from different cortical areas such as enthorinal (Egorov et al., 2002), prefrontal (Winograd et al., 2008; Thuault et al., 2013) and visual cortex (Le Bon-Jego and Yuste, 2007). Some modeling studies of have exploited this idea of intrinsic bistability as mechanisms underlying UP and DOWN states (Parga and Abbott, 2007). However, a recent study in transgenic mice with deletion of HCN1 channels (responsible for I_h current related to persistent activity), exhibit no effect on UP and DOWN states dynamics, suggesting that mechanisms underlying persistent activity and UP and DOWN states might be independent (Thuault et al., 2013).

What maintains cortical neurons in the UP states? One hypothesis says that local reverberation, given the strong recurrent connectivity, keeps the necessary synaptic background in order to give cortical neurons input to sustain their depolarized low firing states (Contreras et al., 1996; Cowan and Wilson, 1994; Sanchez-Vives and McCormick, 2000; Petersen et al., 2003b). The balance between excitatory and inhibitory activity could be keeping the firing at low rates and producing irregular spike trains (Haider et al., 2006). Furthermore, contribution and interplay of active membrane currents might play a fundamental role in sustaining UP states (Compte et al., 2003; Metherate and Ashe, 1993). This is supported by *in*

vitro experiments showing that blocking excitatory transmission prevents the generation of UP states *in vitro* (Sanchez-Vives and McCormick, 2000; Compte et al., 2003).

Patch-clamp recordings have shown that neurons displays average firing rates from 0.4 to 4 Hz during UP states (Constantinople and Bruno, 2011; Waters and Helmchen, 2006; Gentet et al., 2012). Cortical intracellular recordings in cats reveal higher firing rates on an average of 15 Hz pooled across neurons (Steriade et al., 2001). One possible explanation for these differences is that in the last case the recording pipettes are filled with high concentrations of potassium acetate, which likely depolarizes neurons and affects their firing rates (Waters and Helmchen, 2006; Timofeev, 2011). Estimation of firing rates during UP states by extracellular single unit recordings shows an average of 11 Hz (Ruiz-Mejias et al., 2011) whereas the population rates observed by multielectrode recordings are below 5 Hz (Renart et al., 2010).

Intracellular recordings have revealed a balance of excitatory and inhibitory conductances during the UP states *in vitro* (Shu et al., 2003b) and *in vivo* (Haider et al., 2006). In contrast, dynamic clamp recordings suggests that inhibitory conductances dominate during the UP states, although an abrupt decrease in inhibitory conductance is observed towards the offset of the UP state (Rudolph et al., 2007). Consistent with this, a decrease in the firing rate of inhibitory neurons is observed prior to the offset of UP states (Haider et al., 2006; Luczak and Barthó, 2012). The recording of isolated excitatory and events (EPSPs and IPSPs) reveals simultaneous increases/decreases of both events at the initiation/end of UP states *in vivo* (Compte et al., 2009).

DOWN states, on the other hand, are associated with hyperpolarized potentials caused by a lack of synaptic drive, known as disfacilitation (Contreras et al., 1996; Timofeev et al., 2001), and not by GABAergic cortical inhibition as first suggested.

The mechanisms underlying the transitions from the UP to the DOWN state are not entirely clear but a number of non-mutually exclusive mechanisms have been proposed. First, UP to DOWN transitions could occur in response to short-term synaptic depression produced for instance by neurotransmitter depletion (Contreras et al., 1996). Reduction in post-synaptic potentials could be explained through activity-dependent decreases in extracellular Ca^{2+} concentration (Crochet et al., 2005; Boucetta et al., 2013). Alternatively, UP state duration seems to be controlled by Na+ and Ca+ dependent intrinsic K+ currents whereas DOWN duration might be controlled by a K+ dependent intrinsic after-hyperpolarization (AHP) current that acts as a pacemaker for the UP/DOWN generation (Sanchez-Vives and McCormick, 2000; Compte et al., 2003). Moreover, the unspecific intracellular blocking of K+ conductances by the use of Cs- in the recording pipette reduces dramatically the hyperpolarization of voltage membrane observed during DOWN states (Timofeev et al., 2001). Steriade and colleagues concur with this idea by showing that the slow oscillations are suppressed by the presence of neuromodulators that suppress specialized K+ conductances (McCormick and Prince, 1986; Steriade et al., 1993b). However, a gradual increase in input resistance of pyramidal cells during the UP state *in vivo* revealing a steady decrease of the overall membrane conductance, suggests a stronger role of synaptic depression over

the activation of K+ conductances in causing the UP to DOWN transitions (Contreras et al., 1996; Timofeev et al., 2001). However, synaptic depression is notably reduced during slow wave activity (Reig et al., 2006). Furthermore, a recent modeling study suggest that synaptic depression could contribute to the elongation rather than to the termination of UP states (Benita et al., 2012). Another "fatigue" mechanisms proposed is a decrease in adenosine-tryphosphate (ATP) levels occurring during UP states that affect ATP dependant K+ channels (Cunningham et al., 2006).

During DOWN periods, the membrane potential of individual neurons is hyperpolarized at values that are close to the resting membrane potential observed in deafferented slabs (Timofeev et al., 2000) and the firing rates are zero or very low (Ruiz-Mejias et al., 2011). This enables the network to recover from any activity dependent fatigue mechanism. The beginning of a new UP state could be triggered by some neurons that are particularly excitable (LTS) which, after recovery from the fatigue accumulated during the previous UP period, will fire spontaneously and then recruit the rest of the cortical network (Sanchez-Vives and McCormick, 2000; Compte et al., 2003). It also has been proposed that pacemaker cortical neurons, cells which fire rhythmically even in the absence of synaptic activity, could be responsible of UP state initiation based on *in vitro* experiments (Cossart et al., 2003; Le Bon-Jego and Yuste, 2007). On the other hand, spontaneous release of neurotransmitter (Timofeev et al., 2000; Chauvette et al., 2010) or a contribution of astrocytes (Poskanzer and Yuste, 2011) has also been proposed for the initiation of UP states.

Despite the particular way of implementing the fatigue mechanism, it is not straight forward to derive the collective behavior of UP-DOWN switching based on individual cellular-based changes. In this way, it is challenging to reconcile these single cell mechanisms with the high synchrony of the UP-DOWN transitions that is observed in neurons which are several millimeters apart (Amzica and Steriade, 1995a; Volgushev et al., 2006). This suggests "the existence of a network mechanism that switches activity to silence" (Volgushev et al., 2006). As previously described, although the isolated cortex is capable of generating UP and DOWN states, it has been proposed that generation of natural slow-waves during sleep may also rely on input from intrinsic thalamic oscillators, which in turn are driven by cortico-thalamic activity (Crunelli and Hughes, 2010). As reviewed in (Steriade, 2001), "... instead of pure, simple rhythms generated in circumscribed territories as found in simplified *in vitro* preparations, the global electrical activity of the intact brains in living animals displays complex waves sequences...". Indeed, as described in the following section and at least under particular conditions, external inputs to the thalamocortical circuit can also influence the UP-DOWN dynamics in cortical circuits.

In Chapter 4.2 of this Thesis we will scrutinize the evidence supporting a fatigue mechanism in the generation of UP-DOWN switching in *in vivo* data, finding that under urethane anesthesia, there is little or no evidence of this mechanism in the spiking activity of a cortical population. Moreover, in Chapter 4.3 we will use a computational model to explore alternative mechanisms generating the switching.

Coactivation of sub-cortical structures with cortical UP/DOWN transitions

In slices showing slow oscillatory activity, intracortical stimulation is able to evoke transitions from UP to DOWN states and viceversa (Shu et al., 2003b). Studies in thalamocortical slices that exhibit UP and DOWN states, have shown that electrical (MacLean et al., 2005; Rigas and Castro-Alamancos, 2007) or chemical (Rigas and Castro-Alamancos, 2007) thalamic stimulation during DOWN states can induce DOWN to UP transitions, while thalamic stimulation during UP states is not able to trigger UP to DOWN transitions (Rigas and Castro-Alamancos, 2007). This has been proposed to reflect a protective role of the ongoing cortical activity from external thalamic input (Watson et al., 2008). However, many *in vivo* studies have shown that UP-DOWN transitions can be triggered by sensory stimulation (Anderson et al., 2000a; Petersen et al., 2003b; Sachdev et al., 2004; Hasenstaub et al., 2007; Haider et al., 2007; Reig and Sanchez-Vives, 2007; Curto et al., 2009). On the other hand, although some studies show that sensory stimulation in a particular sensory modality can trigger DOWN-UP and UP-DOWN transitions in a reliable way (Hasenstaub et al., 2007), in others studies this effect cannot be observed (Petersen et al., 2003b). Indeed, this difference could be explained by the type of anesthesia and dose combined with the global brain state of the animal, which will have an impact in the strength of the interaction between the ongoing cortical dynamics and the sensory-evoked activity (Livingstone and Hubel, 1981; Marguet and Harris, 2011).

There is growing evidence that the activity in different brain structures occurs in a tight temporal relation with the occurrence of UP-DOWN transitions, presumably having a role in the generation of these transitions. Hippocampal sharp waves have a higher probability to occur during a DOWN state, and are positively correlated with DOWN to UP cortical transitions of the slow-oscillation in the prefrontal cortex during the natural sleep of rats (Battaglia et al., 2004; Hahn et al., 2006), and the firing of hippocampal neurons anticipates ~100ms the firing from prefrontal cortex cells (Wierzynski et al., 2009). During natural sleep of rats, the firing of noradrenergic neurons from locus coeruleus precede the DOWN to UP state transitions in prefrontal cortex, which could provide neuromodulatory input to the cortex in order to momentary increase excitability and promote intracortical plasticity (Eschenko et al., 2012). Moreover, some basal ganglia and reticular thalamic cells activity sometimes precedes the initiation of cortical UP states (Slézia et al., 2011; Ushimaru et al., 2012), and thalamocortical neurons fires bursts of action potentials before firing is observed during cortical UP states (Contreras and Steriade, 1995; Crunelli and Hughes, 2010). This effect is also observed in thalamocortical slices *in vitro* (Rigas and Castro-Alamancos, 2007). Overall, to a greater or lesser extent, although the cortex can generate and maintain UP and DOWN states by itself, the aforementioned evidence suggest that incoming inputs to the neocortex can induce transitions between UP and DOWN states in cortical networks. In the computational model presented in this Thesis (see Chapter 3) the external afferents coming into the cortical network will provide excitatory inputs which will turn essential to trigger DOWN to UP and UP to DOWN transitions.

Regular vs. Irregular UP-DOWN states.

The alternation between UP and DOWN states during the slow-wave sleep or anesthesia is originally described as an oscillation at 0.1-1.0 Hz (Steriade et al., 1993a). However in some instances the aperiodicity observed makes the timing of UP-DOWN transitions very irregular putting into question the oscillatory nature of this pattern (Stern et al., 1997; Lampl et al., 1999). Dynamics of slow waves depend on the level of anesthesia where experimental data suggests that the deeper the anesthesia level the more regular the activity becomes (Steriade et al., 2001; Erchova et al., 2002; Deco et al., 2009a; Chauvette et al., 2011). The regularity might not only depend on the dose levels but also on the anesthetic agent, where e.g. barbiturates tend to display very irregular UP and DOWN states and short-range synchronization of voltage membrane of cortical neurons (Lampl et al., 1999; Okun and Lampl, 2008). Moreover, a recent study comparing the slow waves observed under ketamine anesthesia versus natural slow-wave-sleep, show that the natural slow-wave-sleep displays considerable more irregularity in the UP-DOWN interval durations than under ketamine anesthesia as derived from a comparison of the autocorrelograms of the LFP signals for each condition (Chauvette et al., 2011). In agreement, in cortical chronic recordings in rats, from Bruce McNaughton's lab, the UP+DOWN cycle distribution observed during SWS is observed to be exponential and the authors suggests that DOWN state occurrence is "not due by the presence of an oscillator, but it's a random process" (Johnson et al., 2010).

One study performing a detailed quantitative analysis on the UP and DOWN statistics is provided by the group of Charles Wilson (Stern et al., 1997). In this work, the authors show that although voltage membrane of individual neurons display clear bimodality in cortical & striatal intracellular recordings in urethane-anesthetized rats: i) a broad peak in the power spectrum of voltage membrane at ~1 Hz is observed, ii) UP and DOWN states durations shows gamma-like skewed distributions — with a coefficient of variation (CV), defined as the ration between the standard deviation and the mean, equal to 0.65 and 0.47, respectively — and iii) the serial correlations between consecutive UP and DOWN states are zero (Stern et al., 1997). In the associative cortices of ketamine anesthetized cats, the variability in the duration times seems to be lower with CV(UP)=0.45 and CV(DOWN)=0.31 (Volgushev et al., 2006). Additionally, a recent study on ketamine anesthetized mice have shown that the duration variability of UP and DOWN periods across different areas were quite variable, with prefrontal areas displaying lower variability (CV(UP)=0.2 and CV(DOWN)=0.3) and motor areas displaying higher variability (CV(UP)=0.3 and CV(DOWN)=0.4) (Ruiz-Mejias et al., 2011).

Modeling studies about UP and DOWN states

The majority of the studies proposing the underlying mechanisms causing the transitions between UP and DOWN states does not provide a detailed quantitative analysis of UP and DOWN occurrence, even if the mechanisms producing transitions constrains the UP and DOWN statistics. As previously described, the initial observations from Steriade and colleagues suggested "fatigue" as the key mechanism underlying UP and DOWN switching (Contreras et al., 1996).

Activity dependent adaptive processes have been used in different computational models, implemented as synaptic short-term depression (Bazhenov et al., 2002; Hill and Tononi, 2005; Holcman and Tsodyks, 2006; Benita et al., 2012), synaptic short-term facilitation (Melamed et al., 2008) or spike frequency adaptation (Latham et al., 2000; Compte et al., 2003; Destexhe, 2009). On the other hand, stochastically induced transitions in cortical network models could be implementing synaptic noise (Holcman and Tsodyks, 2006; Mejias et al., 2010). The interplay of fluctuations and adaptation causing transitions between two states has been studied in the context of developing (excitatory) networks and pacemaker central pattern generators (Tabak et al., 2000; Lim and Rinzel, 2010; Tabak et al., 2011; Mattia and Sanchez-Vives, 2012).

On the other hand, other mechanisms have been proposed to cause transitions such as the existence of pacemakers neurons (Kang et al., 2004). Additionally, UP to DOWN transitions have been proposed to be generated via increasing feedback inhibition during the UP state (Melamed et al., 2008; Parga and Abbott, 2007; Chen et al., 2012).

In Chapter 4.3 of this Thesis, we will use a low dimensional model of two inhibitory (I) and excitatory (E) populations in order to explore the contribution of fluctuations and adaptation in causing UP and DOWN switching. We will propose a novel type of bistability based on an asymmetry in the firing threshold of the E and I populations, which can lead to arbitrary low firing rates. We will also performe a qualitative comparison of second order stats in the duration of UP and DOWNs and spiking activity (FF and correlations of spike counts) vs the same measurements performed in the data in Chapter 4.2. Moreover, the model permits to also compare the activity generated by the E and I populations with that obtained after putative classification of narrow and broad spiking isolated neurons from the multi-single unit activity recordings.

1.5. Cortical brain state

By the end of 1920's, Hans Berger observed that brain electrical activity recorded on the scalp of human subjects changes its spectral properties according to different behavioral states of the subject: closing the eyes in the awake calm subject can induce the “alpha” oscillations (with frequency ~10Hz), while opening the eyes cause the presence of “beta” oscillations (~20Hz). Although different states were originally described in terms of cortical electrical activity, it was later understood that they reflect global brain differences associated with different cognitive states.

By means of EEG, cortical activity can be broadly categorized into a continuum of regimes at the extreme of which are the desynchronized state (also called Activated state) and the synchronized state (also called Inactivated state). While desynchronized states are characteristic of wakefulness and REM sleep (that's the reason behind why is also called paradoxical sleep), synchronized states are characteristic of SWS and anesthetized states under most anesthetics (see (Steriade and McCarley, 2005)). Many structures and neurotransmitters seem to be involved in forebrain activation, although the precise mechanisms by which brain states changes ramains largely unknown (see e.g. (Saper et al., 2001; Lee and Dan,

2012) for a review).

How is the cortex desynchronized?

Synchronized states are characterized by slow-waves and UP and DOWN switching, described in previous sections. On the opposite extreme, during desynchronized states neocortical neurons tend to fire tonically although their firing rate is not necessarily higher than during the synchronized state (Steriade, 2001; Rudolph et al., 2007). During waking, periods of cortical silence can be sometimes observed in immobile inattentive animals (Petersen et al., 2003b; Luczak et al., 2009). Sleep pressure, moreover can significantly increase their appearance (Vyazovskiy et al., 2011).

Many structures and neurotransmitters seem to be deeply involved in forebrain activation or desynchronization. Cholinergic projections arising in the basal forebrain (Moruzzi and Magoun, 1949) and the brain stem pedunculopontine tegmental (PPT) nucleus and serotonergic projections arising in the raphe nucleus (Dringenberg and Vanderwolf, 1997) seem to have a privileged role. Stimulation of the Nucleus Basalis (NB) in the basal forebrain can activate the cortex (Buzsaki et al., 1988; Metherate et al., 1992; Alitto and Dan, 2012) as well as stimulation of the PPT nucleus (Sakata and Harris, 2012). Cholinergic neurons in the NB send diffuse projections throughout the neocortex and to subcortical areas such as the reticular nucleus in the thalamus (reviewed in (Lee and Dan, 2012)). Additionally, *in vitro* studies have shown that the activation of cholinergic receptors decreases the efficacy of intracortical feedback connections via muscarinic receptors (Gil et al., 1997), and an enhancement ot thalamocortical transmission via nicotinic receptors (Kawai et al., 2007). Moreover, under the presence of acetylcholine, adaptation related conductances in cortical cells decrease (McCormick and Prince, 1986; Steriade et al., 1993b). In this way these changes seem to set the cortex to be more "sensitive" to sensory inputs, minimizing the impact of the internal dynamics (Curto et al., 2009). Indeed, NB stimulation produced an enhancement in the encoding of natural images by reducing correlations among cortical neurons (Goard and Dan, 2009; Hirata and Castro-Alamancos, 2011), which might improve sensory information coding (Zohary et al., 1994).

On the other hand, electrical stimulation of the raphe nucleus, which contains serotoninergic cells, can induce desynchronization (Dringenberg and Vanderwolf, 1997). In fact, tail pinching can also induce desynchronization (Marguet and Harris, 2011) and this process is blocked by serotonin antagonists (Neuman and Thompson, 1989). Additionally, it has recently shown that noradrenergic signaling is also involved in desynchronized states since the pharmacological blockage prevents the desynchronization when the animal is awake (Constantinople and Bruno, 2011).

It has been suggested that the desynchronized states are consequence of the depolarization of cortical and thalamical cells via cholinergic inputs coming from pedunculopontine and laterodorsal tegmental nuclei which increase the voltage membrane of cortical and thalamic cells near the action potential threshold (Steriade et al., 1982), giving the thalamus a key control of the cortical state (Hirata and Castro-Alamancos, 2010; Poulet et al., 2012). Consistent with this idea, it has been

shown that local application of ACh in the thalamus is enough to activate the cortex, arguing that this could be an alternative pathway by which local microcircuits in the neocortex could be focally desynchronized given the connection specificity of the thalamocortical projections (Hirata and Castro-Alamancos, 2010). However, extensive lesion in the thalamus does not prevent cortical desynchronization (Buzsaki et al., 1988; Constantinople and Bruno, 2011). Altogether these results suggest that thalamus is not necessary but it is sufficient to desynchronize the cortex.

To summarize, although there is a large body of work on the effects of neuromodulators in the activation of the cortex and the thalamocortical loop, the relationship between neuromodulators and brain state is not completely understood.

Brain states under anesthesia

Under most anesthetics, cortical circuits usually display synchronized states. The patterns of activity might depend on the levels of anesthesia. This was shown already in the seminal work from Lord Adrian. In moderate degrees of chloroform and ether anesthesia in the cortex of rabbits, electrophysiological recordings carried with a wire electrode showed that "*...The slow waves have a characteristic frequency of 3-4 per sec. With brief waves at 25-40 per sec superimposed. In very deep anaesthesia, the 3-4 per sec. rhythm gives way to a slower beat at intervals of 1-2 sec. The super imposed brief waves are on the whole more regular and their frequency usually lies in the region of 25-30 per sec...In lighter anesthesia sensory stimulation often abolishes the rhythmic beat and substitutes a continuous train of brief waves...*" (Adrian and Matthews, 1934). It has become clear that under different anesthetics and anesthesia levels, the synchronized brain states exhibit qualitative and quantitative differences (Steriade, 2001; Erchova et al., 2002; Chauvette et al., 2011).

Under moderate levels of urethane anesthesia, cortical activity spontaneously undergoes transitions between synchronized and desynchronized states (Clement et al., 2008; Li et al., 2009; Curto et al., 2009; Sakata and Harris, 2012). Moreover, under a very tight control of the urethane dose, the state of an animal oscillates between desynchronized and synchronized states (Clement et al., 2008) in a way that very closely resembles the alternation between natural SWS and REM (Steriade, 1999). Although some computational studies have been proposed showing different possible regimes of activity across this synchronized and desynchronized axis (Bazhenov et al., 2002; Compte et al., 2003; Hill and Tononi, 2005; Wilson et al., 2005; Curto et al., 2009; Mattia and Sanchez-Vives, 2012), the fundamental mechanisms which account for brain states transitions remains largely unexplored.

Transitions between synchronized and desynchronized brain states occur in a continuum space of possible states defined by spectral properties of brain electrical signals (Gervasoni et al., 2004), and this can be observed both during natural occurring brain states and under anesthesia (Clement et al., 2008; Curto et al., 2009). Moreover — as observed by intracellular recordings— while synchronized states are dominated by UP and DOWN states dynamics, transition

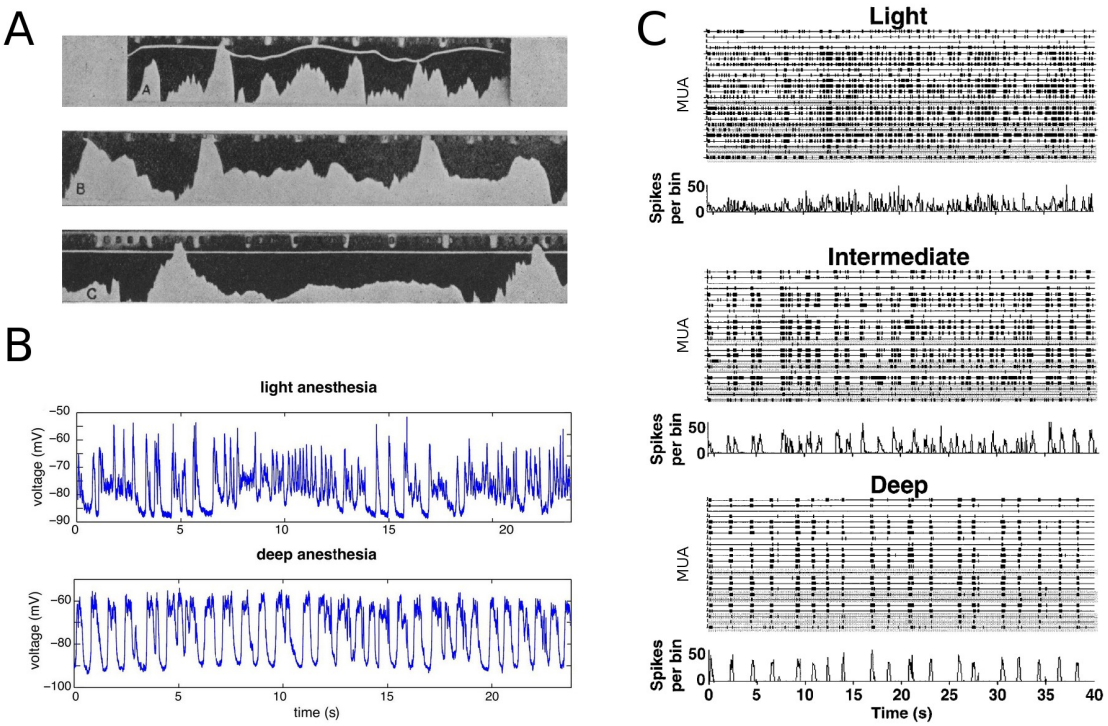

Figure 5. *Anesthesia induces synchronized states in the cortical EEG signals in dose dependent manner.* **A.** Cortical EEG recordings in urethane anesthetized rabbits: A: Moderately light, B-C: deep levels of anesthesia. White squared time markers on the film each 0.25 sec. "In deep anaesthesia the slow waves become more regular. The "brief" waves [observable in A] are just visible" (Adrian and Matthews, 1934)). **B.** Intracellular recordings in the auditory cortex of ketamine-xylazine anesthetized rats under light (top) and deep (bottom) levels of anesthesia (modified from (Deco et al., 2009a)). C. Multi single-unit recordings in somatosensory cortex of urethane anesthetized rats under different doses of anesthesia (modified from (Erchova et al., 2002)).

from synchronized towards desynchonized states are accompanied with a concomitant increase in UP period and decrease DOWN period duration. Moreover, individual neurons fire at their "preferred" brain states, so can either increase or decrease their firing rate according to different states (Steriade et al., 2001; Rudolph et al., 2007).

Understanding how these changes between states are achieved constraints the mechanisms governing the cortical activity in a particular state and could help to elucidate how brain state transitions are achieved. In Chapter 4.4 of this Thesis we will study how cortical states shapes the dynamics of UP and DOWN states in cortical circuits.

2. Objectives

1. To determine the laminar specificity of intracortical fast frequency oscillations across a cortical column during UP intervals from synchronized brain states, and to compare this laminar specificity between *in vivo* experiments and the isolated cortical circuit *in vitro*.

2. To quantify the spiking statistics of cortical populations during synchronized states *in vivo*, and to build computational models to explore the network mechanisms causing the UP and DOWN transitions observed in the experiments.

3. To determine how changes in global brain state impact the dynamics of spontaneous activity in cortical circuits and to investigate the mechanistic network basis of this variations in dynamics

3. Methods

3.1. Experimental methods

In vitro experiments [§]

[§] performed by **Daniel Jercog** and **Ramon Reig** in Sanchez-Vives Laboratory (Chapter 4.1).

In vitro slice preparation. The methods for preparing cortical slices were similar to those previously described in (Compte et al., 2008). Briefly, cortical slices were prepared from 6- to 16-month-old ferrets of either sex that were deeply anesthetized with sodium pentobarbital (40 mg/kg) and decapitated. Four hundred-micrometer-thick coronal slices of the visual cortex were cut on a vibratome. Slices were then placed in an interface-style recording chamber (Fine Sciences Tools, Foster City, CA) and bathed in ACSF containing (in mM): NaCl, 124; KCl, 2.5; $MgSO_4$, 2; $NaHPO_4$, 1.25; $CaCl_2$, 2; $NaHCO_3$, 26; and dextrose, 10, and was aerated with 95% O_2, 5% CO_2 to a final pH of 7.4. Bath temperature was maintained at 34-36°C. In order for spontaneous rhythmic activity to be generated, the solution was switched to "in vivo-like" ACSF which consists in a bathing milieu similar to that present *in viv*o, containing (in mM): NaCl, 124; KCl, 3.5; $MgSO_4$, 1; $NaHPO_4$, 1.25; $CaCl_2$, 1.2; $NaHCO_3$, 26; and dextrose, 10 (Sanchez-Vives and McCormick, 2000).

In vitro recordings. Simultaneous extracellular field potential recordings were obtained from supra (SG) and infragranular (IG) layers with 2-4 MOhm tungsten electrodes (FHC, Bowdoinham, ME) and amplified using a Neurolog system (Digitimer, UK). Electrodes positioned for SG and IG recordings were vertically aligned in order to capture columnar effects (Fig 4.3.A). Electrodes were placed in the first (for SG) and last third (for IG) of the distance from the pial surface to the white matter. The signal was recorded unfiltered (0.1Hz-10 kHz) at a sampling frequency of 10 kHz. Recordings were digitized and acquired using a data acquisition interface and software from Cambridge Electronic Design (Cambridge, UK).

Pharmacology. In a set of experiments (n=10), kainic acid (Tocris Bioscience) was applied to the cortical network by adding up the drug at increasing concentrations to the "in vivo-like" ACSF bathing solution. The action of kainic acid is not reversible and thus no "washed-up" conditions are shown.

Extracellular signals extraction. Two extracellular signals were extracted from the unfiltered extracellular recordings: one for the UP and DOWN state transitions detection and another one for the spectral analysis. In both cases, raw signals were first downsampled to 1KHz for ease of manipulation. LFP signals

for the UP and DOWN state transitions detection were obtained by band-pass filtering the extracellular signals between 10 and 300 Hz using a zero-phase lag third-order Butterworth filter. LFP signals for the spectral analysis were obtained applying the same filter configuration in the 2 to 300 Hz band. Recording length used for the analysis were approximately 300 s.

In vivo experiments

Visual cortex recordings from anesthetized ferrets [§]

[§] performed by **Marcel Ruiz-Mejias** in Sanchez-Vives Laboratory (Chapter 4.1).

Recordings were performed in 3 male ferrets 5 month old. The recordings were performed in both hemispheres. Animals were anesthetized with an intramuscular injection of a mixture of ketamine (30 mg/Kg, Imalgene 1000®, Merial) and medetomidine (1 mg/Kg, Domtor®, Orion Pharma), and were supplemented with intramuscular bolus of ¼ to ½ of the induction dose on demand. ECG and temperature (36-37ºC) were monitored continuously during the experiments. After placing the animal in the stereotaxic frame, a subcutaneous dose of atropine was given to prevent respiratory secretions (0.15 mg/Kg). A craniotomy of 2x2 mm was opened over the area spanning AP -11 to -14 mm and L 5 to 8 mm from bregma (areas 18-21, visual cortex).

Local Field Potential (LFP) recordings were obtained using vertical 16-channel silicon probes (Neuronexus®) with 100 µm of separation between recording sites and impedances ranging 0.4-1 MΩ.. The electrode was introduced perpendicularly to the cortical surface until the top electrode contact disappeared below the surface. Recordings were obtained from both hemispheres in 2 animals and from 1 hemisphere in 1 animal and were amplified with a 16-multichannel system (Multi Channel Systems®). The signal was digitized at 9.920 KHz with a CED acquisition board and Spike 2 software (Cambridge Electronic Design®). Recording length used for the analysis were approximately 300 s.

Somatosensory[¢] and auditory[¤] cortices recordings from anesthetized rats

[¢] Performed by **Peter Bartho** and **Arthur Luczak** in Kenneth Harris' Laboratory (Chapter 4.2), and **Ainhoa Hermoso Mendizabal** in de la Rocha Laboratoy (Chapter 4.4).

[¤] Performed by **Shuzo Sakata** in Sakata Laboratory (Chapter 4.4).

For detailed descriptions of surgery and recording procedures see (Barthó et al., 2004). Briefly, rats (Sprague-Dawley; 400-900 g) were anesthetized with urethane (1.3-1.6 g/kg body weight) and ketamine (25-40 mg/kg) plus additional injections of urethane (0.2 g/kg) as needed. Rats were placed in a stereotaxic frame or naso-orbital restraint, and a window in the scalp was prepared over the somatosensory or auditory cortex. A silicon microelectrode (Neuronexus technologies, Ann Arbor MI) was attached to a micromanipulator and moved gradually to its desired depth position. Probes consisted of four or eight linearly

arranged shanks with 200 μm separation between consecutive shanks. Each shank had eight recording sites arranged in a staggered configuration or in tetrode configuration (20 μm separation). Recordings were performed in deep layers of auditory and somatosensory cortices. Data from several of these animals were used in previous studies (Barthó et al., 2004; Renart et al., 2010).

Extracellular signals were high-pass filtered (1 Hz) and amplified (1,000 gain) by using a 64-channel amplifier (Sensorium, Charlotte,VT), and digitized at 25 kHz (DataMax System; RC Electronics, Santa Barbara, CA) or 20 kHz (United Electronic Industries, Inc., Canton, MA). LFP signals are obtained by high-pass filtering the raw signal either at 1000 kHz or 1250 kHz. Units were isolated by a semiautomatic algorithm (http://klustakwik.sourceforge.net) followed by manual clustering procedures (for Chapter 4.2) (http://klusters.sourceforge.net). We considered MUA as the pool of spikes from isolated units. For some experiments, LFP signals were provided as low-pass filter at 1000 Hz from the original extracellular signals.

3.2. LFP data analysis

UP and DOWN detection. Individual LFP signals were used to identify UP and DOWN state transition times for each recording site. An increase in fast fluctuations in the LFP signals is taken as a signature of an UP state occurrence (Mukovski et al., 2007; Compte et al., 2008). Following previously described methods in (Compte et al., 2008), the instantaneous amplitude (envelope) of the LFP was computed as the absolute value of the complex Hilbert transform which is smoothed with a 100 ms box- kernel. Possible slow (<0.1 Hz) linear trends – drifts the recordings – were removed and transitions were determined by thresholding the resulting signal by it's mean value. In the last set of *in vitro* experiments (kainic acid administration at 400nM, Fig. 4.1.6, 4.1.7 and 4.1.8) UP and DOWN transitions ceased in IG layers as a result of the drug application. In this case, the interval times for analysis of IG recordings were defined as those intervals defined by UP and DOWN transitions detected in the simultaneous SG recordings.

Spectral analysis. Spectral analysis was performed using Chronux software package (Bokil et al., 2010), Matlab Signal Processing Toolbox (The Mathworks, Natick, MA) and the use of in-house algorithms. Chronux built-in multitaper spectral estimation (5 tapers, unpadded configuration, time-bandwidth=3) was used to estimate frequency spectra (power spectra, time-frequency spectrum and coherence estimations). In order to have long enough time series to perform the spectral analysis in the studied range of frequencies, we used a window size of 300 ms (400 ms for *in vivo*) taken from the centre of each UP/DOWN period detected (UP/DOWN periods shorter than the window size were discarded, typically within a few percent of the total number of periods). In order to compare the spectral properties of signals obtained from different recording sites, we normalized each power spectrum by the variance of the signal. Multi-taper time-frequency spectrum

was computed over a moving window of 200 ms with a step size of 100 ms. Coherence analysis across recording sites was performed over a time-window consisting on the intersection (in time) of detected UP state epochs in both recording sites (intervals with duration below the window size for spectral analysis were discarded). Described procedure was repeated changing the window size from 200 ms up to 450 ms and changing the number of tapers from 2 to 5 (time-bandwidth=(#tapers+1)/2), obtaining analogous results.
The parameters for spectrograms calculation were the following:

Chapter	*Window/Step size (s)*	*#Tapers*	*Figure*
4.1	0.2/0.1	4	4.1.3, 4.1.6
4.2	5/3	7	4.2.1
4.4	5/3	7	4.4.1

Error bars for spectral estimation represent jackknife 95%CI.

Peaks detection in Power Spectra. For each mean power spectrum during UP states *P*, the "1/f" power spectral decay of *P* was fitted by the function $a*f^b$, where the coefficients *a* and *b* where obtained through a linear-regression of log(*P*) as a function of log(f) (Miller et al., 2009). Excess power is defined as the power ratio between the lower error band (95% CI) for *P* estimation and the power law fit $a*f^b$. Excess power was used to compare the magnitude of peaks in the power spectrum across different experiments, recording sites and different ranges of frequencies. Thus, a peak in *P* is defined by a local increment in the excess power, exceeding by at least 20% over the fitted power $a*f^b$ (i.e. excess power >1.2). The power law $a*f^b$ was fitted to *P* in the range of frequencies 5 to 105 Hz in the *in vitro* case, and 5 to 20Hz in the in vivo case (Fig 4.1.4.D). This was due to the fact that peaks in the power spectrum in vivo differ very pronouncedly from the power law fit, especially at frequencies > 20 Hz. With these choices, power law fits to our data captured the expected trend of decaying power over the frequencies of interest, as evaluated by visual inspection. Using the residuals from the *P* power-law fit, or computing the power spectra from the residual of a low-order autoregressive model of the LFP signal — a procedure known as signal pre-whitening (Mitra and Pesaran, 1999) — returned analogous results.

Statistical analysis. The significance of paired comparisons (across layers) were assessed using non-parametric Wilcoxon tests. Confidence intervals (95%) were estimated by a non-parametric jackknife procedure. Multi factorial ANOVA analysis was used to assess the significance of changes in detected peak frequency and power across layers under pharmacological manipulations of the slices (factors=layer domain, pharmacological condition (continous), slice id (random); model=interaction).

L/H ratio. Traditionally, the cortical state assessment is based on spectral properties of EEG or LFP. Synchronized states are characterized by slow high amplitude

fluctuations in the LFP signals, whereas desynchronized states are characterized by fast low amplitude fluctuations (Steriade et al., 1993b). Therefore, the power ratio between the low (0.5-4 Hz) and high (20-55 Hz) frequency bands, the L/H ratio, is high when the cortex is in a synchronized state and hence switching between UP and DOWN states occur (Li et al., 2009). To the contrary, when the cortex display low power in low frequency bands and high power in the higher frequency bands, the low/high ratio remains low in desynchronized state and switching between UP and DOWN states are rarely observed. Thus, for each shank we randomly choose the LFP signal from one channel and compute the L/H ratio in non-overlapping windows of 20 sec as the ratio of mean power in (low) 0.5-4 Hz band and mean power in (high) 20-55 Hz band as previously described (Curto et al., 2009; Li et al., 2009).

3.3. MUA data analysis

Silence density. Another way of characterizing the cortical state is by taking into account the spiking activity of individual neurons from a local population (Renart et al., 2010). Even though during UP states individual neurons might fire only a few action potentials, pooling the spiking activity of many individual neurons in the multi-unit activity can reveal the presence of co-fluctuations in the firing activity of the individual neurons. Given that the presence of DOWN state is characterized by quiescent activity in cortical networks (Steriade et al., 1993a), we can also assess the activation level based on the MUA activity by quantifying the Silence density of 20 ms bins with the absence of spikes in the MUA in 20 sec windows (Renart et al., 2010). The mean and standard deviation of the silence density is computed in 50 seconds windows. For data analyzed in Chapter 4.2, periods with mean silence density above 0.5 and standard deviation below 0.1 were considered as sustained synchronized. For last section of Chapter 4.4, in order to compare silence density values across experiments, the window-size to compute the silence density was defined as 5 times the mean inter-spike interval from the MUA.

UP and DOWN detection. We used a hidden semi-Markov probabilistic model to infer a discrete two-state process based on the MUA observation, proposed by (Chen et al., 2009). The simultaneously recorded spike trains are considered as a single stochastic point processes that is modulated by the discrete hidden state and the firing history of the ensemble of neurons recorded. In order to estimate the hidden state and the unknown parameters of the probabilistic models, the method uses the expectation maximization (EM) algorithm for the parameter estimation. Although the discrete-time HMM provides a reasonable state estimate with a rather fast computing speed, the model is restricted to locate the UP and DOWN transition with a certain time bin size (10 ms in our case). The initial parameters that we use for the UP and DOWN detection in our model are the following:

T (bin-size, error in transition detection)	10 ms
μ	-2
α	2
J (# history bins; *J*=0 for Markov process)	1
β (history-dependance weight; β=0 for Markov process)	0.01
P (transition matrix,0 DOWN 1 UP)	$P_{01}=P_{10}=0.9$
	$P_{00}=P_{11}=0.1$

An example of the detection is shown in Fig. M1. MUA spike-count (MUAc) is computed in 20 ms sliding windows of 5ms steps (Fig M1B, gray bars). An expectation-maximization algorithm (a statistical inference algorithm within the maximum likelihood estimation framework) is used for the estimation of model's parameters. Finally, the probability of being in an UP state is assessed by the output of the Viterbi algorithm (Fig M1B, green trace).

About the UP and DOWN intervals detection methods. Many methods for the detection of UP and DOWN transitions have been designed based on intracellular (Stern et al., 1997; Volgushev et al., 2006; Haider et al., 2006; Seamari et al., 2007), LFP (Amzica and Steriade, 1995b; Mukovski et al., 2007; Compte et al., 2008; McFarland et al., 2011), MUA (Luczak et al., 2007; Hasenstaub et al., 2007; Sanchez-Vives et al., 2010) or a combination of these signals (Saleem et al., 2010). These methods are typically "threshold-based", which means that a transition is determined when a threshold is crossed. The pattern of transitions depends therefore

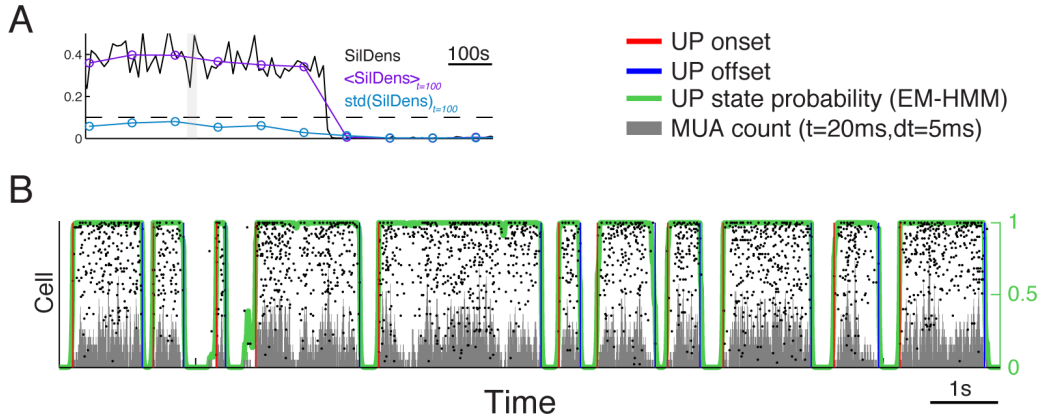

Figure M1. Example of UP and DOWN transitions detections. **A.** Cortical state assessment by silence density (black trace). Mean and standard deviation of the silence density are shown in violet and turquoise traces, respectively. **B.** Hidden Markov Model (HMM) based detection (from Chen et al 2009). Raster plots of the pooled detected units is shown (each row represent one cell and each dot represent a spike from that particular cell). MUA spike-count (MUAc) is computed in 20 ms sliding windows (5ms steps) and normalized for displaying purposes (in gray). Probability of being in an UP state is computed by the Viterbi algorithm and shown in green. Finally, DOWN-TO-UP and UP-to-DOWN transitions are indicated by red and blue vertical lines respectively.

on the value of the threshold which is a priori arbitrary. For this reason the method requires of an independent assesment of the detection errors to optimize the threshold value or of independent arguments to set it (e.g. at the trough of the bimodality found in the voltage membrane histogram). Moreover, given that brain signals exhibit in general large fluctuations, threshold crossings can be caused by a state transition or by a random fluctutation. A common procedure used to distinguish these two has been to assume that fluctuations are short lived and produced much shorter intervals than "real" UP/DOWN intervals, which are merged to the surrounding intervals. It must be noticed however, that imposing a lower cutoff in the duration of UP and DOWN intervals can also modify the distribution of durations and decrease for instance the coefficients of variation CV(U) and CV(D). More recent approaches to detection of transitions consider hidden Markov probabilistic models to infer a two-state (UP/DOWN) process based on the LFP (McFarland et al., 2011; Hahn et al., 2012) or MUA (Chen et al., 2009). This provides a more principled framework than setting a particular threshold and, moreover, better accommodates to non-stationarities of the data (McFarland et al., 2011). We used tthe detection method proposed by (Chen et al., 2009), which might be another cause of the differences with previous reports on UP/DOWN duration variability. However, although we did not merge or discard short UP or DOWN intervals , the large duration variability that we reported here might be more influenced by the long tail in the UP/DOWN duration distributions than by the presence of the short intervals. Moreover, we observed coefficients of variation of D and U close to those reported by intracellular studies in a similar preparation where threshold-based methods were used (Stern et al., 1997). Therefore, we discard the possibility that interval duration statistics reported here are an artifact of the detection method.

Spike trains statistics

We first divide the time in bins of dt=1 ms and define the spike train if the j-th neuron as:

$$s_j(t)=\begin{cases}1 & if\ there\ is\ a\ spike\in(t,t+dt)\\ 0 & otherwise\end{cases} \quad (1)$$

The ***spike count*** of the j-th neuron over a the time window (t-T/2, t+T/2) is obtained

$$n_j(t;T)=(K*s_j)(t) \quad (2)$$

where * refers to a discrete convolution and K(t) is a square kernel which equals one in (-T/2,T/2) and zero otherwise.

The instantaneous ***population count*** is defined as the sum over all neurons of the individual spike counts $n_j(t;T)$:

$$PC(t;T)=\sum_{i=1}^{N} n_j(t;T) \quad (3)$$

where N is the total number of well isolated and simultaneously recorded neurons. The ***instantaneous rate*** of the *j*-th neuron and the ***instantaneous population rate*** are defined as

$$r_i(t)=\frac{n_i(t;T)}{T}$$
$$R(t)=\frac{PC(t;T)}{T\,N} \tag{4}$$

where we have dropped the dependence on T from $r_i(t)$ and R(t) to ease the notation. We also defined the instantaneous E-population and I-populations rates, $R^E(t)$ and $R^I(t)$ respectively, as those based in the population count of E-cells and I-cells separately.

Statistics of U and D durations

We generally used *onset* and *offset* referring to the onset and offset of UP intervals. The time series $\{t_i^{on}\}_{i=1}^{M}$ contains to the onset times and $\{t_i^{off}\}_{i=1}^{M}$ the offset times of the putative UP intervals detected and M being the total number of intervals. We define the ***i-th putative UP and DOWN intervals*** as (see Fig. 4.4.1)

$$U_i=t_i^{off}-t_i^{on}$$
$$D_i=t_{i+1}^{on}-t_i^{off} \tag{5}$$

The mean and the coefficient of variation of U_i are defined as

$$\langle U_i\rangle=\frac{1}{M}\sum_{i=1}^{M}U_i$$
$$CV(U_i)=\frac{\sqrt{Var(U_i)}}{\langle U_i\rangle} \tag{6}$$

and equivalently for $\langle D_i\rangle$ and $CV(D_i)$. The serial correlation between U_i and the consecutive D_i is quantified with the Pearson correlation coefficient defined as:

$$Corr(U_i,D_i)=\frac{Cov(U_i,D_i)}{\sqrt{Var(U_i)Var(D_i)}} \tag{7}$$

where the covariance is defined as:

$$Cov(U_i,D_i)=\frac{1}{M}\sum_{i=1}^{M}(U_i-\langle U_i\rangle)(D_i-\langle D_i\rangle) \tag{8}$$

The correlation between D_i and U_{i+1} (i.e. the DOWN interval and its following UP interval) named $Corr(D_i,U_{i+1})$ was defined equivalently. To remove correlations between U_i and D_i produced by slow covariation of the durations, for instance as those observed during drift in the synchronization state level (Fig. 4.4.2 in Chapter 4.4), we subtracted from the $Cov(U_i,D_i)$ the covariance obtained from a surrogate U and D series obtained from the original by shuffling the values $\{U_i\}_{i=1}^{M}$. Specifically, we defined the *k*-th shuffled series of UP intervals as $\{u_i^k\}_{i=1}^{M}$ as the one obtained by randomly shuffling the order of the Us over

intervals of 10 seconds. The same was done to define the shuffled series $\{d_i^k\}_{i=1}^M$. Because the shuffled was done over 10 second intervals the two series lack any correlation except that introduced by slow co-variations in the statistics (i.e. slower than 10 seconds). We generated S=100 independent shuffled series $\{u_i^k\}_{i=1}^M$ and $\{d_i^k\}_{i=1}^M$ with k =1, ...S, computed the covariance $Cov(u_i^k, d_i^k)$ for each and the averaged over all of them to obtain $Cov(u_i, d_i)=\langle Cov(u_i^k, d_i^k)\rangle_k$. Finally we replaced the covariance in equation 7 by the difference , that is we subtracted the correlations solely due to slow co-variations in the statistics of UP and DOWN periods.

Population firing statistics during Us and Ds

We next defined the average and variance across the onset and offset times of UP intervals. Specifically, given the onset times series $\{t_i^{on}\}_{i=1}^M$ the ***averaged population rate aligned at the onset*** is defined as:

$$R_{on}(t)=\langle R(t)\rangle_{on}=\frac{1}{M}\sum_{t'\in\{t_i^{on}\}} R(t-t') \qquad (9)$$

where the population rate R(t) has been aligned to the onset times as described in Fig. 4.4.4 in Chapter 2. More importantly, the brackets $\langle x(t)\rangle_{on}$ implies the average across UP intervals lasting longer than t, that is the sum in equation 9 runs over $t'\in\{t_i^{on}\}$ only if $(t-t_i^{on})<U_i$. By doing this we remove the trivial decay we would observe in $R_{on}(t)$ as t increases due to the increasing probability to transition into a the consecutive DOWN interval. The average population rate aligned at the offset $R_{off}(t)$ is defined equivalently by replacing $\{t_i^{on}\}_{i=1}^M$ by the series of offset times $\{t_i^{off}\}_{i=1}^M$. We also defined the onset and offset-aligned averaged population rate for excitatory (E) and inhibitory (I) populations, termed $R_{on}^E(t)$ and $R_{off}^E(t)$ for the E case and similarly for the I case.

We also computed the instantaneous second order statistics of the firing activity across putative UP intervals aligned both at the onset and offset. The instantaneous Fano factor of the population spike count $PC(t;T)$ aligned at the U onset was defined as

$$FP_{on}(t;T)=\frac{Var\left(PC(t;T)\right)_{on}}{\langle PC(t;T)\rangle_{on}} \qquad (10)$$

where the variance and the mean are taken across the onset times $\{t_i^{on}\}_{i=1}^M$ as describe in equation 9. The offset-aligned Fano factor $FP_{off}(t;T)$ was obtained equivalently by using the offset times $\{t_i^{off}\}_{i=1}^M$.

The autocorrelogram of the instantaneous population rate is defined as:

$$A(\tau)=\frac{1}{L}\sum_{t=1}^{L} R(t)R(t+\tau)-\langle R(t)\rangle_t^2 \qquad (11)$$

with the sum in t running over the L time bins of the entire period of data analysed (e.g. a ~ 10 min period). The brackets $\langle\cdot\rangle_t$ define an average over time. The autocorrelogram shown in Figure 4.2.3 in Chapter 4.2 was normalized by the value at lag zero $A(\tau=0)$.

Power spectrum of population rate R(t). The power spectrum of the instantaneous population rate R(t) was computed using the Chronux software package (Bokil et al., 2010). Chronux built-in multitaper average spectral estimation (21 tapers, unpadded configuration, time-bandwidth=11) was performed over non-overlapping windows of 60 s. 95% CI error bars are estimated via jackknife procedure.

Individual Neuron firing statistics during Us and Ds

We defined the spike count of the *j*-th neuron during the interval U_i as

$$n_j(U_i)=\sum_{t'\in U_i} s_j(t') \tag{12}$$

and the average firing rate of the *j*-th neuron across U intervals as:

$$r_j^U=\frac{1}{M}\sum_i \frac{n_j(U_i)}{U_i} \tag{13}$$

The average firing rate across D intervals r^D_j was defined equivalently.

As defined above using the population rate (equation 9) we now define the average single neuron rate across the onset and offset times of UP intervals. Specifically, given the onset times series $\{t_i^{on}\}_{i=1}^M$ the ***averaged rate of the j-th neuron aligned at the onset*** is defined as:

$$r_{j,on}(t)=\langle r_j(t)\rangle_{on}=\frac{1}{M}\sum_{t'\in\{t_i^{on}\}} r_j(t-t') \tag{14}$$

We defined the individual Fano factor of the *j*-th neuron spike count $n_i(t;T)$ as

$$FF_{j,on}(t;T)=\frac{Var\left(n_j(t;T)\right)_{on}}{\langle n_j(t;T)\rangle_{on}} \tag{15}$$

and generally show the average of $FF_{i,on}(t;T)$ across neurons

$$FF_{on}(t;T)=\frac{1}{N}\sum_j F_{j,on}(t;T) \tag{16}$$

The instantaneous correlation between the spike counts from cells i and j aligned at the onset was defined as

$$Corr_{ij,on}(t;T)=\frac{Cov\left(n_i(t;T),n_j(t;T)\right)_{on}}{\sqrt{Var\left(n_i(t;T)\right)_{on}Var\left(n_j(t;T)\right)_{on}}} \tag{17}$$

where both the covariance and the variances of the spike counts are obtained across the onset times of UP intervals as shown in equation 9. We generally show the average spike count correlations across neuronal pairs defined as

$$Corr_{on}(t;T)=\frac{1}{N(N-1)}\sum_{i\neq j} Corr_{ij,on}(t;T) \qquad (18)$$

The statistics $r_{j,off}(t)$, $F_{j,off}(t;T)$ and $Corr_{ij,off}(t;T)$ aligned at the U offset, are computed equivalently to equations 14, 15 and 17 but replacing the onset times with the offset times $\{t_i^{off}\}_{i=1}^{M}$

Putative E/I neuronal classification.

Isolated units were classified into putative E or I based on three parameters extracted from their mean spike waveforms (see Fig. 4.2.9A top), grouped into two classes by k-means clustering. Each dot represents a single unit. Putative Is were characterized by narrower spike waveforms and relatively higher asymmetry index. Putative Es were characterized by wider spike waveforms and relatively smaller asymmetry index. Previous studies suggest that the narrow-spiking and wide-spiking cells may correspond primarily to inhibitory INs and excitatory PCs, respectively (Csicsvari et al., 1998; Barthó et al., 2004; Sirota et al., 2008).

3.4. Model data analysis

Simulation details.

Chapter 4.3 Network parameters. The parameters for the network used for the simulations are described in the following table, and changes in parameters for different figures are denoted in the caption of the respective figure.

α_E=1, α_I=4, ω_E=5, ω_I=25,	*transfer function*
J_{EE}=5, J_{EI}=1, J_{iE}=10, J_{II}=0.5,	*connectivity*
θ_E=0, θ_I=0,	*main input to each pop*
τ_E=10, τ_I=2, τ_E=500, τ_N=1,	*time constants*
σ=0	*amplitude of fluctuations*

Chapter 4.4 Network parameters. Parameters are described at Fig. 4.4.6 caption.

Stochastic fluctuations. Stochastic fluctuations were modeled by an Ornstein–Uhlenbeck process, which was computed in the exact form numerically following the methods described (Gillespie, 1996).

Numerical simulation of the differential equations were performed using 4th order Runge-Kutta methods (*dt*):

- Integration step dt=0.1
- Length of each simulation=100000 *dt*

For Fig. 4.3.6, each point from the color plot was generated by 50 simulations.

All simulations were performed by in-house algorithms coded in C++/ MeX and Matlab (The Mathworks, Natick, MA).

Analysis of simulations.

UD detection. U and D intervals were defined by threshold-based detection method (threshold on r_E=1). Intervals with duration less than 50dt were merged with neighboring intervals. We didn't used the HMM detection method used in Chapter 4.2 given that the complexity of the method turns it prohibitive to analyze long numerical simulations.

Fano Factor and correlations in the rate model. In order to compare the results obtained from our rate model with the statistics of the spike counts obtained in the data, we extended the rate model and assumed a two-stage model consisting in two populations of E and I neurons firing inhomogeneous and independent Poisson spike trains with rate given by the trajectories of r_E(t) and r_I(t) defined by equations 1.1 and 1.2 from Chapter 4.3. Notice that the neurons in each population are independent *conditioned* on the trajectories r_E(t) and r_I(t), but because this trajectories are stochastic spike trains from two neurons will show correlations. This model can be interpreted as a double stochastic Poisson process since the rate follows a stochastic differential equation (Eq. 1.1 and 1.2, Chapter 4.3) and the spike trains are stochastically generated from the rate trajectories. The spike count statistics of this model can be computed given the ensemble of rate trajectories during Us (obtained numerically from simulations of the system Eq. Eq. 1.1 and 1.2, Chapter 4.3) without the need of generating the Poisson spike trains because the expectation with respect to the ensemble of spike trains can be analytically expressed. The average spike count $n_i(t;T)$ across Us of the *i*-th E-cell is defined as:

$$\langle n_i(t;T)\rangle = \int_t^{t+T} \langle r_E(s)\rangle\, ds \qquad (19)$$

where we have replaced the integral of r_E(t), i.e. the filtered rate with a Heavie side function of width T, with R_E(t). The brackets $\langle\cdot\rangle$ refer to an average across Us and can be defined both aligned at the onset or offset as defined above (Eq. 14). Here we omit the notation referring to the alignment for brevity. For simplicity, we define the statistics of E-cells but the definitions are the same for the I-cells. The variance of the spike count $n_i(t;T)$ can be decomposed by the law of the total variance in (Shadlen and Newsome, 1998b; Churchland et al., 2011)

$$Var\left(n_i(t;T)\right)=Var\left(\langle n_i(t;T)|r_E(t)\rangle\right)+\langle Var\left(n_i(t;T)|r_E(t)\right)\rangle \qquad (20)$$

In the first term in the r.h.s., called the variance of the conditional expectation, the variance is taken across the ensemble of rate trajectories r_E(t) whereas the brackets $\langle\cdot\rangle$ refer to the ensemble of spike trains at fixed r_E(t) . In the second term of the r.h.s. the variance is taken with respect to the ensemble of spike trains whereas the brackets $\langle\cdot\rangle$ refer to the ensemble of rate trajectories r_E(t). Thus the first term acounts for the variability of the rates (i.e. it would be zero if the rate trajectories are the same in every U) whereas the second accounts for the variability associated to the realization of the spike trains (i.e. it is always larger than zero unless the rate is zero). Since a the variance of the count of a Poisson process equals its mean:

$$\langle Var\left(n_i(t;T)|r_E(t)\right)\rangle=\langle R_E(t)\rangle \qquad (21)$$

The variance of the conditional expectation $Var\left(\langle n_i(t;T)|r_E(t)\rangle\right)$ can be simply expressed as

$$Var\left(\langle n_i(t;T)|r_E(t)\rangle\right)=Var\left(R_E(t)\right) \qquad (22)$$

Putting all these expression together, the Fano factor of the spike count can be expressed as:

$$FF\left(n_i(t;T)\right)=\frac{Var\left(R_E(t)\right)+\langle R_E(t)\rangle}{\langle R_E(t)\rangle} \qquad (23)$$

Both the mean and the variance of R_E(t) were computed numerically from the simulations.

Using the *law of the total covariance* the covariance of two spike counts from the E population can be decomposed in:

$$Cov\left(n_i(t;T),n_j(t;T)\right)=Cov\left(\langle n_i(t;T)|r_E(t)\rangle,\langle n_j(t;T)|r_E(t)\rangle\right)+\langle Cov\left(n_i(t;T),n_i(t;T)|r_E(t)\right)\rangle \qquad (24)$$

Because by definition the spike trains are *conditionally independent,* the second term of the r.h.s. is zero. The first term in the r.h.s. due to the Poisson statistics of the spike trains can be expressed as:

$$Cov\left(n_i(t;T),n_i(t;T)\right)=Var\left(R_E(t)\right) \qquad (25)$$

whereas if the two neurons where from the E and I population the covariance reads,

$$Cov\left(n_i(t;T), n_i(t;T)\right) = Cov\left(R_E(t), R_I(t)\right) \tag{26}$$

Using the expression of the variance derived above (equations 20-22) we can expressed the spike count correlation coefficient as:

$$Corr\left(n_i(t;T), n_j(t;T)\right) = \frac{Var\left(R_E(t)\right)}{Var\left(R_E(t)\right) + \langle R_E(t)\rangle} \tag{27}$$

for pairs within the E population and

$$Corr\left(n_i(t;T), n_j(t;T)\right) = \frac{Cov\left(R_E(t), R_I(t)\right)}{\sqrt{\left(Var\left(R_E(t)\right) + \langle R_E(t)\rangle\right)\left(Var\left(R_I(t)\right) + \langle R_I(t)\rangle\right)}} \tag{28}$$

4. Results

4.1. Laminar profile of fast oscillations during UP states

The microcircuit of cortical columns is defined by specific feedforward and feedback connections between layers. As a result, laminar patterns of activation can differ depending on the activation of incoming inputs or neuromodulation, for example, during evoked sensory responses and spontaneous activity. Neocortical fast oscillations (10-100Hz) occur not only during awareness, but also during UP states in synchronized network states characteristic of anesthesia and natural slow-wave sleep. In this chapter we studied the intracortical synchronization of activity across layers of the cortical column during such synchronized states *in vivo*, and we compared it with analogous synchronized states in the isolated cortical circuit *in vitro*. First, we observed the existence of compartmentalization of fast oscillations during UP states from existing *in vivo* laminar recordings in anesthetized animals. Then, we compared those fast oscillations to the ones observed during UP states of slow-oscillation *in vitro*, which exhibited laminar differences. By doing pharmacology manipulations *in vitro*, we showed that an increase of the isolated network excitability can control inter-laminar couplings and oscillatory dynamics in cortical circuits, leading to a similar laminar profile of fast oscillations as observed in the *in vivo* condition.

Fast oscillations during UP states are compartmentalized in SG and IG

We investigated the laminar profile of fast oscillations (10-100 Hz) during spontaneous UP states in the visual cortex *in vivo* analyzing existing multilaminar LFP recordings (16 electrodes, 100μm inter-electrode distance) in the visual cortex of ketamine-anesthetized ferrets[1] (n=3 animals). The recordings were obtained from both hemispheres (in total 1 hemisphere was damaged during the craneotomy procedure and 1 recording showed drift, consequently both recordings were discarded for further analysis). In order to compare results across different experiments, unfiltered LFP signals were used to assess by visual inspection the location of the phase reversal from the LFP which is produced near the limit between layers IV and V (Buzsaki et al., 1988; Chauvette et al., 2010). Signal reversion was found around channels 7/8 in the 4 experiments analyzed (Fig. 4.1.1A, marked with an asterisk). For each recording channel we independently identified the transition times between UP and DOWN states based on the LFP signals (Compte et al., 2008). In the example shown in Fig. 4.1.1A, the detected UP state onset/offset periods are marked with magenta/black circles, respectively, where

1 Experiments performed by Marcel Ruiz-Mejias from Sanchez-Vives Lab.

the inter UP state periods define the DOWN states.

It has recently been reported that signals recorded from SG and IG layers in

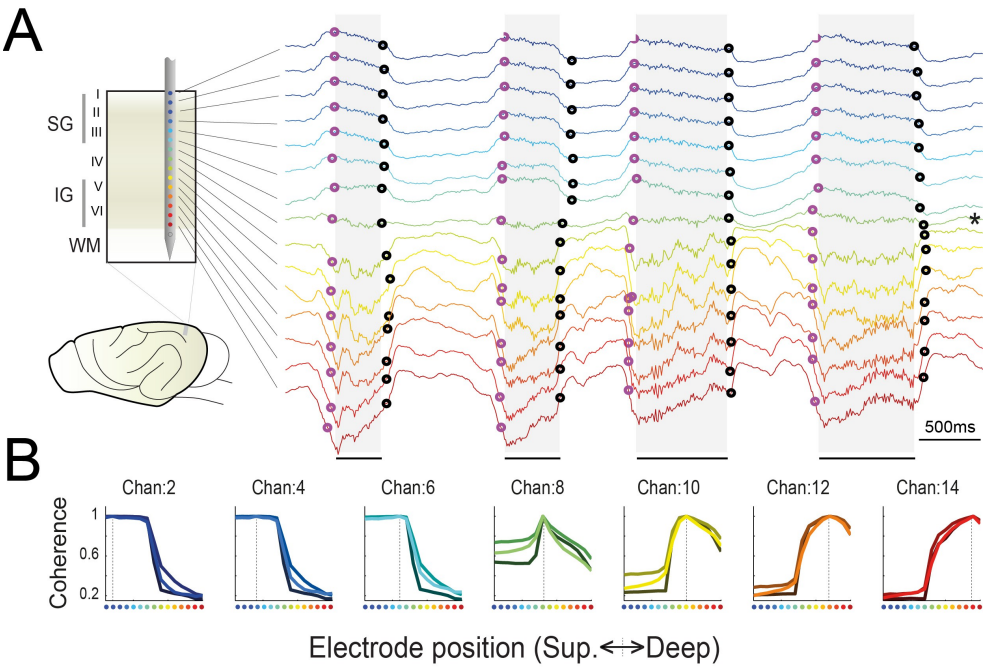

Figure 4.1.1. Laminar recording of spontaneous activity in anesthetized animals shows compartmentalization of fast oscillations in supragranular (SG) and infragranular (IG) visual cortex *in vivo*. *A*, On the left, a schematic illustration of the *in vivo* experimental setup. On the right, an example of laminar LFP data traces. For each signal, UP states are detected (onset in magenta circles, offset in black circles) while DOWN states are defined as inter-UP states intervals. Location of the slow-oscillation phase reversion is marked with an asterisk and is used to compare the results across experiments. ***B***, For the example showed in A and for different reference channels (on top of each panel), mean coherence during UP states between reference and the rest of channels (in the x-axis, same color code as in A). Traces represent the coherence for different bands: light = beta band, intermediate = low gamma, dark = high gamma. Note that signals coming from the same laminar zone (SG/IG) are more coherent within themselves that with signals from other zones. These compartments are separated around channel 8, which corresponds to the identified location of the slow-wave phase reversion.

the visual cortex of monkeys show different spectral signatures, revealing two separate functional domains: LFP signals within each laminar domain (SG/IG) are highly coherent, whereas those across laminar domains are not, both during visual stimulation and rest (Maier et al., 2010)). Similarly, we sought to assess the degree of synchronization across layers during UP states by means of signal coherence to study functional domains in the anesthetized ferret cortex. The independent detection of an UP state in the SG with respect to the IG layer might be shifted in time given that UP states *in vivo* have been observed to predominantly originate in layer 5 and then spread towards superficial layers ((Sanchez-Vives and McCormick, 2000; Sakata and Harris, 2009). For this reason, the coherence analysis was performed over time-windows consisting of the intersections (in time) of detected UP state epochs in all channels (Fig. 4.1.1A, black horizontal lines). For each channel, we computed the mean coherence from this reference channel with the rest

of the channels during UP state intersection intervals (Fig. 4.1.1B). We computed the mean coherence for beta (10-30Hz, Fig. 4.1.1B light traces), low-gamma (30-60Hz, Fig. 4.1.1B mid-dark traces) and high-gamma (60-100Hz, Fig. 4.1.1B dark traces) frequency bands. In 3 out of 5 experiments a clear compartmentalization in SG and IG domains for fast oscillations during spontaneous activity was observed, consisting on high levels of coherence between electrodes from different domains and low levels of coherence between electrodes from different domains. The limit between those compartments coincided with the channel in which slow oscillation phase reversion was detected (eg, channel 8 in Fig. 4.1.1). Thus, the anesthetized cortex of the ferret presents similar functional compartmentalization in SG and IG domains than the visual cortex of the monkey during visual stimulation and at rest, suggesting that this is a general principle of the activation of cortical circuits across species. We next tried to evaluate if, in addition to independent coherence in fast oscillations in the two laminar domains, distinct patterns of fast oscillations characterized SG and IG domains.

A substantial increment in the power of fast frequency fluctuations was present during the UP states compared to the DOWN states. Since we wanted to compare the spectral component of the signals disregarding gain effects, we normalized each computed power spectrum by the variance of the signal during the considered period. To compare the spectral components during UP and DOWN states, we computed the power spectrum of the normalized signal separately for UP and DOWN states. Although power spectra profiles during DOWN states were quite similar, power spectra profiles during UP states differed for different recording sites (Fig. 4.1.2A, error bars displays 95% CI). In order to compute the coherence between SG and IG during UP states intersections, we selected two SG and two IG channels at least 300 microns away from where the phase reversion of the LFP was identified. We computed the coherence between SG-IG pairs (Fig. 4.1.2B, black traces) and the average coherence across those pairs (Fig. 4.1.2.B, red trace), showing a broad band effect which was also observable in the rest of the experiments (Fig. 4.1.2D). In Fig. 4.1.2C from the different *in vivo* experiments, we show the power spectra during UP states for all different channels vertically displaced for displaying purposes (black power spectra corresponds to the slow oscillation phase reversion location). In all the experiments, strong oscillations ranging from 45 to 55 Hz were observed in IG and SG determined as peaks in the power spectral densities, while SG also displayed an oscillation at ~30 Hz that was not present in IG in 3 out of 4 cases (Fig. 4.1.2C). These results suggest that in the anesthetized visual cortex of ferrets, SG and IG display fast oscillations and the low coherence of those oscillations observed across both laminar domains (compartmentalization) suggests that are independently generated. Moreover, gamma oscillations are strong in both domains, while slower beta oscillations, if present, are dominant on SG.

Fast oscillations in vitro are enhanced during UP states in SG and IG

Next, we wanted to compare our observations in the anesthetized ferret

cortex *in vivo* with circuit activations in ferret cortical slices *in vitro*. We performed extracellular recordings from SG and IG layers on active slices of ferret visual cortex[2] (n=55). Slices became spontaneously active after switching from regular ACSF to an "*in vivo* like" ACSF consisting in a bathing milieu with ionic concentrations similar to that present *in vivo* (see Methods, section 3.1), where slow rhythmic activity with alternating UP and DOWN states emerged, as previously

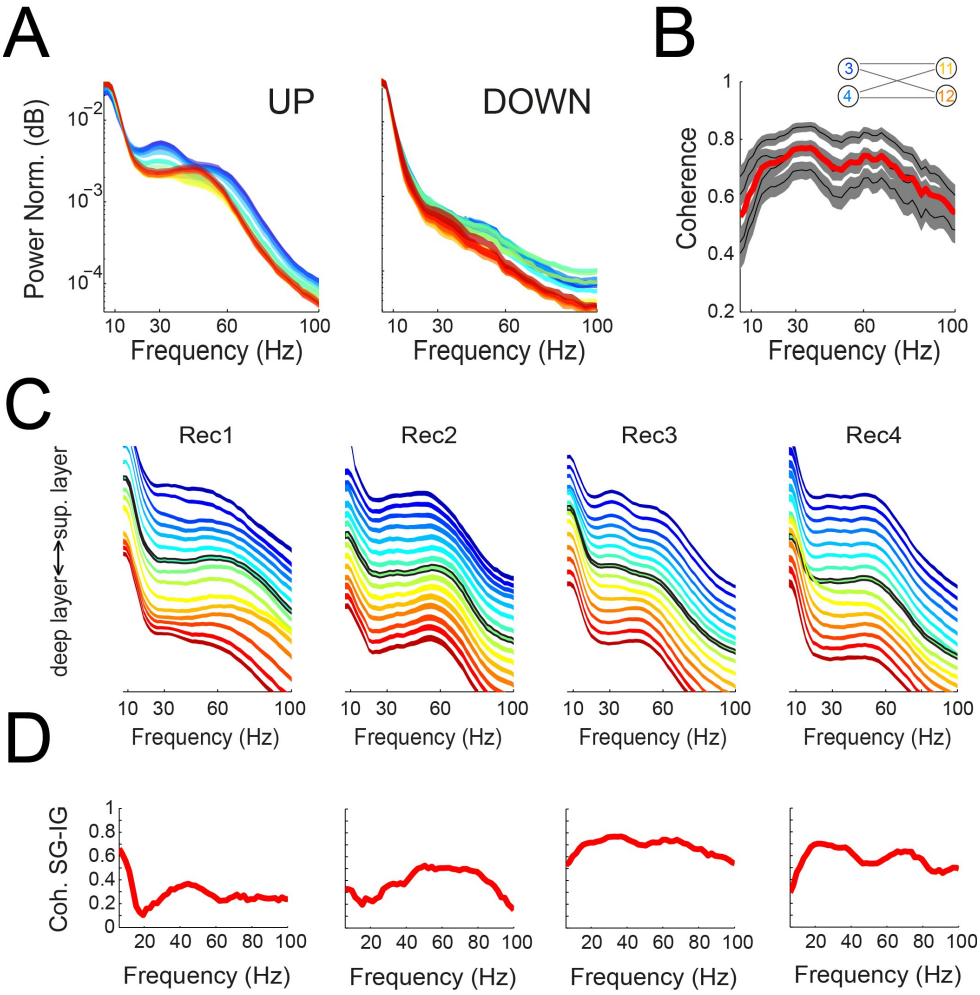

Figure 4.1.2. Laminar profile of fast oscillations during UP states *in vivo* (n=4). **A**, Mean power spectrum during UP states (left) and DOWN states (right) for different channels. **B**, Coherence between different SG and IG channels shown by black traces. Mean coherence shown in red. **C**, Power spectra for different recordings, vertically displaced for displaying purposes. Power spectrum corresponding to the channel where slow-oscillation phase reversion is identified in black. **D,** Mean coherence values as a function of frequency (as in panel B, red trace) for the different experiments.

described (Sanchez-Vives and McCormick, 2000). We recorded the activity simultaneously from SG and IG with two extracellular electrodes, which represent signals from the SG and IG compartments (Fig. 4.1.3A, left). We independently identified periods of transitions between UP and DOWN states as in the *in vivo*

2 Experiments performed by Daniel Jercog and Ramon Reig in Sanchez-Vives Lab.

condition (Fig. 4.1.3A, right).

In both SG and IG recording sites, an increase in the power of signal fluctuations is observed over the beta/gamma range of frequencies (10Hz to 100Hz) during UP states when compared to the DOWN states (Fig. 4.1.3B). However,

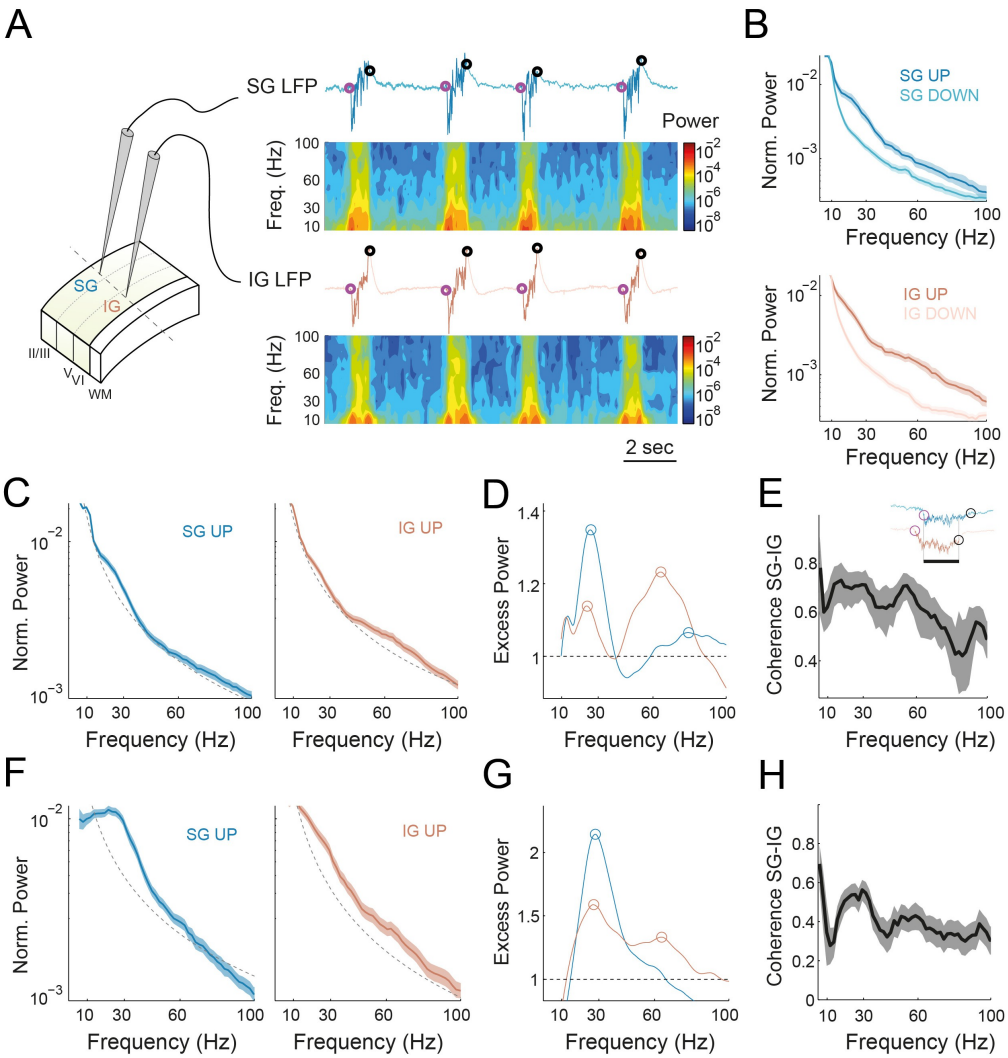

Figure 4.1.3. Fast oscillations during UP states are present in supra-granular (SG) and infra-granular (IG) layers of visual cortex *in vitro*. ***A,*** Schematic illustration of the *in vitro* experimental setup. Example of LFP data traces and spectrograms for SG (top) and IG (bottom), shown for simultaneous UP states are detected (onset in magenta circles, offset in black circles) independently for each signal, while DOWN states are defined as inter-UP states intervals. ***B,*** Mean normalized power spectrum during UP and DOWN states epochs for SG (top) and IG (bottom) recordings. ***C,*** Fit of the "1/f" decay of the power during UP states for each spectrum (dashed gray; SG left, IG right). **D,** Ratio between the power during UP states and the "1/f"-fit, in order to amplify spectral peaks (showed in circles). ***E,*** Mean coherence between SG and IG LFP signals during all UP state intersection periods (defined in the inset). Panels ***F***,***G*** and ***H*** exhibit the results for another example. Jackknife error bars showing 95% CI.

we found that the average power spectra during UP sates in SG and IG layers differed (Fig. 4.1.3C). In the particular example shown in Fig. 4.1.3C, SG shows a weak and broad increase in power spectrum over the "*1/f*" decay for frequencies around ~20 Hz, while IG in addition shows a weak broad peak at ~60Hz. In order to quantify this effect, for each average power spectrum we computed the ratio between the average power spectrum and the a/f^b least square fit in the range of frequencies studied, 10-100Hz (Fig. 4.1.3C, dashed lines represent the fit). Computing the ratio of the lower error bar of the power during UP and the "*1/f*" fit, a measure that we call "excess power", led to amplification of the peaks in the power spectra by removing the power law decay on the power spectral densities from LFPs. We refer to a peak in the power spectra if the local maximum of the excess power was above 1.5 STD of the excess power. In this example, excess power revealed peaks in SG at ~26 Hz and ~79 Hz while IG showed peaks at ~24 Hz and ~64 Hz (Fig. 4.1.3D). We also computed the power spectra from the residual of a low-order autoregressive model of the LFP signal, a process known as signal pre-whitening (Mitra and Pesaran, 1999), which returned analogous results.

In order to assess the degree of synchronization of SG and IG layers during UP states we used signal coherence. As in the *in vivo* condition, UP states *in vitro* also originate in IG and then spread towards superficial layers, although the peak of activity in both domains is reached at the same time (Sanchez-Vives and McCormick, 2000). Coherence analysis was performed over the intersection (in time) of detected UP state epochs in IG and SG LFP. Significant levels of coherency were found over a broad range of frequencies, showing maximal values between 10 and 30 Hz that revealed strong broad-band coherency between signals recorded in the two layers (Fig. 4.1.3E). Figures 4.1.3F, 4.1.3G and 4.1.3H show results obtained for another example recording. Peaks in the power spectra were detected at ~28 Hz in both IG and SG, and at ~64 Hz for IG. Typically, the strongest peaks in the power spectra *in vitro* were observed in SG.

Beta oscillations dominate SG while gamma oscillations dominate IG in vitro

When we computed the mean power spectrum during UP states from SG and IG layers, pooled across experiments, SG showed significant more power on LFP fluctuations for the beta band (10-30Hz) than IG,while gamma frequencies in IG displayed significant more power on fluctuations than SG (Fig. 4.1.4A, non overlapping error bars showing 95% CI).

To quantify possible differences between SG and IG recordings on the power of fast signal fluctuations across different frequency bands, we computed the mean relative area under the power spectra for beta (10-30Hz), low-gamma (30-60Hz) and high-gamma (60-100Hz) frequency bands for pairs of SG and IG recordings obtained from the same column. For SG layers, beta frequencies showed a higher contribution to total spectral power, whereas IG layers had a stronger contribution of the gamma range of frequencies (Fig. 4.1.4B; non-parametric Wilcoxon signed-rank test on SG-IG recording pairs, $p<0.0001$ for beta, low-gamma and high-gamma conditions).

Mean excess power for SG and IG recordings revealed average stronger oscillations for the beta band of frequencies for SG, while IG showed weaker oscillations mainly in the low-gamma range of frequencies (Fig. 4.1.4C, non overlapping error bars showing 95% CI). When significant peaks for individual recordings in the excess power were compared, marginal distributions revealed that SG and IG displayed peaks in the whole range of frequencies studied, with SG showing significant peaks at slower frequencies than those observed in IG (Fig. 4.1.4D; SG median=26.1 Hz, IG median=46.1 Hz; non-parametric Wilcoxon signed-rank test, p=0.0002). On the other hand, SG showed higher excess power values on the peaks compared to those observed in IG (Fig. 4.1.4.D; SG-median=1.54, IG median=1.32; non-parametric Wilcoxon signed-rank test, p=0.0011). The mean coherence over UP state intersections was computed as the mean of the coherence for every SG-IG recording pair during UP

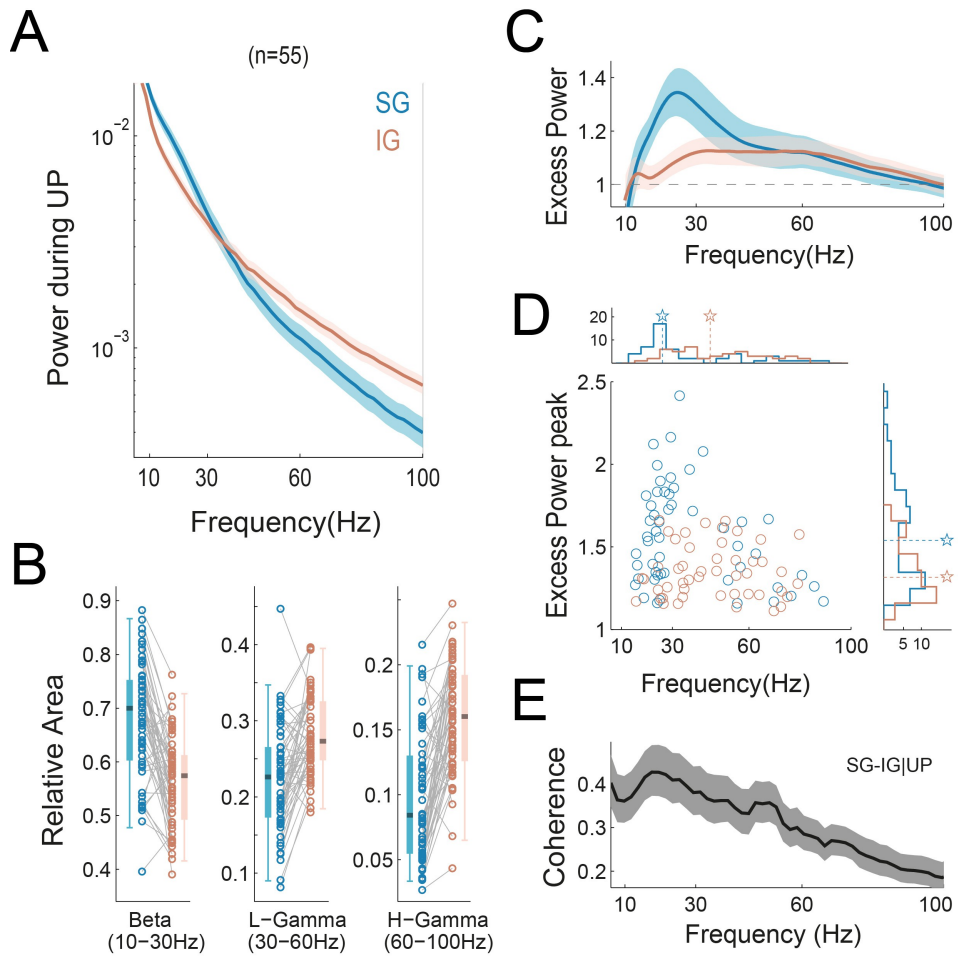

Figure 4.1.4. Fast oscillations during UP states are present in supra-granular (SG) and infra-granular (IG) layers *in vitro* (n=10). **A,** Mean normalized power during UP states for all SG and IG recordings (Jackknife error bars for the mean showing 95% CI). **B,** Relative area under the power spectrum of paired SG and IG recordings for Beta (10-30Hz, left), Low-Gamma (30-60Hz, center) and High-Gamma (60-100Hz, right) frequency bands (each pair joined by a line). Box-plot whiskers display 95%CI. **C,** Mean power during UP and "1/f"-fit ratio (Jackknife error bars for the mean show 95% CI). **D,** Power during UP and "1/f"-fit ratio detected peaks (circles in main panel) as a function of frequency, for all recordings. Marginal distributions are presented, stars showing the location of the median of each distribution. **E,** Mean coherence between SG and IG signals during UP state intersections.

state intersections. Coherence on fast frequencies was found to have significant values in a broad band, although maximum levels were reached at 19Hz in average (Fig. 4.1.4E, error bars showing 95% CI). We found that fast oscillations *in vitro* are segregated in SG and IG, while SG displayed stronger oscillations in the beta range and IG displayed weaker oscillations in the gamma range of frequencies.

Fast oscillations across SG and IG are stronger and at similar frequencies in vivo

In order to compare the *in vitro* results with those obtained *in vivo,* we chose a SG and IG channel (±400 microns away from the channel where the slow oscillation phase reversion was identified) and computed the excess power (Fig. 4.1.5). Although fast oscillations during UP states i*n vitro* displayed different frequency domains for SG and IG, these differences are not clear *in vivo* where SG and IG displayed fast oscillations with similar frequencies, despite the compartmentalization across layers (Fig. 4.1.5.A). Nevertheless, there is a tendency for SG to also display a second slower oscillations (Fig. 4.1.5.A, blue arrows) although we do not have enough statistical power to assess that difference observed.

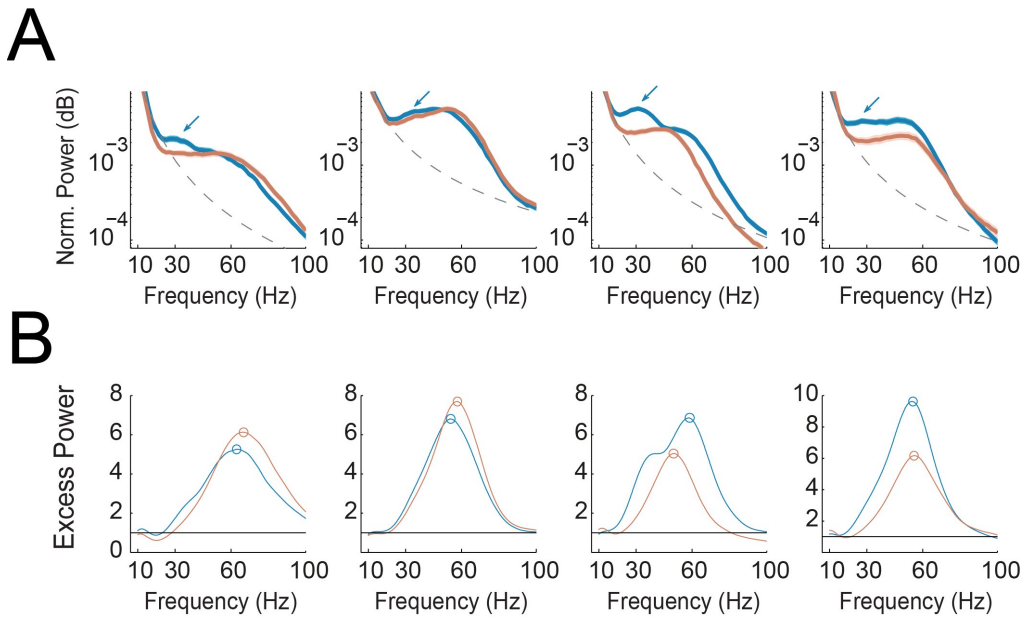

Figure 4.1.5. ***A,*** From each laminar recording, SG and IG channels are selected and fit of "1/f" decay is performed. ***B,*** Excess power for SG and IG, peaks indicated by circles.

Furthermore, fast oscillations in SG displayed more power than in IG *in vitro.* However, those differences in power between SG and IG are not clear *in vivo*, although the excess power of oscillations for both layer domains is at least 2 times larger than for the *in vitro* condition (Fig. 4.1.5D; average excess power peak, SG=7.2 IG=6.2). In sum, the difference in frequency domain and power of the fast oscillations (specially in IG) across SG and IG when *in vitro* and *in vivo* fast oscillations are compared, suggests that the local microcircuit from the slice missed

an ingredient for the generation of fast oscillations as observed in the *in vivo* condition. We address this issue in the following section.

Oscillation dynamics in enhanced excitability with kainic acid in vitro

We observed that fast frequency oscillations were boosted *in vivo* compared to *in* vitro, especially the oscillations observed in IG. In order to test whether these differences were due to a reduced excitability in the slice, we applied kainic acid to the ACSF at different concentrations (200 nM and 400 nM) in a set of *in vitro*

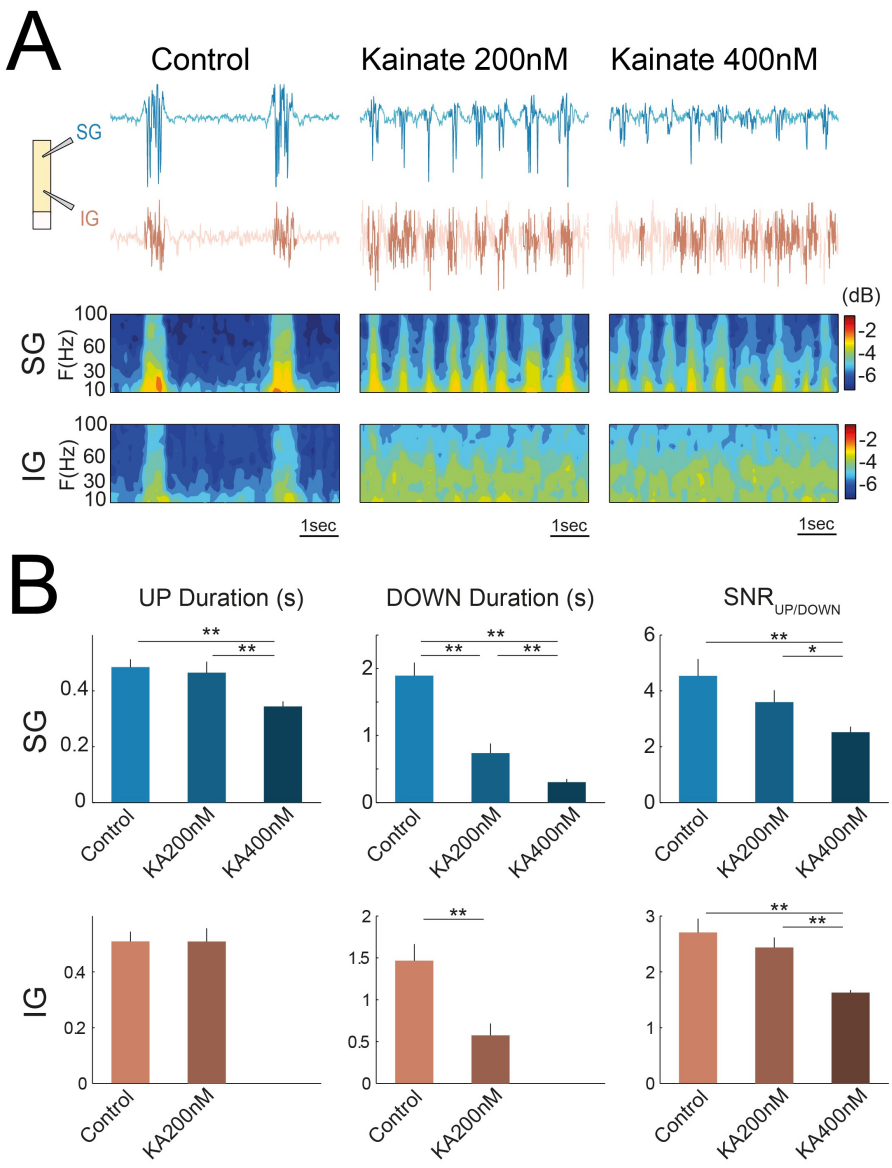

Figure 4.1.6. Increasing the excitability in the slice via kainic acid administration *in vitro* changed the dynamics of the slow oscillation (n=10). ***A,*** Top: raw traces for the SG and IG recordings for Control (left), Kainate 200nM (middle) and Kainate 400nM (right) conditions. Bottom: Spectrogram of signals displayed on top. ***B,*** Statistics of UP durations (left), DOWN durations (center) and ratio between signals STD during UP and DOWN states (SNR) for each pharmacological condition is shown for SG (top) and IG (bottom).

experiments (n=10). Bath perfusion of kainate induced a dose dependent effect on the field activity that was consistent in all slices (Fig. 4.1.6). After the perfusion with the 200 nM concentration of kainic acid, there was an increase in the frequency of the slow oscillation. However, the perfusion with a higher dose of kainic acid (400 nM) resulted in a dissociation of the activity in SG and IG layers in 9 out of 10 cases: while IG layers displayed a continuum UP state with fast oscillations at around 30 Hz, SG layers maintained the slow oscillation rhythm (ca. 1 Hz) similar to the one observed in the presence of 200 nM kainate. An example of this effect is shown in Fig. 4.1.6A.

As in previous analyses, we identified periods of UP and DOWN states under the three different conditions in each SG and IG recordings. Because DOWN states were absent (or not detectable) in IG in the 400 nM condition, we selected the time of UP and DOWN states occurrence on SG as the periods for analyzing the IG signal in order to compare the spectral properties with the SG signals.The effect of kainate was not reversible and therefore there is no "washout" condition.

The presence of kainic acid in the bath not only increased the frequency of the slow oscillations but also changed the statistics of UP/DOWN durations (Fig. 4.1.6B). There were no significant differences between UP duration in control and 200nM kainic acid neither in SG nor in IG (mean±SEM: 0.48±0.03 s vs 0.46±0.04 s for SG, 0.51±0.03 s vs 0.51±0.05 s for IG; Wilcoxon signed-rank test: p=0.56 p=1, respectively). However, DOWN states were significantly shorter comparing kainic acid 200 nM with control condition in SG and IG (1.89±0.19 s vs 0.74±0.14 s for SG and 1.47±0.2 s vs 0.57±0.14 s for IG; p=0.002 for both SG and IG). Increasing the kainic acid concentration from 200 nM to 400 nM disrupted the slow oscillation in IG, and increased the slow oscillation frequency further in SG along with a significant decrease in both UP and DOWN durations in SG (UP duration: 0.34±0.02 s, DOWN duration: 0.3±0.04; Wilcoxon p=0.002). On the other hand, kainic acid increased the activity during the DOWN states period, with respect to control condition, what can be observed in the fluctuations of LFP signals (Fig. 4.1.6A). This effect is captured by the signal-to-noise ratio of UP/DOWN states ($SNR_{UP/DOWN}$), that represents the ratio between standard deviation of LFP signal during UP states and standard deviation during DOWN states (Fig. 4.1.6B, right panel). A decrease in the signal-to-noise ratio in this case is associated with an increase in the LFP fluctuations during DOWN states (Fig. 4.1.6A).

We next explored possible alterations in the LFP spectral content following the enhancement of network excitability. The mean power spectra during UP states for SG and IG revealed spectral changes in the cortical network (Fig. 4.1.7.A). We computed the excess power for each condition, which revealed that an increase in the excitability of the network increased the frequency of dominant oscillatory mode in SG and decreased it in IG towards an intermediate value around 35 Hz (Fig. 4.1.7B, right panel). We repeated the analysis for all the experiments performed in Fig. 4.1.4B by quantifying the relative areas of the power spectra under the beta and low/high gamma frequency bands. The relative difference between SG and IG in the power of fluctuations for the different frequency bands is maintained invariant across the conditions (Fig. 4.1.7C).

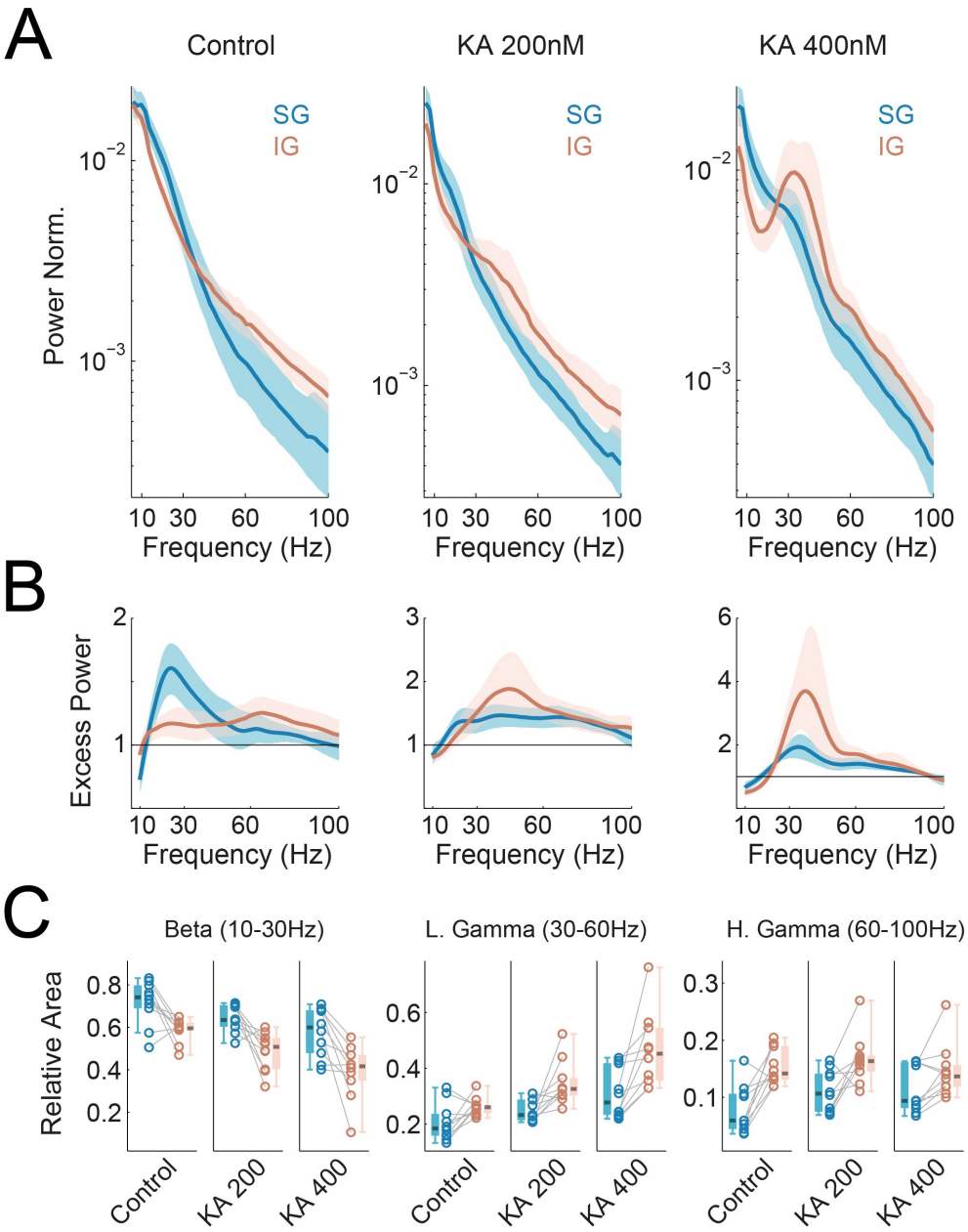

Figure 4.1.7. Kainic acid administration on the ACSF amplified the spectral differences between SG and IG during spontaneous UP states *in vitro* (n=10). ***A,*** Mean power spectrum for SG and IG recordings for the Control (right), Kainate 200 nM (center) and Kainate 400 nM (left) conditions. ***B,*** Mean power during UP and "1/f"-fit ratio for Control (right), Kainate 200 nM (center) and Kainate 400 nM (left). ***C,*** Relative area under the power spectrum of SG and IG recordings for Beta (left), Low-Gamma (center) and High-Gamma (right) frequency bands, for the different pharmacological conditions.

Comparing SG and IG power spectra between control, low and high concentration conditions revealed that kainic acid produced a stronger effect in IG compared to SG (Fig. 4.1.8A-B). The distribution of the frequencies and amplitude of the detected peaks in the excess power are shown in Fig. 4.1.8C and D. Multi

factorial ANOVA analysis (factors = layer domain, pharmacological condition, slice id) revealed a significant main effect on pharmacological condition for the frequency of peaks (p=0.0054). Significant interaction between layer domain and pharmacological condition was found for the amplitude of peaks (p=0.0088), while only a main effect on the condition was found for IG (p=0.0138). The coherence profile did not change significantly for the different conditions between SG and IG during UP states intersection (Fig. 4.1.8E).

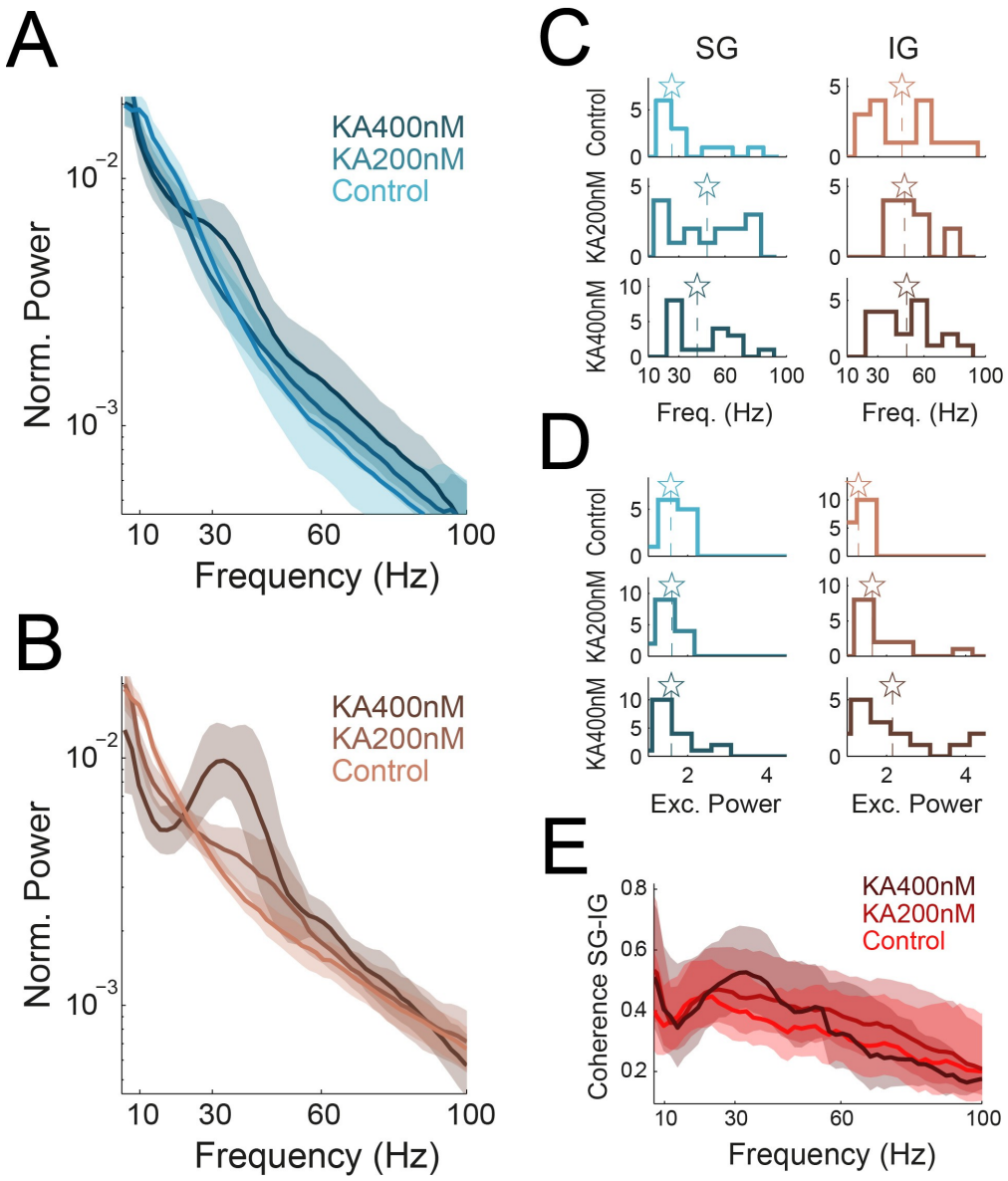

Figure 4.1.8. Kainic acid affected activity in IG and SG layers different. **A,** Mean normalized power during UP states for SG under different pharmacological conditions. **B,** Same as A, but for IG. **C,** Distribution of frequencies of peaks in the Excess power for SG (left column) and IG (rigth column), and the different pharmacological conditions. **D,** Distribution of amplitudes of peaks in the Excess power for SG (left column) and IG (rigth column), and different conditions.

Pharmacological manipulation by kainic acid in the slice had a significant effect on changes in amplitude and frequency of peaks, whereas changes on peaks amplitude for pharmacological condition depended on the layer domain. The presence of an increased excitability in the slice by kainic administration, produced complex change in the structure of the fast oscillations in the different laminar domains. On one hand, increasing the excitability produced a shift in the frequency of fast oscillations in SG towards the frequency of fast oscillations in IG, which remained at similar frequencies. On the other hand, the power of oscillations in SG remained at similar values whereas the power of the oscillations in IG was significantly increased. This result suggest that a tonic increase in excitability disrupts the slow oscillation dynamics in the cortical column, but the boost in the fast oscillations results in a closer match to the fast oscillations observed in the *in vivo* condition.

4.2. Analysis of synchronized state dynamics in vivo

Cortical synchronized states are characterized by the presence of UP and DOWN dynamics. The mechanisms proposed for causing the UP and DOWN transitions during synchronized states include intrinsic cellular or network fatigue mechanisms and incoming external inputs to cortical circuits. However, the nature of each mechanism would imprint different signatures in the transition statistics and in the spiking dynamics. In this chapter, we analyzed existing population recordings of spontaneous activity obtained using multisite silicon electrodes in somatosensory cortex of urethane-anesthetized rats during synchronized states[3]. We show that statistics of UP and DOWN transitions are consistent with the existence of both stochastically generated transitions caused by external inputs and a weak adaptive mechanism.

Cortical state assessment

Under urethane anesthesia, the cortex undergoes spontaneous transitions between synchronized and desynchronized states. The presence of large amplitude slow fluctuations in cortical LFP signals is characteristic of synchronized brain states, whereas during desynchronized states these fluctuations are suppressed (Fig. 4.2.1A). Alternatively, synchronized brain states are characterized by coherent spiking activity of neuronal ensembles, so that MUA spiking activity shows periods of collective silence. We classified cortical brain state using two different methods that quantify these two aspects of synchronized brain states and which give essentially equivalent outcomes: (i) the ratio between the LFP spectral power at low (0.5-4 Hz) and high (20-55 Hz) frequencies, the L/H ratio (Fig. 4.2.1B, green trace) (Goard and Dan, 2009; Marguet and Harris, 2011), (ii) the fraction of 20 ms windows in the MUA recording with no spikes over a period of 10 s, a measure we called “silence density” (Fig. 4.2.1B, black trace) (Renart et al., 2010). For each experiment, we identified sustained periods (~5-10 min) of high silence density values, corresponding to periods of a clear synchronized brain state, and used those periods exclusively to carry out the analysis presented in this Chapter (see methods section 3.3). A characterization of the different levels of synchronization will be carried out in Chapter 4.4 in this Thesis.

We identified putative UP and DOWN intervals, termed U and D respectively, based on the instantaneous spiking activity of the population. For this

3 Experiments performed by Artur Luczak and Peter Barthó in Harris Lab.

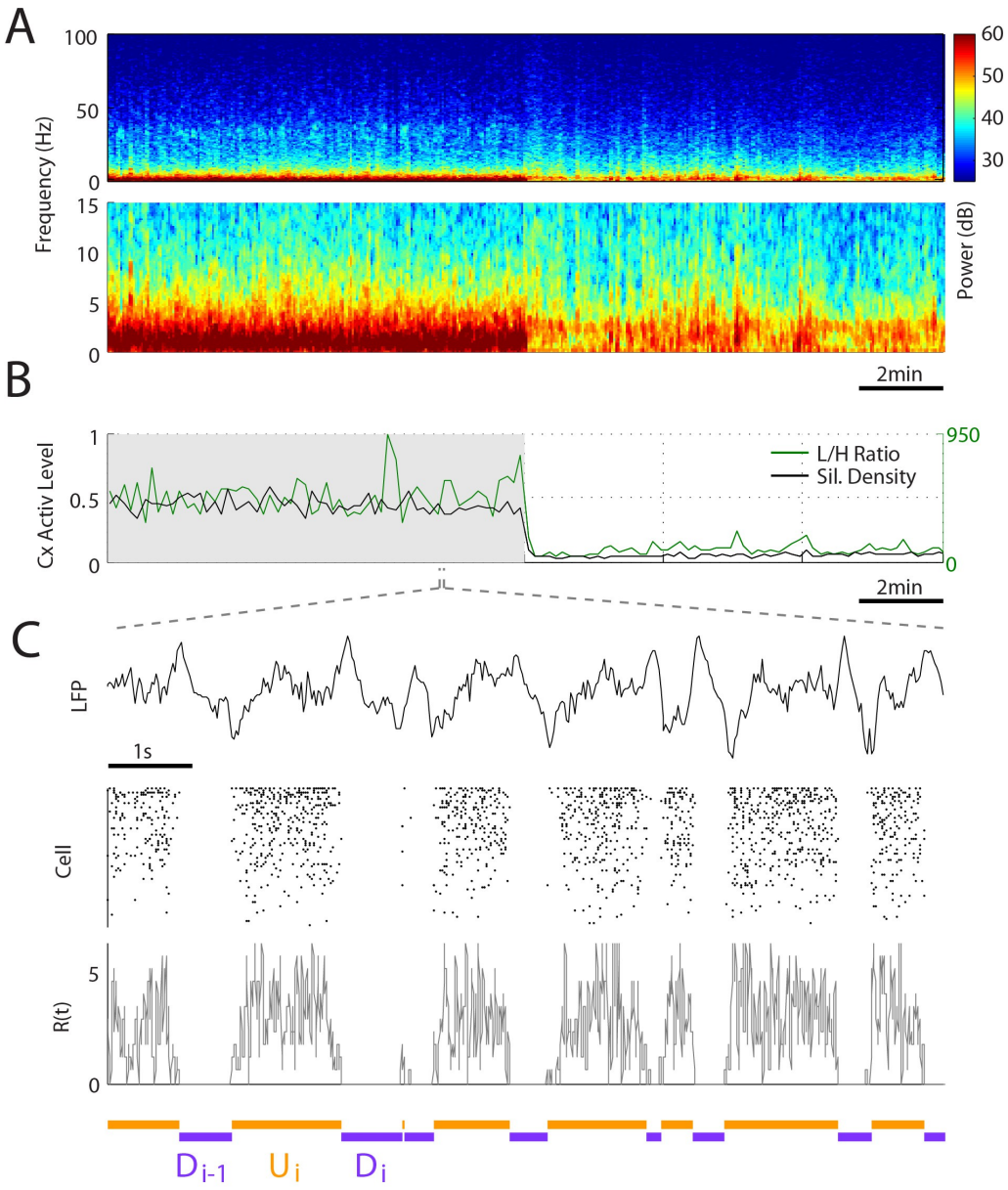

Figure 4.2.1. Cortical state assessment and detection of putative UP & DOWN intervals. **A,** Average spectrogram from simultaneously recorded LFP signals is shown using two different frequency scales (0-100 Hz, top; 0-15 Hz bottom). Notice the abrupt transition from a synchronized to a desynchronized state marked by the decrease in the energy at low frequencies (< 5 Hz; middle panel) **B,** Assessment of cortical state by LFP spectral L/H ratio (green trace) and from MUA Silence density (black trace). MUA was computed using the merged spiking activity of all isolated cells in the recording. Shaded interval indicated the synchronized state period used for analysis. **C,** Example LFP trace during 10 s during the synchronized state shows the characteristic slow fluctuations (top) while the population raster of 85 well isolated single units (middle) shows the corresponding intervals of tonic activity intercalated with intervals of quiescent activity (cells are sorted based on mean firing rate). Instantaneous population rate *R*(t) (bottom) is computed and used to identify UP and DOWN intervals (orange and violet horizontal lines, respectively).

we used a hidden semi-Markov statistical model developed previously that exhibited less classification errors than traditional threshold-based methods (Chen et al., 2009). The method uses the instantaneous population rate $R(t)$ defined as the population-averaged rate of the spike trains of well isolated units, with 20 ms count windows slided in 5ms steps (see equation 4 in Chapter 3.3 from Methods for further details; Fig. 4.2.1C bottom). Based on the trace of $R(t)$, an expectation-maximization algorithm (a recursive method to determine the maximum likelihood estimation of the model parameters) is used for the estimation of the model parameters and the subsequent extraction of the U and D sequence (Fig. 4.2.1C orange and violet horizontal lines, respectively).

From the example shown in Figure 4.2.1, some remarkable features are observable: (i) Us and Ds are variable, (ii) there is no clear relationship between the U and the following or preceding D, (iii) the population rate $R(t)$ during different Us shows large fluctuations, even for Us of similar length. We next performed a quantitative analysis on the statistics of these particular features across our data set (recordings from somatosensory cortex in n=7 rats).

Statistics of UP and DOWN states during synchronized states

We first computed the distribution of U and D and the cycle intervals C, where C=D+U for the example experiment of Fig. 4.2.1C (Fig. 4.2.2A; orange, violet and brown histograms, respectively). For this particular example, the mean U is 0.82 s, mean D is 0.48 s and mean C is simply the sum, i.e. 1.3 s. In order to measure the variability in the U and D duration, we use the coefficient of variation (CV) defined as the standard deviation divided by the mean, commonly used in Neuroscience to quantify the variability of inter-spike-intervals. In this experiment, CV(U)=0.62 and CV(D)=0.69, whereas CV(C)=0.5. The relation between the duration of consecutive periods was assessed by the linear correlation between consecutive (U_i,D_i) and (D_{i-1},U_i) pairs with the subscript i indicating the position in the sequence of U and D intervals (Fig. 4.2.1C). The correlation coefficient displayed positive values $corr(D_{i-1},U_i)=0.12$ and positive trend $corr(U_i,D_i)=0.08$ (Fig. 4.2.2B top and bottom: $p<0.05$, $p>0.05$, respectively). Durations 3 standard deviations away from mean durations were discarded for the correlation estimation. We also corrected for slow drift in the statistics by subtracting the correlation obtained after shuffling of Us and Ds over a running window of 10 s periods. The results for all the experiments (n=7 animals) shows that mean U and D for the different experiments take a wide range of values (mean±SEM: U=0.53±0.1 s, D=0.54±0.05 s; Fig. 4.2.2C left panel). Moreover, the variability of U and D seems consistently large across experiments (mean±SEM: CV(U)=0.68±0.03 CV(D)=0.68±0.04; Fig. 4.2.2C middle panel) while the correlation between consecutive intervals showed consistently positive values (mean±SEM: $corr(D_{i-1},U_i)=0.18\pm0.03$ $corr(U_i, D_i)=0.13\pm0.03$; Fig 2C right panel).

Visual inspection of the data and the distribution of durations, and in particular the broadness of the distribution of the cycle C, suggests that *rhythmicity* in the U and D alternation is weak. We wanted to study to what extent the alternation between states is consistent with an oscillatory mechanism. A standard way of characterizing oscillatory behavior in LFPs or spike trains is by looking at

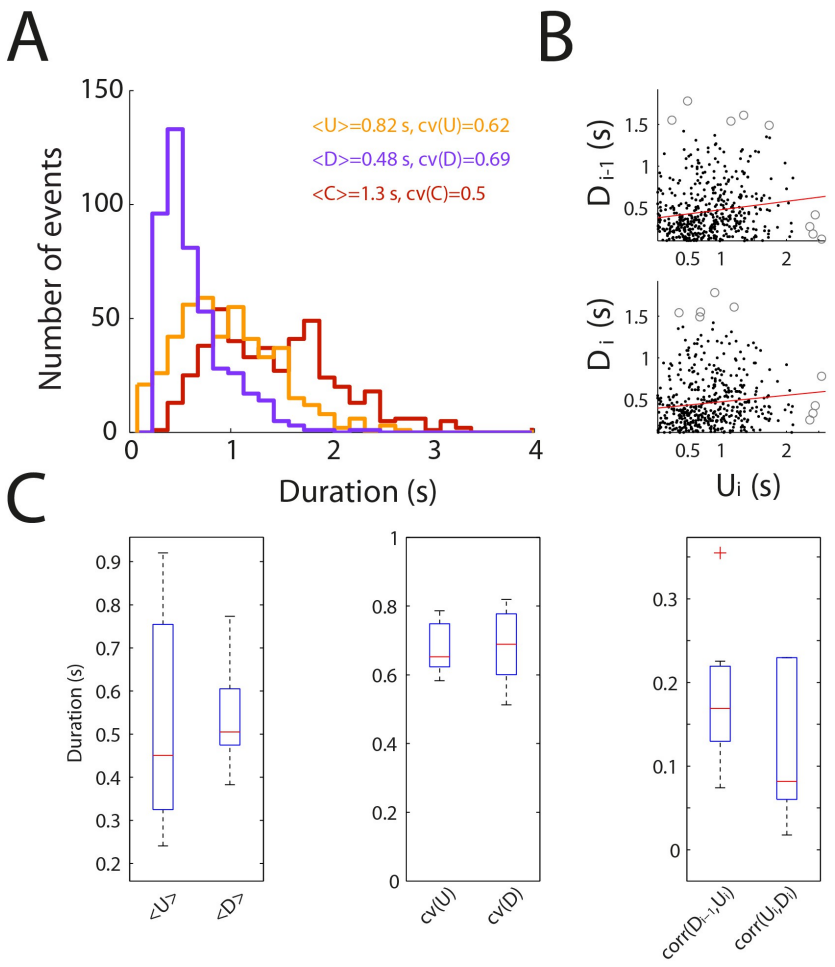

Figure 4.2.2. Statistics of UP and DOWN intervals during synchronized brain states. **A,** Distribution of U, D and C durations in one representative experiment. Inset shows the mean and CV values. **B,** D duration vs the consecutive (top) and the previous (bottom) U duration exhibit weak but significant serial correlations. U or D values 3 standard deviations away from the mean (circles) and discarded for the correlation analysis. **C,** Summary of experimental results (n=7 rats) show the mean (left), the coefficient of variation CV (middle) and the serial correlation (right) of U and D. While the average durations are quite heterogeneous across experiments, the variability is consistently large and the correlations are consistently significantly positive. Boxplots displaying median in red line, box 1st and 3rd quartile and whiskers are defined as 1.5 times the 1st to 3rd quartile distance (outliers in red cross).

the temporal structure of the autocorrelogram (ACG) or equivalently at the structure of the power spectral density. The existence of a *ringing* structure in the ACG, indicative of oscillatory behavior, corresponds to the presence of peaks at the oscillation frequency in the spectral density. To distinguish between the temporal structure given by an oscillatory behavior and non-oscillatory *stochastic switching* behavior, we compared the ACG and the spectral density of the population rate $R(t)$ obtained from the original spike trains against the instantaneous rates obtained from two surrogate data sets: (i) the first surrogate set is generated by drawing Us and Ds

independently from exponential distributions with respective means matching the data, and within each U and D spikes are generated from a homogeneous Poisson process with rate matching the average R(t) during Us or Ds, respectively. The instantaneous rate of this surrogate data, termed R_E(t), corresponds to the statistics expected if the UP/DOWN transitions were purely triggered by fluctuations (i.e. exponentially distributed durations) and there were no fatigue mechanisms which could generate an oscillation (i.e. the firing is stationary within each period). (ii) The second surrogate set, with rate termed R_G(t), is generated identically except that the distributions of U and D durations are not exponential but Gamma distributions, with the mean and the order of the Gamma chosen to match the mean and standard deviation of the original data (e.g Gamma of order 2 yields a CV equal to 0.7 which is approximately the average across experiments). This distribution corresponds to the statistics of a process in which transitions are triggered by fluctuations but with a soft refractory period after each transition preventing the occurrence of very short U or D durations. We reason that none of these two surrogate data sets has an oscillatory nature and we use them as a benchmark against which to compare the original data.

We computed the power spectrum and the ACG of the rate R(t) from the original data and the rates R_E(t) and R_G(t) from the two surrogate sets (Fig. 4.2.3A; bin size 5 ms). As expected, the power spectrum of R_E(t) does not reveal any peaks and the ACG shows an exponential decay with no ringing (Fig. 4.2.3 A-B gray). On the other hand, the power spectrum of R_G(t) shows a clear peak in the power spectrum at low frequencies <1 Hz (Fig. 4.2.3A-B green). The power spectrum of the original R(t) shows a very similar structure than the one obtained from R_G(t) (Fig. 4.2.3A, compare black and green). However, different from R_G(t), the power spectrum of the original R(t) shows a small "bump" at a fast frequency near approximately 30 Hz.

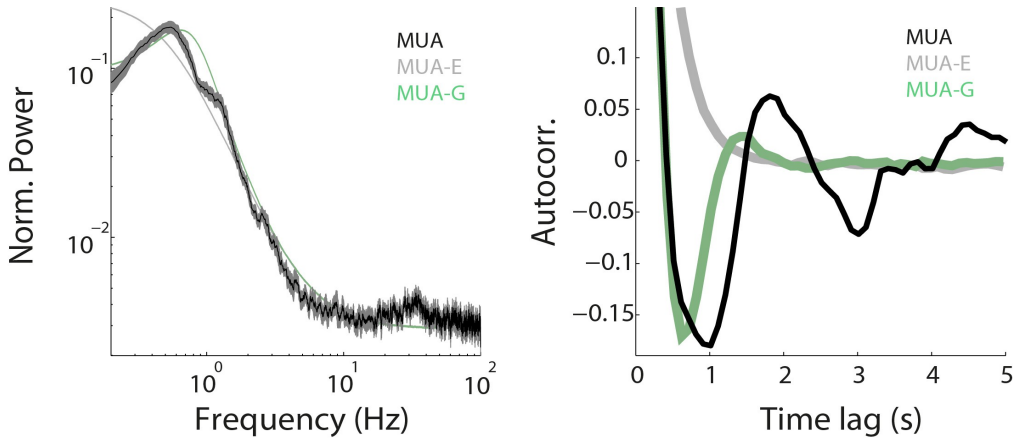

Figure 4.2.3. Periodicity analysis on the instantaneous population rate. A, Power spectra of original population rate R(t) (black), and the rates R_E(t) (gray) and R_G(t) (green) of the exponential and Gamma surrogate sets, respectively, for an example experiment (bin size 5ms; error bars are 95%CI). **B,** Autocorrelograms of R(t), R_E(t) and R_G(t) (same color code as in A), Autocorrelograms are normalized to have amplitude one at zero lag.

The ACG from R_G(t) shows the zero-lag peak sided by a first negative trough and then goes to zero. The ACG of the original R(t) reveals a similar fast decay towards a negative trough and weak noisy ringing (Fig. 4.2.3B). This steep decay towards zero in the ACG from the data was a robust feature confirmed in the rest of the experiments (see Fig. A1 from Appendix).

This analysis shows that stochastic alternation between UP and DOWN intervals can yield ACGs and power spectra showing signatures commonly interpreted as a sign of oscillatory behavior (e.g. the surrogate R_G(t)). Thus we conclude that the temporal structure of the original MUA spike train is approximately consistent with a system showing transitions between two conditions which are driven by fluctuations with a soft refractory period (see e.g. (Moreno-Bote et al., 2007)).

Dynamics of MUA during UP and DOWN states

Motivated by the previous result suggesting that UP/DOWN transitions could be triggered by external fluctuations and not by the accumulation and recovery of a fatigue mechanism, we examine the dynamics of the instantaneous firing rate during UP and DOWN intervals and ask whether there are traces of a fatigue mechanism. We aligned Us at the onset or at the offset (Fig. 4.2.4B) and obtained two population rates averaged across Us: R_{on}(t) is the average rate aligned at the onset, and R_{off}(t) at the offset (Fig. 4.2.4C; see equation 9 in section 3.2 from Methods). The time course of these two quantities gives a measurement of the average instantaneous firing rate of the population across the U (Fig. 4.2.4C). Two things are worth noticing: first, that $R_{on}(t)$ at time t is an average across Us with duration U>t, meaning that the number of Us averaged at every time point is different (see solid gray line indicating number of Us considered as a function of time in Fig. 4.2.4C*)*. Second, that the two traces can not be viewed as the two halves of a U interval, i.e. they cannot be temporally concatenated. Because of the way in which they are built, the temporal relation between them does not remain consistent for all the component Us (Fig. 4.2.4B). When onset and offset-aligned averaged rates are compared for an example experiment, no significant differences in amplitude are observed (Fig. 4.2.4C). This seems to indicate that the population average firing rate during U intervals remains constant.

To further investigate whether the distribution of the rate is also stationary, we compare the activity for two specific 100 ms windows associated to the onset and offset of each U: (i) transient windows are defined just after (before) the onset (offset) times (Fig. 4.2.5A, light gray area); (ii) sustained windows are defined just after (before) the onset (offset) transient window (Fig. 4.2.5A, dark gray area). We plotted the average population rate in the onset transient window versus the average population rate in the offset transient window for each U for one example experiment (Fig. 4.2.5B left). The same was done for the stationary windows (Fig. 4.2.5B right). For this particular case, population rate at offset was higher than population rate at onset for transient periods, whereas population rate at onset was higher than population rate at offset for the stationary period (Wilcoxon signed rank test; p=0.04 and p=0.03, respectively). However, in the the summary for all

experiments, we found no significant differences between the average rate at the onset versus the offset neither for transient nor stationary intervals (Fig. 4.2.5C, Wilcoxon: transient p=0.16, stationary p=0.69).

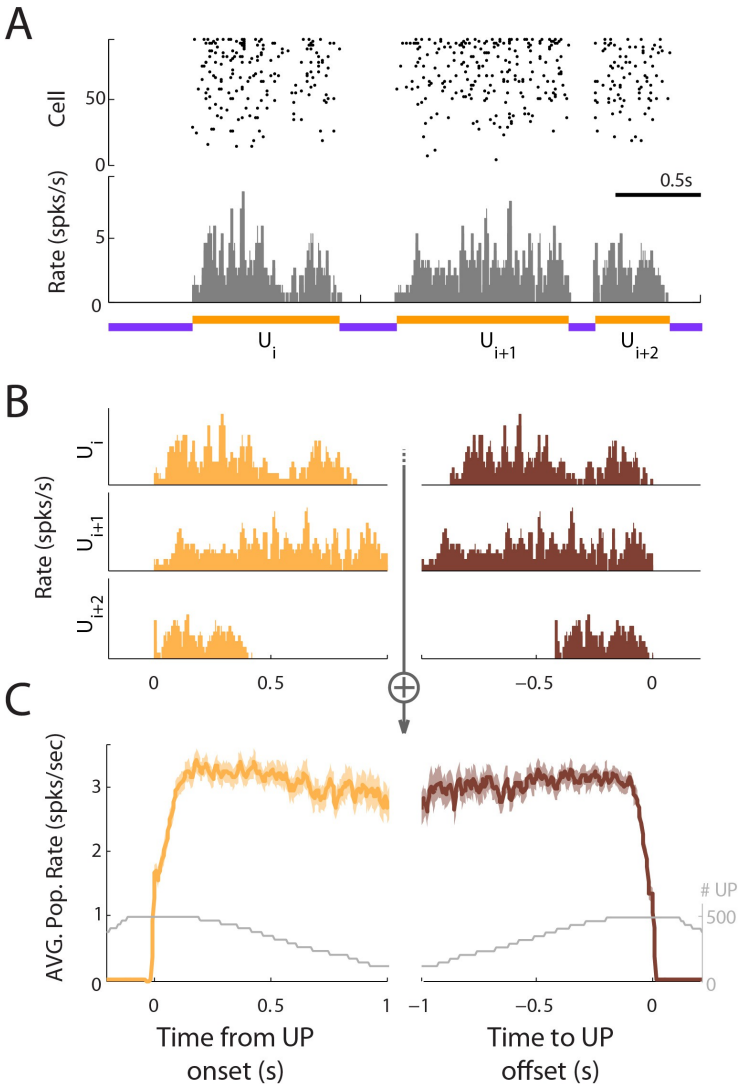

Fig. 4.2.4. Onset and Offset aligned firing statistics. A, Population raster-gram (top), instantaneous population rate *R*(t) (middle)and detected Us and Ds (bottom). **B,** The rate *R*(t) from each U in A (*i*, *i*+1 and *i*+2) is aligned at the onset (left) and at the offset (right). **C,** Averaged Population Rate aligned at the onset (left) and aligned at the offset (right) are obtained by averaging *R*(t) across all Us (equation 9 in Methods 3.2). Error bars indicate 95% confidence intervals. Gray line indicates number of Us considered at each time point.

We reasoned that a fatigue mechanism would be more detectable on long Us in which neurons fire a larger number of spikes and a rate adaptation conductance, for instance, would exhibit a greater increase. We segregated Us into short and long based on whether the duration was below or above the median duration (in the example experiment shown in Fig. 4.2.5, median(U)=0.76 s). For the short group we considered only Us longer than 0.5 s (dashed lines in Fig. 4.2.5D). After 0.5 s

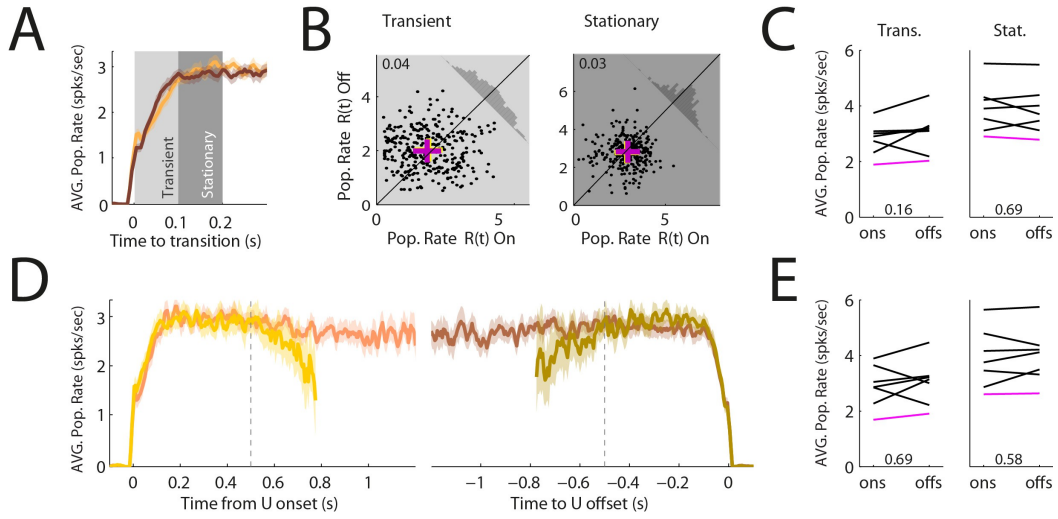

Fig. 4.2.5. Dynamics of the Population Rate at onset and offset of UP intervals. A, Example experiment where the averaged Population Rate aligned at the onset *(*R_{on}(t), orange*)* and at the offset (R_{off}(t), brown) are very similar (notice that the time axes for R_{off}(t) is reversedFig. 4.2.). Transient (light gray) and stationary (dark gray) windows are defined at both the onset and the offset. **B,** Comparison of the rate R(t) at the onset and the offset for each U (same experiment as in A). *Left:* Each dot shows the average of R(t) over the 100 ms offset transient window vs. the onset transient window, in a single U lasting more than 400 ms. Mean values are shown in magenta. *Right:* same as left for the stationary window. **C,** Summary results from n=7 animals. *Left:* Each line compares the population rate averaged across Us at the onset and offset transient windows (magenta cross in B is represented by the magenta line). *Right:* same as left but for the stationary window. **D**, Population averaged rate aligned at the onset (left) and the offset (right) The rates were averaged separately across long (orange and brown) or short Us (yellow and green) defined as being longer or smaller than median(U), respectively. Minimum duration of Us considered is 500ms (dashed vertical lines). **E,** Same analysis as in C, but considering only Us longer than the 85-percentile of the distribution of all Us. Numbers inside the panels indicate the p-values of Wilcoxon two-sided test, respectively.

from the onset, the average rate for short Us decreases due to drop in R(t) produced by the transition into the consecutive D[4]. This example shows that a more pronounced rate decay was not observed either for short or long UP states. Moreover, comparison of the average rates R_{on}(t) and R_{off}(t) obtained from Us above the 85% percentile (i.e. intervals from the tail of the U distribution) averaged over the transient window or over the stationary window, yielded no significant

4 Note that the R_{on}(t) is an average acros Us with $U_i > (t - t_i^{on})$, i.e. at each time point *t*, R_{on}(t) only averages Us longer than *t*. With this we ensure that the rate R_{on}(t) only averages firing during UP intervals and not during the consecutive D. However, the transition into the consecutive D is not instantaneous, but takes between 100 and 200 ms for R(t) to decrease to near zero from the stationary values during the Us (Fig. 4.2.5A and D). The impact of this transient decrease in R(t) during this short window is barely noticeable in the average R_{on}(t), except when we impose an upper bound in U such as for the set of *short* UP intervals with U<0.76 s. This bound reveals the transient drop in rate because as *t* approaches this upper bound R_{on}(t) should mimic the behavior of R_{off}(t) approaching the offset, as it is averaging Us which terminate near the bound. The symmetrical argument is true for the average rate aligned at the offset R_{off}(t) due to the non-instantaneous transition from D to U.

differences (Fig. 4.2.5E; Wilcoxon: p=0.69 transient, p=0.58 stationary windows). In sum, the population average firing rate during UP intervals exhibits no traces of a fatigue mechanism.

Dynamics of single cells during UP states

We now consider the statistics of individual spike trains of isolated cells. We first computed the mean firing rate for individual neurons across each U, i.e. spike count for each U divided by the length U (and analogously for each D). We then averaged these rates across U and D intervals, respectively, for each neuron *j* to obtain r^{U}_{j} and r^{D}_{j} (equation 17 in Methods section 3.2) estimates (Fig. 4.2.6A). The marginal distribution of r^{U}_{j} displays the common Gamma-like shape with a low population mean rate of 2.6 spikes per second (orange marginal distribution in Fig. 4.2.6A; mean±SEM: 2.6±0.004 spks/s). In contrast to the common view describing DOWN intervals as totally silent (Steriade et al., 1993a) many neurons in this experiment showed $r^{D}_{j} > 0$ (violet marginal distribution in Fig. 4.2.6A with mean±SEM: 0.051±0.006 Hz). We obtained an average over experiments (n = 7) of the mean rates during Us and Ds and obtained 3.33±0.28 spks/s and 0.067±0.01 spks/s respectively (mean±SEM; Fig. 4.2.6B). Thus the rate during D periods is around fifty times lower than during U intervals. The correlation between firing rates r^{U}_{j} and r^{D}_{j} displayed positive values although neurons showing higher rates during Us are not necessarily showing higher rates during Ds (Pearson corr(r^{D}_{j},r^{U}_{j})=0.26, p=0.012, Fig. 4.2.6A). This was confirmed across the different experiments (mean(corr(r^{D}_{j},r^{U}_{j}))±SEM=0.42±0.08, Fig. 4.2.6C).

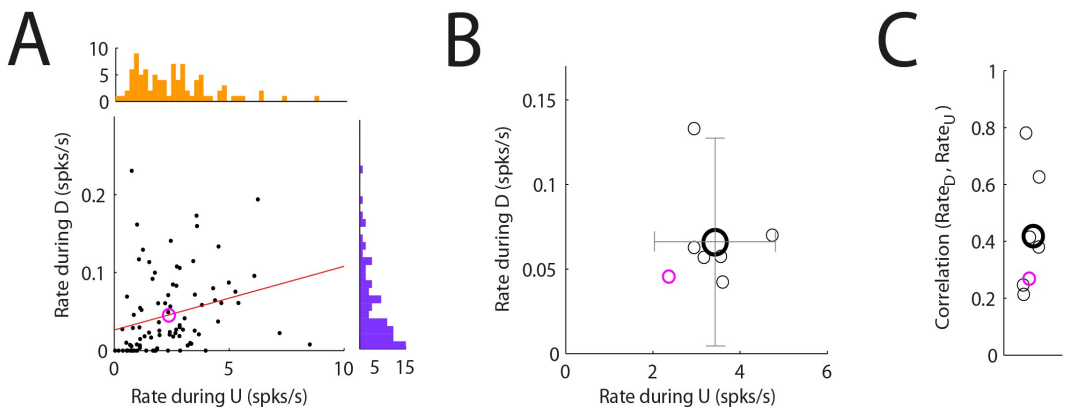

Figure 4.2.6. Firing rate distributions during UP and DOWN intervals. A, Scatter plot of firing rate during UP intervals versus firing rate during DOWN intervals for different isolated cells (r^{U}_{j} vs r^{D}_{j}). Marginal distribution of firing rates r^{U}_{j} . **B,** Mean firing rates r^{U}_{j} and r^{D}_{j} for the different experiments (experiment from panel A showed in magenta). Mean across experiment in thick black circle (gray lines showing 2 standard deviations of the mean; Pearson corr(r^{D},r^{U})= -0.044, p=0.92). **C,** Mean correlation between firing rates during UP and DOWN intervals across neurons for the different experiments.

We next assess the heterogeneity across neurons in the dynamics of the firing rates during UP intervals. We computed the average rate of individual neurons aligned at onset $r_{j,on}(t)$ (equation 14 in Methods section 3.2) and offset

$r_{j,off}(t)$ of U(Fig. 4.2.7A, shows 3 different examples in thick traces). We classified neurons into (i) adaptive, (ii) anti-adaptive or (iii) n.s. depending on whether the average rate decays, increases or shows no significant trend. More specifically, a neuron is adaptive if (1) the area under $r_{j,on}(t)$ is higher than the area under $r_{j,off}(t)$ during the transient and stationary periods, and (2) the slope of the linear regression of $r_{j,on}(t)$ is less than the slope of the linear regression of $r_{j,off}(t)$ (Fig. 4.2.7A, thin traces). If the negation of these two conditions holds, the neuron is anti-adaptive, and otherwise it is classified as n.s. Fig. 4.2.7A shows three example neurons classified as adaptive (top), n.s. (middle) and anti-adaptive (bottom). Averaging $r_{j,on}(t)$ and $r_{j,off}(t)$ across neurons classified as the same type reveals, as expected, different temporal profiles at the onset and offset aligned conditions (Fig. 4.2.7B; inset shows the proportion of classified neurons for this particular experiment). The proportion of neurons classified into adaptive, anti-adaptive and n.s. for different experiments reveals that consistently across experiments there is heterogeneity in the dynamics of individual neurons (Fig. 4.2.7C; colored circles represent different experiments and black circles show mean values). Overall, this simple classification shows that individual cells may exhibit different dynamics during UP intervals.

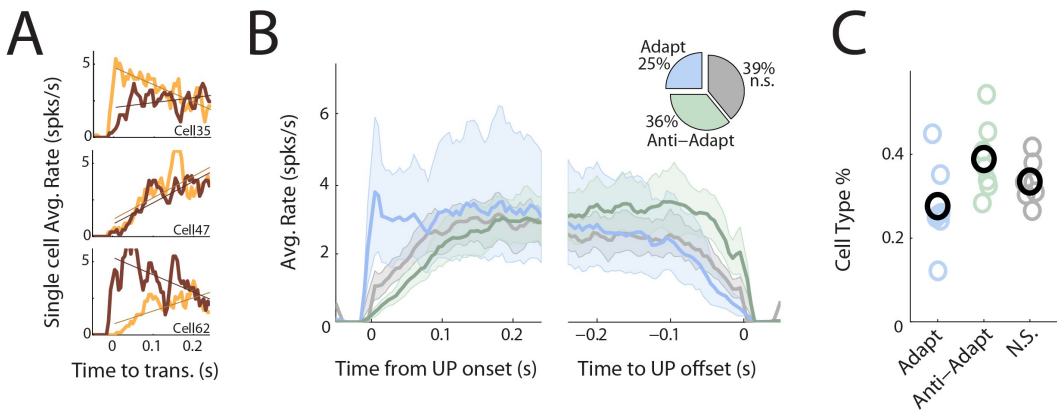

Figure 4.2.7. Firing rate dynamics of individual neurons during UP intervals. A, Three cells examples classiefied as adaptive (top), n.s. (middle) and anti-adaptive (bottom) illustrate the different firing rate dynamics during onset (orange) and offset (brown) aligned conditions. Dashes lines show linear regression of $r_{j,on}(t)$ and $r_{j,off}(t)$). **B,** Mean rate across neurons classified adaptive (blue), anti-adaptive (green) and n.s. (gray). *Inset:* Proportion of cells classified in each category for this example experiment . **C,** Summary results of the proportion of cells in each class are shown for different experiments (colored circles). Means across experiments are shown with black circles.

Second order statistics of spiking activity during UP intervals

In order to obtain a more thorough characterization of the spiking statistics across U intervals, we turn our attention to the interaction of the spike count variability and correlations with the UP and DOWN switching. Analysis of the neuronal variability may reveal many features not captured by the mean

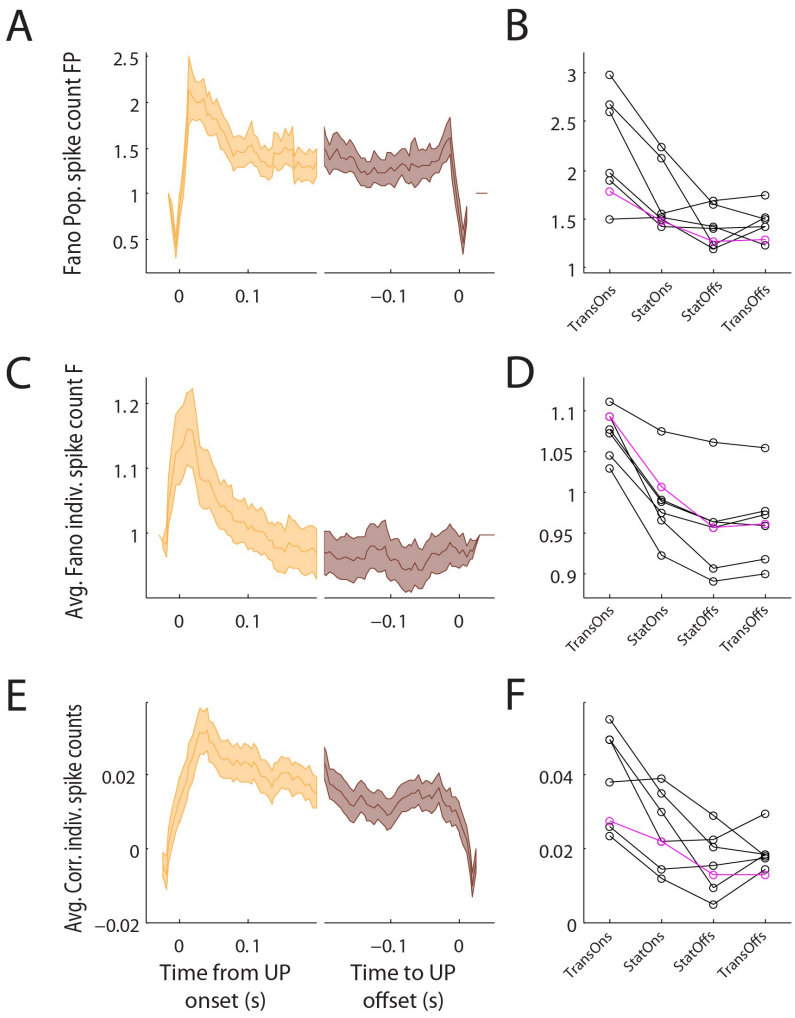

Figure 4.2.8. Second order statistics of spiking activity during UP intervals. A, Fano factor of the population spike count at onset ($FP_{on}(t;T)$, left) and offset ($FP_{on}(t;T)$, right) aligned conditions. Error bars are 95% CI. **B,** Mean FP over the transient and the stationary windows at the onset and offset for n = 7 experiments (each one joined by lines). Example experiment shown in A,C,E is shown in magenta. **C,** Population averaged Fano factor of the spike count for individual cells aligned at the onset ($F_{on}(t;T)$, left) and offset ($F_{off}(t;T)$, right). **D,** Same as B for $F_{on}(t;T)$ and $F_{off}(t;T)$. **E,** Instantaneous spike count pair-wise correlation coefficient averaged across cell pairs aligned at the onset ($Corr_{on}(t;T)$, left) and offset ($Corr_{off}(t;T)$, right) **F,** Same as B for $Corr_{on}(t;T)$ and $Corr_{off}(t;T)$.

activity such as Poisson-like firing across UP intervals or alternatively very repeatable firing produced for instance by reproducible spike train patterns. We computed the instantaneous Fano factor of the population spike count FP(t;T) (equation 10 in Methods section 3.2), which quantifies the spike-count variability across Us in the population activity. The population count variance depends on the variance of the individual cell spike counts, and on the correlations across spike counts. To disentangle the different contributions to the population variability we

computed the Fano factor of individual cells averaged over the population (F(t;T), equation 16 in Methods section 3.2) and the instantaneous spike count pair-wise correlation coefficient averaged across cell pairs in the population of isolated neurons recorded (Corr(t;T) equation 18 in Methods section 3.2). We analyzed these statistics aligned at the onset and at at the offset of Us using T= 20ms sliding windows (5ms step). Two things stand out: first, there is a transient surge in the variability of the population activity at the onset of UP intervals (Fig. 4.2.8A, orange and brown shows the onset and offset aligned condition for a particular example experiment, respectively). Second, after this surge that variability seems to reach a plateau at $FP \sim 1.5$ and does not display a similar strong surge at the offset. Although the example experiment shown in Fig. 4.2.8A shows a small bump in the variability at the offset, this was not a robust feature across experiments (Fig. 4.2.8B). The sharp decrease in $F_{on}(t;T)$ and $F_{off}(t;T)$ at time t=0 is an artifact of the detection of Us and Ds: Our method behaves qualitatively like the threshold based detection of Us and Ds where, by construction, the variability of the population rate is zero at the threshold crossing points. The onset bump in the population variability is also present at the single cell level as exhibited by $F_{on}(t;T)$ and the mean pair-wise correlation coefficient $Corr_{on}(t;T)$ (Fig. 4.2.8C and E, respectively). When we averaged these measurements over the transient and stationary windows at the onset and offset aligned conditions in all the experiments, we observed that the trend is systematic (Fig. 4.2.8B,D,F; example shown in left panels is shown in magenta).

The transient surge of variability observed in the $FP_{on}(t;T)$ could be due to a misalignment in the UP intervals produced by detection inaccuracies. For instance, if the firing rate during each UP interval followed the same ramp-and-plateau profile, but the imprecisions in the U-D detection misaligned the onset of the ramp, the variability of the spike count would show a bump and a plateau similar to what we observe in the data. To control for this possibility, we generated surrogate data sets obtained from the original data but removing the first 100ms of each U. We then repeated the UP and DOWN detection over the surrogate sets and computed $FP_{on}(t;T)$. We reasoned that if the surge in variability was only due to misalignment in the detection, we should observe a similar bump in $FP_{on}(t;T)$ obtained from the surrogate sets. We found however, that the bump in $FP_{on}(t;T)$ was not present in these surrogate data sets (Fig. A5 from Appendix of this Chapter). We also generated surrogates by removing the last 100 ms from each U and performed the full analysis. This manipulation left the absence of bump at the offset unaltered (Fig. A5 from Appendix of this Chapter). This implies that the bump in $FP_{on}(t;T)$ cannot be attributed to imprecisions in the UP onset alignment.

The dynamics of spike count statistics are characterized by a transitory increase in the variability across Us at the onset consistently across experiments. Moreover, the increased onset variability is followed by stationary dynamics and the offset is not preceded by any surge in variability with a magnitude comparable to the onset case. Furthermore, after this transient increase, the mean single cell F(t;T) values are consistent with Poisson spike train statistics with near-zero in average correlations. In the next chapter we will use a computational model to investigate the network mechanisms which could give rise to this transient. In the Discussion we will address possible interpretations and implications of this finding.

Dynamics of putative excitation and inhibition during UP states

Next, we studied the dynamics of excitation and inhibition during UP intervals. In cortical activity, the spike waveform can be used to classify cells into narrow spiking putative fast-spiking (I) and broad spiking putative excitatory (E) cells (Barthó et al., 2004; Sirota et al., 2008). From 5 out of 7 experiments we were able to save the waveforms from individual cells. We used the half-width, trough-to-peak and asymmetry from the average waveform of each neuron to classify the

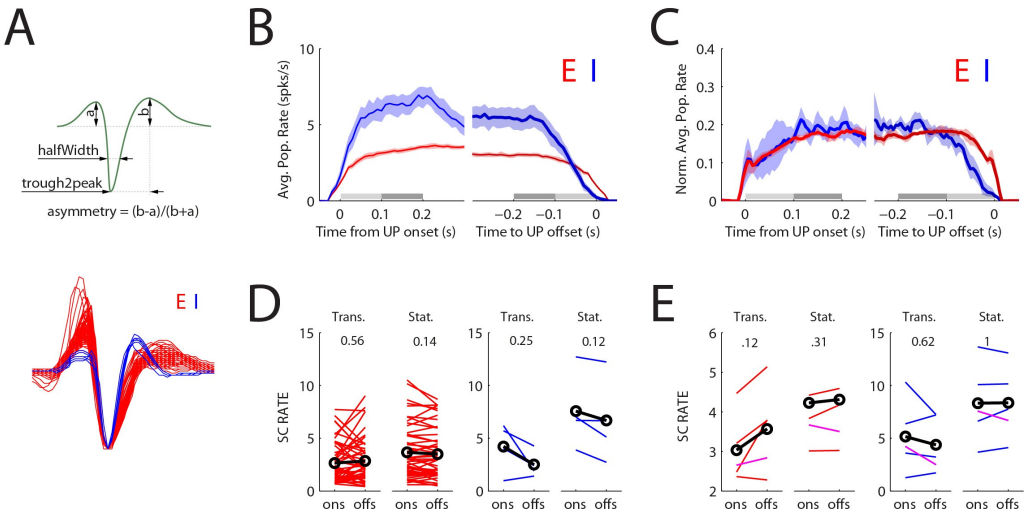

Figure 4.2.9. Dynamics of putative inhibitory (I) and excitatory (E) spiking activity during UP intervals. A, Classification into putative E and I neurons based on waveform. *Top*: definition of the three variables used to classify each waveform. *Middle:* representation of the waveforms in the 3D space defined by those variables shows two separate clusters. *Bottom:* average waveform for each cells colored according to the classification. **B,** Averaged E and I population rates aligned at the onset ($R^{E}_{on}(t)$ and $R^{I}_{on}(t)$, blue and red repectively) and at the offset ($R^{E}_{off}(t)$ and $R^{i}_{off}(t)$) for an example experiment. **C,** Same as in B but with normalized population rates. **D,** Individual firing rates aligned at the onset and offset, compared in the transient (left) and the stationary (right) windows for all cells in the example experiment (each line compares $r_{j,on}$ vs. $r_{j,off}$ of one neuron; average across cells shown in black). **E,** Average rates across neurons for the conditions described in D (black lines) across different experiments. Error bars represent 95% CI. Numbers over each panel indicated the *p* value of the Wilcoxon signed rank test.

population of recorded cells from each experiment into two groups based on a k-means clustering algorithm: putative E cells and putative I cells (Fig. 4.2.9A). The onset-aligned averaged rate for E and I populations, $R^{E}_{on}(t)$ and $R^{I}_{on}(t)$ respectively, displayed relatively similar profiles although the average firing rates were higher for I neurons (Fig. 4.2.9B). However, for the offset-aligned condition the profiles of $R^{E}_{off}(t)$ and $R^{I}_{off}(t)$ were quite different: $R^{I}_{off}(t)$ decreased with an approximately constant slope from around 150ms before the offset, whereas $R^{E}_{off}(t)$ seemed to decrease after $R^{i}_{off}(t)$ and it did so in a more abrupt way (Fig. 4.2.9B). This difference is particularly noticeable when the rates are normalized by the area under the curves to remove differences in the overall magnitude (Fig. 4.2.9.C).

We then compared the average firing rates for individual E and I neurons at the transient and stationary periods for the onset and offset aligned condition. We

found no significant differences neither for E nor for I neurons (Fig. 4.2.9D example experiment from panel A-B; Fig. 4.2.9.E mean rates for I and E are compared across experiments). Note, however that the small number of I neurons identified in our recordings could compromise the detection of a possible rate effect in this neuronal type. As we will see in the following chapter, our computational model makes a specific prediction regarding the rate dynamics during Us for I neurons, which would require additional experiments to be tested.

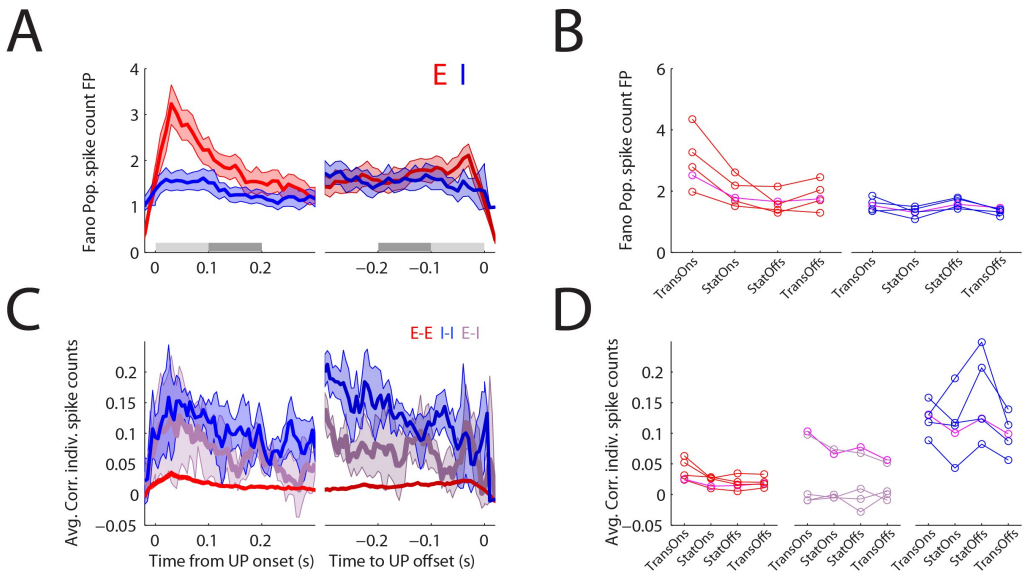

Figure 4.2.10. Instantaneous second order statistics of putative inhibitory (I) and excitatory (E) spiking activity during UP intervals. A, Fano factor of the E and I population spike counts from the example experiment (count window T=20ms). **B,** Summary results across n = 5 experiments of the population Fano factor aligned at the onset and offset for the transient and stationary windows. **C,** Instantaneous mean pair-wise correlation coefficient across E-E (red), I-I (blue) and E-I (purple) pairs of neurons from the example experiment aligned at the onset and offset. **D,** Summary results across experiments for the average instantaneous mean pair-wise correlation for the E-E (left), E-I (center) and I-I (right) pairs aligned at the onset and offset for the transient and stationary windows.

We finally studied the temporal dynamics of the variability and correlations for the I and E populations (as done in Fig. 4.2.8 for all neurons combined). The E population Fano factor showed the surge in variability across Us at the onset, whereas the I population Fano factor remained relatively flat (Fig. 4.2.10.A, single experiment; Fig. 4.2.10.B, all experiments). We also computed the instantaneous mean correlation coefficient for E-E, I-I and E-I pairs of neurons (Fig. 4.2.10C). Our results for all experiments showed that correlations in I-I pairs were higher than in E-E pairs and both were positive, whereas correlations in E-I pairs for 2 experiments were positive and for 3 experiments were around zero (Fig. 4.2.10D). Stronger correlations in I-I pairs during Us have been reported in the past (Hasenstaub et al., 2005) and have commonly been explained by the existence of gap junctions among fast spiking cells (Galarreta and Hestrin, 1999; Lewis and Rinzel, 2003). In the next chapter we present a model which proposes a novel explanation for this difference based on differences in the transfer function of I and E cells.

Appendix

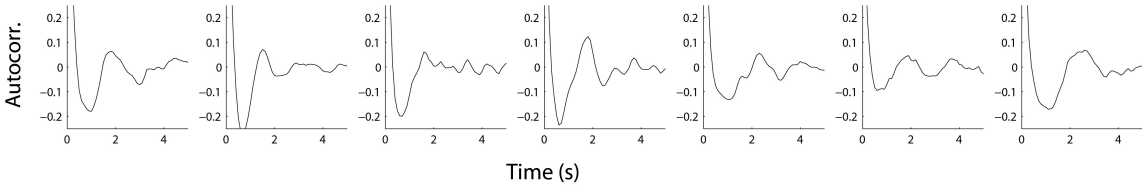

Figure A1. Individual MUA ACGs for the different experiments (n=7) from Chapter 4.2 shown in different panels.

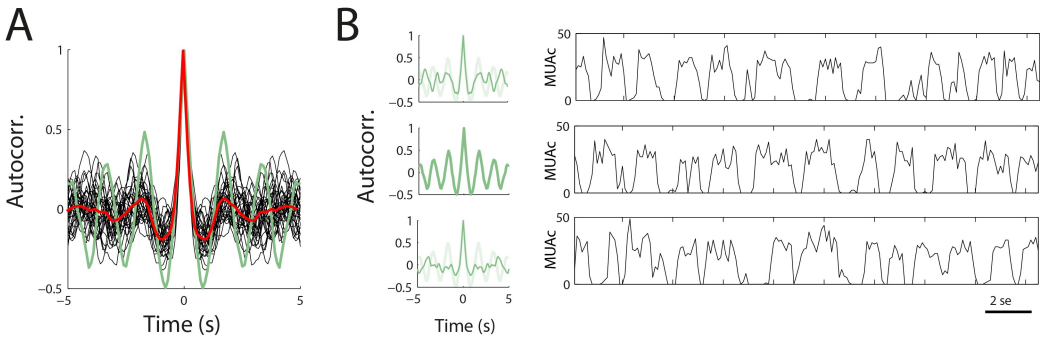

Figure A2. MUA ACGs computed in contiguous small 20 s windows. **A.** Individual ACGs in black and average in red. A particular single window ACG showing strong ringing is shown in green trace. **B,** Comparison of ACGs for the window with strong ringing in the ACG and the neighboring windows: previous 20 s (Top panels), the 20 s with strong ringin showed in A (Middle panels) and the following 20 s (Bottom panels). ACG (left) and MUA count traces (right) shown for each case.

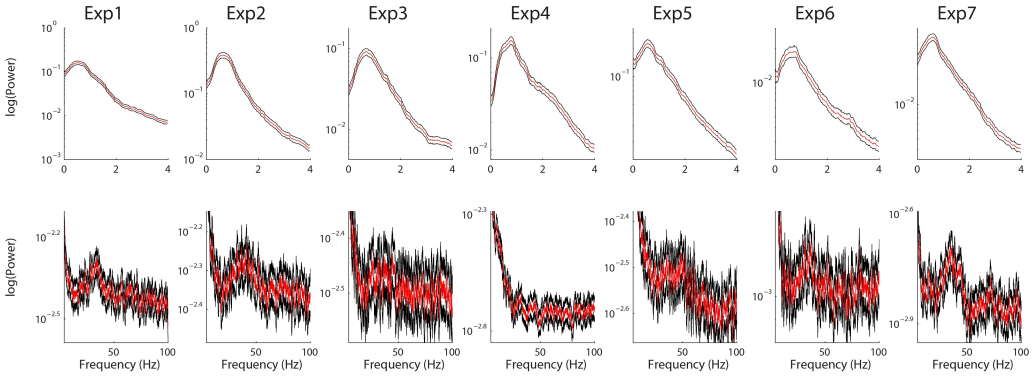

Figure A3. Power spectrum of MUAc during synchronized states of urethane anesthesia for the different experiments (columns) from Chapter 4.2. MUAc is computed in non overlapping windows of 30s, with a count window t=5ms. Averages in red, 95%CI indicated in black lines. Top Panels showing 0-4 Hz band, bottom panel showing 4-100 Hz. (nr. tapers=13, nw=7).

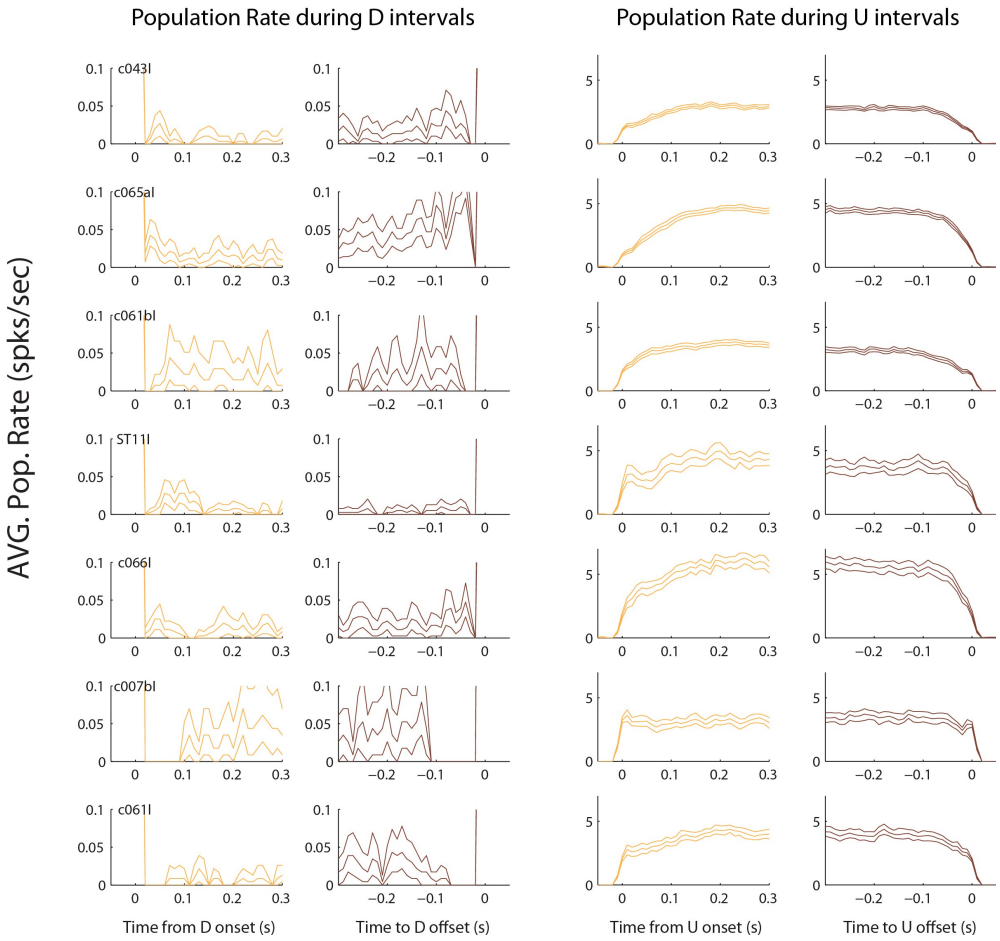

Figure A4. Population rates at onset and offset of DOWN and UP intervals for individual experiments (each row is a different experiment).

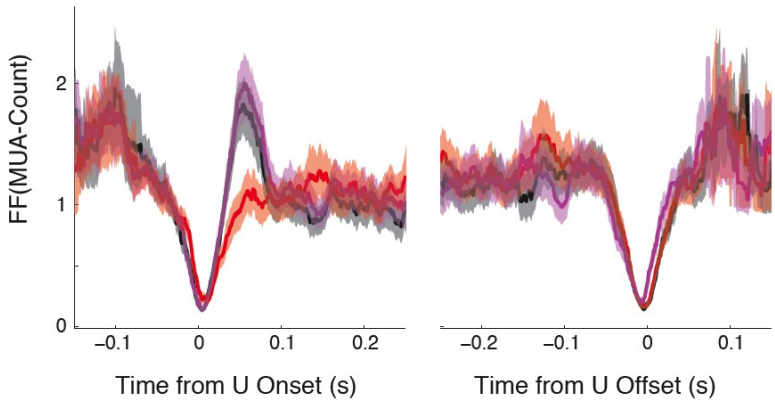

Figure A5. Surge on variability at U onset is not due to missalignment in the transition detection. As a control we repeated the entire analysis (U-D detection + spike stats.) in a surrogate data set obtained from the original data after removing the 100 ms after each U onset (red) or before each U offset (violet). The peak in the FF was only present when the initial 100ms of each U state were included in the analysis. This implies that the FF peak cannot be attributed to imprecision in the U onset alignment.

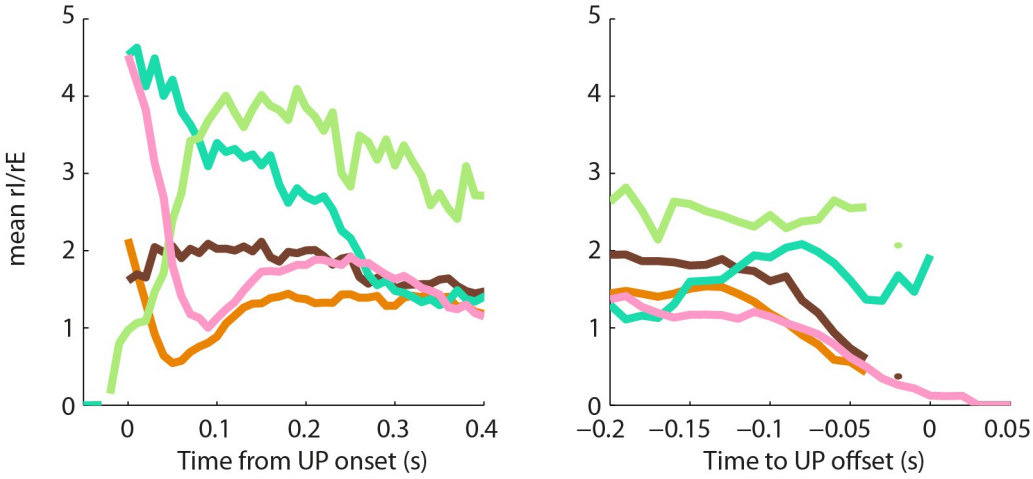

Figure A6 Ratio between the average pop. rate of putative I and E putative neurons (spks/s) for the differents experiments.

4.3. Exploring the mechanisms underlying cortical UP and DOWN dynamics

In the previous chapter we showed that the statistics of UP and DOWN states activity is consistent with both adaptation and random fluctuation mechanisms causing transitions between the two states. On the one hand, the existence of positive correlations between consecutive UP-DOWN permanence times suggests the presence of an adaptation mechanism involved in the transitions between UP and DOWN states. On the other hand, the variability obtained in the permanence times in each state was high, and the firing rates were relatively stationary and without signatures in the spiking statistics as UP state progresses predicting a transition to a DOWN state, which is all consistent with fluctuation mechanisms causing transitions in a bistable regime. In this Chapter we study from a computational perspective the contribution of each aforementioned mechanism to the UP and DOWN state statistics. We propose a simple computational model implementing both mechanisms, which can generate UP and DOWN dynamics based on a novel bistability regime that relies on a low-rate inhibition-stabilized UP state. This model shows that the combination of strong random fluctuations and weak cellular adaptation provides a regime in which the statistics of transitions match those observed in the experimental *in vivo* data.

A novel bistability mechanism based on inhibition stabilization.

The network model proposed is based on the Wilson-Cowan model (Wilson and Cowan, 1972; Latham et al., 2000), and it can be derived as a mean-field approximation to two interconnected populations of excitatory (*E*) and inhibitory (*I*) neurons (Fig. 4.3.1.A). The two populations are recurrently connected and receive external constant inputs for each population θ_X, where $X=\{E,I\}$, and common fluctuations ξ_X of mean amplitude σ.

This rate model represents the dynamics of the excitatory population rate (r_E), inhibitory population rate (r_I) , and is described in Eq. 1.1-1.2, respectively:

$$\tau_E \dot{r_E} = -r_E + \phi_E\left(J_{EE} r_E - J_{EI} r_I + \theta_E + \sigma \xi_E\right) \quad (1.1)$$

$$\tau_I \dot{r_I} = -r_I + \phi_I\left(J_{IE} r_E - J_{II} r_I + \theta_I + \sigma \xi_I\right) \quad (1.2)$$

The time constants for each dynamical variable are denoted by τ_E, τ_I. The parameters J_{XY} , where X,Y=*{E,I}*, describe the strength of the respective connections (from Y to X). Each population receives constant external input θ_X. Each population receives a fluctuating input (ξ_X) and σ defines the amplitude of

these fluctuations. The transfer functions Φ_X are described by piece-wise linear functions, in which the gains and thresholds are defined by α_X and ω_X, respectively:

$$\phi_X(k)=\left[\alpha_X k-\omega_X\right]_+ \qquad ,X=\{E,I\} \qquad (1.3)$$

An appropriate selection of the connectivity, transfer functions and time constant parameters leads to a bistable regime, and the critical conditions for the emergence of this bistability is that firing threshold and gain for inhibitory neurons is higher than the threshold and gain for excitatory neurons. This can be understood graphically in the 2-dimensional phase plane r_E vs r_I, where E and I nullclines of the system are obtained by setting the right side of Eq. 1.1 and 1.2 equal to zero (Fig. 4.3.1C; E-nullcline in red, I-nullcline in blue). Both E and I nullclines determine 3 fixed-points (Fig 4.3.1.C, circles) from which 2 of them are stable solutions of the system (Fig 4.3.1.C, filled circles) and one is an unstable solution (Fig 1.C, empty circle). The phase plane is divided into 2 different regions split by the separatrix of

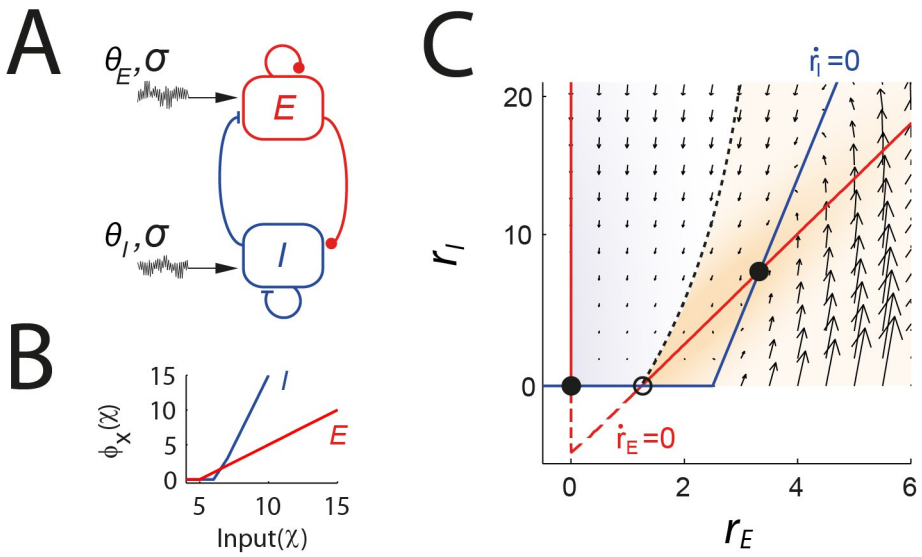

Figure 4.3.1. A novel bistability mechanism based on inhibition stabilizations. A, Scheme of the network architecture. **B,** Transfer functions for the E and I populations. **C,** Phase plane analysis (r_E vs r_I). E-nullcline (red) and I-nullcline (blue) intersections define the fixed points of the system (circles), where 2 of them are stable (filled circles) and 1 unstable (empty circle). The separatrix (dashed line) divides the phase plane into 2 different semi-planes (indicated in violet and orange colors). According to the separatrix, given an initial condition the system relaxes towards the stable fixed-point of the corresponding semi-plane. black arrows indicate the flow of the system, which are indicative of the trajectories described by the network relaxation dynamics in the absence of noise, (i.e. $\sigma=0$). Parameters: $\alpha_E=1$, $\alpha_I=4$, $\omega_E=5$, $\omega_I=25$, $J_{EE}=5$, $J_{EI}=1$, $J_{iE}=10$, $J_{II}=0.5$, $\theta_E=0$, $\theta_I=0$, $\tau_E=10$, $\tau_I=2$, $\tau_N=1$, $\sigma=0$ are maintained for the rest of the Chapter if not specified.

the system (Fig. 4.3.1.C, dashed line). Thus, depending on the initial conditions for r_I and r_E, the network evolves towards one of the two steady state solutions determined by the positions of the stable fixed-points. Notice that modifying the

threshold values ω_X in the transfer functions of the *E* and *I* populations does not change the slope of the nullclines, but rather produces their displacement in the vertical (for the *E*-nullcline) and horizontal (for the *I*-nullcline) axis. It is also clear in this representation that a critical condition to obtain bistability is that the inhibitory threshold is sufficiently high and that the effective gain of the inhibitory nullcline (which depends on both the transfer function gain a_I and the connectivity couplings J_{II} and J_{IE}) is larger than that of the excitatory nullcline. Moreover, by tuning these thresholds and effective gains it is possible to achieve bistable states of r_E and r_I at arbitrary low values. For the remainder of this chapter, we will focus on this bistable regime, and we assume higher gain for the inhibitory than excitatory populations, i.e. $\alpha_E < \alpha_I$, and higher threshold for the *I* population, i.e. $\omega_E < \omega_I$ (Fig. 4.3.1B). Notably, these conditions are supported by electrophysiological data in cortical slices in vitro (Schiff and Reyes, 2012).

The role of random fluctuations in generating UP and DOWN transitions

In this bistable scenario, we turned to consider the role of random fluctuating inputs in generating UP and DOWN transitions. These inputs are assumed to reflect neural activity in other brain areas, non-correlated with the network's internal dynamics. We modeled this as an Ornstein-Uhlenbeck process with zero mean $d\xi_X(t) = -\xi_X/\tau_N\, dt + s\, dW_t$, where W_t is the Wiener process or Brownian motion, and τ_N is the time constant of the fluctuations (typically $\tau_N = 1$). We assume for the rest of the Chapter that the time constant units represent milliseconds.

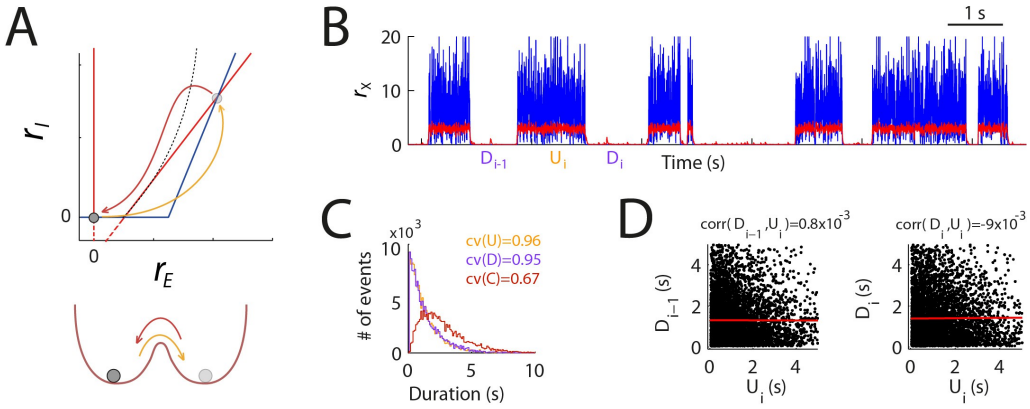

Figure 4.3.2. Fluctuations induced transitions in the bistable regime. A, Rates from E and I, in red and blue respectively, as a function of time. **B,** Distribution of permanence times: DOWN in violet, UP in orange, Cycle (defined as $D_{i-1}+U_i$) in brown. CV values are displayed in legend. **C,** Correlation of the permanence time in consecutive periods (Left: D_{i-1},U_i , Right: D_i ,U_i). Parameters: $\theta_E = -0.5$, $\sigma = 3$.

If the network is in one of the two stable states (UP or DOWN) in the bistable regime, a large enough incoming fluctuation (ξ) can perturb the system, making it cross the separatrix and, therefore, produce a transition from one to the

other state (Fig. 4.3.2A). This effect can be interpreted from a physical perspective as a potential energy landscape conformed by a double-well representing the two states, in which external fluctuations produce transitions from one to the other state (Fig. 4.3.2A, Bottom). A critical parameter therefore for the effectiveness of random fluctuations in producing these transitions is the amplitude of the fluctuations σ, which needs to be sufficiently large to reach the separatrix from each of the stable fixed points of the system (Fig. 4.3.2A). However, this is not the only relevant parameter. It is also important that the timescale of the fluctuations is at least of the same order of magnitude as those of the rates in order to make fluctuations effective in producing transitions among the states. Thus, taking into account this considerations, we can find a set of parameters in which stochastic transitions between UP and DOWN states occur (Fig. 4.3.2B).

In this fluctuation induced transitions scenario we achieve a very high irregularity in the duration of UP and DOWN states: the distributions of dwell times are exponential, with high CV values close to 1 (Fig. 4.3.2C). However, correlations between consecutive UP and DOWN durations are zero: Since transitions occur at random times based on the random occurrence of large current fluctuations, the duration of a given DOWN (UP) state is totally uncorrelated with the subsequent UP (DOWN) state (Fig. 4.3.2D). This is in disagreement with our experimental analysis shown in Chapter 4.2, since we found that correlations between adjacent durations were systematically positive. We thus conclude that a pure fluctuation-driven mechanism in a bistable system is not a good description for the cortical UP and DOWN state dynamics observed *in vivo*.

A model for UP and Down dynamics

We next introduce an adaptation mechanism in the system to study the impact of this particular mechanism in the UP and DOWN dynamics. We add spike frequency adaptation to the excitatory population *E*: it receives a negative feedback from an adaptation variable (*a*) that grows with the activity of the *E* population (Eq. 1.4 & 1.6, Fig. 4.3.3A). We did not consider an analogous negative feedback for the inhibitory population I for simplicity (Eq. 1.5 is equal to Eq. 1.2), and because inhibitory neurons show little or no spike frequency adaptation when depolarized with current injections (McCormick et al., 1985). The dynamics for the adaptation variable is described by Eq. 1.6, and the system now is described by:

$$\tau_E \dot{r_E} = -r_E + \phi_E\left(J_{EE} r_E - J_{EI} r_I - a + \theta_E + \sigma\xi_E\right) \quad (1.4)$$

$$\tau_I \dot{r_I} = -r_I + \phi_I\left(J_{IE} r_E - J_{II} r_I + \theta_I + \sigma\xi_I\right) \quad (1.5)$$

$$\tau_a \dot{a} = -a + \beta r_E \quad (1.6)$$

The time constant of the adaptation variable is denoted by τ_a. The parameter β describes the strength of the adaptation affecting the *E* population. We further assume that the time constant for the adaptation is much larger (2 orders of magnitude larger) than the *E* and *I* time constants, i.e. $\tau_a << \{\tau_E, \tau_I\}$ (Latham et al., 2000).This allows us to dissect the system into fast (r_E, r_I) and slow (*a*) components: r_E and r_I relax rapidly to their steady-state while *a* is slow enough to be considered

constant in the r_E, r_I dynamics (Rinzel and Lee, 1987; Latham et al., 2000).

We first describe the effect produced by the adaptation a while fluctuations in the system are suppressed (σ=0). The effect produced by increasing a is a downward displacement of the E-nullcline. Thus, if a is large enough the UP state fixed point loses the stability and the only stable fixed-point is the DOWN state (Fig. 4.3.3B, Top). In the same way as before, this effect can be interpreted from a physical perspective as a potential energy landscape conformed by a double-well representing the two states, but now adaptation deforms the wells producing transitions from one state to another (Fig. 4.3.3B, Bottom).

In this way, the increase and decrease of the adaptation variable a following its own deterministic dynamics can induce transitions between the quiescent and elevated firing rate states. Indeed, we can find parameters of β, θ_E, and θ_I, such that UP and DOWN state dynamics emerges in the absence of noise, driven by the negative feedback from a (Fig. 4.3.3C, top panel shows the values of r_X as a function of time in arbitrary units and the bottom panel shows the time course of adaptation a). When adaptation is recovered, the system shows a single high-rate stable fixed point and rates relax towards this stable solution (Fig. 4.3.3C, yellow-box inset). As soon as the network is in this UP state, adaptation accumulates displacing downwards the E-nullcline, and a second stable fixed-point emerges at r_E=0, r_I=0 which corresponds to the DOWN state (Fig. 4.3.3C, black-box inset). As the E-nullcline continues moving downwards driven by adaptation, the intersection between the E and I nullclines at (r_E>0, r_I>0) eventually disappears. At this point the UP state loses stability and the network relaxes towards the only remaining stable fixed-point, the DOWN state (Fig. 4.3.3C, dark red-box inset). While the system remains in the DOWN state, the adaptation variable a recovers so that the E-nullcline moves upwards, and eventually a second stable fixed point at the UP state emerges (Fig. 4.3.3C, analogous to black-box inset). At some point the adaptation is low enough to make the intersection determining the fixed-point of the DOWN state disappear, the system loses stability in the DOWN state and it transitions again to the UP state, thus initiating a new cycle (Fig. 4.3.3C, yellow-box inset).

Interestingly, a particular feature of this model is that although the adaptation mechanism is introduced only in the E population, it is the firing rate of the I population the one that presents a more pronounced rate decay during the UP state. This is a direct consequence of the specific conditions that allow for bistability in our model: the higher threshold and gain in the I-nullcline impose that r_I decays from the initial value achieved at the UP onset all the way to zero rate at the moment of the UP-to-DOWN transition, while r_E shows a decay going from the rate reached at the onset to the value of rate determined by the knee of the I-nullcline (see gray inset in Fig. 4.3.3C). Thus, increasing the slope of the I-nullcline would reduce even more the rate decay during UP states observed in the E population. A particularly pronounced decay of firing rates in inhibitory neurons would thus be a signature of the role of cellular adaptation in excitatory neurons in driving UP and DOWN dynamics, according to our model. We will study this particular feature later in the present Chapter.

This regime of adaptation induced transitions generates oscillatory network activity with deterministic UP and DOWN state transitions. As a result, permanence times in each state are constant and do not display any variability (CV=0).

Moreover, although adaptation provides a "memory" of the permanence time in the previous state, under the lack of variability the correlations are undefined. Both of these statistical features are also in contrast with our observations in the previous chapter of this Thesis.

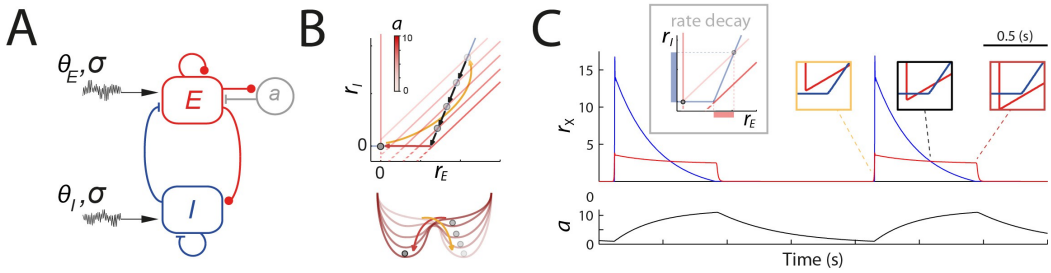

Figure 4.3.3. UP & DOWN states in the model induced by adaptation. A, Adding adaptation to the model. while supressing the effect of fluctuations (σ=0) **B,** Top: Effect of slow adaptation a in the phase plane. When a is small enough, the only fixed point is an elevated rate state (UP state), and the system relaxes towards it (orange arrow). As a increases (a depends on r_E), the E nullcline moves downwards and so does the UP state fixed point (following the black arrows). When a is large enough, the high-rate intersection of the E and I nullclines is lost and the system evolves to the only remaining stable fixed point, the DOWN state (following the dark red arrow). Bottom: Schematic representation of a double well inducing transition from UP to DOWN states. **C,** Transitions induced by adaptation in the model. The rates of E and I populations are displayed on top and the adaptation variable a on bottom panels, both as function of time. Parameters: τ_a=500, β=5, θ_E= 6**,** σ=0.

Although pure-adaptation or pure-fluctuation regimes cannot explain the statistics observed in UP and DOWN switching *in vivo*, the scenario changes when both mechanisms are intermixed (Fig. 4.3.4). In this case, the adaptation-induced transitions (oscillatory) regime (b>0) under the presence of fluctuations (σ>0) can generate variability in the permanence times (Fig. 4.3.4.B) and positive correlations between the dwell times in consecutive intervals (Fig. 4.3.4.C). Hence, a mixture of both mechanisms can explain the statistics that we observed experimentally (Chapter 4.2), at least qualitatively. In the following, we investigate in a quantitative way how the interplay between both mechanism impacts the statistics of UP and DOWN states permanence times.

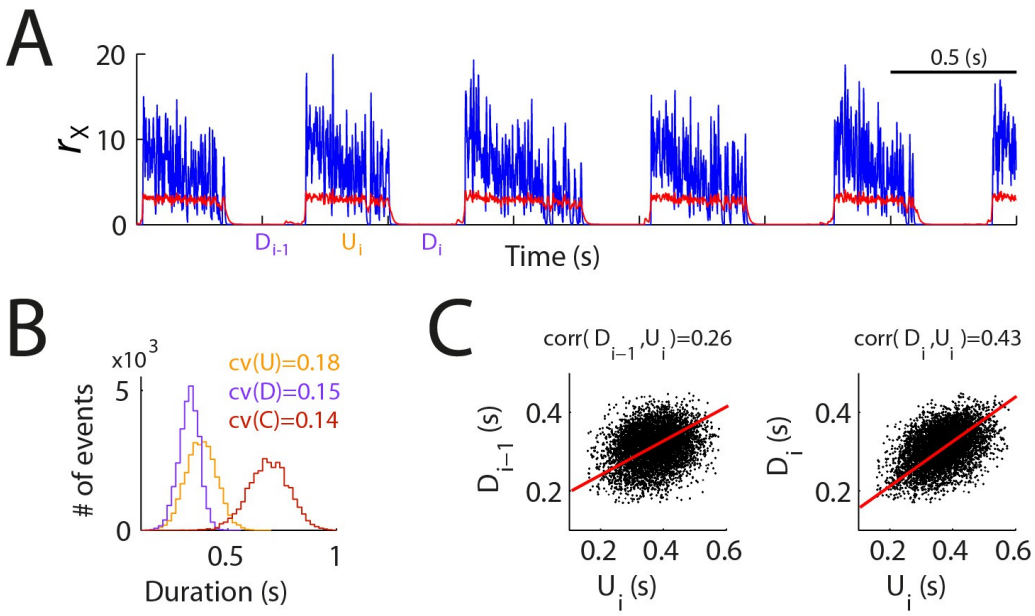

Figure 4.3.4. UP & DOWN states caused by adaptation + fluctuations. A, Rates from E and I, in red and blue respectively, as a function of time. **B,** Distribution of permanence times: DOWN in violet, UP in orange, Cycle (defined as $D_{i-1}+U_i$) in brown. CV values are displayed in legend. **C,** Correlation of the permanence time in consecutive periods (Left: D_{i-1},U_i , Right: D_i ,U_i). Parameters: β=5, θ_E= 8, σ=2.

UP and DOWN state statistics for different regimes

Although until this point we considered the stability analysis by doing the fast/slow dissection and freezing *a*, for the following analysis we incorporate the slow analysis to the dynamics. We analyze the different regimes of activity obtained by modifying the strength of adaptation (β), and the input to the excitatory population (θ_E) in the absence of fluctuations σ=0. Instead of dissecting fast/slow variables and freezing *a* in the dynamics for the stability analysis, as we did before, we now incorporate the slow variable in the dynamics. Based on the nullcline equations, the simplicity of the system permits to easily obtain the different regimes that arise by changing β and θ_E , which are summarized in Fig. 4.3.5.A. Here, we consider stationary a state if adaptation is unable to make the system transition away from it, while a non-stationary state is a fixed-point that is stable temporarily while adaptation increases or decreases, but eventually loses stability to the other state due to adaptation dynamics. In the absence of random fluctuations, six qualitatively different regions are observed: 1. single stationary DOWN (in dark blue); 2. stationary-DOWN nonstationary-UP (light blue); 3. nonstationary-DOWN stationary-UP (light brown); 4. single stationary UP (dark brown); 5. nonstationary-DOWN nonstationary-UP or oscillatory (green); 6. stationary-DOWN stationary-UP or bistable (pink). The bifurcation diagrams of r_E (in red) and r_I (in blue) showing the existence of stationary states as a function of the input θ_E for three different values of β={0,3,6}, are shown in Fig. 4.3.5.B. This summarizes how the stationary rates are modified as θ_E changes in the absence of fluctuations.

When β is increased, the range in θ_E with co-stationary states (where both the DOWN and UP states are stationary) is reduced (Fig. 4.3.5B, middle and bottom panels, range indicated by horizontal pink lines). When β is large enough (β>4) the range θ_E values for co-stationary states (bistable range) vanishes and an oscillatory regime emerges for a range of θ_E values (Fig. 4.3.5B, horizontal green line in top panel). Once the system dynamics is considered in the presence of random fluctuations, transitions can be caused by either fluctuations+adaptation if a stationary state is present, or purely by fluctuations, if both states are non-stationary (i.e., adaptation is unable to cause a transition on its own) (Fig. 4.3.5A, see arrow code). In this way, it is expected that the time spent on a stationary state will be more variable than in a non-stationary state. Indeed, while stochastic fluctuations are the only mechanism to move out of a stationary state, non-stationary states will on average decay away deterministically in a time scale of the range of τ_a and the stochasticity of the fluctuations gets diluted in the regularity of deterministic adaptation. For this reason, we expect to find regimes compatible with the high irregularity in both UP and DOWN durations observed experimentally in the co-stationary or bistable regimes represented by the pink region in Fig. 4.3.5A or the bistable ranges of Fig. 4.3.5B, i.e. for relatively low adaptation strength β. We thus turned to testing this in numeric simulations with different amplitudes of random input fluctuations.

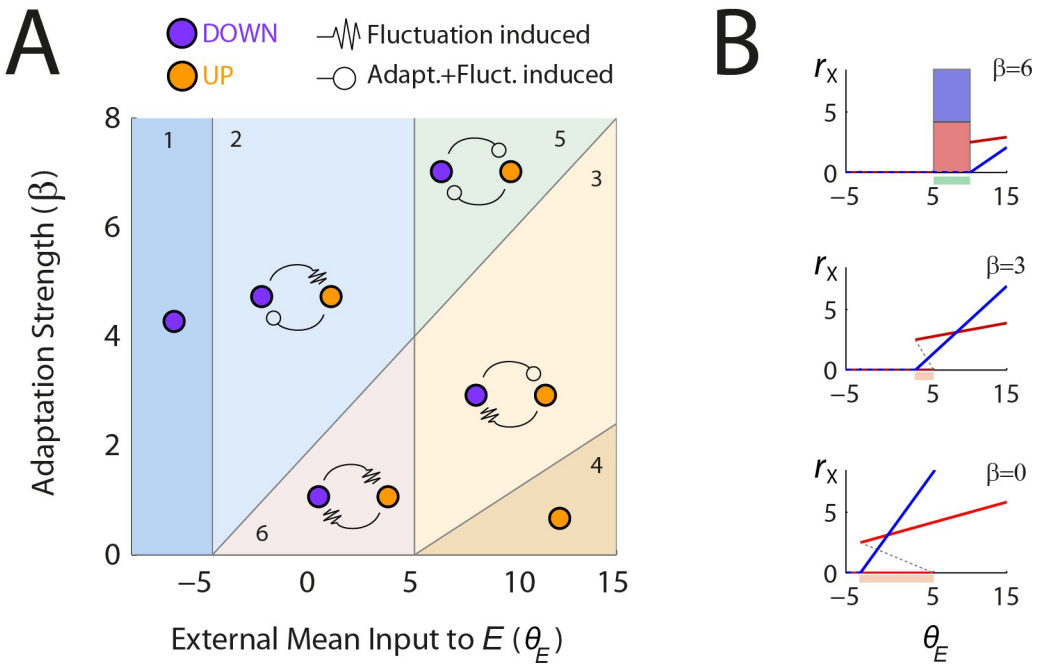

Figure 4.3.5. Different dynamical regimes in the model. A, Six regimes of activity as function of β and θ_E. Violet and orange circles represent the presence of DOWN and UP states. Each state can be stationary or meta-stationary according to if transitions from that state are induced by fluctuations or adaptation+fluctuations, respectively (see arrow code legend). **B,** Bifurcation diagram for three values of β={6,3,0} showing r_E and r_I as a function of θ_E. Bistable range indicated by pink horizontal line. Oscillatory range indicated in green horizontal line and bicolor thick bar.

How do changes in β, θ_E, σ impact the statistics of UP and DOWN states permanence times? For the remainder of this section we denote the duration of UP and DOWN states U and D, respectively, as in the previous Chapter. We run long simulations of the model dynamics and we compute the statistics of U and D for each point in the (β, θ_E) plane and for different levels of the random fluctuations amplitude σ={0,1,2,3,4} (Fig. 4.3.6). We find that in order to obtain high

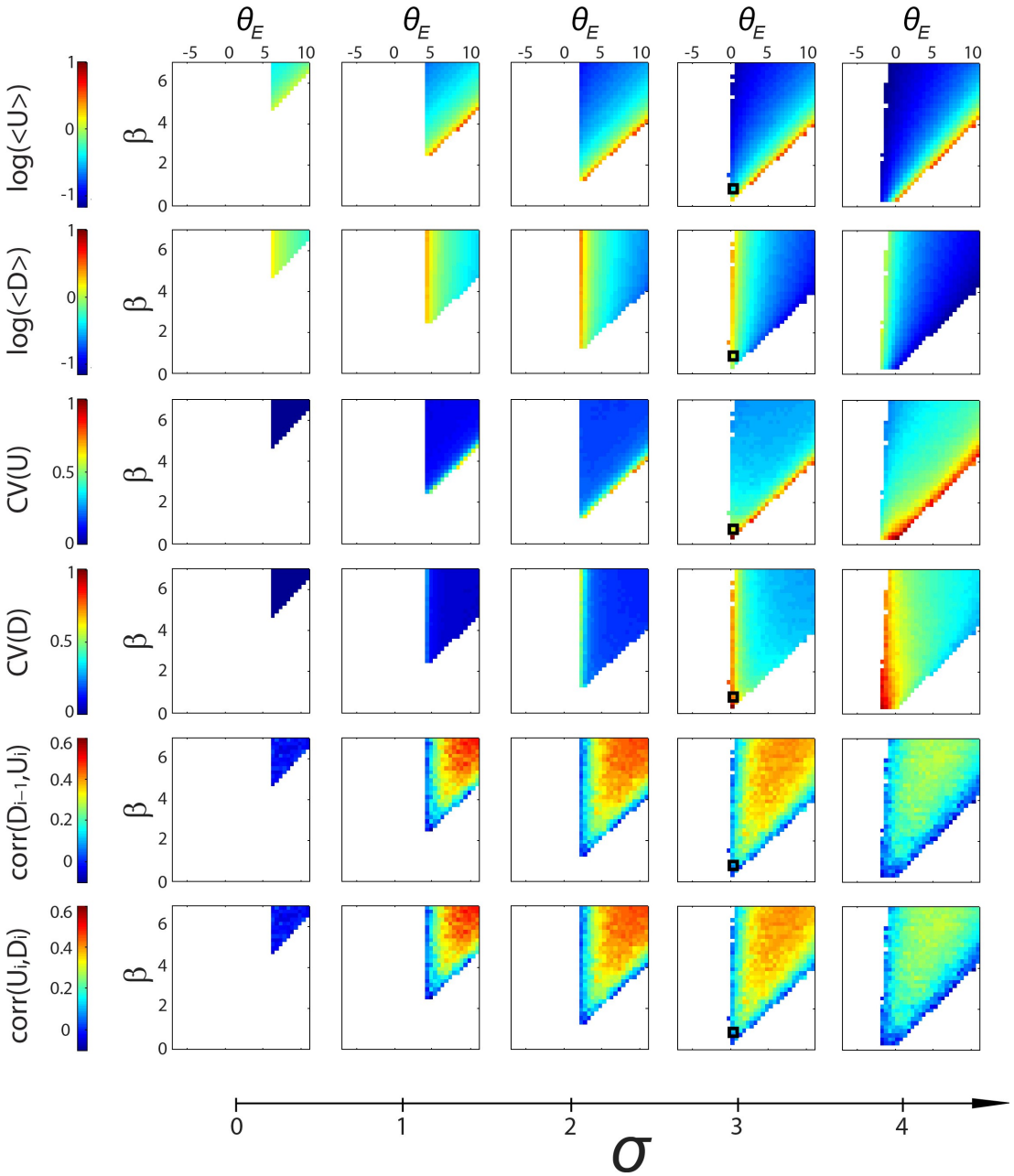

Figure 4.3.6. U and D statistics as a function of β, θ_E and σ. Each row of color plots correspond to the different statistic studied indicated at the left and together with the respective color scale for the row. The absence of color for a specific value of (β, θ_E) is due to the absence or low amount of transitions achieved during the simulations. From top row: logarithm of mean U, logarithm of mean D, CV of U, CV of D, correlation between consecutive D-U and between consecutive U-D. Each panel shows in colour plot the statistics obtained by changing β and θ_E. Different columns show the effect on the statistics of changing the amplitude of fluctuations.

variability in the permanence times (CV(U),CV(D) > 0.5), we must consider large fluctuation amplitudes (with at least σ>3). On the other hand, we observe in Figure 4.3.5 that high values of CV(D) are achieved in the vertical edge while high values of CV(U) are achieved in the slanting edge of the region displaying UP and DOWN dynamics. Therefore, a regime in which both CV(U) and CV(D) are large enough (>0.5) implies low values of β (where the two aforementioned edges meet, see square mark on Fig. 4.3.6). This is the regime where the UP and DOWN state are co-stationary in the sense of Figure 4.3.5, i.e. both of them are stable with respect to the adaptation dynamics and only random fluctuations can cause transitions.

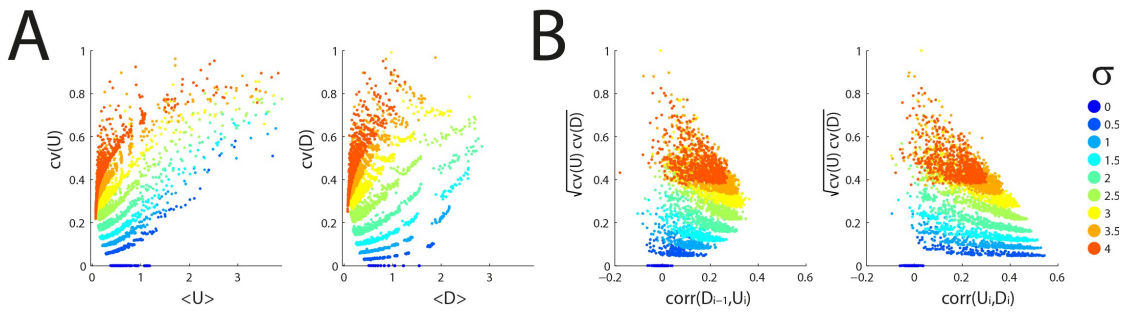

Figure 4.3.7. CV and correlation values for different amplitudes of fluctuations s. A, CV of U versus mean U on the left and CV of D versus mean D on the right. **B,** Correlation between consecutive D-U (left) and U-D (right) versus the square root of CV(U) times CV(D), as a measure of combined value of CV(U) and CV(D).

Although the range of high variability in U and D is increased for higher values of σ, the correlation between consecutive intervals decreases towards values of zero as σ increases. We study the role of fluctuations in determining the values of CV and correlations between consecutive UP/DOWN periods by pooling the results from different values of β and θ_E (Fig. 4.3.7). For different values of σ, we compute the CV changes for different values of mean permanence time in the UP or DOWN state (Fig. 4.3.6A left and right panels, respectively). Given that we are interested in a regime in which both CV(U) and CV(D) are high, we compute the correlation between consecutive intervals and we plot it against a measure of combined U and D variability ($\sqrt{cv(U)cv(D)}$) (Fig. 4.3.7.B). In this way, in order to achieve values of CV around 0.6 and positive correlation values around 0.1, as observed in the experimental data (see Chapter 2), we must consider σ >=3.

Altogether, this analysis suggests that a regime with random input fluctuations of high amplitude and weak adaptation will be able to match in our model the statistics of variability in the permanence time in each state and correlations between consecutive intervals observed in the experimental data (Chapter 2). Indeed, an example of a simulation in this particular regime is shown in Figure 4.3.8. Panel A shows the traces of r_E and r_I on top, while a is shown in the bottom panel. The contribution of adaptation is drastically reduced compared to the adaptation induced regime (Fig. 4.3.2.B), but its dynamics of accumulation during UP periods and recovery during DOWN periods have an impact on the D and U statistics. Panel B shows, on left, the distribution of permanence times of U and D and the cycle C, where the CV are 0.59, 0.66 and 0.48, respectively. Right panels

show the correlation between consecutive intervals, where corr(D_{i-1},U_i)=0.13 and corr(D_i,U_i)=0.14. Thus, this simulation presents both the high variability of U and D caused by random fluctuating inputs and the weak correlation between consecutive D and U of adaptation mechanisms. These statistics resemble those observed in our experimental data analysis in recordings in vivo (Chapter 4.2, see Fig. 4.2.2).

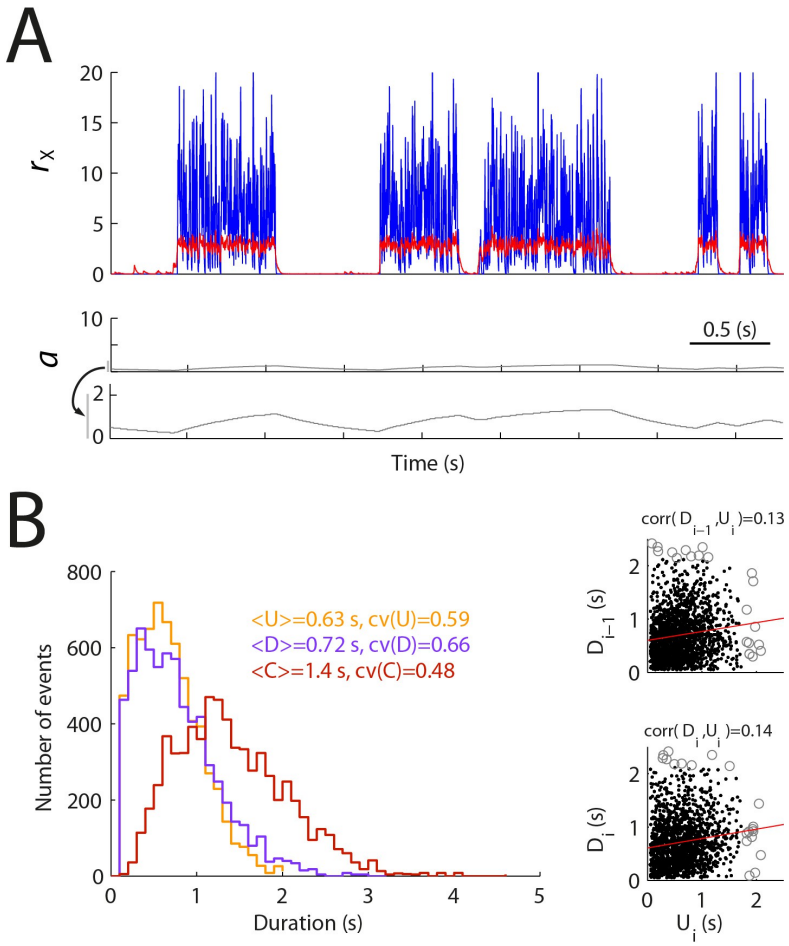

Figure 4.3.8. UP & DOWN states in the weak adaptation and strong fluctuation regime. A, The rates for *E* and *I* populations are shown on top and the adaptation variable on bottom (lowest panel is an expanded view). **B,** Left, distribution of permanence time (in arbitrary units) for U, D and C with mean and CV shown on the inset. Right, consecutive D-U periods (top) and U-D periods (bottom) are indicated in dots, and used to compute the correlation between the duration of consecutive periods (U or D values 3 standard deviations away from the mean are shown in circles and discarded for the correlation analysis). Parameters from this regime marked in black square in Figure 4.3.5. Parameters: β=0.5, θ_E= 0, σ=3.

Oscillations in the rate model

We want to characterize the dynamics of activity in the system during the UP state. Stability analysis of the high-rate solution (Appendix) shows that this model can produce a regime with oscillations occurring during the UP states, for slow enough inhibitory time constant τ_I (Brunel and Wang, 2003). Since we observe no clear stable oscillations in the firing rates during UP states in the experimental

data (Chapter 4.2), we assume for the rest of our analyses that we are not in such conditions, so that we take for our model $\tau_I < 7.5$ (Appendix). However, even in this condition the UP state shows some interesting transient dynamics: depending on parameters there is a more or less prominent rate peak at UP state onset or offset (Fgiure 4.3.9). We characterize this behavior in the phase plane of the full model of Figure 4.3.7. When the E-nullcline moves downwards during the UP state (*a* increases, or θ_E decreases) and the UP fixed-point gets closer to becoming unstable, the separatrix folds surrounding the UP fixed-point and reducing its basin of stability. This effect is more evident as the τ_I value is increased τ_I={2,..,7} (Fig. 4.3.9A). These effects in the phase plane explain the dynamics during UP states, as we discuss below.

When computing the mean rate at the onset and offset aligned conditions for simulations of the model, we observe that increasing the τ_I value generates peaks in firing rate at the transition times at the onset and offset of the UP state (Fig. 4.3.9B). The average trajectory in phase plane at the onset and offset of the UP states for a time interval of [-0.05,0.05] shows that at the UP onset average trajectories describe a spiral that becomes larger with τ_I, despite the strong presence of fluctuations (Fig. 4.3.9C, left). Also the offset average firing rate describes a spiral, of even larger amplitude (Fig. 4.3.9C, right). Although the oscillation described at the onset is related with the fact that the UP fixed point is a stable focus, the oscillation

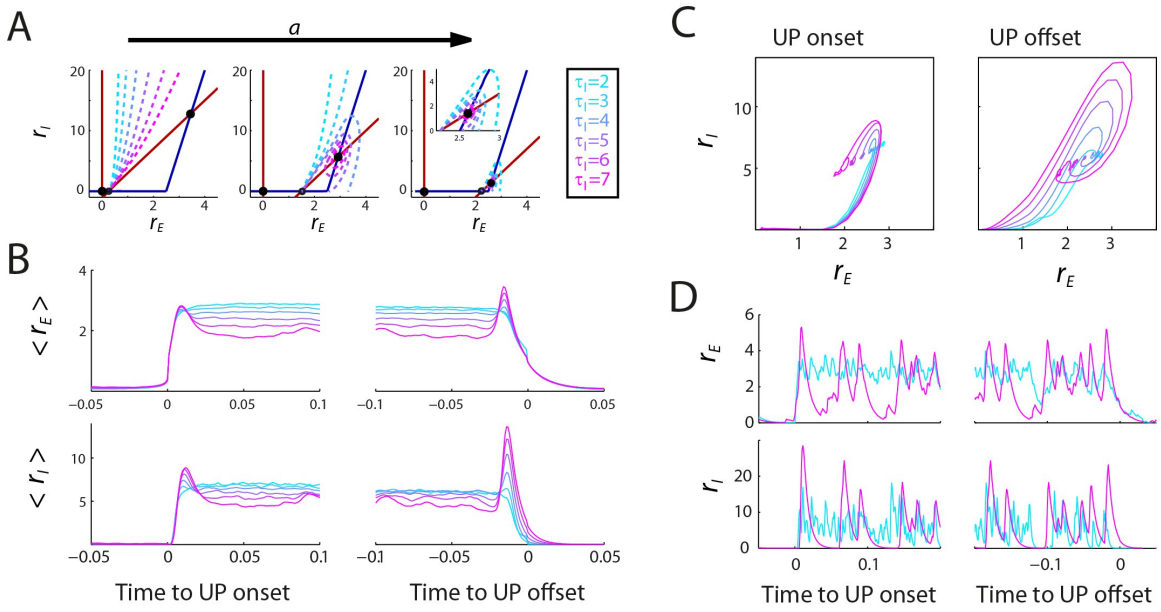

Figure 4.3.9. Dynamics of activity during UP states at onset and offset aligned conditions for different τ_I values. A, Phase plane and separatrix in dashed lines for different τ_I values and bistable scenarios. **B,** Mean rate for *E* (top) and *I* (bottom) populations at onset and offset aligned conditions for the model in the sweet-spot region of parameters. **C,** Mean average trajectories in the phase plane at time *t*=[-0.05,0.05] from transition time (same as in B). **D,** Example of activity from a single UP state for different τ_I (τ_I=2 in cyan, τ_I=7 in magenta) Parameters: β=0.5, θ_E= 0, σ=3.

described at the offset is produced by changes in the separatrix, which determines the way in which transitions from UP to DOWN states occur. Indeed, when the separatrix folds surrounding the UP fixed-point at UP state offset, positive large

fluctuations impinging on r_E will be effective in causing a transition to the DOWN state via a large spiral excursion (Fig. 4.3.9C, right). This analysis reveals that large values of τ_I, approaching the time constant of the E population, produce signatures at the temporal edges of UP states that we do not observe in the experimental data. We thus conclude that the regime observed experimentally corresponds to a condition of significantly faster inhibition than excitation, and we consider in the following the lower value of τ_I (=2ms), which does not induce ringing in the rates at the UP state transition times.

In these conditions of fast enough inhibition, the average firing rate aligned to UP state onset or offset shows little temporal dynamics (Fig. 4.3.9B, cyan traces). Adaptation seems insufficient to imprint a characteristic rate dynamics on the UP state. We analyzed this by considering two models, one has strong adaptation and weak fluctuations (Fig. 4.3.10A) and the other has strong fluctuations and weak adaptation (Fig. 4.3.10.B), which matches better the experimental data. For both regimes we observe a decay in r_E and r_I as the UP state progresses (Fig. 4.3.10.A-B, central panel). However, the decay in rate is especially prominent for the I population, and is barely observable in the E population in any of the two conditions. AThis can be illustrated directly in the ratio between r_I and r_E, which reveals that the decay in rate for the *I* population is stronger throughout the UP state

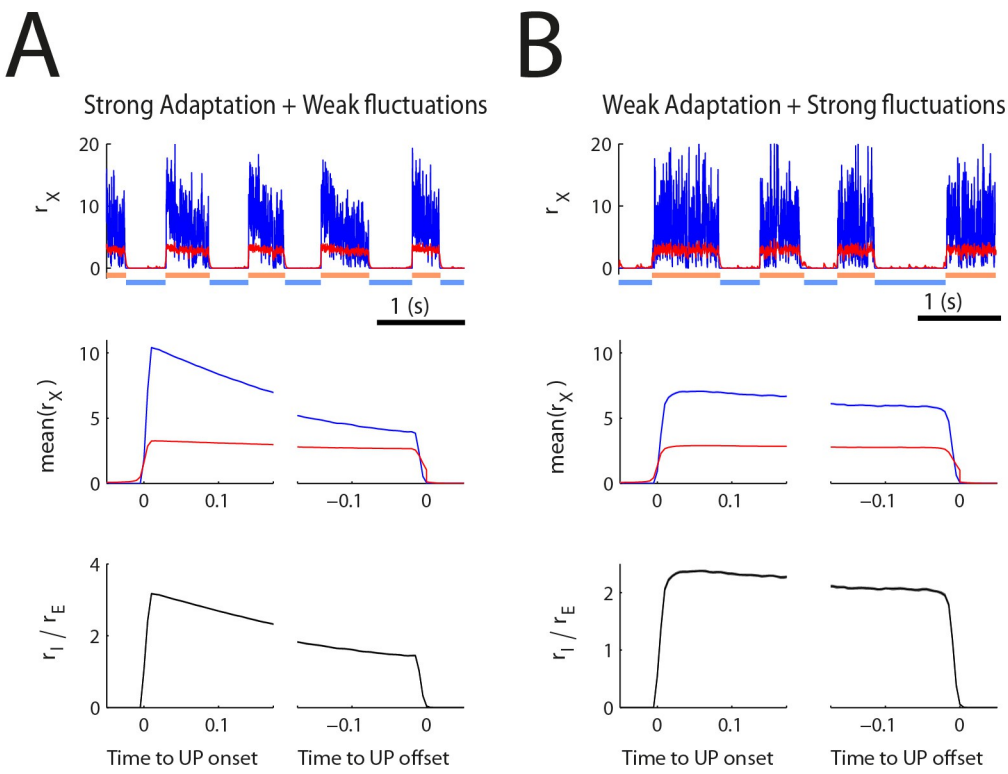

Figure 4.3.10. Dynamics of activity during UP states for adaptation and fluctuation driven regimes. A, Strong adaptation and weak fluctuation regime. Top: sample traces of r_I and r_E and UP and DOWN period detections (horizontal lines). Middle: mean rate of r_I and r_E for onset (left) and offset (right) aligned conditions. Bottom: ratio between r_I and r_E for onset and offset aligned conditions. **B,** Same plots as in A for the weak adaptation and strong fluctuation regime. Parameters A: β=4, θ_E= 6**,** σ=2; B: β=0.5, θ_E= 0**,** σ=3.

and for both models (Fig. 4.3.8A-B, bottom panel). This is related to the way in which bistability is achieved as previously mentioned (see Fig. 4.3.3C inset) Notice also that the UP offset is preceded by a faster decay towards zero for the *I* population, due to the faster decay time constant (τ_I) compared to the time constant from the *E* population (τ_E).

Temporal profile of variability during UP states in the model

We next studied the time course of neural variability across UP periods (quantified by the Fano Factor) and pairwise neuronal correlations through the UP state. We considered the onset and offset aligned conditions in the model, and we explored the impact of both mechanisms in the second order statistics.

In order to study those second order statistics, we assumed a population of inhomogeneous Poisson independent spike trains with a rate obtained from the output of the model simulations. Notice that, although we assume that all neurons are unrealistically describing the same firing rate, in this way we can define the Fano Factor and correlations (see Eq. 23 and 28, respectively, from Methods section 3.4).

We analyze two models corresponding to strong adaptation or strong fluctuation regimes (as in Fig. 4.3.10). For both models, the onset and offset of the UP states are associated with a transient increase in variability (Fig. 4.3.11). In the case of strong adaptation and weak fluctuations, the Fano Factor and correlation display a "ramp". This is due to two factors: On the one hand in this model there is a mean rate decay as the UP state progresses (Fig. 4.3.10). On the other hand, there is an increase in variance (Fig. 4.3.11A, top), due to the increasing instability of the

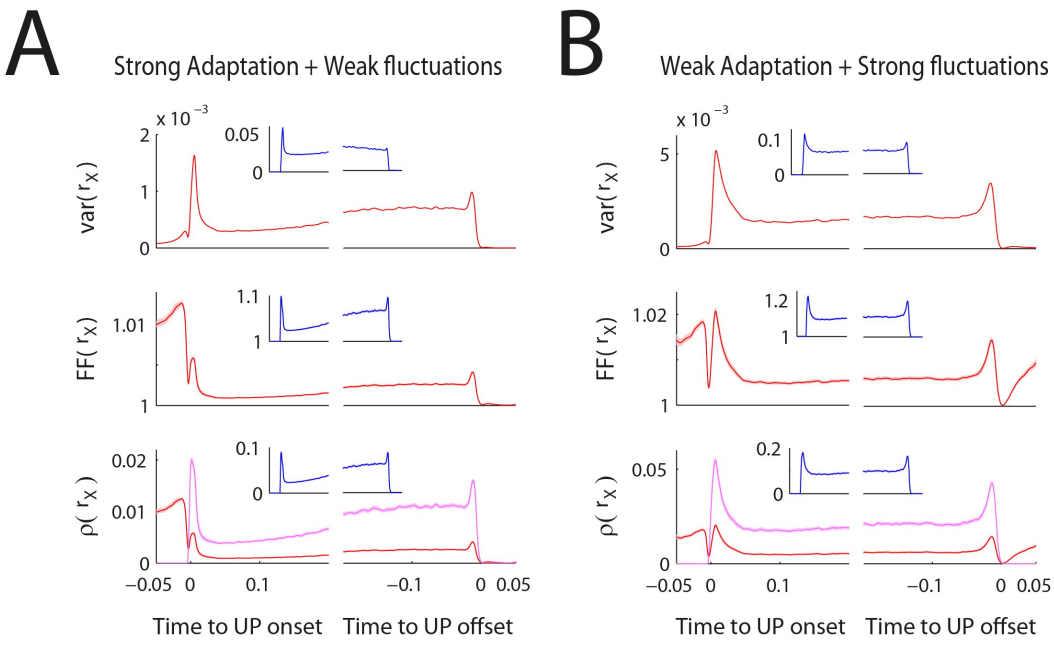

Figure 4.3.11. Dynamics of variability during UP states for adaptation and fluctuation driven regimes. A, Strong adaptation and weak fluctuations regime. **B,** Weak adaptation and strong fluctuations regime. From top to bottom: variance of rate r_E and r_I (inset), fano factor of the rate, correlations between r_E-r_E (red), r_E-r_I (magenta) and r_I-r_I (blue, inset).

UP produced by the adaptation process (Mattia and Sanchez-Vives, 2012). In the same way, a weak adaptation and strong fluctuations regime also displays this "ramp", but it is a weaker effect since both the mean rate and the variance of the rate during the UP state exhibit much weaker dynamics (4.3.10B, middle, and Fig. 4.3.11B, top).

The surge on variability observed for the *E* population at the UP onset condition precedes the UP onset, whereas the surge on variability for the UP to DOWN transition is observed only prior to the UP offset and after this transition the variability is reduced, reflecting an asymmetry in the way that the network evolves from one attractor state towards the other (Fig. 4.3.9A-B, middle and bottom panels). Although changes between the attractor states could be systematically associated with an increase in variability, the aforementioned asymmetry of this variability could be model dependent. Additionally, beside the surge of variability at the temporal edges of UP states, correlations display positive values generally with the highest values for r_I-r_I correlations and intermediate values for r_E-r_I correlations (Fig. 4.3.11A-B, bottom panels).

What is the origin of this surge of variability observed at the temporal edges of the UP states? To study the origin of this surge, we consider both weak adaptation and strong fluctuation regimes. We first analyze a possible role of the imprecision of

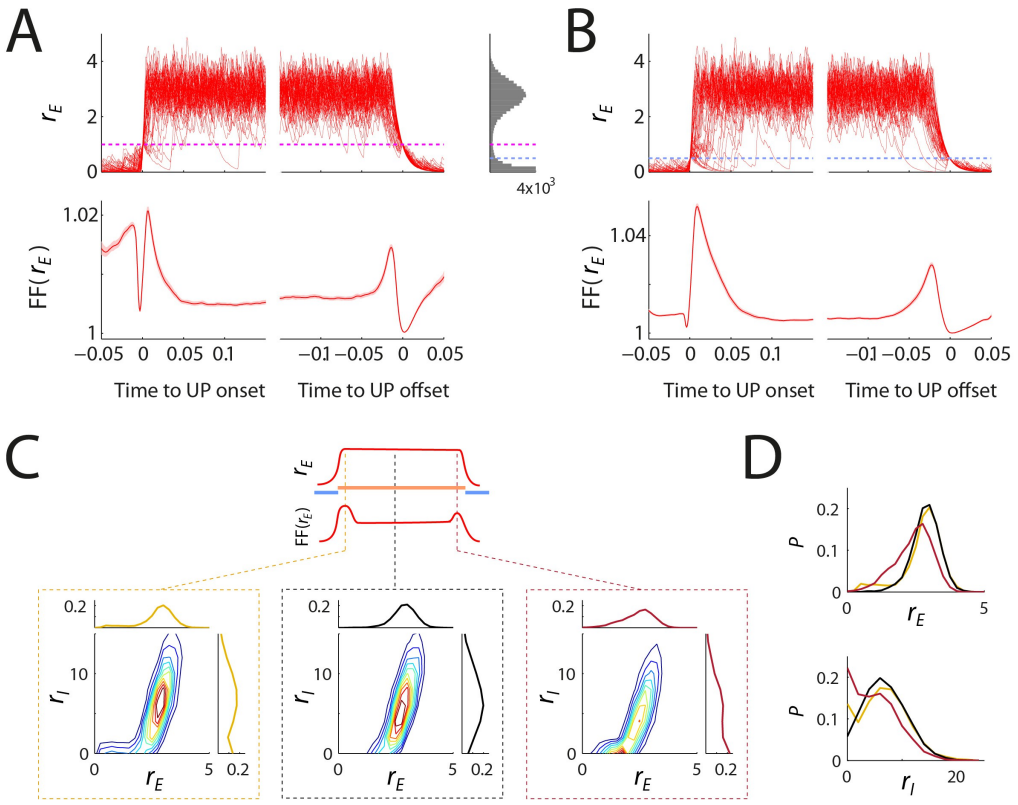

Figure 4.3.12. Asymmetry in the surge of variability associated with state transitions. A, Fano Factor and overlapped single UP traces when the detection threshold is set right at the trough of the r_E bimodal distribution. **B,** Same as A, but for threshold set at half of the trough of the r_E bimodal distribution. **C,** Contour values showing the joint and marginal *E*,*I* rate distributions at different time points: onset (orange), middle (black) and offset (dark red) of UP states. **D,** Comparison of marginal distributions for r_E and r_I shown in C.

UP-DOWN transition detection on this variability. We compare Fano Factor and rates for 2 different conditions: when the threshold for UP detection is set in the trough of the bimodal r_E distribution, and when the threshold is lowered at half of this value (Fig. 4.3.12A-B, respectively). Overlapping the r_E traces from different UP states for the onset and offset aligned conditions reveals that UP to DOWN transitions are less variable and are followed by more reduced activity than the DOWN to UP transitions (Fig. 4.3.12A). Moreover, when the detection threshold is reduced, it is observable the same behavior in the Fano Factor and rate traces (Fig. 4.3.12B). Therefore, it confirms that the surge on variability at the temporal edges of UP states is related to the variability of the rate trajectories at the transition times at onset and offset is not due to the detection method. Although we initially study this phenomenon on r_E, we observe an analogous effect on r_I when we consider the distribution of combined rates at the time of the surges occurrence, where marginal distributions are more skewed at the onset-surge than the middle-UP and offset-surge conditions (Fig. 4.3.12C). The surge in variability at the onset is therefore higher, and this is observed also when comparing the marginal distributions of the rates for both *E* and *I* populations (Fig. 4.3.12D). These results show that changes between states are associated with periods of increased rate variability in the model, and these transitions between the two states are asymmetric possibly due to the differences in the two basins of attraction.

Average time course of incoming fluctuations at transition times

To further investigate the role of fluctuations in transitions, we computed the transition-triggered (UP onset and offset) average fluctuations at the onset and offset in the strong fluctuation and weak adaptation regime. Typically, the onset of the UP state in the model is preceded by positive input fluctuations arriving to the *E* population. Instead, the average fluctuations to the *I* population are flat around UP state onset showing that incoming fluctuations to the *I* population do not play any role in the DOWN to UP transitions (Fig. 4.3.13.A, left panel). Before the positive fluctuations into the E population triggering the UP state, average fluctuations for the E population are biased below zero (Fig. 4.3.13.A, left panel inset). During the

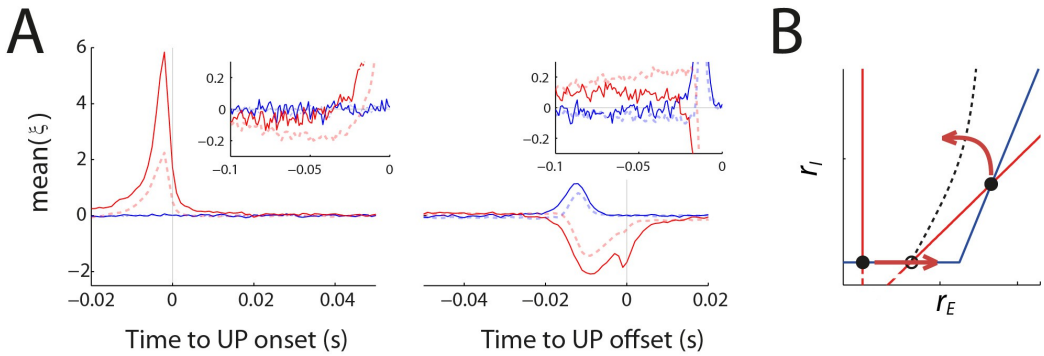

Figure 4.3.13. Transition triggered average fluctuations. A, Transition-triggered averages of time courses of the input fluctuations (ξ_X) to *E* and *I* populations (red and blue traces) the for weak adaptation strong fluctuations regime at the onset and offset aligned condition (dashed line is the results for strong adaptation weak fluctuations regime). **B,** Schematics of the more effective fluctuations causing transitions in the model.

UP state periods, fluctuations in the *E* population are above zero on average whereas fluctuations in the *I* population are below zero (Fig. 4.3.13A, right panel inset). UP state offset is preceded by a coincident positive incoming fluctuation to the *I* population followed by a negative fluctuation to the *E* population in order to drive the UP to DOWN transition (Fig. 4.3.13A, right panel). This is another asymmetry observable in the way that network transitions from one to the other attractor, and it is a robust feature of the model since it is also observable in the strong adaptation weak fluctuations regime (Fig. 4.3.13A, dashed line). Moreover, this analysis shows the way in which fluctuations are more effective to cause transitions in the model (Fig. 4.3.13B).

Appendix

Stability analysis. The stability of fixed points is determined not only by the connectivity of the network (J_{XY} values) but also by the time constant of the rate for the *E* and *I* populations (τ_E and τ_I, respectively). We explore how changes in the time constant of the *I* population impact the stability of UP states and the network dynamics during UP states. The behaviour of the dynamical system near a fixed point is determined by the eigenvalues of the Jacobian matrix of the dynamical system. If we consider $\beta=0$ and a regime with one fixed point in the UP (large enough θ_E), The eigenvalues of the system are given by Eq. 1.7:

$$\lambda=\frac{1}{2}\left(\frac{\alpha_E J_{EE}-1}{\tau_E}-\frac{\alpha_I J_{II}+1}{\tau_I}\pm\sqrt{\left(\frac{\alpha_E J_{EE}-1}{\tau_E}-\frac{\alpha_I J_{II}+1}{\tau_I}\right)^2-\frac{4\,\alpha_E\alpha_I J_{EI}J_{IE}}{\tau_E\tau_I}}\right) \quad (1.7)$$

Considering fixed $\tau_E=10$ and the previously defined connectivity, we vary the value of τ_I. For $\tau_I < 7.5$ the eigenvalues are complex with negative real part (Fig. 4.3.8.A), so that the UP state fixed point is a stable focus. This means that for an initial condition close to the fixed point the system describes a spiral trajectory in the phase plane collapsing into the UP state, thus producing damped rate oscillations as the rates from *E* and *I* settle down to the stable fixed point (Fig. 4.3.8.B). When $\tau_I > 7.5$, the real part of the complex eigenvalues becomes positive and the fixed point becomes an unstable focus: trajectories in the phase plane describe a spiral expanding outwards from the fixed point. Without any rectification in the transfer functions, the spiral would grow indefinitely (Fig. 4.3.8.C, dashed lines). However, the rectification non-linearity in the threshold transfer functions prevents the trajectory from expanding and it stabilizes a limit cycle (Fig. 4.3.8.C, solid lines). Additionally, under the presence of a DOWN state fixed point (in the bistable regime), these trajectories collapses into the DOWN state.

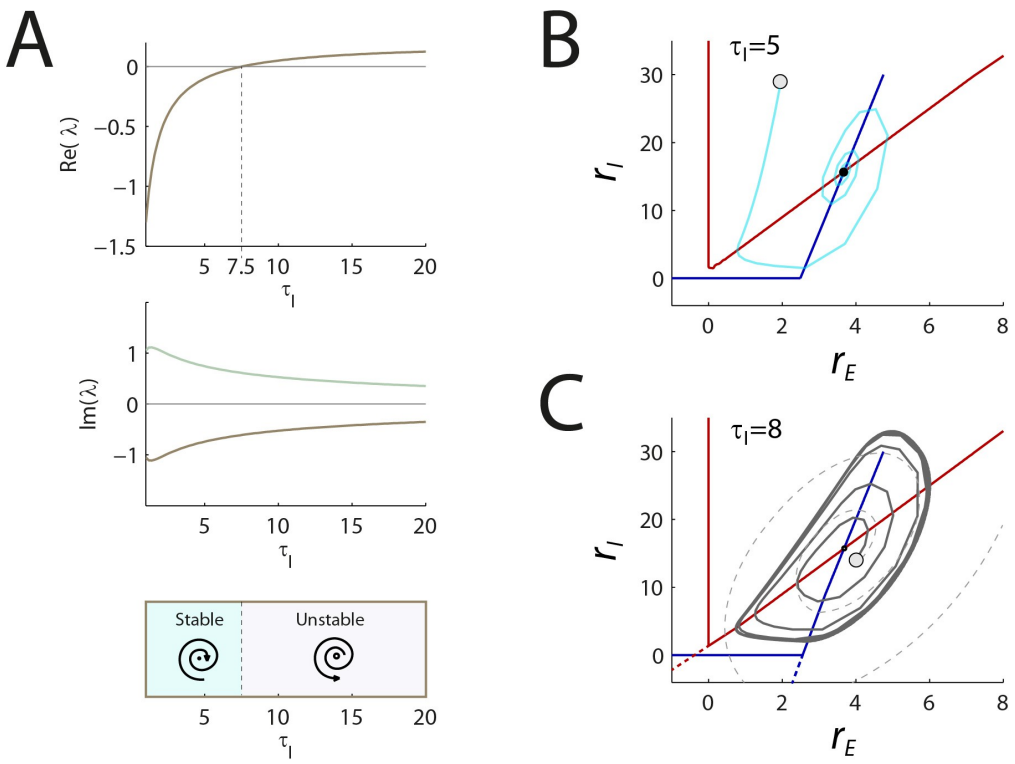

Figure 4.3.8. Activity in the network model. A, Real (top panel) and imaginary (middle panel) parts of the eigenvalues determining the stability of the UP state fixed point as function of τ_I (bottom panel). **B,** Trajectories in the phase plane for stable focus fixed points in the UP for different values of τ_I <7.5. Open circle marks the initial condition. **C,** Trajectories in the phase plane for unstable focus (τ_I =10) that stabilizes into a limit cycle (solid line). Without the threshold definition of the transfer functions, trajectory expands indefinitely (dashed line).

4.4. Statistics of spontaneous activity across brain states

The neocortex is thought to operate in a continuum of regimes in which desynchronized and synchronized states are loosely defined as categorical extremes in a high dimensional continuous space of possible brain states. Although there are numerous studies about the role of different neuromodulators and subcortical structures in forebrain activation, the precise mechanisms underlying cortical desynchronization remain to a large extent unknown. As shown in the previous chapter, the nature of the mechanisms underlying the generation of UP/DOWN transitions constrains the statistics of switching times. In this chapter, we analyzed population recordings of ongoing activity obtained using multisite silicon electrodes in auditory and somatosensory cortices of urethane-anesthetized rats during spontaneous transitions across a broad range of brain states, going from desynchronized to strongly synchronized. We characterized the statistics of UP and DOWN intervals as brain state varies and found systematic and continuous changes in all the statistics of the UP and DOWN intervals which were consistent for the two cortical areas studied. We proposed a mechanistic rate model with adaptation which can qualitatively reproduce the changes in the statistics of UP-DOWN intervals observed in the data, as a few of the model parameters are continuously varied.

Brain state assessment

We first characterized the changes in brain state in long recordings (up to 2 hours), from auditory (n=6 rats) or somatosensory cortices (n=4 rats) using the same methods employed in Chapter 4.2 and described in the section 3.3. We used (i) the silence density (fraction of 20 ms windows with no spikes over a period of 10 s) and (ii) the L/H ratio (ratio of the LFP spectral power of low (0.5-4 Hz) over high frequencies (20-55 Hz)) to quantify the instantaneous variations in brain state and found spontaneous transitions across the spectrum of synchronized and desynchronized states (Fig. 4.4.1). Low values for both L/H ratio and silence density correspond to more desynchronized states whereas high values are associated with more synchronized states. We observed that silence density provided a one-to-one mapping over a larger domain of brain states than the L/H ratio. This can be observed by the non-monotonic relation between L/H ratio and silence density (Fig. 4.4.1C). For states yielding very high silence density the frequency of slow fluctuations was clearly reduced (Fig. 4.4.1D; period iii versus ii and iv), which produced a drop in the L/H ratio given the reduction in power for low frequencies (Fig. 4.4.1B; period iii shows lower L/H power ratio than periods ii

and iv, but higher silence density). Based on this comparison, in this chapter we used the silence density to assess the degree of cortical state synchronization.

In several experiments an extra dose of urethane was administered towards the end of the experiment which tended to cause a similar change in brain state: first becoming desynchronized and after progressively becoming more synchronized (Fig. 4.4.1A-B, administration time indicated by red lines). The example experiment shown in figure 4.1.1 shows that under this increased level of anesthesia state variations showed similar values of L/H ratio and silence density as they displayed before injecting the anesthesia boost (Fig. 4.4.1C, compare black and red dots). This indicates that the brain states visited were the same across a broad range of anesthesia concentrations (Fig. 4.4.1D; compare points ii and iv with an addition of 20% of urethane).

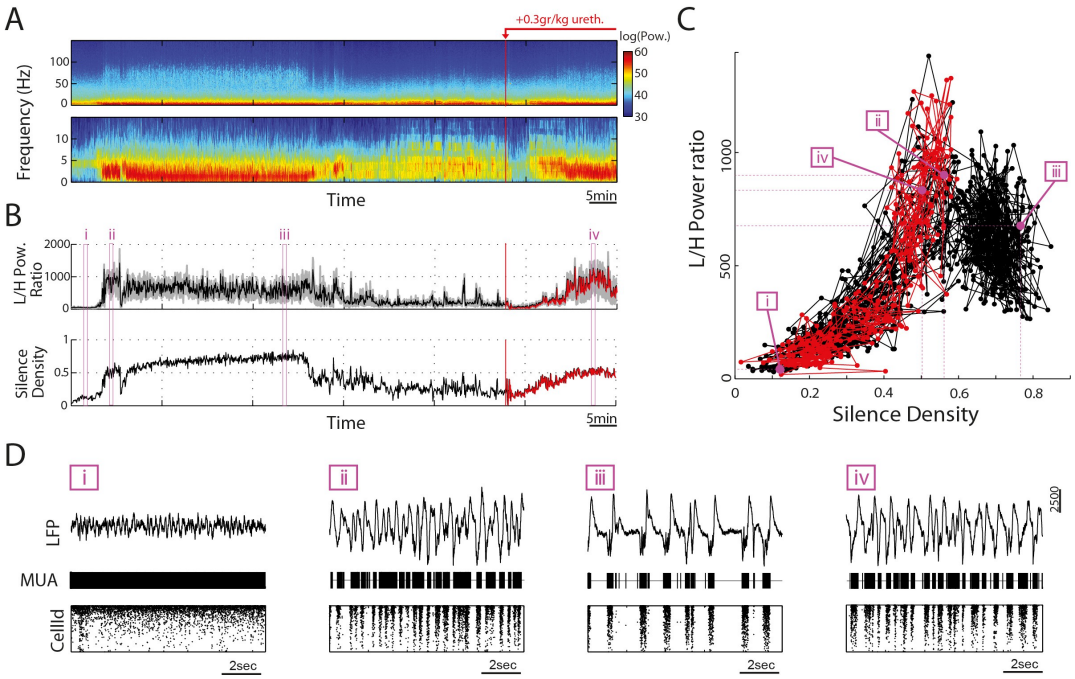

Figure 4.4.1. Brain State assessment from spontaneous activity recordings in the urethane anesthetized rat. Animals are initially anesthetized with 1.5gr/kg urethane. For this example, additional supplement of 0.3 gr/kg is administered (indicated by red arrow and vertical lines on panels A and B). **A.** Spectrogram from the local field potential for 1-to-100 Hz (top) and 1-to-15 Hz (bottom) **B.** On top, L/H (LFP power) ratio computed as the ratio between power at 0.4-to-5Hz/20-55Hz. Bottom, silence density computed from the multi-unit activity spike train (MUA). **C.** L/H power ratio versus silence density (every point corresponds to 10 s of recording). Red dots indicate the period after the urethane supplementary dose. Magenta boxes showing values for particular periods indicated in magenta vertical lines in panel B. **D.** LFP and MUA from different 10 seconds sampled periods (indicated by gray bars in B). Note that periods ii and iv showing similar values in panel B show similar traces on panel D, disregarding the different levels of anesthesia in both periods. In panel B, period iii shows lower L/H power ratio than periods ii and iv, but higher silence density, because the frequency of UP/DOWN transitions inperiod iii is lower than in ii and iv (D).

Spontantaneous activity across the desyncrhonized and synchronized brain state axis

As explained in the Introduction of this thesis, spontaneous activity during

synchronized states is characterized by UP and DOWN dynamics, whereas during desynchronized states DOWN periods are nearly absent. To study the mechanistic basis underlying this repertoire of dynamics displayed by cortical circuits, we performed a quantitative analysis on how spontaneous population activity is affected by brain state transitions.

In non-overlapping epochs W (length(W)=50 seconds) we first computed the mean silence density value from the spike train of multiunit activity (MUA), i.e. without performing spike sorting and unit isolation (Fig. 4.4.2A). For each of these epochs, we detected UP and DOWN intervals using the same methods used for the detection in in Chapter 4.3.2 (described in section 3.3 from Methods). The UP and DOWN interval detection algorithm assumes the existence of 2 different states in

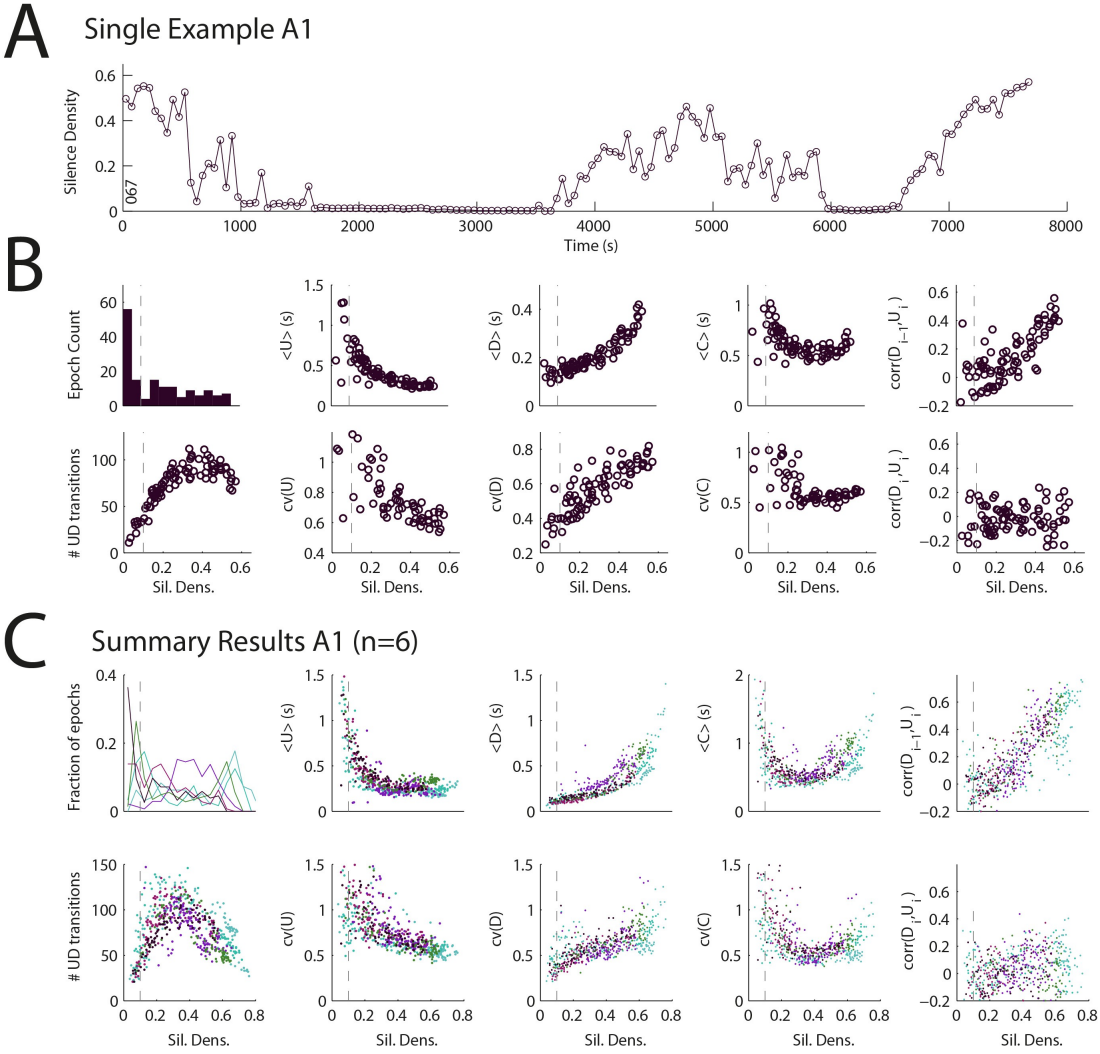

Figure 4.4.2. Statistics of U and D durations as function of silence density for auditory cortex recordings. **A.** Silence density computed in W=50 s epochs (using T=5<ISI_MUA>=0.011) for the whole experiment, showing spontaneous variations over a broad interval indicative of transitions between brain states. **B,** Top: Distribution of Silence density values, mean U, mean D, mean cycle (C), correlation between (D_{i-1},U_i) . Bottom: Number of U to D transitions detected, CV of U, CV of D, CV of C, correlation between (U_i,D_i). **C,** Summary results for n=6 experiments for the same statistics. Different experiments are indicated by different colors. Vertical dashed line corresponds to Silence density value of 0.1 below which the method detecting of U and D intervals is starts to be inaccurate.

the population rate, and estimates the parameters of the hidden-Markov model in an iterative way (Chen et al., 2009). Thus, we expected that the detection accuracy would decrease during desynchronized states where such 2 different stationary rates are not necessarily observed because DOWN intervals occur very sporadically. Indeed, visual inspection of the detection results showed that the DOWN detection was not reliable for intervals with silence density values less than 0.1. This was further confirmed by running the detection routines on surrogate data obtained from a rudimentary generative model of state transitions (not shown). Despite of this limitation of the method, if the amount of DOWN intervals in one epoch was sufficiently large (>20) we computed the same statistics of UP and DOWN interval duration (U and D, respectively) as in Chapter 4.3.2, and plotted them as a function of silence density for the whole range of silence density values measured. In the following, results for silence density values below 0.1 should be interpreted with caution. Changes in mean and coefficient of variation of U and D and correlation between consecutive U/D periods as a function of silence density, described manifolds showing that changes between synchronized and desynchronized states occured in a continuous way (Fig. 4.4.2B).

We first analyzed an example experiment from auditory cortex (Fig. 4.4.2B). As the state became more synchronized, Us became shorter and less variable whereas Ds did the contrary, they became longer and more variable (Fig. 4.4.2B). The mean and CV of the cycle C described a non-monotonic behavior with a minimum at around 0.4 in silence density (Fig. 4.4.2B). Correlation between consecutive U-D periods vanished towards desynchronized states. For the synchronized states, consecutive (U_i,D_i) remained uncorrelated, while correlations between consecutive (D_{i-1},U_i) periods turned positive, presenting higher correlation values than those observed in the somatosensory cortex recordings of Chapter 4.2 (see below).

In order to compare the different U and D statistics across experiments, we needed to “renormalize” the silence density to be able to compare it across experiments with different number of neurons and different overall density of spikes. We did that by tailoring the size of the silence window used to compute the silence density in each experiment. We computed the average rate R of the multi-unit spike train containing all the detected spikes, and defined the silence window equal to T=5/R, that is five times the mean ISI value of the multi-unit spike train. With this definition, if the spikes had a uniform probability to occur across time, i.e. they were a homogeneous Poisson process, the silence density would be $\exp(-RT)=\exp(-5)=0.007$ for any experiment, thus providing a common baseline for all experiments to compare against. We compared the U and D statistics across n= 6 experiments from auditory cortex and found that they exhibited remarkably similar behavior as a function of this renormalized silence density (Fig. 4.4.2C). This implies two things: (i) that silence density, despite its simplicity, provides a very accurate assessment of brain state synchronization; and (ii) that the changes observed in U and D statistics as silence density varies are systematically found across experiments.

We analyzed another badge of long experiments recording population spiking activity from somatosensory cortex (with duration > 2 hours) and repeated the analysis regarding brain state variations and U and D statistics. Although somatosensory experiments displayed a smaller silence density range, the comparison of the population averages for somatosensory and auditory experiments revealed that the statistics evolved in general agreement across similar manifolds (Fig. 4.4.3). The only noticeable difference was the apparent asymmetry between the serial correlations between consecutive Us and Ds at high silence density: while in auditory cortex $Corr(U_i, D_i) < Corr(D_{i-1}, U_i)$ in somatosensory cortex $Corr(U_i, D_i) \approx Corr(D_{i-1}, U_i)$.

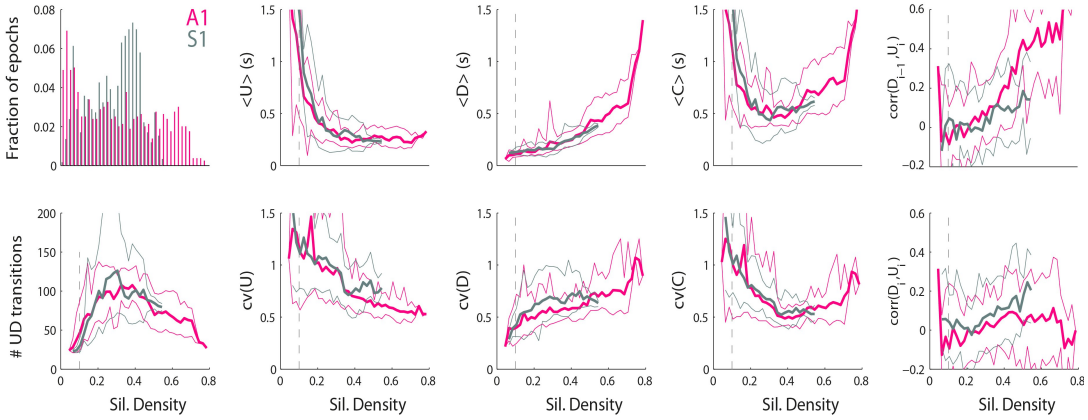

Figure 4.4.3. Average U and D statistics as function of silence density for auditory (n=6, magenta) and somatosensory (n=4, gray) recordings. Same panel layout as figure 4.4.2B-C. Thick lines show mean values across experiments and thin lines show 95% CI. Notice that the range of silence density values obtained in experiments from somatosensory cortex is narrower than the range obtained from auditory cortex experiments. Despite this difference, the behavior of U and D statistics vs. silence density is very similar.

Population spiking activity across brain states

We next characterized the spiking activity of the population across epochs with different silence density values spanning a range of brain state synchronization levels (Fig. 4.4.4A top). We observed that average population rate during UP intervals, aligned at the onset and the offset, was surprisingly lower for desynchronized epochs compared to synchronized epochs (Fig. 4.4.4A bottom traces). We computed overall average population rate in each epoch (i.e. population spike count in an epoch divided by epoch length W) and then averaged epochs with similar silence density (density bins of width 0.1). As expected, the overall population rate decays as silence density increases, i.e. the more silence the fewer spikes (Fig. 4.4.4A top). We then computed the same averaged population rate but considering only U intervals. As expected from the analysis shown in figure 4.4.4A (bottom traces), the averaged rate showed an increase as a function of the silence density in all experiments except for one recording from S1 (Fig. 4.4.4B bottom). This indicates that the population rate during U intervals tends to increase as the

brain state becomes more synchronized. This increase compensates partly the decrease in the overall average rate (considering both Us and Ds) that would be obtained by only introducing more silence (compare dotted line with the rest of the experiments).

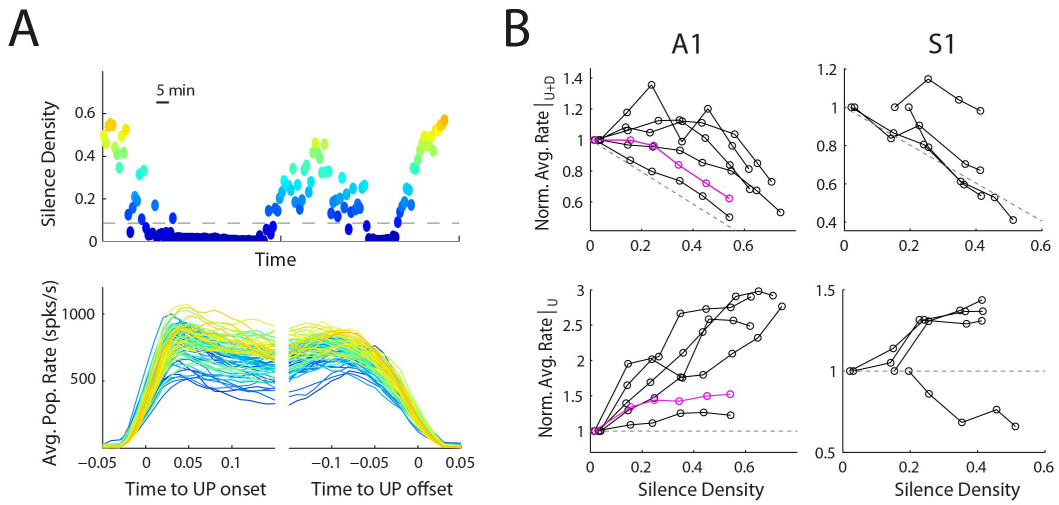

Figure 4.4.4. Average Population rate during UP intervals as a function of Silence Density. **A,** Top: An example experiment showing spontaneous changes silence density levels (same experiment is shown in Fig. 4.4.2A-B). Bottom: Averaged population rate *R*(t) aligned at the onset and the offset of Us for the different epochs showed in the top panel. The color of the rate trace indicates the silence density observed in that epoch (see top trace). **B,** Summary of *n*=6 A1 and *n*=4 S1 experiments. *Top:* population rate averaged within W= 50 s epochs versus silence density (dots represent averaged of all epochs within silence density bins of size 0.1) normalized by the rate obtained at the lower value of silence density reached in that experiment. *Bottom:* same as top plots except that population rates were averaged exclusively during UP intervals. Experiment shown in A is marked in magenta. Vertical dashed line indicate the silence density value below which the detection of U and D can be inaccurate.

Network model exhibiting changes between synchronized and desynchronized states

Can a model that shows adaptation and fluctuations capture the features of UP and DOWN statistics across different brain states? We considered a low-dimensional model describing the collective dynamics of a single excitatory population, characterized by the rate *r*(t) (expressed in Hz), which exhibits rate adaptation, *a*(t) (in arbitrary units; Fig. 4.4.5A). This is a particular instance of an extensively used class of models describing the activity of a self-excitable population with a slow negative feedback, here provided by the adaptation, which can induce transitions between quiescent and sustained firing rate intervals (Latham et al., 2000; Holcman and Tsodyks, 2006; Curto et al., 2009; Melamed et al., 2008; Mejias et al., 2010; Mattia and Sanchez-Vives, 2012) (Fig. 4.4.5A). The dynamics of these variables are described by:

$$\tau_r \frac{dr(t)}{dt} = -r(t) + \phi\left(J\, r(t) - a(t) + \theta + \sigma\,\xi(t)\right) \qquad (1.1)$$

$$\tau_a \frac{da(t)}{dt} = -a(t) + \beta r(t) \qquad (1.2)$$

The time constants for each dynamical variable are denoted by τ_r and τ_a (taking the values 10 and 1000 ms, respectively) and the strength of the excitatory recurrent connection is J (with units of Hz^{-1}). The population receives an external fluctuating current with mean input θ and standard deviation σ (in arbitrary units). $\xi(t)$ is a stochastic Gaussian process (see Methods section 3.4 for details). As in the previous chapter, these *ad hoc* fluctuating term represents inputs coming from other brain areas plus the fluctuations of the network activity whose mean rate is $r(t)$. The parameter β, with units of Hz^{-1}, sets the strength of the adaptation. We use the transfer function Φ (Fig. 4.4.5B; (Brunel, 2003)) described by

$$\phi(x) = \begin{cases} 0 & x < 0 \\ \frac{x^2}{3} & 0 \le x < 1 \\ \frac{\sqrt{4x-3}}{3} & x \ge 1 \end{cases} \qquad (1.3)$$

This function captures nicely the change of concavity observed in the transfer function of cell recorded *in vitro* or spiking neuronal models. In contrast to the classic sigmoid function, it does not saturate but exhibits a square root behavior at high rates (Fig. 4.4.5C). We set the output rate of the inflection point where the function changes its concavity at unrealistically low values (Fig. 4.4.5C). This is necessary to obtain stable solutions of the system at low rates representing the UP state. As mentioned in Chapter 4.3 this is a problem when using this type of models with sigmoid-like transfer function and slow negative feedback to generate bistability: the state with high rate is obtained at values of the rate where the transfer function is already "saturating" (i.e. concave down) which generally occurs for much higher rates (20-40 spikes/s) than those observed during UP intervals (~3 spikes/s).

Based on the nullclines of the system (Fig. 4.4.5C), in the absence of fluctuations σ=0, according to the mean input θ and adaptation strength β the system can operate in qualitatively different regimes in a similar way as it was observed in the previous chapter[5]: mono-stable DOWN (violet), mono-stable UP (orange), bi-stable UP and DOWN(magenta) and oscillatory (turquoise) (Fig. 4.4.5C). An example of the UP and DOWN dynamics produced by the model in the oscillatory regime in the presence of external fluctuations is shown in figure 4.4.5D.

5 We consider a state as stationary if adaptation was unable to make the system transition away from it, while a non-stationary state is a fixed-point that is stable temporarily while adaptation increases or decreases, but eventually loses stability and switches to the other state.

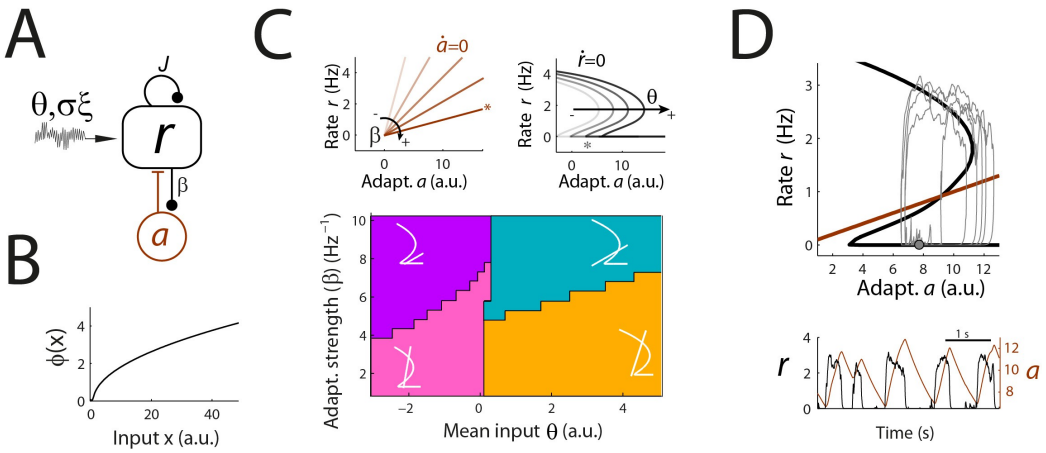

Figure 4.4.5. Model of UP and DOWN switching dynamics. **A,** Scheme of the network architecture showing a single population of recurrently connected excitatory cells, characterized by its population rate $r(t)$, which exhibit spike frequency adaptation, characterized by the variable $a(t)$, and receiving and external fluctuating input with mean θ and standard deviation σ. **B**, Transfer function shows the dependence of the population rate on its input current. **C,** *Top left*: a-nullcline for various values of the strength of adaptation (β). *Top right*: r-nullcline for various values of the mean external input θ. *Bottom*: stability regimes in the noise-free system (σ=0) as a function of β and θ can be mono-stable (UP-stable is purple and DOWN-stable is orange), bistable (UP and DOWN stable, pink) or show a limit cycle (turquoise). **D,** *Top*: phase-plane (r,a) showing the r-nullcline (black) and a-nullcline (brown) superimposed with an example trajectory showing UP and DOWN transitions. *Bottom*: the same example trajectory is shown as r and a versus time. Parameters: β=8 Hz^{-1}, θ=3 (see asterisk in C), σ=3 and J=10 Hz^{-1}.

The next question was if such a simple model could reproduce qualitatively the changes observed in UP and DOWN statistics along the desynchronized-synchronized axis by gradually changing some of the model's parameters along a specific trajectory in the parameter space. As we observed in our data, different levels of silence density were associated with systematic changes in the statistics of UP and DOWN states. For the rest of the analysis we focus on on the statistics of the extremes of high and low values of silence density observed in auditory cortex (summarized in Fig. 4.4.2C), and tried to *qualitatively* reproduce the changes in the UP and DOWN statistics observed between those extremes.

The low silence density periods showed high values of mean(U) and CV(U) and low values of mean (D) and CV(D) (Fig. 4.4.6A). The longer Us versus shorter Ds, suggested that this state corresponded to the the mono-stable UP regime (Fig. 4.4.5C orange). In this regime, the transitions UP to DOWN are triggered by the external fluctuations (because the UP is a stable fixed point) thus yielding high CV(U). In contrast the transitions DOWN to UP result from the recovery from adaptation and fluctuations do not play an important role yielding low mean(D) and low CV(D) (Fig. 4.4.6B-C). Equivalent arguments apply for the high density periods with mean(D)>mean(U) and CV(D)>CV(U). In the mono-stable DOWN regime the system spends more time around the DOWN fixed point (large mean(D)) and external fluctuations play a larger role triggering the transitions to the UP (increased CV(D)).

Modeling serial correlations between D and U

Next we turned our attention to the serial correlations between Us and Ds and their dependence on brain state. In the data, during periods with low silence density, both corr(U_i,D_i) and corr(D_{i-1},U_i) were close to zero (Fig. 4.4.6A right). In contrast, high silence density periods were characterized by an asymmetry with large corr(D_{i-1},U_i) and corr(U_i,D_i) close to zero (Fig. 4.4.6A right). This scenario is remarkably similar to the correlations between inter-burst-interval and burst duration observed in the spontaneous activity of developing spinal cord (Tabak et al., 2001) which led Rinzel and colleagues to investigate the mechanisms yielding serial correlations extensively. The key observation from those studies was that the amount of correlation between consecutive intervals was determined by the broadness of the distribution of the adaptation variable at the transition times (Tabak et al., 2001; Lim and Rinzel, 2010). This means that to obtain corr(D_{i-1},U_i)>0 the transitions between the lower and the upper branch of the *r*-nullcline must occur at different points along the *a*-axes (see how the trajectories at the D to U transitions in Fig. 4.4.6B right are quite scattered). When the variability of the adaptation is large at the transitions times, the transitions do not reset the system because the value of *a(t)* acts as a buffer that "stores" the information about the length of the previous interval and correspondingly impacts the length of the current one: if a strong fluctuation kicked the system early during D to the U (short D), the value of *a* is rather large at transition time (far from the lower knee), and the following U will tend to be short because the system is closer to the upper knee. This necessary condition is also sufficient to obtain corr(D_{i-1},U_i)>0 in the oscillatory regime (Fig. 4.4.5C turquoise region) (Tabak et al., 2001; Lim and Rinzel, 2010). However, under the presence of a stable fixed point in the upper brunch (Fig. 4.4.6B left), the value of *a(t)* at the transition, i.e. the distance to the UP fix point, does not have a great impact on the U duration anymore. This is simply because the system spends most of the U around this UP fixed point until a large fluctuation triggers a transition to the lower branch. For an equivalent argument an UP fixed point prevents the system from generating corr(U_i,D_i)>0. This is the reason why our network model yields near zero corr(U_i,D_i) and corr(D_{i-1},U_i) during desynchronized states of low silence density (Fig. 4.4.6C bottom).

During synchronized states the system has now a DOWN fixed point (Fig. 4.4.6B right) but, in contrast to the desynchronized case, it does not effectively spend much time around it because the fluctuations, which are now bigger (σ=1), are very effective triggering transitions to the upper branch before the system reaches the fixed point (see D-to-U transitions in 4.4.6B right panel). These D-to-U transitions occurring at different values along the lower branch generate a broad distribution of *a(t)* values at the transition times (condition 1) and, because there is no fixed point in the upper branch (condition 2), yield large corr(D_{i-1},U_i)>0 (Fig. 4.4.6C bottom). The asymmetry between the upper and the lower branches, caused by the shape of the transfer function Φ (Eq. 1.3), makes the fluctuations much less effective triggering U to D transitions at different values of the upper branch making corr(U_i,D_i)~0 as observed in the data (compare Fig. 4.4.6A right with C bottom). Replacing Φ by the standard sigmoid function made the *r*-nullcline symmetric and

impaired the ability of the system to generate asymmetric serial correlations as observed in the data (not shown).

All the changes in the U and D statistics observed in the data along the silence density axis (Fig. 4.4.6A), are schematically reproduced by two sets of model parameters (Fig. 4.4.6C). The two sets only differed in the values of β, σ and θ which were chosen based on the mechanistic arguments given above. Therefore, the model predicts that more synchronized states are associated with an increase in the strength of adaptation β, an increase in the amplitude of fluctuations σ and a reduction of the mean input θ received by the network. The plausibility of changes in adaptation and external input mediating changes in brain state will be discuss in the next chapter (Discussion).

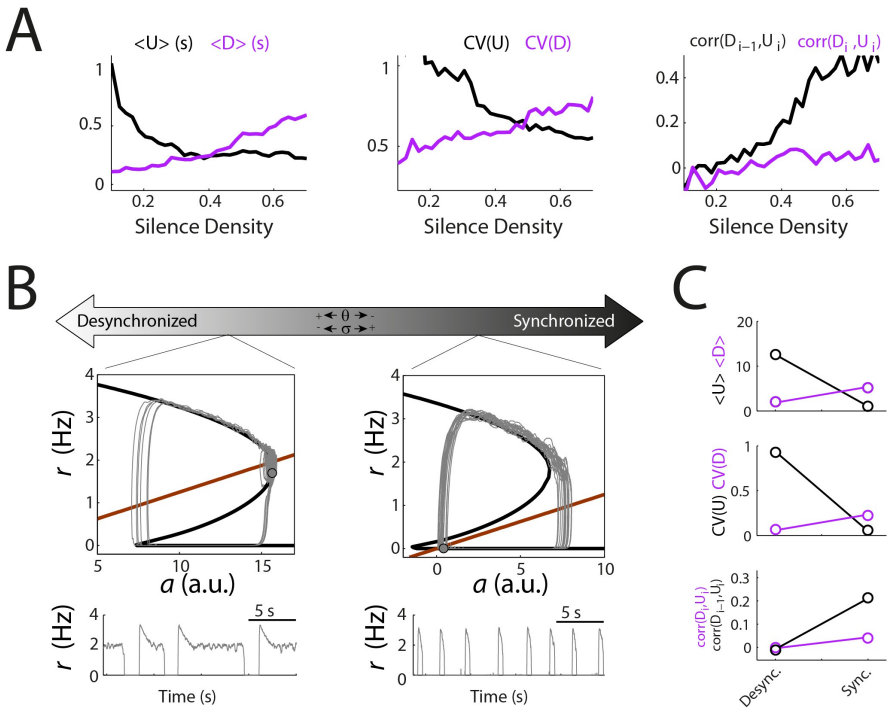

Figure 4.4.6. Model of UP and DOWN transitions reproducing changes in dynamics like those caused by brain state variations. **A,** Summary of variations of the U and D statistics versus silence density observed in A1 experiments: mean duration (left), coefficient of variation (center) and serial correlations (right) averaged across n=6 animals (replotted from Figure 4.4.3 pink solid lines). **B,** Phase plane (*r*,*a*) and bottom *r* traces as in figure 4.4.5D. Variation of β, θ and σ generates different model regimes qualitatively mimicking the variations in U and D statistics observed in A . *Left*: a desynchronized state generates long and irregular Us and short and regular Ds (see bottom trace) with negligible (D_{i-1},U_i) and (U_i,D_i) correlations (see C). *Right:* the synchronized state generates shorter and more regular Us and longer and more irregular Ds compared to the desynchronized state. It also exhibits strong (D_{i-1},U_i) correlations but negligible (U_i,D_i) correlations (C). **C,** U and D statistics in the desynchronized and synchronized states obtained in the model. Parameters: J=10 Hz^{-1}, τ_r=10 ms, τ_a=1000 ms, τ_{noise}=5 ms; Desynchronized: β=5 Hz^{-1}, σ=0.5 and θ=1.5 (a.u.); Synchronized: β=8 Hz^{-1}, σ=1 and θ=-1 (a.u.).

5. Discussion

In this Thesis we studied different aspects of neocortical spontaneous slow waves. First, we studied how fast oscillations observed during UP periods are expressed across the cortical layers both *in vitro* and *in vivo*. Second, we analyzed the dynamics of slow waves *in vivo* to test the hypothesis that adaptation and random fluctuations are mechanisms participating in their generation. Third, we built a computational model to explore how those two mechanisms would affect the dynamics and statistics of UP and DOWN periods in a recurrently sustained bistable network. Fourth, we characterized how brain state shapes the dynamics of slow waves in the neocortex.

Fast oscillations across the cortical layers during UP states

We found that fast oscillations occurring during UP periods *in vivo* had similar spectral characteristics across cortical laminae. However, fast oscillations were "compartmentalized" in SG and IG domains: coherence between recording sites from the same domain was high while coherence between recording sites from different domains was significantly reduced. This suggests that fast oscillations in SG and IG are locally generated in these two domains while they are coupled more weakly with each other. Fast oscillations in SG and IG were also observable *in vitro*. However, the spectral properties for both domains were different: while SG fast oscillations were stronger and in the beta range of frequencies, IG fast oscillations where weaker and tended to reside in the gamma range. Fast oscillations *in vivo* were stronger than those observed *in vitro* for both domains. We hypothesized that the differences between the isolated cortical network *in vitro* and the same cortex *in situ* could be due to a reduced excitability in the *in vitro* preparation. In order to increase excitability, we applied kainic acid *in vitro*, an agonist of excitatory kainate receptors. Kainic acid produced dramatic changes in the slow wave dynamics, leading to a specific disruption of slow waves in IG. In addition, kainic acid also boosted the power of the oscillations observed in control ACSF and increased the frequency of the primary fast oscillation in SG while reducing that in IG towards an intermediate approximately common value. Therefore, from the perspective of fast oscillatory dynamics, increasing excitability produced a more similar laminar pattern to the one observed *in vivo*.

Fast oscillations during UP periods in vivo are compartmentalized in SG and IG domains

Fast oscillations in the LFP across the cortical column during the UP states have been described to occur in-phase across the cortical layers in anesthetized and natural sleeping animals, based on cross-correlation analysis

between neighbouring pairs of electrodes at different cortical depths and on visual comparison of 15-80 Hz filtered traces (Steriade et al., 1996). In this way, the phase-locking of fast oscillations between adjacent LFP cortical signals in the same column is preserved during REM and desynchronized states in anesthetized cats after electrical stimulation of brainstem areas related to the activating systems (Steriade et al., 1996). In contrast, laminar recordings in the visual cortex of awake monkeys during resting or visual stimulation shows that coherence between electrodes from different laminar domains (supra/infra granular) is substantially decreased even when fast oscillations coherence between electrodes from the same domain is high (Maier et al., 2010). This compartmentalization of fast oscillations observed would imply a lack of consistency in the oscillatory phases from SG and IG. By doing a detailed analysis of laminar recordings on the visual cortex of ketamine anesthetized ferrets, we revised this apparent contradiction in the literature.

We observed that fast oscillations occurring during the UP states *in vivo* were also compartmentalized in the SG and IG domains, and the limits between those compartments coincided with the location of the phase reversion of the slow waves. Our results in the anesthetized ferret are in agreement with those reported in the awake monkey (Maier et al., 2010), but contrast with those in anesthetized and natural sleeping cats, where in-phase fast oscillations were concluded to occur across the cortical laminae (Steriade et al., 1996). However, it is important to note that the results from Steriade and colleagues based on cross-correlation analysis of neighboring electrodes could mask the drop in coherence that might occur across distant recording sites. Considering this, our observations can be reconciled with those from (Steriade et al., 1996) since compartmentalization implies that neighboring electrodes exhibit high coherence except at the edge of the compartments.

Another result in our analysis supports a compartmentalization of fast rhythms in SG and IG *in vivo*; fast oscillations observed in the average power spectrum during UP periods *in vivo* for SG and IG showed similar spectral properties, but in 3 out of 4 cases a second oscillatory peak at slower frequencies (beta range) appeared in SG recordings (Figure 4.1.2, Figure 4.1.5, blue arrows). This sets a qualitative difference between fast rhythms generated in these two domains. Steriade and colleagues did not report this effect, even when the precise location of peaks in their example cross-correlograms varies for different layers in the same direction (i.e., see Figure 5.1 below).

As Steriade et al 1996, our recordings were obtained under ketamine-xylazine anesthesia. This specific pharmacological manipulation could have an effect on the layer specificity of fast oscillations. Indeed, NDMA receptor activation controls different microcircuits involved in gamma rhythm generation in superficial layers of enthorinal cortex *in vitro* (Middleton et al., 2008). Moreover, the use of ketamine *in vitro* reduces the power of gamma oscillations in superficial layers of enthorinal cortex, while IG gamma oscillation properties are not altered (Cunningham et al., 2006). In addition, anesthetic agents *per se* may alter fast cortical dynamics without changing cortical activations to slow wave patterns. Subanesthetic administration of ketamine *in vivo* induces an enhancement of gamma oscillations in neocortex (Pinault, 2008), and volatile anesthetics such as halotane or

isofluorane — which potentiate $GABA_A$ transmission while inhibiting AMPA receptors — can produce an enhancement in spontaneous gamma oscillations at low doses (Vanderwolf, 2000; Imas et al., 2004). Further studies are needed in order to assess if the compartmentalization of fast oscillations observed during UP periods in ketamine-anesthetized animals is also present across different brain states, in natural sleeping, unanesthetized preparations and under different anesthetics. Nevertheless, the similarity of the compartmentalization reported here and that observed in the awake monkey across different brain states (Maier et al., 2010), suggest that SG and IG compartmentalization of fast-frequency oscillations might be a general feature of neocortical operation.

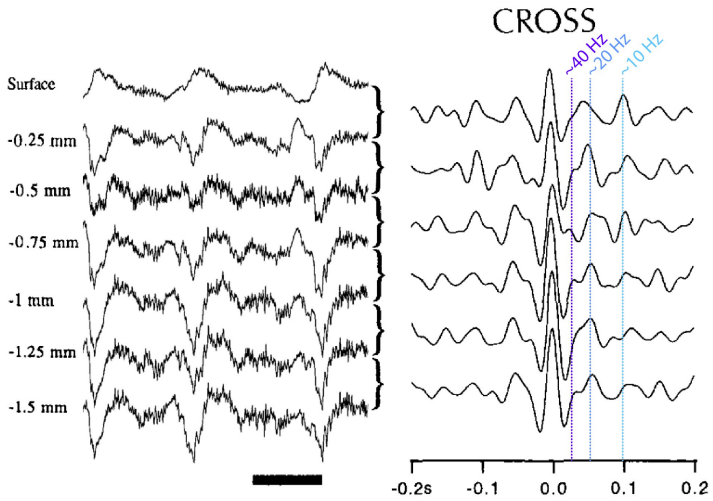

Figure 5.1. Cross correlation analysis of LFP signals from neocortex of ketamine-anesthetized cats during slow-wave activity at different depths (modified from (Steriade et al., 1996)). On the left, simultaneous LFP signals at different depths. Phase reversion of slow-waves is obtained around -0.5 mm (darkest trace). Negative peaks in the LFPs are used as trigger signal for choosing 2-seconds windows in order to perform cross-correlation analysis. On the right, cross-correlation of pairs of electrodes indicated by curly brackets. Coloured lines for different frequencies are shown.

Laminar specificity of fast oscillations during UP states in vitro

Given the compartmentalization observed *in vivo*, we considered that during UP periods cortical layers from visual cortex can be grouped into SG and IG as two functional blocks from the oscillatory perspective. We then studied if the isolated cortical circuit can generate such laminar patterns of fast oscillations as observed *in vivo*.

Fast oscillations have also been observed during spontaneously generated UP states in neocortical slices maintained *in vitro*, showing that the local cortical circuit has the necessary components for their generation (Compte et al., 2008). Although these spontaneous UP states are propagated across the cortical column (Sanchez-Vives and McCormick, 2000), the laminar specificity of these fast oscillations has not been explored, and this was one of the central aims of the present study.

We observed that during UP states *in vitro* fast oscillations occur in SG and IG domains and display clear different frequency domains: while SG fast oscillations dominated the beta range of frequencies, IG fast oscillations tended to occur in the gamma range. Moreover, the power of oscillations in SG was stronger than in IG. These results differ from our observations *in vivo*, where fast oscillations tended to occur at approximately similar frequencies, although also *in vivo* SG often displayed an additional beta-frequency oscillation in parallel to our *in vitro* results. A clear difference between *in vivo* and *in vitro* was that both SG and IG oscillations were stronger *in vivo* than *in vitro* (Figure 4.1.5).

Mechanisms of fast oscillations potency and coherence

Balanced excitatory and inhibitory forces have been suggested to be at the root of fast rhythms (Compte et al., 2008). Slowing down the time course of fast inhibition by $GABA_A$ agonist thiopental displaces the peak of fast rhythms towards lower values, suggesting that $GABA_A$ time course is critical to determine the oscillatory frequency (Compte et al., 2008). We hypothesized that the differences observed between the *in vivo* and *in vitro* preparations might arise in the slices by a decrease of excitability. Therefore, we investigated to what degree an excitability increase in the slice mimics cortical dynamics observed *in vivo*. To this end, we administered kainic acid (an agonist for kainate receptors) into the perfusion bath, a common procedure to activate cortical slices (Ainsworth et al., 2011).

Kainic acid administration produced changes in the slow wave dynamics *in vitro*. Increasing the excitability with the lower dose (200nM) of kainic acid produced an increase in the frequency of UP states by reducing DOWN state durations. The blockage of $GABA_A$ receptor by bicuculine in cortical slabs, increasing the excitability of the slab, produces a decrease in the duration of both UP and DOWN intervals (Chen et al., 2012). Moreover, a previous study using our slices preparation shows that bicuculine reduce UP durations and increases DOWN durations (Sanchez-Vives et al., 2010). Altogether, these result suggests that depending on the way that excitability is modulated, alterations in slow wave dynamics are diverse.

The presence of 200 nM kainic acid boosted the power of fast oscillations in IG significantly. In the 400nM kainic acid, fast oscillations were even stronger across the cortical column, although the UP and DOWN states dynamics was disrupted in IG. Furthermore, in the average across experiments, the frequency of oscillations in IG was reduced, while it was increased in SG towards an intermediate and approximately equal value. Altogether, our results indicate that an excitability increase boosts fast frequency oscillations and homogenizes the frequency of the rhythms generated in the two domains of the cortical column, as in the *in vivo* condition. This suggests that local cortical excitability modulates inter-laminar coupling and intra-laminar oscillatory dynamics, and is an important factor in understanding dynamical differences between *in vitro* and *in vivo* cortical network dynamics.

Our *in vitro* study the mechanisms of fast frequency modulation across the cortical laminae. Previous experimental and computational studies have rather concentrated on synaptic mechanisms, but not on the role of network excitability on

fast oscillations. In particular, inhibitory synaptic transmission and mutual inhibition are key components for gamma oscillations, based on studies in the hippocampus (reviewed by (Bartos et al., 2007)). Computational network models of gamma-range synchronization with sparse neuronal participation have implicated time scales and strengths of fast excitatory and inhibitory currents in the control of the oscillation frequency (Brunel and Wang, 2003). In the context of UP and DOWN states, fast oscillations during UP states might also rely on the interplay between excitatory and inhibitory populations (Compte et al., 2008).

Our data brings forward network excitability as a modulatory mechanism of fast rhythms in the cortex. Note that even if we employ a synaptic receptor agonist in our manipulation, this does not potentiate synapses functionally but instead activates kainate receptors, resulting in a sustained increase in excitability without significant synaptic strength modulation (Campbell et al., 2007). Can we mechanistically understand such an effect of excitability? Is an increase of excitability responsible for the increase of power of fast oscillations in IG? Are SG oscillations getting synchronous with the oscillations boosted in IG? One way to test these hypothesis is to use the model proposed by (Compte et al., 2003) and decrease the leak conductance to mimic the increase in the excitability of the network.

The laminar distribution of kainate receptor shows maximal concentration in layers V-VI in the visual cortex of adult ferrets, whereas the expression in the rest of layers remains low (Smith and Thompson, 1994). This suggests that our manipulation could indeed have engaged differently the two layer domains of the cortical circuit, triggering changes associated with their specific coupling dynamics. More detailed computational models with SG and IG compartments (as in (Roopun et al., 2008; Ainsworth et al., 2011)), might help to elucidate the mechanisms underlying the fast oscillations occurring during kainate-evoked UP states in the cortical laminae.

Relation to other in vitro preparations to study fast oscillations in vitro.

To our knowledge, this study is the first to investigate the laminar specificity of fast oscillatory activity during UP states *in vitro*. However, different previous *in vitro* studies explored the mechanisms of fast oscillations in other brain emergent patterns. Indeed, *in vitro* models have often been used to study the mechanisms underlying the generation of fast oscillations in cortex by electrical (Metherate and Cruikshank, 1999) or pharmacological (Cunningham et al., 2003; Roopun et al., 2006, 2008, 2010; van Aerde et al., 2009; Oke et al., 2010; Ainsworth et al., 2011) activation of the slices. Under exogenous activation, the generated fast oscillations in some of these *in vitro* preparations shows strong and narrow peaks in their power spectra. However, this feature differs to what is typically observed in the neocortex *in vivo* (Wang, 2010). Neverthless, they are succesful to reproduce the laminar decoupling observed in awake monkeys (Buffalo et al., 2011; Spaak et al., 2012; Xing et al., 2012). Moreover, different drugs and concentrations on some of these *in vitro* preparations can generate diverse laminar activation profiles (Roopun et al., 2010; Ainsworth et al., 2011), showing that the isolated circuitry of the neocortex is capable to generate distinct laminar profiles of fast oscillatory activity.

Although other *in vitro* preparations display slow waves in SG but not in IG

(Cunningham et al., 2006), our preparation spontaneously displays robust slow waves both in SG and IG (Sanchez-Vives and McCormick, 2000). Moreover, our *in vitro* preparation showed robust UP and DOWN states and generated layer-specific fast oscillations during UP periods in the absence of externally applied neuromodulators, synaptic agonists or electrical stimulation protocols (Compte et al., 2008).

Kainic acid produce different laminar profile of fast oscillations in different cortical areas *in vitro*. On the one hand, in secondary somatosensory cortex kainic acid at 400nM generates two independent local fast oscillators in SG and IG, where SG expresses gamma oscillations and IG beta oscillations (Roopun et al., 2006). A similar profile is observed in the visual cortex when the agonist carbachol is also added on the bath, where SG and IG exhibit gamma oscillations with faster frequencies in IG (Oke et al., 2010). On the other hand, the same researchers reported the reverse situation using the same preparation but in primary auditory cortex in vitro: kainic acid generated two independent local gamma generators at 30-45 and 50-80 Hz in layer 2/3 and layer 4, respectively (Ainsworth et al., 2011). While the emergence of the faster oscillation in layer 4 occurs at maximal (800nM) kainate concentration, for lower concentrations (<=600nM) slower fast oscillations are present in both layers and the frequency of the oscillation depends linearly on the concentration (Ainsworth et al., 2011).

In our *in vitro* experiments, kainic acid administration produced an opposite effect in SG and IG: while spontaneous UP states *in vitro* show fast oscillations at different frequencies in SG and IG, with higher frequency for IG than SG, addition of kainic acid tends to equalize the frequency of fast oscillations towards an intermediate value. Moreover, in our *in vitro* preparation, increasing kainic acid concentration further than 400 nM leads to spreading depression and epileptiform activity in the slice.

Regarding the mechanisms regulating laminar segregation of fast oscillations, computational simulations suggest that inhibitory interlaminar connections could facilitate the frequency segregation in auditory cortical slices (Ainsworth et al., 2011). In the secondary somatosensory cortex, SG and IG local networks fast oscillatory activity has been suggested to rely on electrical and chemical synapses, respectively, in order to produce the segregation of frequencies (Roopun et al., 2006). However, pharmacological blockage of gap junctions by carbenoxolone in visual cortical slices supresses fast oscillatory activity in a more robust way for the faster rhythm that is present in SG, suggesting that the mechanisms underlying different frequencies in SG and IG might depend on experimental conditions (Oke et al., 2010). In our case, the mechanisms by which the local SG and IG networks equalize their fast oscillation frequencies (without significant coherence increase) by increasing neuronal excitability are still to be determined. Further *in vitro* pharmacological manipulations and computational models might be required to understand how fast oscillations are generated across the cortical column during UP states.

Methodological caveats in our in vitro studies

Fast oscillations in IG *in vivo* were remarkable strong, whereas *in vitro* fast

oscillations were weaker and often difficult to identify distinctly in the bare power spectrum. This is due to the fact that LFP power spectra are dominated by a power law both *in vitro* and *in vivo* (Buzsáki and Draguhn, 2004). A rhythm is manifested by the existence of a small peak superimposed on such a broad-band power-law power spectrum (Wang, 2010). While such bumps are readily observable *in vivo*, *in vitro* they are generally small as previously described (Compte et al., 2008). To overcome this problem we used an analysis method to emphasize departures from the power-law baseline power spectrum (excess power, see Methods for Chapter 4.1 in section 3.2 from Methods). This analysis has been used before to characterize the power-law observed in the power spectra of human EEG recordings (Miller et al., 2009). This analysis allowed us to better compare the frequency of oscillations in spite of the different power *in vivo* and *in vitro*. One possible caveat of this approach is the fact that *in vitro*, the method would emphasize random fluctuations in the power spectrum, falsely attributing them to oscillations. However, this is unlikely to be the case since this would imply that the identified bumps should be either uniformly distributed along the frequency axis, or equally biased to high or low frequencies for IG and SG recordings. Instead, we found that SG peaks were distributed over the beta range of frequencies whereas IG peaks were more spread but more preferentially on the gamma band.

A second possible caveat in our *in vitro* study is the fact that we used two different electrodes to record from SG and IG domains. Systematic differences observed in these two domains could therefore reflect not a difference in layer, but the different band-pass properties of the two electrodes. We ruled out this possibility in three different ways. Firstly, we randomly selected the electrodes used to perform the recordings in each cortical domain for each *in vitro* experiment, so the same electrode used to record in SG in one experiment was subsequently used to record in IG in another experiment. Population averages would therefore average out possible differences in filtering properties of the electrodes. Secondly, we computed LFP power spectra in both UP and DOWN states and computed the ratio of these power spectra, i.e. the relative increase of power in UP relative to DOWN state for each frequency. We computed this relative power independently for SG and IG domains, so that any possible difference due to filtering properties of the electrodes would be eliminated through this analysis. The qualitative results of such analysis were the same as reported in the Results section. Thirdly, in some experiments we placed both electrodes in the same layer and recorded LFP signals separated horizontally on the slice. We then analyzed signals from the two electrodes using the same methods as we used for vertically separated recordings. The resulting power spectra overlapped in all cases, with no significant power deviation from one another. Taken together, this confirms that differences measured in LFP signals recorded from the two different electrodes in SG and IG domains reflected actual differences in neural activity in the two cortical domains.

Finally, we assumed that the compartmentalization of fast oscillations observed *in vivo* also applied *in vitro*. Another possibility would be that fast oscillations *in vitro* have multiple laminar generators. Laminar recordings *in vitro* would be necessary to test this hypothesis. In our *in vitro* recordings, single electrodes for SG and IG recordings were placed on the first and last third of cortical depth. Similar to *in vivo*, we observed that fast oscillations in SG and IG *in*

vitro were segregated in different frequency bands, and coherence levels between SG and IG were in the range 0.4-0.6. The analogy between our results *in vitro* and those obtained *in vivo*, suggest that the assumption of two domains for fast frequency generation is justified *in vitro*.

UP and DOWN statistics in vivo

A quantitative analysis of population spiking activity during synchronized states under urethane anesthesia has revealed that the statistics of UP and DOWN intervals together with the statistics of the instantaneous population rate in our experimental data indicates that the role of an adaptive process in causing transitions is weak, whereas fluctuations might have a larger impact driving the dynamics of UP-DOWN transitions.

We found that during synchronized states, U and D durations displayed skewed gamma-like distributions, exhibiting large coefficients of variation (mean±SEM: CV(U)=0.68±0.03 CV(D)=0.68±0.04, Figure 4.2.2.C). Consistently, UP and DOWN dynamics where characterized by a weak periodicity in the temporal pattern of the population rate. However, U an D durations showed positive correlations between consecutive periods (Figure 4.2.2.C), a common signature of slow fatigue processes which carry the information about previous activity to subsequent intervals. We searched for that fatigue process but found that during UP intervals the population firing rates did not revealed significant traces of rate adaptation, as indicated by a lack or non-evident progressive decrease of average population rate. Together, these seemingly contradictory results suggest that an adaptive mechanism exists but has a weak but significant role in determining the durations of Us and Ds, and that fluctuations, in the external inputs or in the local activity, might have a large impact driving the dynamics of UP-DOWN transitions.

We found a skewed average rate distribution of individual cells during UP or DOWN intervals with low and near-zero population mean, respectively. The temporal profile of population spike count variability across UP intervals was characterized by a transient surge at the U onset followed by relative stationary dynamics.

Irregular UP and DOWN intervals during synchronized states under urethane anaesthesia

During synchronized states, in particular those observed in natural slow-wave sleep (SWS) and under different anesthetics, cortical UP and DOWN transitions have been described to be modulated by a slow oscillation with a depolarizing and hyperpolarizing phase at less than 1 Hz that also groups faster population oscillatory events such as delta waves or spindles during those depolarizing phases (Steriade et al., 1993b, 1996).

The ability of cortical microcircuits to generate slow oscillatory activity with alternating UP and DOWN intervals has been shown in isolated cortex preparations (Sanchez-Vives and McCormick, 2000; Timofeev et al., 2000). This suggests a central role of cortex in their generation since no slow oscillatory activity

is displayed in the thalamus of decorticated animals (Timofeev and Steriade, 1996b). In this context, fatigue mechanisms, such as spike frequency adaptation or synaptic depression, are appealing candidates to explain the oscillatory switching. This idea has been implemented by different computational modeling studies ((Bazhenov et al., 2002; Compte et al., 2003), to name some examples). Moreover, if this type of mechanisms underlie the switching between UP and DOWN intervals it would be reflected as low variability in the U and D durations, positive correlation between consecutive periods and, a decrease in population firing rate as UP interval progresses. For this reason, a previous quantitative analysis of *in vivo* intracellular recordings during synchronized states in urethane anesthetized rats, questioned the characterization of the activity as a slow oscillation since they found skewed U and D distributions and correlation between consecutive intervals not significantly different than zero (Stern et al., 1997). In agreement with those results, during natural SWS of rats the statistics of D and cycle duration times display exponential shape distributions (Johnson et al., 2010). In contrast, the variability of U and D duration observed in ketamine–xylazine anesthetized mice is smaller for various cortical areas (CV<0.4, on average) with a special reduction in variability in prefrontal areas (CV<0.2) (Ruiz-Mejias et al., 2011).

Our results are in agreement with those reported in (Stern et al., 1997) where distribution of U and D durations are skewed with high coefficient of variation. However, we observed significant positive correlations between consecutive U-D and D-U (Figure 4.2.2) when they don't. A possible explanation of this discrepancy might be the reduced amount of considered intervals (30 in their case; we usually consider at the order of thousands of intervals) leading to difficulties in detecting the presence of weak correlations. Another possibility could be related with differences in cortical state. At moderate doses of urethane (similar to those used in our experimental data set and in (Stern et al., 1997)), spontaneous transitions between synchronized and desynchronized states are observed (Clement et al., 2008; Curto et al., 2009; Steriade et al., 1994). For this reason, we focused our analysis on sustained periods of synchronized states in the far end of the synch./desynch. spectrum (Fig. 4.2.1). The study by Stern and colleagues might have analyzed desynchronized periods where serial correlations between U and D become weaker (Fig. 4.4.2C). The difference with (Ruiz-Mejias et al., 2011) might be related with the anesthesia, ketamine vs. urethane, which generally has a strong impact in the UP and DOWN dynamics as discussed below.

Comparison of UP and DOWN dynamics across different anesthetics.

Deep levels of ketamine–xylazine tend to generate regular UP and DOWN dynamics with approximately Gaussian U and D distributions (Deco et al., 2009a), while low levels induce exponential shapes (Deco et al., 2009a). In a similar way, under light levels of barbiturate sodium thiopental anesthesia, UP and DOWN intervals are irregular with duration spanning from tens of milliseconds to seconds (Lampl et al., 1999).

Urethane is commonly used to induce synchronized states (Steriade et al., 1993a; Luczak et al., 2007, 2009). At high doses it induces sustained synchronized states (Détári et al., 1997) were more regular slow waves appear compared to what is

observed during SWS (Steriade et al., 1993a). However, moderate levels produce spontaneous cyclic alternations between synchronized and desynchronized states, which closely resemble the alternations observed between SWS and REM in rats natural sleep. For this reason, moderate levels of urethane have been proposed as a good model of sleep (Clement et al., 2008; Pagliardini et al., 2013). Moreover, the alternations of cortical states observed under urethane are not caused by variations in its concentration in the blood (Clement et al., 2008). Thus, with the doses used in our experiments and in contrast to what is sometimes assumed, synchronized and desynchronized periods are uniformly distributed over several hours following the administration of the anesthesia (i..e there is no drift towards desynchronized states as the drug is being metabolized). This does not mean that the dose of anesthesia does not affect the brain state (e.g. desynchronized periods can be triggered by a strong boost of urethane, Fig. 4.4.1A) but that the spontaneous alternations in brain state are observable for a considerable range of dose levels (Clement et al., 2008). Additionally, neural activity during synchronized states under urethane resembles that observed during natural SWS (Wolansky et al., 2006; Clement et al., 2008), although differences in the spontaneous firing properties of neurons have been reported (Luczak et al., 2007).

Ketamine-xylazine induces faster and stronger slow waves than those observed under urethane (Steriade et al., 1993a; Sharma et al., 2010).Moreover, ketamine-xylazine also induces greater mean D values than those observed during natural SWS conditions (Chauvette et al., 2011). When ketamine-xylazine and urethane anesthesias are compared, visual inspection of LFP ((Sharma et al., 2010), Fig. 2) and intracellular ((Steriade et al., 1993a), Fig. 5) traces during synchronized states suggest that the periodicity is weaker in the last condition. Although no rigorous comparison has been made under both anesthetics regarding the differences in UP and DOWN dynamics, these observations somewhat explain the difference between our results and those reported by (Ruiz-Mejias et al., 2011). Given that properties of slow fluctuations depend on experimental conditions (Chauvette et al., 2011; Contreras and Steriade, 1997), further quantitative comparisons of the UP-DOWN dynamics under different anesthetics would be necessary to clarify this discrepancy.

Weak periodicity of the slow global fluctuations during synchronized states under urethane anesthesia

In the seminal work of Steriade and colleagues on natural sleep in cats, UP and DOWN states appear in a slow oscillatory manner, which generates a strong rhythmicity manifested as ringing in the auto-correlogram (ACG) of the membrane voltage and LFPs and, therefore, causes the UP and DOWN intervals to be regular (Steriade et al., 1993a). In contrast, later work from the same group reported data showing ACGs with a steep decay and little ringing obtained from 20 sec time windows during SWS. The authors suggested that higher levels of rhythmicity (i.e. ACG ringing) can be revealed when ACGs are calculated from smaller time windows (Destexhe et al., 1999). In a control analysis we used small time windows and found that in some individual windows the ACG displayed ringing comparable to those reported by (Steriade et al., 1993a; Contreras and Steriade, 1997) (Figure A2.A from Appendix). However, the rhythmicity was temporally confined to

particular windows and decreased at neighboring windows. We conclude therefore that the rythmicity was not a robust and representative pattern of the global dynamics observed (Fig. A2.B). Power spectrum of the MUAc revealed a broad peak at ~0.7 Hz, which is consistent with previous studies that suggests this evidence as against a single oscillatory process causing UP/DOWN switching (Stern et al., 1997).

Although deep ketamine–xylazine anesthesia is commonly used as a model of SWS, a quantitative comparison of the two conditions reveals differences in the dynamics of spontaneous activity such as a robust UP/DOWN periodicity expressed by strong ringing in ACG under ketamine–xylazine that is greatly reduced in SWS (Chauvette et al., 2011). On the other hand, during synchronized states under moderate levels of urethane anesthesia, the ACG of cortical LFPs exhibit low levels of ringing (Figure 4.2.3) in agreement with previous results (Wolansky et al., 2006; Clement et al., 2008), and with those observed during natural SWS (Chauvette et al., 2011; Destexhe et al., 1999).

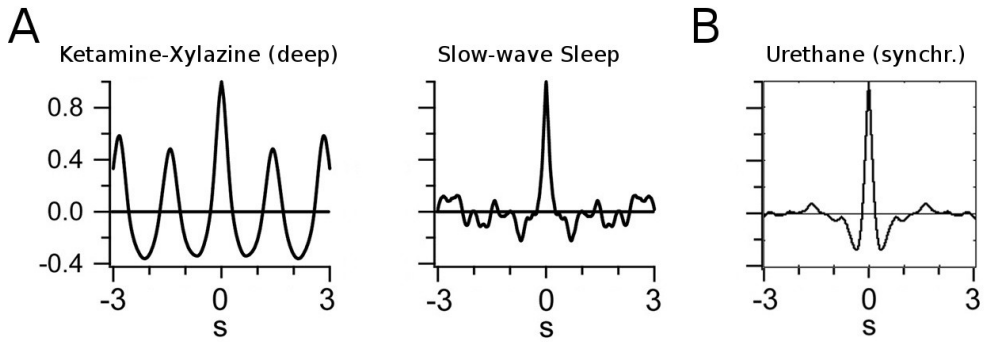

Figure 5.2. A. Rhythmicity of slow waves in local field potential is higher during ketamine–xylazine anesthesia than in SWS (modified from (Chauvette et al., 2011)). B, Example of autocorrelogram of local field potential during synchronized states of urethane anesthesia (same experiment as in Fig. 4.2.3).

Average Population rate during UP intervals does not display adaptation

UP and DOWN switching is thought to be generated by adaptive processes which build up during UP intervals and recover during DOWN intervals (Contreras et al., 1996; Sanchez-Vives and McCormick, 2000; Timofeev et al., 2000). This type of process generally cause a decrease in the population rate along the UP intervals. This decrease is observed during the UP/DOWN switching observed *in vitro*, where the rate of multiunit spiking activity decreases as evidenced by comparing the rate at the onset and the offset (Mattia and Sanchez-Vives, 2012). Our results showed in contrast that averaged population rates were stable during the UP intervals presenting no significant decrease between the onset and offset. Moreover, we performed the same analysis over D intervals and compared the average population rate at the onset and offset but found again no significant differences (data not shown). This finding is consistent with the idea of UP and DOWN intervals correspond to transitions between two attractor of the network dynamics (Cossart et al., 2003). Transitions between the two attractors in this framework must be caused my external inputs which “kick” the system from one basin of attraction to the other

(Martí et al., 2008; Deco et al., 2009a, 2009b) or by intrinsic fluctuations generated in the local activity of the circuit (Braun and Mattia, 2010) (particularly during the UP intervals since DOWN intervals are quiescent). It has been proposed that thalamic neurons showing rhythmic firing might cause DOWN to UP transitions (Crunelli and Hughes, 2010). This mechanism, however, causes in principle rhythmic transitions and, unless elaborated further to account for the lost of rythmicity in the UP/DOWN transitions, is not directly compatible with our findings.

Stationary variability of MUA activity during UP states and the surge at UP onset

Besides the strong rhythmicity usually observed during slow waves, another observed feature in the spiking activity from *in vitro* UP/DOWN transitions is an increase in the variability of the multiunit spike count at the UP offset compared to the onset (i.e. the spike count distribution at the offset is broader) (Mattia and Sanchez-Vives, 2012). This might be caused by an increase in activity-dependent self-inhibition that reduces the stability of the UP attractor yielding larger fluctuations in the population activity (Mattia and Sanchez-Vives, 2012). In contrast to this, our results showed that variability displays a surge at the onset of UP intervals that is followed by stationary dynamics (i.e. a plateau in the Fano factor of the population spike count). We also observed that the offset is not preceded by an increase in variability. Moreover, after the transient surge in variability, mean single cell Fano factors are approximately one, consistent with Poisson statistics, and the mean instantaneous pair-wise correlation coefficient does not exhibit any build-up but just stationary positive and near-zero values. Simultaneous intracellular recordings during UP/DOWN dynamics of multiple cells have shown an increased variability across the membrane voltages of the recorded neurons at the onset but not at offset of UP intervals (Chen et al., 2012). Although the variability in this study refers to the degree to which neurons transition synchronously from DOWN to UP and viceversa (the study did not measure variability across UP intervals), together with our finding describes a system exhibiting a repertoire of different ways to undergo DOWN to UP transitions but a homogenous way to undergo UP to DOWN transitions. This is reminiscent of the observation reporting a variety of different traveling waves causing the initiation of UP intervals (Massimini et al., 2004; Sanchez-Vives and McCormick, 2000; Luczak et al., 2007, 2013). Additionally, the initial portion of UP states might reflect different patterns (Luczak et al., 2007, 2009) that might be related to consolidation processes (Chauvette et al., 2012). We summarized our finding in Figure 5.3 showing a cartoon of the population instantaneous rate during various individual UP intervals: at the DOWN to UP transition, the rate follows a variety of trajectories until it reaches the steady state. The transitions from UP to DOWN occur in a stereotyped fashion (something for which there is no mechanistic explanation).

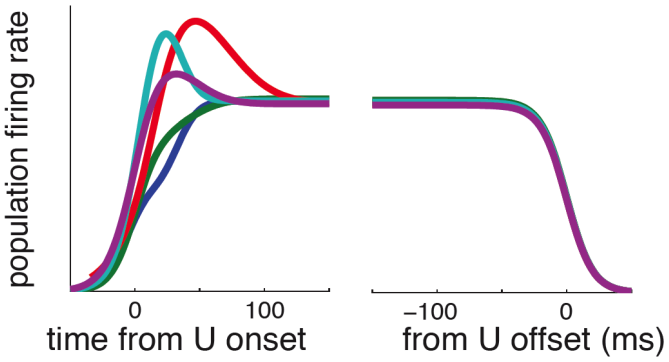

Figure 5.3. Schematics of population instantaneous rates during different UP intervals.

We found that the average individual firing rate during UP intervals, 3.6 spikes per second, was comparable with recent patch clamp studies(Waters and Helmchen, 2006; Constantinople and Bruno, 2011; Gentet et al., 2012) and extra/juxta cellular recordings (Sakata and Harris, 2009; Massi et al., 2012). Nevertheless, this value overestimates the real average rate in the cortical network given that our extracellular recording method is not sensitive to the presence of neurons in the local network that do not fire spontaneous action potentials during synchronized states (Rudolph et al., 2007; Steriade et al., 2001). Moreover, the spike sorting method is biased towards high firing rate neurons, because isolating a handful of waveforms is statistically more difficult than a large cluster. Regarding the average rate during DOWN intervals, 0.08 spikes/s, it is to our knowledge the first report of this magnitude and cannot therefore be compared with previous analysis.

Dynamics of putative E and I neurons during UP states

Classification of units based on waveforms into narrow spiking (putative inhibitory, I) and broad spiking cells (putative excitatory, E) revealed that the UP offset was preceded by a drop in firing rate of the I population which was the followed by a fast decrease of E population rate. In agreement with our observations, intracellular studies *in vivo,* comparing onset and offset aligned conditions, show that excitatory RS cells display sustained firing rates during the UP intervals whereas inhibitory FS cells show firing rates that decrease towards the end of the UP interval (Haider et al., 2006). The same temporal profiles were observed in the excitatory and inhibitory synaptic conductances inferred from voltage clamp recordings (Haider et al., 2006). In the same way, other intracellular studies have shown similar dynamics in the conductances with a drop of inhibitory conductance preceding the UP offset (Rudolph et al., 2007), despite differences observed in the conductance values. Altogether, these results contradict previous theoretical work suggesting that UP intervals are terminated by an increase in inhibitory activity (Compte et al., 2003; Parga and Abbott, 2007; Melamed et al., 2008; Chen et al., 2012).

Mechanisms underlying UP and DOWN dynamics in neocortex

We have investigated the mechanisms of intrinsic UP-and-DOWN dynamics in cortical networks using a computational low dimensional model that implements cellular adaptation and random input fluctuations. We studied the contribution of each mechanism to the statistics of UP and DOWN states and the interplay between excitation and inhibition that can lead to stable quiescent and low firing rate states. In particular, we showed that a network model with: i) bistability based on a specific asymmetry in the *f-I* curves of excitatory and inhibitory cells (larger threshold and gain for the inhibitory population), ii) a weak activity-dependent adaptation current in the excitatory population, and iii) large-amplitude external input fluctuations, can reproduce the key features of UP and DOWN statistics observed during the synchronized states of cortical activity under urethane anesthesia presented in Chapter 4.2.

Bistablity at low rates

In the isolated cortex, UP and DOWN state dynamics has been proposed to emerge as a consequence of synaptically amplified spontaneous activity. Such activity would be initiated by spontaneous release of neurotransmitter (Timofeev et al., 2000) or by spontaneously active cells (Sanchez-Vives and McCormick, 2000; Compte et al., 2003), and then it would be amplified by strong recurrent excitation in the cortical circuit. Eventually, synaptically sustained activity is overcome by an activity-dependent negative feedback provided by a fatigue mechanism such as synaptic depression (Contreras et al., 1996; Timofeev et al., 2001) or adaptation membrane currents (Sanchez-Vives and McCormick, 2000). These principles have been implemented in detailed computational models (Bazhenov et al., 2002; Compte et al., 2003; Kang et al., 2004; Hill and Tononi, 2005; Cunningham et al., 2006; Parga and Abbott, 2007; Destexhe, 2009; Benita et al., 2012). Additionally, alternation between two rate states using these principles have been studied in different low-dimensional rate models and mean-field approximations (Latham et al., 2000; van Vreeswijk and Hansel, 2001; Holcman and Tsodyks, 2006; Melamed et al., 2008; Deco et al., 2009a; Lim and Rinzel, 2010; Mejias et al., 2010; Mattia and Sanchez-Vives, 2012).

Although there are numerous computational studies exploiting these ideas, there are few studies concerned about the low firing rates observed during UP periods (Latham et al., 2000) and the variability and correlations observed in the permanence times of UP and DOWN states (Holcman and Tsodyks, 2006; Mejias et al., 2010). Our modeling effort in Chapter 4.3 of this Thesis sought to address these statistical constraints, and their implications for the mechanistic hypotheses currently formulated in the literature. This was done in direct relationship to the experimentally observed statistics of UP and DOWN state dynamics reported in Chapter 4.2.

Our model is based on the Wilson-Cowan equations (Wilson and Cowan, 1972), which describe the activity of a local network of excitatory and inhibitory

neurons and which has been used to study many different neuroscience problems from a computational perspective (Destexhe and Sejnowski, 2009). In the seminal paper by Wilson and Cowan (1972), it was shown that it is possible to obtain a bistable regime of quiescent and active states with a network composed of an excitatory and an inhibitory population (EI network). However, the bistable active state was obtained on the saturating parts of the *f-I* curves (Wilson and Cowan, 1972), thus leading to high firing rates. In addition, Latham and colleagues (Latham et al., 2000) concluded that robust bistability could only be achieved in an EI network if the active state had high firing rates. Indeed, a bistable active state could be obtained at lower rates, but it was restricted to a very small parameter region (Fig. 4B in (Latham et al., 2000)), which is in addition incompatible with the straight phase-plane nullclines expected in high connectivity networks (van Vreeswijk and Sompolinsky, 1998). This must now be revised on the light of our modeling results. Our model shows that bistability can be achieved with "straight" nullclines from linear-threshold *f-I* curves based on one additional key assumption: firing threshold for *I* neurons is higher than for *E* neurons. In agreement with this assumption, patch clamp experiments *in vitro* reveal that the firing threshold for inhibitory fast-spiking neurons is higher than for excitatory regular-spiking neurons (Cruikshank et al., 2007; Schiff and Reyes, 2012). These differences in firing thresholds were measured in the absence of synaptic input (silent slices) in similar conditions to DOWN state periods, which are characterized by synaptic silence (Contreras et al., 1996; Timofeev et al., 2001). Therefore, we show that one additional parameter, the threshold of the inhibitory population, allows an EI network of the type considered by Latham et al. (2000) to have a robust bistable regime with an active state with arbitrarily low firing rate in the absence of fluctuations.

Impact of adaptation and fluctuations on the UP and DOWN state statistics

Transitions between UP and DOWN states can occur by a mixture of adaptation and fluctuation mechanisms in our model, and a regime of weak adaptation and strong fluctuations predicts the experimental statistics reported in Chapter 4.2 of this Thesis.

As discussed before, the cellular and network mechanisms involved in the initiation, maintenance and termination of UP states are still a matter of debate. On the one hand, an adaptive process might be responsible for generating the alternation between activity states in the isolated cortex. This is consistent with the firing rates and statistics of permanence times observed in some *in vitro* experiments, where Gaussian permanence time distributions and firing rate decay through the UP states are observed (Mattia and Sanchez-Vives, 2012). On the other hand, the cortical network *in vivo* can generate more complex patterns of slow waves, with increased variability in the alternating dynamics, and additional mechanisms such as the role of subcortical input causing transitions have been proposed (Battaglia et al., 2004; Crunelli and Hughes, 2010; Slézia et al., 2011; Ushimaru et al., 2012). In this context, previous computational studies have stressed

the role of external input fluctuations in generating irregular UP and DOWN states dynamics (Holcman and Tsodyks, 2006; Mejias et al., 2010) that reproduce the large variability observed in permanence times in some *in vivo* preparations (Lampl et al., 1999; Deco et al., 2009a). Our model also stresses the role of fluctuations in order to obtain high variability in permanence times. Additionally, it emphasizes the presence of a weak adaptation mechanism, which provides a memory trace of the amount of time spent in the previous DOWN/UP state and it constrains the permanence time in the current UP/DOWN state, thus introducing positive correlations between consecutive permanence times. The effect of fluctuations in state switching and their impact on permanence time correlation has been studied in the context of self excitatory systems with activity-dependent depression such as central pattern generators and models of the developing spinal cord (Tabak et al., 2001; Lim and Rinzel, 2010; Tabak et al., 2011).

We found that in a noise-driven regime, where fluctuations are necessary to induce transitions between UP and DOWN states, weak adaptation was needed to introduce positive correlations between consecutive states and shape the permanence time distributions to match the experimental data. In a different context, this interplay between strong noise and weak adaptation has been proposed to underly perceptual bistability processes (Moreno-Bote et al., 2007; Shpiro et al., 2009). Again, in that context the criteria to identify the plausible mechanistic regime was to compare with experimental distributions of perceptual permanence times and correlations. Interestingly, they reached similar conclusions to us even if their network dynamics was totally different from ours. Those perceptual bistability models consist of two populations that compete to determine the dominant population in a winner-take-all regime. Instead, our UP and DOWN state model also includes two populations, but they do not interact symmetrically through competition, and the ensuing dynamics is not winner-take-all (Deco et al., 2009a) but both populations are simultaneously active or silent in the dynamics. The convergence onto similar mechanisms based on different alternating network dynamics suggests that this interplay between noise and adaptation might be a basic principle of neuronal networks operation.

Oscillations in the rate model

The model proposed can operate in two different regimes. In one, the UP state fixed point is an unstable focus, and robust periodic oscillations develop during the UP state as the system stabilizes in a limit cycle. In the second regime, the UP state fixed point is a stable focus, and damping oscillations are observable as the system relaxes to the focus through a spiral dynamics. These damped oscillations are more prevalent at the temporal edges of UP states, but they will also persist through the UP state when the system is subject to random fluctuations that continuously move the system away from the focus. This is consistent with our experimental data in the first chapters of these thesis. In Chapter 4.1, we found that fast oscillations (30-80 Hz) can be detected in LFPs recorded in both supragranular and infragranular layers during UP states, especially *in vivo* but also in *in vitro* recordings. In Chapter 4.2, we showed that fast oscillations are also observable in the MUA activity of deep

layers of cortex during UP states (see Appendix from Chapter 4.2, Fig. A3).

The ability of linear threshold neuronal networks to generate oscillations has been studied previously (Hahnloser, 1998; Tang et al., 2005). Although our model is capable of generating robust oscillations during the UP states, for sufficiently slow inhibitory time constant, we restricted our analysis to the stable focus regime because our experimental data did not reveal large-amplitude robust oscillations during UP states but rather weak dynamics. However, we observed that also in this regime the lengthening of the inhibitory time constant generates a surge in rate right at the temporal edges of the UP states, and specially in the UP to DOWN transition due to changes in the shape of the UP basin of attraction. Interestingly, spontaneous termination of self-sustained (persistent) activity in integrate and fire spiking networks can also be associated with a strong transient population event (Kumar et al., 2008). In contrast, as shown in Chapter 4.2, we did not observe such a surge in firing rate at the temporal edges of UP states in the experimental data. This suggests that the effective time constants of the excitatory and the inhibitory populations *in vivo* are approximately the same. This is in agreement with some experimental studies, which have reported equal time constants for both EPSCs and IPSCs (Matsumura et al., 1996), but at variance with other *in vitro* studies that found slower inhibitory than excitatory synaptic currents (Tarczy-Hornoch et al., 1998; Williams and Stuart, 2002). Slower inhibition than excitation generates in our model firing rate peaks at the onset and offset of the UP state that we do not see experimentally.

Transition between attractor states associated with a transitory increase in variability

The evidence of relatively stable rates during UP and DOWN states (Chapter 4.2) is in agreement with the view of UP and DOWN states as attractor states as previously suggested (Cossart et al., 2003). In this thesis we also explored the signature of different network regimes in the dynamics of variability across UP states. In Chapter 4.2, we showed that experimentally the transition from DOWN to UP is associated with a surge in variability, whereas in the UP to DOWN transition this variability was generally smaller. Moreover, throughout the UP state the variability showed stationary values. When we study this in the model, we observe that transitions between states are also generally associated with a brief period of increased variability. Instead, the dynamics of rate variability in the course of the UP state is different for different network regimes. In the oscillatory regime, with periodic transitions between UP and DOWN states, rate variability increases during the time course of the UP state. This is consistent with previous experimental observations in UP and DOWN states *in vitro (Mattia and Sanchez-Vives, 2012)*. However, in the regime with strong fluctuations and weak adaptation that provides permanence time statistics compatible with the *in vivo* data from Chapter 4.2, variability remains stationary through the UP state, consistent with the view of UP states a stable attractor states.

Predictions and Future work

Electrophysiological recording techniques have improved dramatically in the last decades, and we are now able to record the activity of hundreds to thousands of neurons and to manipulate selectively network activity through optogenetic techniques. Such new techniques open exciting new possibilities to test predictions and mechanisms suggested by computational models of the cortical network.

Bistability in our model relies on the assumption that the firing threshold of inhibitory neurons is higher than for excitatory neurons. Although this is reported to occur *in vitro* (Cruikshank et al., 2007; Schiff and Reyes, 2012), as discussed above, the question of whether firing threshold is larger for inhibitory cells during DOWN states, when synaptic background is abolished, remains to be explored *in vivo*. Some problems like the fact that DOWN states can occur locally (Sirota and Buzsáki, 2005), might be necessary to tackle in order to provide an answer to this question.

Moreover, our model predicts that the rate decay of *I* neurons is stronger than the rate decay observed in *E* neurons during UP states . We test this hypothesis in the experimental data from Chapter 4.2, where E and I neurons are putatively defined based on their extracellular spike form. The reduced number of putative I neurons obtained makes this ratio noisy, although for some experiments this effect was present (see Figure A5 in Appendix from Chapter 4.2). Further experiments need to be performed in order to confirm this prediction.

Another feature observed in the model is the average incoming fluctuations causing transitions, which determine the most effective way of stimulating the network in order to cause transitions in a state dependent manner (Fig. 4.4.13). In this way, selective stimulation of inhibitory and excitatory cells by optogenetic manipulations (Beltramo et al., 2013) could test this hypothesis. Specifically, the model predicts that a concomitant excitation of inhibitory cells followed by inhibition of excitatory cells is the most effective way of causing UP to DOWN transitions, whereas the solely stimulation of excitatory cells would trigger DOWN to UP transitions.

Our model also suggests future computational work. We have considered a single source of fluctuations modelled as an Ornstein-Uhlenbeck stochastic process, although it is meant to capture two possible sources of noise in the system: subcortical inputs and self-generated noise by the recurrent network. The time scales of these two sources might be different, and this could have an impact on the dynamics. On the one hand, the external input coming from subcortical structures could be modelled as sporadic “shot noise”, with very rare but very high amplitude fluctuation events which would potentially increase the variability. Moreover, self-generated fluctuations by the network could have two different components (such as additive or multiplicative on the rate). Furthermore, another possibility is that noise-induced amplification of oscillations (Bressloff, 2010) could also increase the variability of the permanence time and capture better the statistics observed experimental data.

Finally, the principles of our low-dimensional EI network model can be used to implement a more realistic spiking network model in the future. Such a model would allow to explore in detail additional network dynamics emerging from the interactions between single cells during UP states, and would allow a more

principled biological implementation of both the adaptation and the random fluctuation mechanisms that we have found to play an important role in generating UP and DOWN dynamics in the cortical network *in vivo*.

Statistics of UP and DOWN dynamics across synchronized and desynchronized states

In Chapter 4.4 we showed that the spontaneous and continuous variations in brain state observe in the rat cortex under urethane anesthesia were associated with systematic changes in the UP and DOWN statistics, and that brain state along this broad range was well described by the silence density. . The changes in UP/DOWN statistics as the brain changes from desynchronized to more synchronized states can be summarized as: i) Ds became longer and more variable, whereas Us became shorter and less variable; ii) correlation between consecutive periods increased and correlation between (D_{i-1},U_i) pairs was strongly increased for A1 experiments; iii) population firing rates during UP intervals increased. Although it has been shown that spontaneous brain states as those induced by anesthesia have an impact in cortical dynamics (Adrian and Matthews, 1934; Steriade et al., 2001; Erchova et al., 2002; Curto et al., 2009; Deco et al., 2009a; Clement et al., 2008), the results presented in this Thesis are to our knowledge the first statistical characterization of the changes in UP/DOWN dynamics as brain states varies continuously. The results obtained for this analysis (Chapter 4.4) from the somatosensory cortex experiments that were performed in different setups and by different experimenters (see Methods), support the robustness of our estimations described in Chapter 4.2, since the statistics of U and D at the maximum silence density (~0.5) for the somatosensory experiments are similar to those reported there (see Fig. 4.2.2)

The characterization of UP and DOWN dynamics *in vivo* varies in different studies and preparations. On one extreme, UP duration duration ranges from hundreds of milliseconds to seconds (Lampl et al., 1999; Anderson et al., 2000a). On the other extreme, a recent study states that UP intervals are manifested as "rare" transitory bumps (DeWeese and Zador, 2006; Hromádka et al., 2013). In between, UP and DOWN states are characterized to appear as slow oscillations (Steriade et al., 1993a; Petersen et al., 2003b; Haider et al., 2006; Poulet and Petersen, 2008; Sakata and Harris, 2009; Ruiz-Mejias et al., 2011), to name some studies). The heterogeneity of these dynamics shows the different possible repertoire of regimes in the cortical spontaneous activity dynamics under different anesthetics and brain states. Despite this seemingly contradictory set of possible UP/DOWN dynamics, we showed that spontaneous transitions between synchronized and synchronized states altered the statistics of UP and DOWN dynamics in a robust and continuous manner and that these changes could be related by means of a simple computational network model

Mechanisms underlying transitions between synchronized and desynchronized states

Cortical desynchronization via basal forebrain stimulation induces an increase in the firing rate of thalamocortical neurons (Castro-Alamancos and Oldford, 2002). Moreover, cortical desynchronization caused by either cholinergic

thalamic stimulation or basal forebrain stimulation in urethane anesthetized rats is associated with a reduction of spontaneous firing rate for most RS cortical cells while the firing rate of cortical FS is increased (Hirata and Castro-Alamancos, 2010). In addition, recordings in alert/nonalert awake rabbits shows that firing rate of L4 pyramidal cells does not change across brain states, whereas L4 FS increase their firing rate towards alert (more desynchronized) states in unanesthetized rabbits (Stoelzel et al., 2008). Desynchronized states are overall associated with a reduction in the firing rate in superficial layers of cortex of RS and FS cells, so the effect in firing rates seems layer dependent(Gentet et al., 2012; Sakata and Harris, 2012). The picture might be even more complex since a recent study in layer II/III has shown that the firing rate of excitatory and parvalbumin-positive cells increases at low levels of cortical desynchronization as a result of activation of muscarinic receptors and decreases under strong desynchronization as a result of activation of nicotinic receptors (Alitto and Dan, 2012). Indeed, the mechanisms by which arousal affect cortical dynamics are unclear and the precise role of neuromodulators is still debated. The common description that emerges from these studies is that acetylcholine decreases the efficacy of intracortical EPSPs (via muscarinic receptors) (Gil et al., 1997) and enhances thalamocortical synaptic transmission (via nicotinic receptors) (Gil et al., 1997; Kawai et al., 2007; Disney et al., 2007). Moreover, the presence acetylcholine blocks or reduces the magnitude of K+ conductances that are responsible for spike frequency adaptation in cortical neurons in thalamocortical cells *in vitro* (McCormick, 1992), which presumably would produce the same effect in cortical cells *in vivo (Steriade et al., 1993b)*. However, the central role of acetylcholine has been recently challenged by a study which suggests that norepinephrine is the crucial neuromodulator responsible for cortical desynchronization (Constantinople and Bruno, 2011).

Consistent with this common view derived largely from *in vitro* experiments, previous computational work have modeled the transitions from synchronized to desynchronized states by modeling the effects of an increase in acetylcholine in the network: (i) decreasing K^+ conductances and (ii) decreasing the strength of intra-cortical excitatory connections, constrained by experimental observations regarding input resistance values and voltage membrane traces in sleep and awake recordings (Bazhenov et al., 2002; Compte et al., 2003; Hill and Tononi, 2005; Rudolph et al., 2005; Destexhe, 2009). Moreover, the phenomenology of the transitions had also been study from a mean-field approximation (Wilson et al., 2005). However, the impact on the statistics of UP and DOWN transitions has not been a matter of discussion in the aforementioned computational studies, despite that each particular mechanism imprints a particular signature in those statistics, as described in Chapter 4.4.

To understand the changes in network dynamics caused by the transitions between desynchronized and synchronized states, we proposed a simple rate model including adaptation and external fluctuating inputs as the underlying mechanisms generating UP and DOWN switching. The model qualitatively reproduced the experimental observations regarding UP/DOWN statistics in the extremes desynchronized and synchronized axes, by changing two parameters. As the state became more synchronized i) the mean external input decreased, ii) the amplitude of fluctuations increased. The first condition is supported by the

electrophysiological aforementioned evidence (Castro-Alamancos and Oldford, 2002).

Moderate levels of urethane anesthesia induce cyclic alternations between desynchronized and synchronized states resembling those observed during SWS and REM sleep (Clement et al., 2008; Pagliardini et al., 2013). Alternatively to the idea of a central role of acetylcholine and monoamines in cortical desynchronization, it has also been proposed that there are two inhibitory populations in the brain stem that compete via mutual inhibition producing alternation between REM and SWS (the "flip-flop" model) (Lu et al., 2006). This mechanism has been proposed to underlie the sleep regulation (Borbély and Achermann, 1999) and has been used from a computational perspective (Rempe et al., 2010; Phillips et al., 2010). The picture, however, gets more complicated when considering that alternations between REM and SWS during natural sleep alter the properties of slow waves and the firing rates of individual cells when going from early to late phases of sleep (Vyazovskiy et al., 2009). The impact of subsequent cyclic alternations in the UP and DOWN dynamics is however beyond the scope of this Thesis.

The model presented in Chapter 4.4 is the first step towards the understanding of the basis of cortical desynchronization. We did not explore the possibility that changes in other model parameters such as the connectivity (J), the adaptation strength (β) or the statistical structure of the external fluctuations could explain better the observations from the experimental results. Moreover, the bistability at low rates obtained in the Chapter 4.4 model relies in unrealistic assumptions of the transfer function which "start to saturate" at low values of firing rate. Regarding this, the EI model proposed in Chapter 4.3 could be used to explain how cortical desynchronization in achieved in a more realistic way. In sum, there are still a number of questions to solve about the impact of changes in different model parameters to understand the fundamental aspects playing a role in shaping the UP and DOWN statistics changes towards cortical desynchronization, and this will be explored in future work.

6. Conclusions

(From Chapter 4.1):

1. Segregation in different laminar domains of fast oscillations (10-100 Hz) can be observed during spontaneous cortical UP states *in vivo*, despite the strong intracolumnar vertical connectivity and the highly synchronous cortical activation patterns during slow oscillations.

2. Although supra and infragranular cortical layers displayed fast oscillations at different frequency ranges *in vitro*, increasing the excitability homogenized the frequency of fast oscillations across the cortical column, mimicking our observations *in vivo*. This suggests that modulation of local excitability can control inter-laminar couplings and oscillatory dynamics in cortical circuits.

(From Chapter 4.2):

3. The statistics of the duration of UP and DOWN intervals during synchronized states under urethane anesthesia together with the lack of a decrease in average rate during UP intervals, stress the role of external fluctuating inputs in causing UP-DOWN transitions, although positive correlations among consecutive UP and DOWN intervals suggest the existence of a slow fatigue process (such as spike frequency adaptation) contributing in the generation of transitions.

(From Chapter 4.3):

4. A low dimensional rate model of a EI network with: i) bistability based on an asymmetry in the *f-I* curves of E and I cells (larger I threshold & gain), ii) spike frequency adaptation in the E cells, iii) external input fluctuations, can reproduce the key features of UP and DOWN statistics observed under urethane anesthesia.

(From Chapter 4.4):

5. Spontaneous variations in brain state (i) can be easily tracked by computing the silence density over short epochs (~1 min) and (ii) have an enormous impact on the statistics of UP and DOWN intervals. This impact can be quantitatively described by relations between silence density and UP/DOWN statistics which are consistently observed across animals.

6. A simple rate model of a recurrent network including both adaptation and noisy inputs can produce UP and DOWN statistics similar to the experimental data. Changes observed in the statistics across the desynchronized and synchronized extremes can qualitatively be reproduced by changes in the model parameters.

7. Bibliography

Achermann, P., and Borbély, A.A. (1997). Low-frequency (< 1 Hz) oscillations in the human sleep electroencephalogram. Neuroscience *81*, 213–222.

Adrian, E.D., and Matthews, B.H. (1934). The interpretation of potential waves in the cortex. J. Physiol. *81*, 440–471.

Van Aerde, K.I., Mann, E.O., Canto, C.B., Heistek, T.S., Linkenkaer-Hansen, K., Mulder, A.B., van der Roest, M., Paulsen, O., Brussaard, A.B., and Mansvelder, H.D. (2009). Flexible spike timing of layer 5 neurons during dynamic beta oscillation shifts in rat prefrontal cortex. J. Physiol. *587*, 5177–5196.

Ainsworth, M., Lee, S., Cunningham, M.O., Roopun, A.K., Traub, R.D., Kopell, N.J., and Whittington, M.A. (2011). Dual γ rhythm generators control interlaminar synchrony in auditory cortex. J. Neurosci. Off. J. Soc. Neurosci. *31*, 17040–17051.

Alitto, H.J., and Dan, Y. (2012). Cell-type-specific modulation of neocortical activity by basal forebrain input. Front. Syst. Neurosci. *6*, 79.

Amatrudo, J.M., Weaver, C.M., Crimins, J.L., Hof, P.R., Rosene, D.L., and Luebke, J.I. (2012). Influence of highly distinctive structural properties on the excitability of pyramidal neurons in monkey visual and prefrontal cortices. J. Neurosci. Off. J. Soc. Neurosci. *32*, 13644–13660.

Amzica, F., and Steriade, M. (1995a). Short- and long-range neuronal synchronization of the slow (< 1 Hz) cortical oscillation. J. Neurophysiol. *73*, 20–38.

Amzica, F., and Steriade, M. (1995b). Disconnection of intracortical synaptic linkages disrupts synchronization of a slow oscillation. J. Neurosci. Off. J. Soc. Neurosci. *15*, 4658–4677.

Anderson, J., Lampl, I., Reichova, I., Carandini, M., and Ferster, D. (2000a). Stimulus dependence of two-state fluctuations of membrane potential in cat visual cortex. Nat. Neurosci. *3*, 617–621.

Anderson, J.S., Lampl, I., Gillespie, D.C., and Ferster, D. (2000b). The contribution of noise to contrast invariance of orientation tuning in cat visual cortex. Science *290*, 1968–1972.

Arieli, A., Shoham, D., Hildesheim, R., and Grinvald, A. (1995). Coherent spatiotemporal patterns of ongoing activity revealed by real-time optical imaging coupled with single-unit recording in the cat visual cortex. J. Neurophysiol. *73*, 2072–2093.

Arieli, A., Sterkin, A., Grinvald, A., and Aertsen, A. (1996). Dynamics of ongoing activity: explanation of the large variability in evoked cortical responses. Science *273*, 1868–1871.

Ascoli, G.A., Alonso-Nanclares, L., Anderson, S.A., Barrionuevo, G., Benavides-Piccione, R., Burkhalter, A., Buzsáki, G., Cauli, B., Defelipe, J., Fairén, A., et al. (2008). Petilla terminology: nomenclature of features of GABAergic interneurons of the cerebral cortex. Nat. Rev. Neurosci. *9*, 557–568.

Baker, S.N., Olivier, E., and Lemon, R.N. (1997). Coherent oscillations in monkey motor cortex and hand muscle EMG show task-dependent modulation. J. Physiol. *501 (Pt 1)*, 225–241.

Baldissera, F., and Gustafsson, B. (1971). Regulation of repetitive firing in motoneurones by the afterhyperpolarization conductance. Brain Res. *30*, 431–434.

Barbour, D.L., and Callaway, E.M. (2008). Excitatory local connections of superficial neurons in rat auditory cortex. J. Neurosci. Off. J. Soc. Neurosci. *28*, 11174–11185.

Barthó, P., Hirase, H., Monconduit, L., Zugaro, M., Harris, K.D., and Buzsáki, G. (2004). Characterization of neocortical principal cells and interneurons by network interactions and extracellular features. J. Neurophysiol. *92*, 600–608.

Bartos, M., Vida, I., and Jonas, P. (2007). Synaptic mechanisms of synchronized gamma oscillations in inhibitory interneuron networks. Nat. Rev. Neurosci. *8*, 45–56.

Battaglia, F.P., Sutherland, G.R., and McNaughton, B.L. (2004). Hippocampal sharp wave bursts coincide with neocortical “up-state” transitions. Learn. Mem. Cold Spring Harb. N *11*, 697–704.

Bazhenov, M., Timofeev, I., Steriade, M., and Sejnowski, T.J. (2002). Model of thalamocortical slow-wave sleep oscillations and transitions to activated States. J. Neurosci. Off. J. Soc. Neurosci. *22*, 8691–8704.

Beltramo, R., D’Urso, G., Dal Maschio, M., Farisello, P., Bovetti, S., Clovis, Y., Lassi, G., Tucci, V., De Pietri Tonelli, D., and Fellin, T. (2013). Layer-specific excitatory circuits differentially control recurrent network dynamics in the neocortex. Nat. Neurosci. *16*, 227–234.

Benita, J.M., Guillamon, A., Deco, G., and Sanchez-Vives, M.V. (2012). Synaptic depression and slow oscillatory activity in a biophysical network model of the cerebral cortex. Front. Comput. Neurosci. *6*, 64.

Binzegger, T., Douglas, R.J., and Martin, K.A.C. (2004). A quantitative map of the circuit of cat primary visual cortex. J. Neurosci. Off. J. Soc. Neurosci. *24*, 8441–8453.

Biswal, B.B., Mennes, M., Zuo, X.-N., Gohel, S., Kelly, C., Smith, S.M., Beckmann, C.F., Adelstein, J.S., Buckner, R.L., Colcombe, S., et al. (2010). Toward discovery science of human brain function. Proc. Natl. Acad. Sci. U. S. A. *107*, 4734–4739.

Bokil, H., Andrews, P., Kulkarni, J.E., Mehta, S., and Mitra, P.P. (2010). Chronux: a platform for analyzing neural signals. J. Neurosci. Methods *192*, 146–151.

Bonhoeffer, T., and Grinvald, A. (1991). Iso-orientation domains in cat visual cortex

are arranged in pinwheel-like patterns. Nature *353*, 429–431.

Le Bon-Jego, M., and Yuste, R. (2007). Persistently active, pacemaker-like neurons in neocortex. Front. Neurosci. *1*, 123–129.

Borbély, A.A., and Achermann, P. (1999). Sleep homeostasis and models of sleep regulation. J. Biol. Rhythms *14*, 557–568.

Boucetta, S., Crochet, S., Chauvette, S., Seigneur, J., and Timofeev, I. (2013). Extracellular Ca2+ fluctuations in vivo affect afterhyperpolarization potential and modify firing patterns of neocortical neurons. Exp. Neurol. *245*, 5–14.

Braun, J., and Mattia, M. (2010). Attractors and noise: twin drivers of decisions and multistability. Neuroimage *52*, 740–751.

Bressloff, P.C. (2010). Metastable states and quasicycles in a stochastic Wilson-Cowan model of neuronal population dynamics. Phys. Rev. E Stat. Nonlin. Soft Matter Phys. *82*, 051903.

Brodmann, K. (1909). Vergleichende Lokalisationslehre der Grosshirnrinde (Barth-Verlag).

Brunel, N. (2003). Dynamics and plasticity of stimulus-selective persistent activity in cortical network models. Cereb. Cortex New York N 1991 *13*, 1151–1161.

Brunel, N., and Wang, X.-J. (2003). What determines the frequency of fast network oscillations with irregular neural discharges? I. Synaptic dynamics and excitation-inhibition balance. J. Neurophysiol. *90*, 415–430.

Buffalo, E.A., Fries, P., Landman, R., Buschman, T.J., and Desimone, R. (2011). Laminar differences in gamma and alpha coherence in the ventral stream. Proc. Natl. Acad. Sci. U. S. A. *108*, 11262–11267.

Buzsaki, G., Bickford, R.G., Ponomareff, G., Thal, L.J., Mandel, R., and Gage, F.H. (1988). Nucleus basalis and thalamic control of neocortical activity in the freely moving rat. J. Neurosci. Off. J. Soc. Neurosci. *8*, 4007–4026.

Buzsáki, G. (2006). Rhythms of the Brain.

Buzsáki, G., and Draguhn, A. (2004). Neuronal oscillations in cortical networks. Science *304*, 1926–1929.

Buzsáki, G., Anastassiou, C.A., and Koch, C. (2012). The origin of extracellular fields and currents–EEG, ECoG, LFP and spikes. Nat. Rev. Neurosci. *13*, 407–420.

La Camera, G., Rauch, A., Thurbon, D., Lüscher, H.-R., Senn, W., and Fusi, S. (2006). Multiple time scales of temporal response in pyramidal and fast spiking cortical neurons. J. Neurophysiol. *96*, 3448–3464.

Campbell, S.L., Mathew, S.S., and Hablitz, J.J. (2007). Pre- and postsynaptic effects of kainate on layer II/III pyramidal cells in rat neocortex. Neuropharmacology *53*, 37–47.

Cash, S.S., Halgren, E., Dehghani, N., Rossetti, A.O., Thesen, T., Wang, C.,

Devinsky, O., Kuzniecky, R., Doyle, W., Madsen, J.R., et al. (2009). The human K-complex represents an isolated cortical down-state. Science *324*, 1084–1087.

Castro-Alamancos, M.A. (2004). Absence of rapid sensory adaptation in neocortex during information processing states. Neuron *41*, 455–464.

Castro-Alamancos, M.A., and Oldford, E. (2002). Cortical sensory suppression during arousal is due to the activity-dependent depression of thalamocortical synapses. J. Physiol. *541*, 319–331.

Chauvette, S., Volgushev, M., and Timofeev, I. (2010). Origin of active states in local neocortical networks during slow sleep oscillation. Cereb. Cortex New York N 1991 *20*, 2660–2674.

Chauvette, S., Crochet, S., Volgushev, M., and Timofeev, I. (2011). Properties of slow oscillation during slow-wave sleep and anesthesia in cats. J. Neurosci. Off. J. Soc. Neurosci. *31*, 14998–15008.

Chauvette, S., Seigneur, J., and Timofeev, I. (2012). Sleep oscillations in the thalamocortical system induce long-term neuronal plasticity. Neuron *75*, 1105–1113.

Chen, J.-Y., Chauvette, S., Skorheim, S., Timofeev, I., and Bazhenov, M. (2012). Interneuron-mediated inhibition synchronizes neuronal activity during slow oscillation. J. Physiol. *590*, 3987–4010.

Chen, Z., Vijayan, S., Barbieri, R., Wilson, M.A., and Brown, E.N. (2009). Discrete- and continuous-time probabilistic models and algorithms for inferring neuronal UP and DOWN states. Neural Comput. *21*, 1797–1862.

Churchland, A.K., Kiani, R., Chaudhuri, R., Wang, X.-J., Pouget, A., and Shadlen, M.N. (2011). Variance as a signature of neural computations during decision making. Neuron *69*, 818–831.

Clement, E.A., Richard, A., Thwaites, M., Ailon, J., Peters, S., and Dickson, C.T. (2008). Cyclic and sleep-like spontaneous alternations of brain state under urethane anaesthesia. PloS One *3*, e2004.

Compte, A., Sanchez-Vives, M.V., McCormick, D.A., and Wang, X.-J. (2003). Cellular and network mechanisms of slow oscillatory activity (<1 Hz) and wave propagations in a cortical network model. J. Neurophysiol. *89*, 2707–2725.

Compte, A., Reig, R., Descalzo, V.F., Harvey, M.A., Puccini, G.D., and Sanchez-Vives, M.V. (2008). Spontaneous high-frequency (10-80 Hz) oscillations during up states in the cerebral cortex in vitro. J. Neurosci. Off. J. Soc. Neurosci. *28*, 13828–13844.

Compte, A., Reig, R., and Sanchez-Vives, M.V. (2009). Timing Excitation and Inhibition in the Cortical Network. In Coherent Behavior in Neuronal Networks, K. Josic, J. Rubin, M. Matias, and R. Romo, eds. (Springer New York), pp. 17–46.

Connors, B.W., and Gutnick, M.J. (1990). Intrinsic firing patterns of diverse neocortical neurons. Trends Neurosci. *13*, 99–104.

Constantinople, C.M., and Bruno, R.M. (2011). Effects and mechanisms of wakefulness on local cortical networks. Neuron *69*, 1061–1068.

Constantinople, C.M., and Bruno, R.M. (2013). Deep cortical layers are activated directly by thalamus. Science *340*, 1591–1594.

Contreras, D. (2004). Electrophysiological classes of neocortical neurons. Neural Networks Off. J. Int. Neural Netw. Soc. *17*, 633–646.

Contreras, D., and Steriade, M. (1995). Cellular basis of EEG slow rhythms: a study of dynamic corticothalamic relationships. J. Neurosci. Off. J. Soc. Neurosci. *15*, 604–622.

Contreras, D., and Steriade, M. (1997). State-dependent fluctuations of low-frequency rhythms in corticothalamic networks. Neuroscience *76*, 25–38.

Contreras, D., Timofeev, I., and Steriade, M. (1996). Mechanisms of long-lasting hyperpolarizations underlying slow sleep oscillations in cat corticothalamic networks. J. Physiol. *494 (Pt 1)*, 251–264.

Cortes, J.M., Marinazzo, D., Series, P., Oram, M.W., Sejnowski, T.J., and van Rossum, M.C.W. (2012). The effect of neural adaptation on population coding accuracy. J. Comput. Neurosci. *32*, 387–402.

Cossart, R., Aronov, D., and Yuste, R. (2003). Attractor dynamics of network UP states in the neocortex. Nature *423*, 283–288.

Cowan, R.L., and Wilson, C.J. (1994). Spontaneous firing patterns and axonal projections of single corticostriatal neurons in the rat medial agranular cortex. J. Neurophysiol. *71*, 17–32.

Crochet, S., and Petersen, C.C.H. (2006). Correlating whisker behavior with membrane potential in barrel cortex of awake mice. Nat. Neurosci. *9*, 608–610.

Crochet, S., Chauvette, S., Boucetta, S., and Timofeev, I. (2005). Modulation of synaptic transmission in neocortex by network activities. Eur. J. Neurosci. *21*, 1030–1044.

Crook, S.M., Ermentrout, G.B., and Bower, J.M. (1998). Spike frequency adaptation affects the synchronization properties of networks of cortical oscillations. Neural Comput. *10*, 837–854.

Cruikshank, S.J., Lewis, T.J., and Connors, B.W. (2007). Synaptic basis for intense thalamocortical activation of feedforward inhibitory cells in neocortex. Nat. Neurosci. *10*, 462–468.

Cruikshank, S.J., Urabe, H., Nurmikko, A.V., and Connors, B.W. (2010). Pathway-specific feedforward circuits between thalamus and neocortex revealed by selective optical stimulation of axons. Neuron *65*, 230–245.

Crunelli, V., and Hughes, S.W. (2010). The slow (<1 Hz) rhythm of non-REM sleep: a dialogue between three cardinal oscillators. Nat. Neurosci. *13*, 9–17.

Csercsa, R., Dombovári, B., Fabó, D., Wittner, L., Eross, L., Entz, L., Sólyom, A.,

Rásonyi, G., Szucs, A., Kelemen, A., et al. (2010). Laminar analysis of slow wave activity in humans. Brain J. Neurol. *133*, 2814–2829.

Csicsvari, J., Hirase, H., Czurko, A., and Buzsáki, G. (1998). Reliability and state dependence of pyramidal cell-interneuron synapses in the hippocampus: an ensemble approach in the behaving rat. Neuron *21*, 179–189.

Cunningham, M.O., Davies, C.H., Buhl, E.H., Kopell, N., and Whittington, M.A. (2003). Gamma oscillations induced by kainate receptor activation in the entorhinal cortex in vitro. J. Neurosci. Off. J. Soc. Neurosci. *23*, 9761–9769.

Cunningham, M.O., Pervouchine, D.D., Racca, C., Kopell, N.J., Davies, C.H., Jones, R.S.G., Traub, R.D., and Whittington, M.A. (2006). Neuronal metabolism governs cortical network response state. Proc. Natl. Acad. Sci. U. S. A. *103*, 5597–5601.

Curto, C., Sakata, S., Marguet, S., Itskov, V., and Harris, K.D. (2009). A simple model of cortical dynamics explains variability and state dependence of sensory responses in urethane-anesthetized auditory cortex. J. Neurosci. Off. J. Soc. Neurosci. *29*, 10600–10612.

Dean, A.F. (1981). The variability of discharge of simple cells in the cat striate cortex. Exp. Brain Res. Exp. Hirnforsch. Expérimentation Cérébrale *44*, 437–440.

Deco, G., Martí, D., Ledberg, A., Reig, R., and Sanchez Vives, M.V. (2009a). Effective reduced diffusion-models: a data driven approach to the analysis of neuronal dynamics. PLoS Comput. Biol. *5*, e1000587.

Deco, G., Rolls, E.T., and Romo, R. (2009b). Stochastic dynamics as a principle of brain function. Prog. Neurobiol. *88*, 1–16.

Descalzo, V.F., Nowak, L.G., Brumberg, J.C., McCormick, D.A., and Sanchez-Vives, M.V. (2005). Slow adaptation in fast-spiking neurons of visual cortex. J. Neurophysiol. *93*, 1111–1118.

Destexhe, A. (2009). Self-sustained asynchronous irregular states and Up-Down states in thalamic, cortical and thalamocortical networks of nonlinear integrate-and-fire neurons. J. Comput. Neurosci. *27*, 493–506.

Destexhe, A., and Sejnowski, T.J. (2009). The Wilson-Cowan model, 36 years later. Biol. Cybern. *101*, 1–2.

Destexhe, A., Contreras, D., and Steriade, M. (1999). Spatiotemporal analysis of local field potentials and unit discharges in cat cerebral cortex during natural wake and sleep states. J. Neurosci. Off. J. Soc. Neurosci. *19*, 4595–4608.

Détári, L., Rasmusson, D.D., and Semba, K. (1997). Phasic relationship between the activity of basal forebrain neurons and cortical EEG in urethane-anesthetized rat. Brain Res. *759*, 112–121.

DeWeese, M.R., and Zador, A.M. (2006). Non-Gaussian membrane potential dynamics imply sparse, synchronous activity in auditory cortex. J. Neurosci. Off. J. Soc. Neurosci. *26*, 12206–12218.

Diba, K., and Buzsáki, G. (2007). Forward and reverse hippocampal place-cell sequences during ripples. Nat. Neurosci. *10*, 1241–1242.

Disney, A.A., Aoki, C., and Hawken, M.J. (2007). Gain modulation by nicotine in macaque v1. Neuron *56*, 701–713.

Douglas, R.J., and Martin, K.A.C. (2004). Neuronal circuits of the neocortex. Annu. Rev. Neurosci. *27*, 419–451.

Douglas, R.J., Martin, K.A.C., and Whitteridge, D. (1989). A Canonical Microcircuit for Neocortex. Neural Comput. *1*, 480–488.

Dringenberg, H.C., and Vanderwolf, C.H. (1997). Neocortical activation: modulation by multiple pathways acting on central cholinergic and serotonergic systems. Exp. Brain Res. Exp. Hirnforsch. Expérimentation Cérébrale *116*, 160–174.

Druckmann, S., Hill, S., Schürmann, F., Markram, H., and Segev, I. (2012). A Hierarchical Structure of Cortical Interneuron Electrical Diversity Revealed by Automated Statistical Analysis. Cereb. Cortex New York N 1991.

Von Economo, C., and Koskinas, G. (1925). Die Cytoarchitektonik der Hirnrinde des erwachsenen Menchen. (Springer).

Egorov, A.V., Hamam, B.N., Fransén, E., Hasselmo, M.E., and Alonso, A.A. (2002). Graded persistent activity in entorhinal cortex neurons. Nature *420*, 173–178.

Erchova, I.A., Lebedev, M.A., and Diamond, M.E. (2002). Somatosensory cortical neuronal population activity across states of anaesthesia. Eur. J. Neurosci. *15*, 744–752.

Eschenko, O., Ramadan, W., Mölle, M., Born, J., and Sara, S.J. (2008). Sustained increase in hippocampal sharp-wave ripple activity during slow-wave sleep after learning. Learn. Mem. Cold Spring Harb. N *15*, 222–228.

Eschenko, O., Magri, C., Panzeri, S., and Sara, S.J. (2012). Noradrenergic neurons of the locus coeruleus are phase locked to cortical up-down states during sleep. Cereb. Cortex New York N 1991 *22*, 426–435.

Euston, D.R., Tatsuno, M., and McNaughton, B.L. (2007). Fast-forward playback of recent memory sequences in prefrontal cortex during sleep. Science *318*, 1147–1150.

Fanselow, E.E., and Connors, B.W. (2010). The roles of somatostatin-expressing (GIN) and fast-spiking inhibitory interneurons in UP-DOWN states of mouse neocortex. J. Neurophysiol. *104*, 596–606.

Fanselow, E.E., Richardson, K.A., and Connors, B.W. (2008). Selective, state-dependent activation of somatostatin-expressing inhibitory interneurons in mouse neocortex. J. Neurophysiol. *100*, 2640–2652.

Farkhooi, F., Muller, E., and Nawrot, M.P. (2011). Adaptation reduces variability of the neuronal population code. Phys. Rev. E Stat. Nonlin. Soft Matter Phys. *83*, 050905.

Feller, M.B. (1999). Spontaneous correlated activity in developing neural circuits. Neuron *22*, 653–656.

Fiser, J., Chiu, C., and Weliky, M. (2004). Small modulation of ongoing cortical dynamics by sensory input during natural vision. Nature *431*, 573–578.

Fox, M.D., and Raichle, M.E. (2007). Spontaneous fluctuations in brain activity observed with functional magnetic resonance imaging. Nat. Rev. Neurosci. *8*, 700–711.

Fries, P., Reynolds, J.H., Rorie, A.E., and Desimone, R. (2001). Modulation of oscillatory neuronal synchronization by selective visual attention. Science *291*, 1560–1563.

Friston, K.J., Buechel, C., Fink, G.R., Morris, J., Rolls, E., and Dolan, R.J. (1997). Psychophysiological and modulatory interactions in neuroimaging. Neuroimage *6*, 218–229.

Fuhrmann, G., Markram, H., and Tsodyks, M. (2002). Spike frequency adaptation and neocortical rhythms. J. Neurophysiol. *88*, 761–770.

Fujisawa, S., Amarasingham, A., Harrison, M.T., and Buzsáki, G. (2008). Behavior-dependent short-term assembly dynamics in the medial prefrontal cortex. Nat. Neurosci. *11*, 823–833.

Gabernet, L., Jadhav, S.P., Feldman, D.E., Carandini, M., and Scanziani, M. (2005). Somatosensory integration controlled by dynamic thalamocortical feed-forward inhibition. Neuron *48*, 315–327.

Galarreta, M., and Hestrin, S. (1999). A network of fast-spiking cells in the neocortex connected by electrical synapses. Nature *402*, 72–75.

Gentet, L.J., Kremer, Y., Taniguchi, H., Huang, Z.J., Staiger, J.F., and Petersen, C.C.H. (2012). Unique functional properties of somatostatin-expressing GABAergic neurons in mouse barrel cortex. Nat. Neurosci. *15*, 607–612.

Gervasoni, D., Lin, S.-C., Ribeiro, S., Soares, E.S., Pantoja, J., and Nicolelis, M.A.L. (2004). Global forebrain dynamics predict rat behavioral states and their transitions. J. Neurosci. Off. J. Soc. Neurosci. *24*, 11137–11147.

Gibson, J.R., Beierlein, M., and Connors, B.W. (1999). Two networks of electrically coupled inhibitory neurons in neocortex. Nature *402*, 75–79.

Gil, Z., Connors, B.W., and Amitai, Y. (1997). Differential regulation of neocortical synapses by neuromodulators and activity. Neuron *19*, 679–686.

Gillespie (1996). Exact numerical simulation of the Ornstein-Uhlenbeck process and its integral. Phys. Rev. E Stat. Phys. Plasmas Fluids Relat. Interdiscip. Top. *54*, 2084–2091.

Girardeau, G., Benchenane, K., Wiener, S.I., Buzsáki, G., and Zugaro, M.B. (2009). Selective suppression of hippocampal ripples impairs spatial memory. Nat. Neurosci. *12*, 1222–1223.

Goard, M., and Dan, Y. (2009). Basal forebrain activation enhances cortical coding of natural scenes. Nat. Neurosci. *12*, 1444–1449.

Gonchar, Y., Wang, Q., and Burkhalter, A. (2007). Multiple distinct subtypes of GABAergic neurons in mouse visual cortex identified by triple immunostaining. Front. Neuroanat. *1*, 3.

Grenier, F., Timofeev, I., and Steriade, M. (2001). Focal synchronization of ripples (80-200 Hz) in neocortex and their neuronal correlates. J. Neurophysiol. *86*, 1884–1898.

Haegens, S., Nácher, V., Hernández, A., Luna, R., Jensen, O., and Romo, R. (2011). Beta oscillations in the monkey sensorimotor network reflect somatosensory decision making. Proc. Natl. Acad. Sci. U. S. A. *108*, 10708–10713.

Hahn, T.T.G., Sakmann, B., and Mehta, M.R. (2006). Phase-locking of hippocampal interneurons' membrane potential to neocortical up-down states. Nat. Neurosci. *9*, 1359–1361.

Hahn, T.T.G., McFarland, J.M., Berberich, S., Sakmann, B., and Mehta, M.R. (2012). Spontaneous persistent activity in entorhinal cortex modulates cortico-hippocampal interaction in vivo. Nat. Neurosci. *15*, 1531–1538.

Hahnloser, R.L.T. (1998). On the piecewise analysis of networks of linear threshold neurons. Neural Networks Off. J. Int. Neural Netw. Soc. *11*, 691–697.

Haider, B., and McCormick, D.A. (2009). Rapid neocortical dynamics: cellular and network mechanisms. Neuron *62*, 171–189.

Haider, B., Duque, A., Hasenstaub, A.R., and McCormick, D.A. (2006). Neocortical network activity in vivo is generated through a dynamic balance of excitation and inhibition. J. Neurosci. Off. J. Soc. Neurosci. *26*, 4535–4545.

Haider, B., Duque, A., Hasenstaub, A.R., Yu, Y., and McCormick, D.A. (2007). Enhancement of visual responsiveness by spontaneous local network activity in vivo. J. Neurophysiol. *97*, 4186–4202.

Han, F., Caporale, N., and Dan, Y. (2008). Reverberation of recent visual experience in spontaneous cortical waves. Neuron *60*, 321–327.

Hasenstaub, A., Shu, Y., Haider, B., Kraushaar, U., Duque, A., and McCormick, D.A. (2005). Inhibitory postsynaptic potentials carry synchronized frequency information in active cortical networks. Neuron *47*, 423–435.

Hasenstaub, A., Sachdev, R.N.S., and McCormick, D.A. (2007). State changes rapidly modulate cortical neuronal responsiveness. J. Neurosci. Off. J. Soc. Neurosci. *27*, 9607–9622.

Hebb, D.O. (1949). The Organization of Behavior: A Neuropsychological Theory.

Van den Heuvel, M.P., Mandl, R.C.W., Kahn, R.S., and Hulshoff Pol, H.E. (2009). Functionally linked resting-state networks reflect the underlying structural connectivity architecture of the human brain. Hum. Brain Mapp. *30*, 3127–3141.

Hill, S., and Tononi, G. (2005). Modeling sleep and wakefulness in the thalamocortical system. J. Neurophysiol. *93*, 1671–1698.

Hirata, A., and Castro-Alamancos, M.A. (2010). Neocortex network activation and deactivation states controlled by the thalamus. J. Neurophysiol. *103*, 1147–1157.

Hirata, A., and Castro-Alamancos, M.A. (2011). Effects of cortical activation on sensory responses in barrel cortex. J. Neurophysiol. *105*, 1495–1505.

Hoffman, K.L., and McNaughton, B.L. (2002). Coordinated reactivation of distributed memory traces in primate neocortex. Science *297*, 2070–2073.

Holcman, D., and Tsodyks, M. (2006). The emergence of Up and Down states in cortical networks. PLoS Comput. Biol. *2*, e23.

Hounsgaard, J., and Kiehn, O. (1985). Ca++ dependent bistability induced by serotonin in spinal motoneurons. Exp. Brain Res. Exp. Hirnforsch. Expérimentation Cérébrale *57*, 422–425.

Hromádka, T., Zador, A.M., and DeWeese, M.R. (2013). Up states are rare in awake auditory cortex. J. Neurophysiol. *109*, 1989–1995.

Hughes, S.W., Cope, D.W., Blethyn, K.L., and Crunelli, V. (2002). Cellular mechanisms of the slow (<1 Hz) oscillation in thalamocortical neurons in vitro. Neuron *33*, 947–958.

Hughes, S.W., Lörincz, M., Cope, D.W., Blethyn, K.L., Kékesi, K.A., Parri, H.R., Juhász, G., and Crunelli, V. (2004). Synchronized oscillations at alpha and theta frequencies in the lateral geniculate nucleus. Neuron *42*, 253–268.

Imas, O.A., Ropella, K.M., Wood, J.D., and Hudetz, A.G. (2004). Halothane augments event-related gamma oscillations in rat visual cortex. Neuroscience *123*, 269–278.

Isomura, Y., Sirota, A., Ozen, S., Montgomery, S., Mizuseki, K., Henze, D.A., and Buzsáki, G. (2006). Integration and segregation of activity in entorhinal-hippocampal subregions by neocortical slow oscillations. Neuron *52*, 871–882.

Ji, D., and Wilson, M.A. (2007). Coordinated memory replay in the visual cortex and hippocampus during sleep. Nat. Neurosci. *10*, 100–107.

Johnson, L.A., Euston, D.R., Tatsuno, M., and McNaughton, B.L. (2010). Stored-trace reactivation in rat prefrontal cortex is correlated with down-to-up state fluctuation density. J. Neurosci. Off. J. Soc. Neurosci. *30*, 2650–2661.

Jones, E.G. (2000). Microcolumns in the cerebral cortex. Proc. Natl. Acad. Sci. U. S. A. *97*, 5019–5021.

Kang, S., Kitano, K., and Fukai, T. (2004). Self-organized two-state membrane potential transitions in a network of realistically modeled cortical neurons. Neural Networks Off. J. Int. Neural Netw. Soc. *17*, 307–312.

Van Kan, P.L., Scobey, R.P., and Gabor, A.J. (1985). Response covariance in cat visual cortex. Exp. Brain Res. Exp. Hirnforsch. Expérimentation Cérébrale *60*, 559–

563.

Kätzel, D., Zemelman, B.V., Buetfering, C., Wölfel, M., and Miesenböck, G. (2011). The columnar and laminar organization of inhibitory connections to neocortical excitatory cells. Nat. Neurosci. *14*, 100–107.

Kawaguchi, Y., and Kubota, Y. (1997). GABAergic cell subtypes and their synaptic connections in rat frontal cortex. Cereb. Cortex New York N 1991 *7*, 476–486.

Kawai, H., Lazar, R., and Metherate, R. (2007). Nicotinic control of axon excitability regulates thalamocortical transmission. Nat. Neurosci. *10*, 1168–1175.

Kenet, T., Bibitchkov, D., Tsodyks, M., Grinvald, A., and Arieli, A. (2003). Spontaneously emerging cortical representations of visual attributes. Nature *425*, 954–956.

Kisley, M.A., and Gerstein, G.L. (1999). Trial-to-trial variability and state-dependent modulation of auditory-evoked responses in cortex. J. Neurosci. Off. J. Soc. Neurosci. *19*, 10451–10460.

Kohn, A., and Smith, M.A. (2005). Stimulus dependence of neuronal correlation in primary visual cortex of the macaque. J. Neurosci. Off. J. Soc. Neurosci. *25*, 3661–3673.

Von Krosigk, M., Bal, T., and McCormick, D.A. (1993). Cellular mechanisms of a synchronized oscillation in the thalamus. Science *261*, 361–364.

Kumar, A., Schrader, S., Aertsen, A., and Rotter, S. (2008). The high-conductance state of cortical networks. Neural Comput. *20*, 1–43.

Kurth, S., Ringli, M., Geiger, A., LeBourgeois, M., Jenni, O.G., and Huber, R. (2010). Mapping of cortical activity in the first two decades of life: a high-density sleep electroencephalogram study. J. Neurosci. Off. J. Soc. Neurosci. *30*, 13211–13219.

Lampl, I., Reichova, I., and Ferster, D. (1999). Synchronous membrane potential fluctuations in neurons of the cat visual cortex. Neuron *22*, 361–374.

Latham, P.E., Richmond, B.J., Nelson, P.G., and Nirenberg, S. (2000). Intrinsic dynamics in neuronal networks. I. Theory. J. Neurophysiol. *83*, 808–827.

Lee, S.-H., and Dan, Y. (2012). Neuromodulation of brain states. Neuron *76*, 209–222.

Léger, J.-F., Stern, E.A., Aertsen, A., and Heck, D. (2005). Synaptic integration in rat frontal cortex shaped by network activity. J. Neurophysiol. *93*, 281–293.

Lewis, B.L., and O'Donnell, P. (2000). Ventral tegmental area afferents to the prefrontal cortex maintain membrane potential "up" states in pyramidal neurons via D(1) dopamine receptors. Cereb. Cortex New York N 1991 *10*, 1168–1175.

Lewis, T.J., and Rinzel, J. (2003). Dynamics of spiking neurons connected by both inhibitory and electrical coupling. J. Comput. Neurosci. *14*, 283–309.

Lewis, C.M., Baldassarre, A., Committeri, G., Romani, G.L., and Corbetta, M. (2009). Learning sculpts the spontaneous activity of the resting human brain. Proc. Natl. Acad. Sci. U. S. A. *106*, 17558–17563.

Li, C.-Y.T., Poo, M.-M., and Dan, Y. (2009). Burst spiking of a single cortical neuron modifies global brain state. Science *324*, 643–646.

Lim, S., and Rinzel, J. (2010). Noise-induced transitions in slow wave neuronal dynamics. J. Comput. Neurosci. *28*, 1–17.

Lisman, J.E., and Idiart, M.A. (1995). Storage of 7 +/- 2 short-term memories in oscillatory subcycles. Science *267*, 1512–1515.

Livingstone, M.S., and Hubel, D.H. (1981). Effects of sleep and arousal on the processing of visual information in the cat. Nature *291*, 554–561.

Loewenstein, Y., Mahon, S., Chadderton, P., Kitamura, K., Sompolinsky, H., Yarom, Y., and Häusser, M. (2005). Bistability of cerebellar Purkinje cells modulated by sensory stimulation. Nat. Neurosci. *8*, 202–211.

Lu, J., Sherman, D., Devor, M., and Saper, C.B. (2006). A putative flip-flop switch for control of REM sleep. Nature *441*, 589–594.

Luczak, A., and Barthó, P. (2012). Consistent sequential activity across diverse forms of UP states under ketamine anesthesia. Eur. J. Neurosci. *36*, 2830–2838.

Luczak, A., Barthó, P., Marguet, S.L., Buzsáki, G., and Harris, K.D. (2007). Sequential structure of neocortical spontaneous activity in vivo. Proc. Natl. Acad. Sci. U. S. A. *104*, 347–352.

Luczak, A., Barthó, P., and Harris, K.D. (2009). Spontaneous events outline the realm of possible sensory responses in neocortical populations. Neuron *62*, 413–425.

Luczak, A., Bartho, P., and Harris, K.D. (2013). Gating of sensory input by spontaneous cortical activity. J. Neurosci. Off. J. Soc. Neurosci. *33*, 1684–1695.

Ma, W.J., Beck, J.M., Latham, P.E., and Pouget, A. (2006). Bayesian inference with probabilistic population codes. Nat. Neurosci. *9*, 1432–1438.

MacKay, W.A., and Mendonça, A.J. (1995). Field potential oscillatory bursts in parietal cortex before and during reach. Brain Res. *704*, 167–174.

MacLean, J.N., Watson, B.O., Aaron, G.B., and Yuste, R. (2005). Internal dynamics determine the cortical response to thalamic stimulation. Neuron *48*, 811–823.

Maier, A., Adams, G.K., Aura, C., and Leopold, D.A. (2010). Distinct superficial and deep laminar domains of activity in the visual cortex during rest and stimulation. Front. Syst. Neurosci. *4*.

Mann, E.O., Kohl, M.M., and Paulsen, O. (2009). Distinct roles of GABA(A) and GABA(B) receptors in balancing and terminating persistent cortical activity. J. Neurosci. Off. J. Soc. Neurosci. *29*, 7513–7518.

Maquet, P., Laureys, S., Peigneux, P., Fuchs, S., Petiau, C., Phillips, C., Aerts, J., Del Fiore, G., Degueldre, C., Meulemans, T., et al. (2000). Experience-dependent changes in cerebral activation during human REM sleep. Nat. Neurosci. *3*, 831–836.

Marguet, S.L., and Harris, K.D. (2011). State-dependent representation of amplitude-modulated noise stimuli in rat auditory cortex. J. Neurosci. Off. J. Soc. Neurosci. *31*, 6414–6420.

Markram, H., Toledo-Rodriguez, M., Wang, Y., Gupta, A., Silberberg, G., and Wu, C. (2004). Interneurons of the neocortical inhibitory system. Nat. Rev. Neurosci. *5*, 793–807.

Marshall, L., Helgadóttir, H., Mölle, M., and Born, J. (2006). Boosting slow oscillations during sleep potentiates memory. Nature *444*, 610–613.

Martí, D., Deco, G., Mattia, M., Gigante, G., and Del Giudice, P. (2008). A fluctuation-driven mechanism for slow decision processes in reverberant networks. PloS One *3*, e2534.

Mason, A., and Larkman, A. (1990). Correlations between morphology and electrophysiology of pyramidal neurons in slices of rat visual cortex. II. Electrophysiology. J. Neurosci. Off. J. Soc. Neurosci. *10*, 1415–1428.

Massi, L., Lagler, M., Hartwich, K., Borhegyi, Z., Somogyi, P., and Klausberger, T. (2012). Temporal dynamics of parvalbumin-expressing axo-axonic and basket cells in the rat medial prefrontal cortex in vivo. J. Neurosci. Off. J. Soc. Neurosci. *32*, 16496–16502.

Massimini, M., Rosanova, M., and Mariotti, M. (2003). EEG slow (approximately 1 Hz) waves are associated with nonstationarity of thalamo-cortical sensory processing in the sleeping human. J. Neurophysiol. *89*, 1205–1213.

Massimini, M., Huber, R., Ferrarelli, F., Hill, S., and Tononi, G. (2004). The sleep slow oscillation as a traveling wave. J. Neurosci. Off. J. Soc. Neurosci. *24*, 6862–6870.

Matsumura, M., Chen, D., Sawaguchi, T., Kubota, K., and Fetz, E.E. (1996). Synaptic interactions between primate precentral cortex neurons revealed by spike-triggered averaging of intracellular membrane potentials in vivo. J. Neurosci. Off. J. Soc. Neurosci. *16*, 7757–7767.

Mattia, M., and Sanchez-Vives, M.V. (2012). Exploring the spectrum of dynamical regimes and timescales in spontaneous cortical activity. Cogn. Neurodyn. *6*, 239–250.

McCormick, D.A. (1992). Cellular mechanisms underlying cholinergic and noradrenergic modulation of neuronal firing mode in the cat and guinea pig dorsal lateral geniculate nucleus. J. Neurosci. Off. J. Soc. Neurosci. *12*, 278–289.

McCormick, D.A., and Prince, D.A. (1986). Acetylcholine induces burst firing in thalamic reticular neurones by activating a potassium conductance. Nature *319*, 402–405.

McCormick, D.A., Connors, B.W., Lighthall, J.W., and Prince, D.A. (1985).

Comparative electrophysiology of pyramidal and sparsely spiny stellate neurons of the neocortex. J. Neurophysiol. *54*, 782–806.

McFarland, J.M., Hahn, T.T.G., and Mehta, M.R. (2011). Explicit-duration hidden Markov model inference of UP-DOWN states from continuous signals. PloS One *6*, e21606.

Mejias, J.F., Kappen, H.J., and Torres, J.J. (2010). Irregular dynamics in up and down cortical states. PloS One *5*, e13651.

Melamed, O., Barak, O., Silberberg, G., Markram, H., and Tsodyks, M. (2008). Slow oscillations in neural networks with facilitating synapses. J. Comput. Neurosci. *25*, 308–316.

Metherate, R., and Ashe, J.H. (1993). Ionic flux contributions to neocortical slow waves and nucleus basalis-mediated activation: whole-cell recordings in vivo. J. Neurosci. Off. J. Soc. Neurosci. *13*, 5312–5323.

Metherate, R., and Cruikshank, S.J. (1999). Thalamocortical inputs trigger a propagating envelope of gamma-band activity in auditory cortex in vitro. Exp. Brain Res. Exp. Hirnforsch. Expérimentation Cérébrale *126*, 160–174.

Metherate, R., Cox, C.L., and Ashe, J.H. (1992). Cellular bases of neocortical activation: modulation of neural oscillations by the nucleus basalis and endogenous acetylcholine. J. Neurosci. Off. J. Soc. Neurosci. *12*, 4701–4711.

Middleton, S., Jalics, J., Kispersky, T., Lebeau, F.E.N., Roopun, A.K., Kopell, N.J., Whittington, M.A., and Cunningham, M.O. (2008). NMDA receptor-dependent switching between different gamma rhythm-generating microcircuits in entorhinal cortex. Proc. Natl. Acad. Sci. U. S. A. *105*, 18572–18577.

Miller, K.J., Sorensen, L.B., Ojemann, J.G., and den Nijs, M. (2009). Power-law scaling in the brain surface electric potential. PLoS Comput. Biol. *5*, e1000609.

Mitchell, J.F., Sundberg, K.A., and Reynolds, J.H. (2007). Differential attention-dependent response modulation across cell classes in macaque visual area V4. Neuron *55*, 131–141.

Mitra, P.P., and Pesaran, B. (1999). Analysis of dynamic brain imaging data. Biophys. J. *76*, 691–708.

Mohajerani, M.H., McVea, D.A., Fingas, M., and Murphy, T.H. (2010). Mirrored bilateral slow-wave cortical activity within local circuits revealed by fast bihemispheric voltage-sensitive dye imaging in anesthetized and awake mice. J. Neurosci. Off. J. Soc. Neurosci. *30*, 3745–3751.

Moreno-Bote, R., Rinzel, J., and Rubin, N. (2007). Noise-induced alternations in an attractor network model of perceptual bistability. J. Neurophysiol. *98*, 1125–1139.

Moruzzi, G., and Magoun, H.W. (1949). Brain stem reticular formation and activation of the EEG. Electroencephalogr. Clin. Neurophysiol. *1*, 455–473.

Mountcastle, V.B. (1957). Modality and topographic properties of single neurons of cat's somatic sensory cortex. J. Neurophysiol. *20*, 408–434.

Mountcastle, V.B., Talbot, W.H., Sakata, H., and Hyvärinen, J. (1969). Cortical neuronal mechanisms in flutter-vibration studied in unanesthetized monkeys. Neuronal periodicity and frequency discrimination. J. Neurophysiol. *32*, 452–484.

Mukovski, M., Chauvette, S., Timofeev, I., and Volgushev, M. (2007). Detection of active and silent states in neocortical neurons from the field potential signal during slow-wave sleep. Cereb. Cortex New York N 1991 *17*, 400–414.

Murakami, M., Kashiwadani, H., Kirino, Y., and Mori, K. (2005). State-dependent sensory gating in olfactory cortex. Neuron *46*, 285–296.

Murphy, B.K., and Miller, K.D. (2009). Balanced amplification: a new mechanism of selective amplification of neural activity patterns. Neuron *61*, 635–648.

Nauhaus, I., Busse, L., Carandini, M., and Ringach, D.L. (2009). Stimulus contrast modulates functional connectivity in visual cortex. Nat. Neurosci. *12*, 70–76.

Neuman, R.S., and Thompson, P.M. (1989). Serotonin mediates suppression of focal epileptiform activity induced by noxious stimulation. Epilepsia *30*, 307–313.

Ngo, H.-V.V., Martinetz, T., Born, J., and Mölle, M. (2013). Auditory closed-loop stimulation of the sleep slow oscillation enhances memory. Neuron *78*, 545–553.

Nir, Y., Mukamel, R., Dinstein, I., Privman, E., Harel, M., Fisch, L., Gelbard-Sagiv, H., Kipervasser, S., Andelman, F., Neufeld, M.Y., et al. (2008). Interhemispheric correlations of slow spontaneous neuronal fluctuations revealed in human sensory cortex. Nat. Neurosci. *11*, 1100–1108.

Nishihara, K., and Horiuchi, S. (1998). Changes in sleep patterns of young women from late pregnancy to postpartum: relationships to their infants' movements. Percept. Mot. Skills *87*, 1043–1056.

Nowak, L.G., Sanchez-Vives, M.V., and McCormick, D.A. (1997). Influence of low and high frequency inputs on spike timing in visual cortical neurons. Cereb. Cortex New York N 1991 *7*, 487–501.

Nowak, L.G., Azouz, R., Sanchez-Vives, M.V., Gray, C.M., and McCormick, D.A. (2003). Electrophysiological classes of cat primary visual cortical neurons in vivo as revealed by quantitative analyses. J. Neurophysiol. *89*, 1541–1566.

Ohl, F.W., Scheich, H., and Freeman, W.J. (2001). Change in pattern of ongoing cortical activity with auditory category learning. Nature *412*, 733–736.

Oke, O.O., Magony, A., Anver, H., Ward, P.D., Jiruska, P., Jefferys, J.G.R., and Vreugdenhil, M. (2010). High-frequency gamma oscillations coexist with low-frequency gamma oscillations in the rat visual cortex in vitro. Eur. J. Neurosci. *31*, 1435–1445.

Okun, M., and Lampl, I. (2008). Instantaneous correlation of excitation and inhibition during ongoing and sensory-evoked activities. Nat. Neurosci. *11*, 535–537.

Pagliardini, S., Gosgnach, S., and Dickson, C.T. (2013). Spontaneous sleep-like brain state alternations and breathing characteristics in urethane anesthetized mice.

PloS One *8*, e70411.

Palva, J.M., Palva, S., and Kaila, K. (2005). Phase synchrony among neuronal oscillations in the human cortex. J. Neurosci. Off. J. Soc. Neurosci. *25*, 3962–3972.

Parga, N., and Abbott, L.F. (2007). Network model of spontaneous activity exhibiting synchronous transitions between up and down States. Front. Neurosci. *1*, 57–66.

Partridge, L.D., and Stevens, C.F. (1976). A mechanism for spike frequency adaptation. J. Physiol. *256*, 315–332.

Perrin, F., García-Larrea, L., Mauguière, F., and Bastuji, H. (1999). A differential brain response to the subject's own name persists during sleep. Clin. Neurophysiol. Off. J. Int. Fed. Clin. Neurophysiol. *110*, 2153–2164.

Petersen, C.C.H., Grinvald, A., and Sakmann, B. (2003a). Spatiotemporal dynamics of sensory responses in layer 2/3 of rat barrel cortex measured in vivo by voltage-sensitive dye imaging combined with whole-cell voltage recordings and neuron reconstructions. J. Neurosci. Off. J. Soc. Neurosci. *23*, 1298–1309.

Petersen, C.C.H., Hahn, T.T.G., Mehta, M., Grinvald, A., and Sakmann, B. (2003b). Interaction of sensory responses with spontaneous depolarization in layer 2/3 barrel cortex. Proc. Natl. Acad. Sci. U. S. A. *100*, 13638–13643.

Peyrache, A., Khamassi, M., Benchenane, K., Wiener, S.I., and Battaglia, F.P. (2009). Replay of rule-learning related neural patterns in the prefrontal cortex during sleep. Nat. Neurosci. *12*, 919–926.

Phillips, A.J.K., Robinson, P.A., Kedziora, D.J., and Abeysuriya, R.G. (2010). Mammalian sleep dynamics: how diverse features arise from a common physiological framework. PLoS Comput. Biol. *6*, e1000826.

Pinault, D. (2008). N-methyl d-aspartate receptor antagonists ketamine and MK-801 induce wake-related aberrant gamma oscillations in the rat neocortex. Biol. Psychiatry *63*, 730–735.

Portas, C.M., Krakow, K., Allen, P., Josephs, O., Armony, J.L., and Frith, C.D. (2000). Auditory processing across the sleep-wake cycle: simultaneous EEG and fMRI monitoring in humans. Neuron *28*, 991–999.

Poskanzer, K.E., and Yuste, R. (2011). Astrocytic regulation of cortical UP states. Proc. Natl. Acad. Sci. U. S. A. *108*, 18453–18458.

Poulet, J.F.A., and Petersen, C.C.H. (2008). Internal brain state regulates membrane potential synchrony in barrel cortex of behaving mice. Nature *454*, 881–885.

Poulet, J.F.A., Fernandez, L.M.J., Crochet, S., and Petersen, C.C.H. (2012). Thalamic control of cortical states. Nat. Neurosci. *15*, 370–372.

Prescott, S.A., and De Koninck, Y. (2003). Gain control of firing rate by shunting inhibition: roles of synaptic noise and dendritic saturation. Proc. Natl. Acad. Sci. U. S. A. *100*, 2076–2081.

Priebe, N.J., and Ferster, D. (2008). Inhibition, spike threshold, and stimulus selectivity in primary visual cortex. Neuron *57*, 482–497.

Qin, Y.L., McNaughton, B.L., Skaggs, W.E., and Barnes, C.A. (1997). Memory reprocessing in corticocortical and hippocampocortical neuronal ensembles. Philos. Trans. R. Soc. Lond. B. Biol. Sci. *352*, 1525–1533.

Raichle, M.E., and Mintun, M.A. (2006). Brain work and brain imaging. Annu. Rev. Neurosci. *29*, 449–476.

Reig, R., and Sanchez-Vives, M.V. (2007). Synaptic transmission and plasticity in an active cortical network. PloS One *2*, e670.

Reig, R., Gallego, R., Nowak, L.G., and Sanchez-Vives, M.V. (2006). Impact of cortical network activity on short-term synaptic depression. Cereb. Cortex New York N 1991 *16*, 688–695.

Reimann, M.W., Anastassiou, C.A., Perin, R., Hill, S.L., Markram, H., and Koch, C. (2013). A biophysically detailed model of neocortical local field potentials predicts the critical role of active membrane currents. Neuron *79*, 375–390.

Rempe, M.J., Best, J., and Terman, D. (2010). A mathematical model of the sleep/wake cycle. J. Math. Biol. *60*, 615–644.

Renart, A., de la Rocha, J., Bartho, P., Hollender, L., Parga, N., Reyes, A., and Harris, K.D. (2010). The asynchronous state in cortical circuits. Science *327*, 587–590.

Ribeiro, S., Gervasoni, D., Soares, E.S., Zhou, Y., Lin, S.-C., Pantoja, J., Lavine, M., and Nicolelis, M.A.L. (2004). Long-lasting novelty-induced neuronal reverberation during slow-wave sleep in multiple forebrain areas. PLoS Biol. *2*, E24.

Rigas, P., and Castro-Alamancos, M.A. (2007). Thalamocortical Up states: differential effects of intrinsic and extrinsic cortical inputs on persistent activity. J. Neurosci. Off. J. Soc. Neurosci. *27*, 4261–4272.

Rinzel, J., and Lee, Y.S. (1987). Dissection of a model for neuronal parabolic bursting. J. Math. Biol. *25*, 653–675.

Roopun, A.K., Middleton, S.J., Cunningham, M.O., LeBeau, F.E.N., Bibbig, A., Whittington, M.A., and Traub, R.D. (2006). A beta2-frequency (20-30 Hz) oscillation in nonsynaptic networks of somatosensory cortex. Proc. Natl. Acad. Sci. U. S. A. *103*, 15646–15650.

Roopun, A.K., Kramer, M.A., Carracedo, L.M., Kaiser, M., Davies, C.H., Traub, R.D., Kopell, N.J., and Whittington, M.A. (2008). Temporal Interactions between Cortical Rhythms. Front. Neurosci. *2*, 145–154.

Roopun, A.K., Lebeau, F.E.N., Rammell, J., Cunningham, M.O., Traub, R.D., and Whittington, M.A. (2010). Cholinergic neuromodulation controls directed temporal communication in neocortex in vitro. Front. Neural Circuits *4*, 8.

Rudolph, M., Pelletier, J.G., Paré, D., and Destexhe, A. (2005). Characterization of

synaptic conductances and integrative properties during electrically induced EEG-activated states in neocortical neurons in vivo. J. Neurophysiol. *94*, 2805–2821.

Rudolph, M., Pospischil, M., Timofeev, I., and Destexhe, A. (2007). Inhibition determines membrane potential dynamics and controls action potential generation in awake and sleeping cat cortex. J. Neurosci. Off. J. Soc. Neurosci. *27*, 5280–5290.

Rudy, B., and McBain, C.J. (2001). Kv3 channels: voltage-gated K+ channels designed for high-frequency repetitive firing. Trends Neurosci. *24*, 517–526.

Ruiz-Mejias, M., Ciria-Suarez, L., Mattia, M., and Sanchez-Vives, M.V. (2011). Slow and fast rhythms generated in the cerebral cortex of the anesthetized mouse. J. Neurophysiol. *106*, 2910–2921.

Ruthazer, E.S., and Stryker, M.P. (1996). The role of activity in the development of long-range horizontal connections in area 17 of the ferret. J. Neurosci. Off. J. Soc. Neurosci. *16*, 7253–7269.

Sachdev, R.N.S., Ebner, F.F., and Wilson, C.J. (2004). Effect of subthreshold up and down states on the whisker-evoked response in somatosensory cortex. J. Neurophysiol. *92*, 3511–3521.

Sakata, S., and Harris, K.D. (2009). Laminar structure of spontaneous and sensory-evoked population activity in auditory cortex. Neuron *64*, 404–418.

Sakata, S., and Harris, K.D. (2012). Laminar-dependent effects of cortical state on auditory cortical spontaneous activity. Front. Neural Circuits *6*, 109.

Saleem, A.B., Chadderton, P., Apergis-Schoute, J., Harris, K.D., and Schultz, S.R. (2010). Methods for predicting cortical UP and DOWN states from the phase of deep layer local field potentials. J. Comput. Neurosci. *29*, 49–62.

Salinas, E., and Sejnowski, T.J. (2000). Impact of correlated synaptic input on output firing rate and variability in simple neuronal models. J. Neurosci. Off. J. Soc. Neurosci. *20*, 6193–6209.

Sanchez-Vives, M., and McCormick, D. (2000). Cellular and network mechanisms of rhythmic recurrent activity in neocortex. Nat. Neurosci. *3*, 1027–1034.

Sanchez-Vives, M.V., Descalzo, V.F., Reig, R., Figueroa, N.A., Compte, A., and Gallego, R. (2008). Rhythmic spontaneous activity in the piriform cortex. Cereb. Cortex New York N 1991 *18*, 1179–1192.

Sanchez-Vives, M.V., Mattia, M., Compte, A., Perez-Zabalza, M., Winograd, M., Descalzo, V.F., and Reig, R. (2010). Inhibitory modulation of cortical up states. J. Neurophysiol. *104*, 1314–1324.

Saper, C.B., Chou, T.C., and Scammell, T.E. (2001). The sleep switch: hypothalamic control of sleep and wakefulness. Trends Neurosci. *24*, 726–731.

Schabus, M., Dang-Vu, T.T., Heib, D.P.J., Boly, M., Desseilles, M., Vandewalle, G., Schmidt, C., Albouy, G., Darsaud, A., Gais, S., et al. (2012). The Fate of Incoming Stimuli during NREM Sleep is Determined by Spindles and the Phase of the Slow Oscillation. Front. Neurol. *3*, 40.

Schiff, M.L., and Reyes, A.D. (2012). Characterization of thalamocortical responses of regular-spiking and fast-spiking neurons of the mouse auditory cortex in vitro and in silico. J. Neurophysiol. *107*, 1476–1488.

Seamari, Y., Narváez, J.A., Vico, F.J., Lobo, D., and Sanchez-Vives, M.V. (2007). Robust off- and online separation of intracellularly recorded up and down cortical states. PloS One *2*, e888.

Sejnowski, T.J., and Destexhe, A. (2000). Why do we sleep? Brain Res. *886*, 208–223.

Shadlen, M.N., and Newsome, W.T. (1998a). The variable discharge of cortical neurons: implications for connectivity, computation, and information coding. J. Neurosci. Off. J. Soc. Neurosci. *18*, 3870–3896.

Shadlen, M.N., and Newsome, W.T. (1998b). The variable discharge of cortical neurons: implications for connectivity, computation, and information coding. J. Neurosci. Off. J. Soc. Neurosci. *18*, 3870–3896.

Sharma, A.V., Wolansky, T., and Dickson, C.T. (2010). A comparison of sleeplike slow oscillations in the hippocampus under ketamine and urethane anesthesia. J. Neurophysiol. *104*, 932–939.

Shepherd, G.M.G., and Svoboda, K. (2005). Laminar and columnar organization of ascending excitatory projections to layer 2/3 pyramidal neurons in rat barrel cortex. J. Neurosci. Off. J. Soc. Neurosci. *25*, 5670–5679.

Shpiro, A., Moreno-Bote, R., Rubin, N., and Rinzel, J. (2009). Balance between noise and adaptation in competition models of perceptual bistability. J. Comput. Neurosci. *27*, 37–54.

Shu, Y., Hasenstaub, A., Badoual, M., Bal, T., and McCormick, D.A. (2003a). Barrages of synaptic activity control the gain and sensitivity of cortical neurons. J. Neurosci. Off. J. Soc. Neurosci. *23*, 10388–10401.

Shu, Y., Hasenstaub, A., and McCormick, D.A. (2003b). Turning on and off recurrent balanced cortical activity. Nature *423*, 288–293.

Silberberg, G., Gupta, A., and Markram, H. (2002). Stereotypy in neocortical microcircuits. Trends Neurosci. *25*, 227–230.

Singer, W. (1993). Synchronization of cortical activity and its putative role in information processing and learning. Annu. Rev. Physiol. *55*, 349–374.

Sirota, A., and Buzsáki, G. (2005). Interaction between neocortical and hippocampal networks via slow oscillations. Thalamus Relat. Syst. *3*, 245–259.

Sirota, A., Montgomery, S., Fujisawa, S., Isomura, Y., Zugaro, M., and Buzsáki, G. (2008). Entrainment of neocortical neurons and gamma oscillations by the hippocampal theta rhythm. Neuron *60*, 683–697.

Skaggs, W.E., and McNaughton, B.L. (1996). Replay of neuronal firing sequences in rat hippocampus during sleep following spatial experience. Science *271*, 1870–1873.

Slézia, A., Hangya, B., Ulbert, I., and Acsády, L. (2011). Phase advancement and nucleus-specific timing of thalamocortical activity during slow cortical oscillation. J. Neurosci. Off. J. Soc. Neurosci. *31*, 607–617.

Smith, A.L., and Thompson, I.D. (1994). Distinct laminar differences in the distribution of excitatory amino acid receptors in adult ferret primary visual cortex. Neuroscience *61*, 467–479.

Softky, W.R., and Koch, C. (1993). The highly irregular firing of cortical cells is inconsistent with temporal integration of random EPSPs. J. Neurosci. Off. J. Soc. Neurosci. *13*, 334–350.

Spaak, E., Bonnefond, M., Maier, A., Leopold, D.A., and Jensen, O. (2012). Layer-specific entrainment of gamma-band neural activity by the alpha rhythm in monkey visual cortex. Curr. Biol. CB *22*, 2313–2318.

Stafstrom, C.E., Schwindt, P.C., and Crill, W.E. (1984). Repetitive firing in layer V neurons from cat neocortex in vitro. J. Neurophysiol. *52*, 264–277.

Stein, R.B., Gossen, E.R., and Jones, K.E. (2005). Neuronal variability: noise or part of the signal? Nat. Rev. Neurosci. *6*, 389–397.

Steriade, M. (1999). Brainstem activation of thalamocortical systems. Brain Res. Bull. *50*, 391–392.

Steriade, M. (2001). Impact of network activities on neuronal properties in corticothalamic systems. J. Neurophysiol. *86*, 1–39.

Steriade, M. (2006). Grouping of brain rhythms in corticothalamic systems. Neuroscience *137*, 1087–1106.

Steriade, M., and Amzica, F. (1996). Intracortical and corticothalamic coherency of fast spontaneous oscillations. Proc. Natl. Acad. Sci. U. S. A. *93*, 2533–2538.

Steriade, M., and Contreras, D. (1998). Spike-wave complexes and fast components of cortically generated seizures. I. Role of neocortex and thalamus. J. Neurophysiol. *80*, 1439–1455.

Steriade, M., and McCarley, R.W. (2005). Brain control of wakefulness and sleep (New York: Springer).

Steriade, M., Oakson, G., and Ropert, N. (1982). Firing rates and patterns of midbrain reticular neurons during steady and transitional states of the sleep-waking cycle. Exp. Brain Res. Exp. Hirnforsch. Expérimentation Cérébrale *46*, 37–51.

Steriade, M., Dossi, R.C., and Nuñez, A. (1991). Network modulation of a slow intrinsic oscillation of cat thalamocortical neurons implicated in sleep delta waves: cortically induced synchronization and brainstem cholinergic suppression. J. Neurosci. Off. J. Soc. Neurosci. *11*, 3200–3217.

Steriade, M., Nuiiez, A., Neurophysiologie, L.D., Mbdecine, F.D., Laval, U., and Glk, C. (1993a). A Novel Slow (less I Hz) Oscillation Depolarizing and Hyperpolarizing of Neocortical NATURAL. *73*.

Steriade, M., McCormick, D.A., and Sejnowski, T.J. (1993b). Thalamocortical oscillations in the sleeping and aroused brain. Science *262*, 679–685.

Steriade, M., Nuñez, A., and Amzica, F. (1993c). Intracellular analysis of relations between the slow (< 1 Hz) neocortical oscillation and other sleep rhythms of the electroencephalogram. J. Neurosci. Off. J. Soc. Neurosci. *13*, 3266–3283.

Steriade, M., Contreras, D., and Amzica, F. (1994). Synchronized sleep oscillations and their paroxysmal developments. Trends Neurosci. *17*, 199–208.

Steriade, M., Contreras, D., Amzica, F., and Timofeev, I. (1996). Synchronization of fast (30-40 Hz) spontaneous oscillations in intrathalamic and thalamocortical networks. J. Neurosci. Off. J. Soc. Neurosci. *16*, 2788–2808.

Steriade, M., Timofeev, I., and Grenier, F. (2001). Natural waking and sleep states: a view from inside neocortical neurons. J. Neurophysiol. *85*, 1969–1985.

Stern, E.A., Kincaid, A.E., and Wilson, C.J. (1997). Spontaneous subthreshold membrane potential fluctuations and action potential variability of rat corticostriatal and striatal neurons in vivo. J. Neurophysiol. *77*, 1697–1715.

Stern, E.A., Jaeger, D., and Wilson, C.J. (1998). Membrane potential synchrony of simultaneously recorded striatal spiny neurons in vivo. Nature *394*, 475–478.

Stoelzel, C.R., Bereshpolova, Y., Gusev, A.G., and Swadlow, H.A. (2008). The impact of an LGNd impulse on the awake visual cortex: synaptic dynamics and the sustained/transient distinction. J. Neurosci. Off. J. Soc. Neurosci. *28*, 5018–5028.

Stroh, A., Adelsberger, H., Groh, A., Rühlmann, C., Fischer, S., Schierloh, A., Deisseroth, K., and Konnerth, A. (2013). Making waves: initiation and propagation of corticothalamic Ca2+ waves in vivo. Neuron *77*, 1136–1150.

Tabak, J., Senn, W., O'Donovan, M.J., and Rinzel, J. (2000). Modeling of spontaneous activity in developing spinal cord using activity-dependent depression in an excitatory network. J. Neurosci. Off. J. Soc. Neurosci. *20*, 3041–3056.

Tabak, J., Rinzel, J., and O'Donovan, M.J. (2001). The role of activity-dependent network depression in the expression and self-regulation of spontaneous activity in the developing spinal cord. J. Neurosci. Off. J. Soc. Neurosci. *21*, 8966–8978.

Tabak, J., Rinzel, J., and Bertram, R. (2011). Quantifying the relative contributions of divisive and subtractive feedback to rhythm generation. PLoS Comput. Biol. *7*, e1001124.

Tang, H.J., Tan, K.C., and Zhang, W. (2005). Analysis of cyclic dynamics for networks of linear threshold neurons. Neural Comput. *17*, 97–114.

Tarczy-Hornoch, K., Martin, K.A., Jack, J.J., and Stratford, K.J. (1998). Synaptic interactions between smooth and spiny neurones in layer 4 of cat visual cortex in vitro. J. Physiol. *508 (Pt 2)*, 351–363.

Tateno, T., Harsch, A., and Robinson, H.P.C. (2004). Threshold firing frequency-current relationships of neurons in rat somatosensory cortex: type 1 and type 2 dynamics. J. Neurophysiol. *92*, 2283–2294.

Thomson, A.M., and Bannister, A.P. (2003). Interlaminar connections in the neocortex. Cereb. Cortex New York N 1991 *13*, 5–14.

Thuault, S.J., Malleret, G., Constantinople, C.M., Nicholls, R., Chen, I., Zhu, J., Panteleyev, A., Vronskaya, S., Nolan, M.F., Bruno, R., et al. (2013). Prefrontal Cortex HCN1 Channels Enable Intrinsic Persistent Neural Firing and Executive Memory Function. J. Neurosci. Off. J. Soc. Neurosci. *33*, 13583–13599.

Timofeev, I. (2011). Neuronal plasticity and thalamocortical sleep and waking oscillations. Prog. Brain Res. *193*, 121–144.

Timofeev, I., and Steriade, M. (1996a). Low-frequency rhythms in the thalamus of intact-cortex and decorticated cats. J. Neurophysiol. *76*, 4152–4168.

Timofeev, I., and Steriade, M. (1996b). Low-frequency rhythms in the thalamus of intact-cortex and decorticated cats. J. Neurophysiol. *76*, 4152–4168.

Timofeev, I., Grenier, F., Bazhenov, M., Sejnowski, T.J., and Steriade, M. (2000). Origin of slow cortical oscillations in deafferented cortical slabs. Cereb. Cortex New York N 1991 *10*, 1185–1199.

Timofeev, I., Grenier, F., and Steriade, M. (2001). Disfacilitation and active inhibition in the neocortex during the natural sleep-wake cycle: an intracellular study. Proc. Natl. Acad. Sci. U. S. A. *98*, 1924–1929.

Tolhurst, D.J., Dean, A.F., and Thompson, I.D. (1981). Preferred direction of movement as an element in the organization of cat visual cortex. Exp. Brain Res. Exp. Hirnforsch. Expérimentation Cérébrale *44*, 340–342.

Tolhurst, D.J., Movshon, J.A., and Dean, A.F. (1983). The statistical reliability of signals in single neurons in cat and monkey visual cortex. Vision Res. *23*, 775–785.

Ts'o, D.Y., Gilbert, C.D., and Wiesel, T.N. (1986). Relationships between horizontal interactions and functional architecture in cat striate cortex as revealed by cross-correlation analysis. J. Neurosci. Off. J. Soc. Neurosci. *6*, 1160–1170.

Tsodyks, M., Kenet, T., Grinvald, A., and Arieli, A. (1999). Linking spontaneous activity of single cortical neurons and the underlying functional architecture. Science *286*, 1943–1946.

Ushimaru, M., Ueta, Y., and Kawaguchi, Y. (2012). Differentiated participation of thalamocortical subnetworks in slow/spindle waves and desynchronization. J. Neurosci. Off. J. Soc. Neurosci. *32*, 1730–1746.

Valderrama, M., Crépon, B., Botella-Soler, V., Martinerie, J., Hasboun, D., Alvarado-Rojas, C., Baulac, M., Adam, C., Navarro, V., and Le Van Quyen, M. (2012). Human gamma oscillations during slow wave sleep. PloS One *7*, e33477.

Vanderwolf, C.H. (2000). Are neocortical gamma waves related to consciousness? Brain Res. *855*, 217–224.

Le Van Quyen, M., Staba, R., Bragin, A., Dickson, C., Valderrama, M., Fried, I., and Engel, J. (2010). Large-scale microelectrode recordings of high-frequency gamma oscillations in human cortex during sleep. J. Neurosci. Off. J. Soc. Neurosci. *30*,

7770–7782.

Villablanca, J.R. (2004). Counterpointing the functional role of the forebrain and of the brainstem in the control of the sleep-waking system. J. Sleep Res. *13*, 179–208.

Vincent, J.L., Patel, G.H., Fox, M.D., Snyder, A.Z., Baker, J.T., Van Essen, D.C., Zempel, J.M., Snyder, L.H., Corbetta, M., and Raichle, M.E. (2007). Intrinsic functional architecture in the anaesthetized monkey brain. Nature *447*, 83–86.

Volgushev, M., Chauvette, S., Mukovski, M., and Timofeev, I. (2006). Precise long-range synchronization of activity and silence in neocortical neurons during slow-wave oscillations [corrected]. J. Neurosci. Off. J. Soc. Neurosci. *26*, 5665–5672.

Van Vreeswijk, C., and Hansel, D. (2001). Patterns of synchrony in neural networks with spike adaptation. Neural Comput. *13*, 959–992.

Van Vreeswijk, C., and Sompolinsky, H. (1998). Chaotic balanced state in a model of cortical circuits. Neural Comput. *10*, 1321–1371.

Vyazovskiy, V.V., Olcese, U., Lazimy, Y.M., Faraguna, U., Esser, S.K., Williams, J.C., Cirelli, C., and Tononi, G. (2009). Cortical firing and sleep homeostasis. Neuron *63*, 865–878.

Vyazovskiy, V.V., Olcese, U., Hanlon, E.C., Nir, Y., Cirelli, C., and Tononi, G. (2011). Local sleep in awake rats. Nature *472*, 443–447.

Walker, M.P., and Stickgold, R. (2006). Sleep, memory, and plasticity. Annu. Rev. Psychol. *57*, 139–166.

Wang, X.-J. (2010). Neurophysiological and computational principles of cortical rhythms in cognition. Physiol. Rev. *90*, 1195–1268.

Wang, X.J. (1998). Calcium coding and adaptive temporal computation in cortical pyramidal neurons. J. Neurophysiol. *79*, 1549–1566.

Waters, J., and Helmchen, F. (2006). Background synaptic activity is sparse in neocortex. J. Neurosci. Off. J. Soc. Neurosci. *26*, 8267–8277.

Watson, B.O., MacLean, J.N., and Yuste, R. (2008). UP states protect ongoing cortical activity from thalamic inputs. PloS One *3*, e3971.

Weiler, N., Wood, L., Yu, J., Solla, S.A., and Shepherd, G.M.G. (2008). Top-down laminar organization of the excitatory network in motor cortex. Nat. Neurosci. *11*, 360–366.

Weliky, M., and Katz, L.C. (1997). Disruption of orientation tuning in visual cortex by artificially correlated neuronal activity. Nature *386*, 680–685.

Wierzynski, C.M., Lubenov, E.V., Gu, M., and Siapas, A.G. (2009). State-dependent spike-timing relationships between hippocampal and prefrontal circuits during sleep. Neuron *61*, 587–596.

Williams, S.R., and Stuart, G.J. (2002). Dependence of EPSP efficacy on synapse location in neocortical pyramidal neurons. Science *295*, 1907–1910.

Wilson, M. (1996). Dynamics of hippocampal memory formation in waking and sleep states. J. Physiol. Paris *90*, 351–352.

Wilson, C.J., and Groves, P.M. (1981). Spontaneous firing patterns of identified spiny neurons in the rat neostriatum. Brain Res. *220*, 67–80.

Wilson, H.R., and Cowan, J.D. (1972). Excitatory and inhibitory interactions in localized populations of model neurons. Biophys. J. *12*, 1–24.

Wilson, M.T., Steyn-Ross, M.L., Steyn-Ross, D.A., and Sleigh, J.W. (2005). Predictions and simulations of cortical dynamics during natural sleep using a continuum approach. Phys. Rev. E Stat. Nonlin. Soft Matter Phys. *72*, 051910.

Winograd, M., Destexhe, A., and Sanchez-Vives, M.V. (2008). Hyperpolarization-activated graded persistent activity in the prefrontal cortex. Proc. Natl. Acad. Sci. U. S. A. *105*, 7298–7303.

Wolansky, T., Clement, E.A., Peters, S.R., Palczak, M.A., and Dickson, C.T. (2006). Hippocampal slow oscillation: a novel EEG state and its coordination with ongoing neocortical activity. J. Neurosci. Off. J. Soc. Neurosci. *26*, 6213–6229.

Xing, D., Yeh, C.-I., Burns, S., and Shapley, R.M. (2012). Laminar analysis of visually evoked activity in the primary visual cortex. Proc. Natl. Acad. Sci. U. S. A. *109*, 13871–13876.

Xu, X., Olivas, N.D., Levi, R., Ikrar, T., and Nenadic, Z. (2010). High precision and fast functional mapping of cortical circuitry through a novel combination of voltage sensitive dye imaging and laser scanning photostimulation. J. Neurophysiol. *103*, 2301–2312.

Yuste, R., MacLean, J.N., Smith, J., and Lansner, A. (2005). The cortex as a central pattern generator. Nat. Rev. Neurosci. *6*, 477–483.

Zohary, E., Shadlen, M.N., and Newsome, W.T. (1994). Correlated neuronal discharge rate and its implications for psychophysical performance. Nature *370*, 140–143.